

PURDUE UNIVERSITY

THIS IS TO CERTIFY THAT THE THESIS PREPARED UNDER MY SUPERVISION

BY Abd el-Kerim Mohamed Ata

ENTITLED HYPER-ELASTIC PURE BENDING TREATED BY TRUE-STRESS

TRUE-STRAIN RELATIONSHIP

COMPLIES WITH THE UNIVERSITY REGULATIONS ON GRADUATION THESES

AND IS APPROVED BY ME AS FULFILLING THIS PART OF THE REQUIREMENTS

FOR THE DEGREE OF

Doctor of Philosophy

E. O. Stitz

PROFESSOR IN CHARGE OF THESIS

William R. B. Wiley

HEAD OF SCHOOL OR DEPARTMENT

October 11, 1950

TO THE LIBRARIAN:—

THIS THESIS IS NOT TO BE REGARDED AS CONFIDENTIAL.

E. O. Stitz

PROFESSOR IN CHARGE

**HYPER-ELASTIC PURE BENDING
TREATED BY TRUE-STRESS TRUE-STRAIN RELATIONSHIP**

A Thesis

Submitted to the Faculty

of

Purdue University

by

Abd el-Kerim Mohamed Ata

**In Partial Fulfillment of the
Requirements for the Degree**

of

Doctor of Philosophy

February, 1951

ProQuest Number:27714179

All rights reserved

INFORMATION TO ALL USERS

The quality of this reproduction is dependent upon the quality of the copy submitted.

In the unlikely event that the author did not send a complete manuscript and there are missing pages, these will be noted. Also, if material had to be removed, a note will indicate the deletion.



ProQuest 27714179

Published by ProQuest LLC (2019). Copyright of the Dissertation is held by the Author.

All rights reserved.

This work is protected against unauthorized copying under Title 17, United States Code
Microform Edition © ProQuest LLC.

ProQuest LLC.
789 East Eisenhower Parkway
P.O. Box 1346
Ann Arbor, MI 48106 – 1346

TABLE OF CONTENTS

| | Page |
|---|------|
| LIST OF FIGURES | v |
| LIST OF TABLES | ix |
| ACKNOWLEDGMENTS | x |
| ABSTRACT | xi |
| INTRODUCTION | 1 |
| CHAPTER I: STRESS STRAIN RELATIONSHIP | 3 |
| 1. Review of literature | 3 |
| 2. Discussion of the stress strain relationship | 6 |
| 3. Proposed stress strain relationship | 8 |
| 4. Stress-strain relationship in tension and compression for mild steel, stainless steel, aluminum, and magnesium . . . | 11 |
| A. Tests | 11 |
| B. Test Results | 17 |
| C. Sample of derivation of the stress strain relationship equation from test data | 29 |
| 5. The relation between the stress and the slope of the true stress true strain diagram for the tensile specimen at necking | 38 |
| A. Theoretical derivation | 38 |
| B. Experimental verification | 43 |
| C. Value of strain at necking for a tensile specimen . . | 46 |

| | Page |
|--|------|
| CHAPTER II: HYPER-ELASTIC PURE BENDING | 51 |
| 1. Introduction | 51 |
| 2. Review of literature | 52 |
| A. Solutions based on ordinary stress strain diagram | 55 |
| B. Solutions based on approximating the ordinary stress strain diagram | 58 |
| 3. Discussion of the previous methods | 64 |
| 4. New method for computing the moment of resistance in hyper-elastic state | 66 |
| Procedure of the Method: | 67 |
| A. Effect of lateral deformation on relation between stress and strain | 67 |
| B. Position of the neutral axis | 69 |
| C. The moment of resistance | 70 |
| 5. Application of the new method for various cross sections | 71 |
| A. Rectangular cross section | 71 |
| B. Square on edge cross section | 73 |
| C. Trapezoidal cross section | 74 |
| D. Circular cross section | 76 |
| 6. Theoretical application of the new method to beams of square cross sections in pure bending for different materials | 78 |
| A. Sample of computation for mild steel | 79 |
| B. Results | 86 |

| | Page |
|---|------|
| 7. Experimental verification of the new theory. | 87 |
| A. Test equipment and procedure | 87 |
| B. Test results | 108 |
| CHAPTER III: SPRING BACK CURVATURE | 131 |
| 1. Review of literature | 131 |
| 2. Discussion | 135 |
| 3. Proposed method | 135 |
| 4. Application of the new method to beams of square cross sections to different materials | 137 |
| CHAPTER IV: YIELD STRENGTH IN TENSION, COMPRESSION AND BENDING . | 141 |
| 1. Introduction | 141 |
| 2. Review of some previous tests | 141 |
| 3. Discussion of the factors tending to produce different results | 142 |
| 4. Elements to be considered in the experiments to obtain sound comparison between tension, compression and bending results | 145 |
| 5. Tests | 146 |
| A. Description | 146 |
| B. Results | 152 |
| 6. Comparison between yield strength in tension and com- pression and the beginning of yielding in bending . . . | 152 |
| CHAPTER V: SUMMARY AND SIGNIFICANCE OF THE RESULTS | 154 |
| BIBLIOGRAPHY | 161 |
| APPENDIX | 164 |
| 1. Tensile ordinary stress strain diagrams | 165 |

| | Page |
|--|------|
| 2. Compressive ordinary stress strain diagrams | 173 |
| 3. Tensile true-stress true-strain diagrams | 181 |
| 4. Compressive true-stress true-strain diagrams | 189 |
| 5. Tensile logarithmic true stress true strain diagrams . . | 197 |
| 6. Compressive logarithmic true stress true strain diagrams | 200 |
| 7. Clip gage | 203 |
| VITA | 211 |

LIST OF FIGURES

| | Page |
|---|------|
| 1. Ordinary Stress Strain Diagram in Tension | 4 |
| 2. True Stress True Strain Diagram | 4 |
| 3. Tensile or Compressive True Stress True Strain Relationship Diagram | 9 |
| 4. Riehle Testing Machine | 12 |
| 5. Position of Tension, Compression and Bending Specimens | 13 |
| 6. Tension and Compression Specimens | 13 |
| 7. Tension Specimens Showing Plastic Mounting Disc | 15 |
| 8. Compression Specimens | 15 |
| 9. Strain Indicator and Balancing Unit | 16 |
| 10. Caps for Centering Compression Specimens | 18 |
| 11. Ordinary Stress Strain Diagram for Mild Steel in Tension | 19 |
| 12. Ordinary Stress Strain Diagram for Mild Steel in Compression | 20 |
| 13. True Stress True Strain Diagram for Mild Steel in Tension | 23 |
| 14. True Stress True Strain Diagram for Mild Steel in Compression | 24 |
| 15. Mild Steel Fracture | 26 |
| 16. Stainless Steel Fracture | 26 |
| 17. Aluminum Fracture | 27 |
| 18. Aluminum Compressive Specimens | 27 |
| 19. Magnesium Tensile Fracture | 28 |
| 20. Magnesium Compressive Fracture | 28 |
| 21. Elastic Plastic Region of Mild Steel Tensile True Stress True Strain Diagram | 31 |

| | Page |
|--|------|
| 22. Logarithmic True Stress True Strain for Mild Steel in Tension | 32 |
| 23. Loads vs Cross Section Area for Mild Steel and Stainless Steel Tensile Specimens | 41 |
| 24. Loads vs Cross Section Area for Aluminum and Magnesium Tensile Specimens | 42 |
| 25. Beam under Pure Bending | 53 |
| 26. Stress and Strain Distribution over Cross Section in Pure Bending. | 54 |
| 27. Plastic Bending Factor K | 57 |
| 28. Moment of Resistance Using Approximate Stress Strain Distribution | 59 |
| 29. $\frac{M_t}{M_{y.p.}}$ and $\frac{\epsilon_t}{\epsilon_{y.p.}}$ Diagram for Different Cross Sections . . | 60 |
| 30. Modified Stress Strain Diagram Method for M_t | 62 |
| 31. Kuntze's Theory | 63 |
| 32. Theory Taking Care of Upper and Lower Yield Points | 63 |
| 33. Trapezoidal Distribution Method | 63 |
| 34. Cross Sections in Pure Bending | 72 |
| 35. σ_t vs M_t for Mild Steel Beam | 88 |
| 36. ϵ_t vs M_t for Mild Steel Beam | 89 |
| 37. σ_t vs Shift of the Neutral Axis for Mild Steel Beam | 90 |
| 38. ϵ_t vs ϵ_c for Mild Steel Beam | 91 |
| 39. σ_t vs M_t for Stainless Steel Beam | 92 |
| 40. ϵ_t vs M_t for Stainless Steel Beam | 93 |
| 41. σ_t vs Shift of the Neutral Axis for Stainless Steel Beam . . | 94 |
| 42. ϵ_t vs ϵ_c for Stainless Steel Beam | 95 |
| 43. σ_t vs M_t for Aluminum Beam | 96 |
| 44. ϵ_t vs M_t for Aluminum Beam | 97 |
| 45. σ_t vs Shift of the Neutral Axis for Aluminum Beam | 98 |
| 46. ϵ_t vs ϵ_c for Aluminum Beam | 99 |

| | Page |
|--|------|
| 47. σ_t vs M_t for Magnesium Beam | 100 |
| 48. ϵ_t vs M_t for Magnesium Beam | 101 |
| 49. σ_t vs Shift of the Neutral Axis for Magnesium Beam | 102 |
| 50. ϵ_t vs ϵ_c for Magnesium Beam | 103 |
| 51. Bending Apparatus | 104 |
| 52. Range Extender on the Strain Indicator | 107 |
| 53. Mild Steel Beam During Test | 109 |
| 54-A. Mild Steel Beam after Test | 110 |
| 54-B. Beams after Test | 111 |
| 55. Strain Distribution over Central Cross Section of Bent Mild Steel Beam | 113 |
| 56. Strain Distribution over Central Cross Section of Bent Stainless Steel Beam | 114 |
| 57. Strain Distribution over Central Cross Section of Bent Aluminum Beam | 115 |
| 58. Strain Distribution over Central Cross Section of Bent Magnesium Beam | 116 |
| 59. Poisson's Ratio Diagram for Mild Steel Bending Specimen | 117 |
| 60. Poisson's Ratio Diagram for Stainless Steel Bending Specimen | 118 |
| 61. Poisson's Ratio Diagram for Aluminum Bending Specimen | 119 |
| 62. Poisson's Ratio Diagram for Magnesium Bending Specimen | 120 |
| 63. Central Deflection Diagram for Mild Steel Bending Specimen | 123 |
| 64. Central Deflection Diagram for Stainless Steel Bending Specimen | 124 |
| 65. Central Deflection Diagram for Aluminum Bending Specimen | 125 |
| 66. Central Deflection Diagram for Magnesium Bending Specimen | 126 |
| 67. Central Extreme Fiber Strain Diagram for Mild Steel Bending Specimen | 127 |
| 68. Central Extreme Fiber Strain Diagram for Stainless Steel Bending Specimen | 128 |
| 69. Central Extreme Fiber Strain Diagram for Aluminum Bending Specimen. | 129 |

| | Page |
|---|---------|
| 70. Central Extreme Fiber Strain Diagram for Magnesium Bending Specimen | 130 |
| 71. Beam Bent over Elastic Limit | 132 |
| 72. Elastic Behavior Diagram of Unloading Above Elastic Limit. . | 132 |
| 73. R_2 vs M_t Diagram | 139 |
| 74. R_1 vs R_2 Diagram | 140 |
| 75. Fosterite Beam Before Bending | 141 |
| 76. Fosterite Beam After Bending | 148 |
| 77. Photoelastic Testing Set Up | 149 |
| 78. Fringe Pattern of Fosterite Beam | 150 |
| 79. Fringe Order Distribution over Central Section of Fosterite Beam | 151 |
| 80. Comparison Between the New and the Previous Methods | 160 |
| 81-87. Ordinary Tensile Stress Strain Diagrams | 166-172 |
| 88-94. Ordinary Compressive Stress Strain Diagrams | 174-180 |
| 95-101. Tensile True Stress True Strain Diagrams | 182-188 |
| 102-108. Compressive True Stress True Strain Diagrams | 190-196 |
| 109-112. Tensile Logarithmic True Stress True Strain Diagrams. . | 198-199 |
| 113-116. Compressive Logarithmic True Stress True Strain Diagrams | 201-202 |
| 117. Clip Gage | 206 |
| 118. Calibration of Clip Gage by Micrometer | 207 |
| 119. Calibration of Clip Gage by SR-4 Gage | 207 |
| 120. Micrometer Deformations vs Clip Gage Strains | 208 |
| 121. SR-4 Strains vs Clip Gage Strains for 1" x 1" Mild Steel Beam | 209 |
| 122. SR-4 Strains vs Clip Gage Strains for 1 31/32" x 1 31/32" Mild Steel Beam | 210 |

LIST OF TABLES

| | Page |
|---|------|
| 1. Stress Strain Relationship | 5 |
| 2. Percentage of Increase of Yield Point in Outer and Inner Specimens | 22 |
| 3. Stress Strain Relations for Mild Steel | 34 |
| 4. Stress Strain Relations for Stainless Steel | 35 |
| 5. Stress Strain Relations for Aluminum | 36 |
| 6. Stress Strain Relations for Magnesium | 37 |
| 7. Slope and Stress of True Stress True Strain Diagram at Necking | 44 |
| 8. Values of Stress at Necking for Tensile Specimens | 45 |
| 9. Strain and Strain Hardening Exponent at Necking | 49 |
| 10. Stress, Strain, Slope, Strain Hardening Exponent of True Stress True Strain Diagram of Compression Specimen at Transition from Elastic Plastic to Plastic State | 50 |
| 11. Comparison between Tension and Compression Yield Strength and the Beginning of Yielding in Bending | 153 |

ACKNOWLEDGMENT

The writer wishes to express his thanks and sincere gratitude to Dr. H. Shweizer and Dr. R. G. Sturm for their suggestions and encouragement. The writer is especially indebted to Professor E. O. Stitz for his valuable advice, tireless help, and inspiration he contributed during the course of the work reported in this thesis. He also thanks Professors L. T. Wyly, R. Hull and N. Little for their advice. It is a pleasure to acknowledge the help given by Graver Tank and Manufacturing Co., Joslyn Manufacturing Company, Aluminum Company of America, and Dow Chemical Company for furnishing the tested materials. It is of importance to mention the assistance given to the writer by the Purdue Engineering Experiment Station for furnishing the strain gages and the School of Civil Engineering and Engineering Mechanics for financing the machining of the apparatus and specimens. The writer wishes to thank also M. E. Beck for the machining work, the staff of the Purdue Materials Testing Laboratory for facilities offered to conduct the tests and Dr. A. C. Ruge for furnishing the 17-4 post yield gages. The writer is indebted to Professor C. W. Lawton for his help with photography.

September, 1950

A. K. Ata

ABSTRACT

The object of this investigation is to treat the problem of hyper-elastic pure bending. The approximate assumptions used in previous solutions are avoided. The ordinary stress strain relationship usually used in such a case is not applicable in the hyper-elastic state and therefore the true stress true strain relationship was tried. Incidentally some relations governing the stress, strain, slope at necking and the strain hardening exponent for the true stress true strain diagram in tension were obtained. These relations, derived mathematically and verified experimentally, are based on different assumptions from those given in the literature. The treatment of hyper-elastic pure bending by the new theory was carried out for beams of square, square on edge, circular, and trapezoidal cross sections. As an application, analytical computations followed by experimental tests were made for beams of square cross sections of mild steel, stainless steel, aluminum and magnesium. The theoretical values and the experimental results show close agreement for all the materials, which proves the generality of the method. To show the use of this new hyper-elastic pure bending method, a treatment for spring back curvature was developed; this can give the value of the required moment and the die radius for any required radius of a bent beam. As an application for this forming operation, computation resulting in handy graphs were made for beams of square cross sections of mild steel, stainless steel, aluminum and magnesium. Moreover, since it was necessary to obtain the data of

tension, compression and bending tests for all the tested materials, a comparison between tension and compression yield strength and the bending stress at beginning of yielding could be made. This shows that they are all practically equal to each other. This result--obtained by the use of several metals--disproves the observation found by some investigators that the beginning of yielding in bending is 40% higher than the tensile yield strength.

HYPER-ELASTIC PURE BENDING TREATED BY THE
TRUE-STRESS TRUE-STRAIN RELATIONSHIP

INTRODUCTION

Hyper-elastic pure bending is the pure bending action above the proportional limit of the material i.e. in the elastic-plastic and plastic states. The idea of treating this problem came to the writer while conducting bending tests on mild steel beams in 1947 at the materials laboratory of Fouad 1st University, Giza, Egypt. The results of these tests showed marked increase in the value of the moment of resistance above that given by the methods developed in the literature. The experiments were carried out carefully and repeated, and still the same results were obtained. It seemed then that the basis and assumptions used in the literature are different from the actual action, causing this decrease in the computed moment. These methods were worked on the basis of using the ordinary stress-strain relationship. Since this is based on the original area and original strain, then it does not agree with the action in the hyper-elastic state. Which relationship may we try?

The object of this investigation is to apply the true stress true strain relationship to the problem of hyper-elastic pure bending and to use the relationship in such a form that simplifies the analytical computations. The treatment is based on the assumptions listed in detail in Chapter II. The approximate assumptions used in other treatments were avoided.

The detailed work including some interesting new aspects of the true-stress true-strain relations, analytical computations for different cross sections and experimental verification of the new theory for square cross sections of four different metals, application to forming of bent beams, and a comparison between yielding in tension, compression and bending are treated in the following chapters.

CHAPTER I

Stress-Strain Relationship

1. Review of Literature.

The stress-strain relations of a material in tension and compression are the main and essential requirements to define the behavior of this material if subjected to static loads. Since the engineer has continuously striven to improve design and increase the efficiency of various types of engineering structures and operations, the stress-strain diagrams in tension and compression have gained and still hold the interest of many investigators in the field of materials. In 1680, Hooke made the statement due to his observations that the elongation is proportional to the load, "Ut tensio sic vis" (as the extension, so is the force). Engineers still use the more general form that the stress is proportional to the strain in the elastic state of stress.^{1*} Hooke, therefore, began the study of the stress-strain relationship and other investigators followed the same path.^{2,3,4,5} Their results are equations based on good fit of experimental data of ordinary stress-strain diagrams of tension and compression tests (Fig. 1) where the stress = $\frac{\text{Applied Load}}{\text{Original cross sectional area}}$

and the corresponding strain is = $\frac{\text{Measured length} - \text{original length}}{\text{Original length}}$.

These equations give stress in terms of strains or vice versa, having parameters which differ for different materials as obtained by fitting the experimental data. The curve represented by a given equation goes through the origin and has a slope there equal to the modulus of elasticity. A review of some of these relationships between stress and strain in tension or compression is given in Table 1.

* Superscript numbers refer to the Bibliography, page 161.

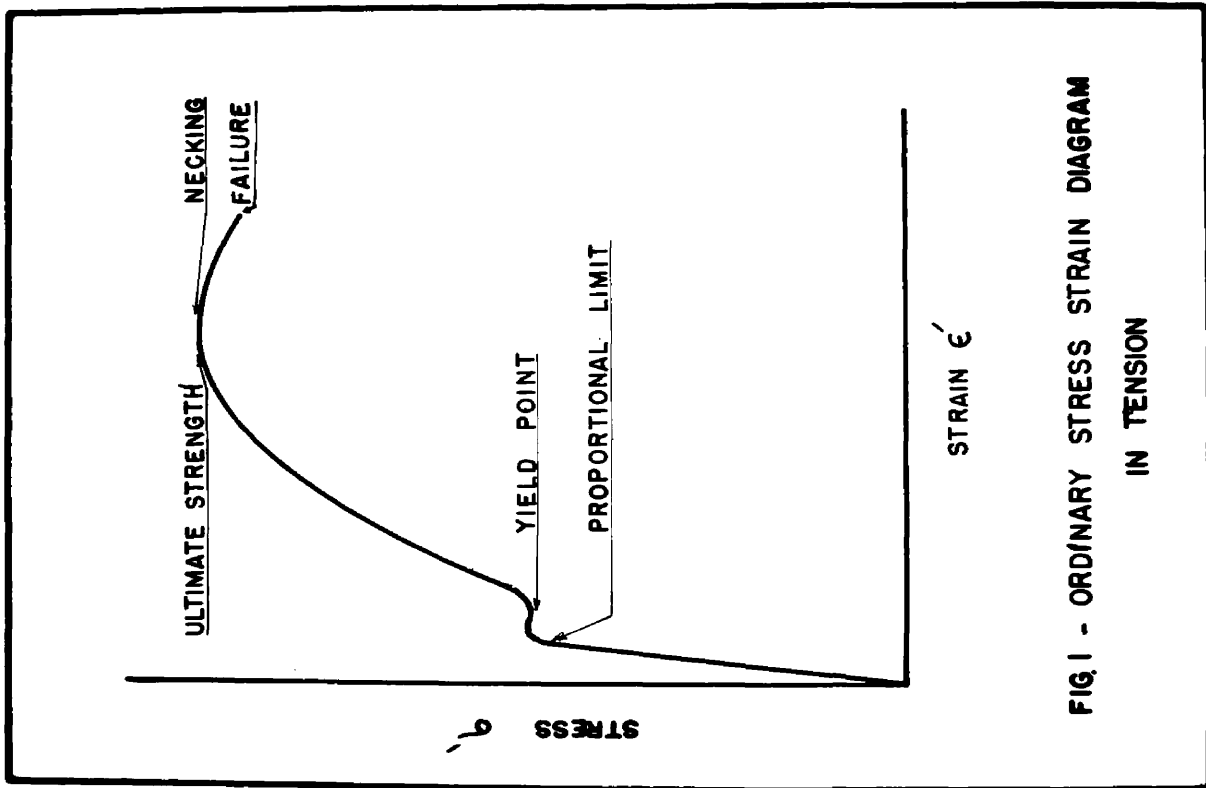


FIG. 1 - ORDINARY STRESS STRAIN DIAGRAM
IN TENSION

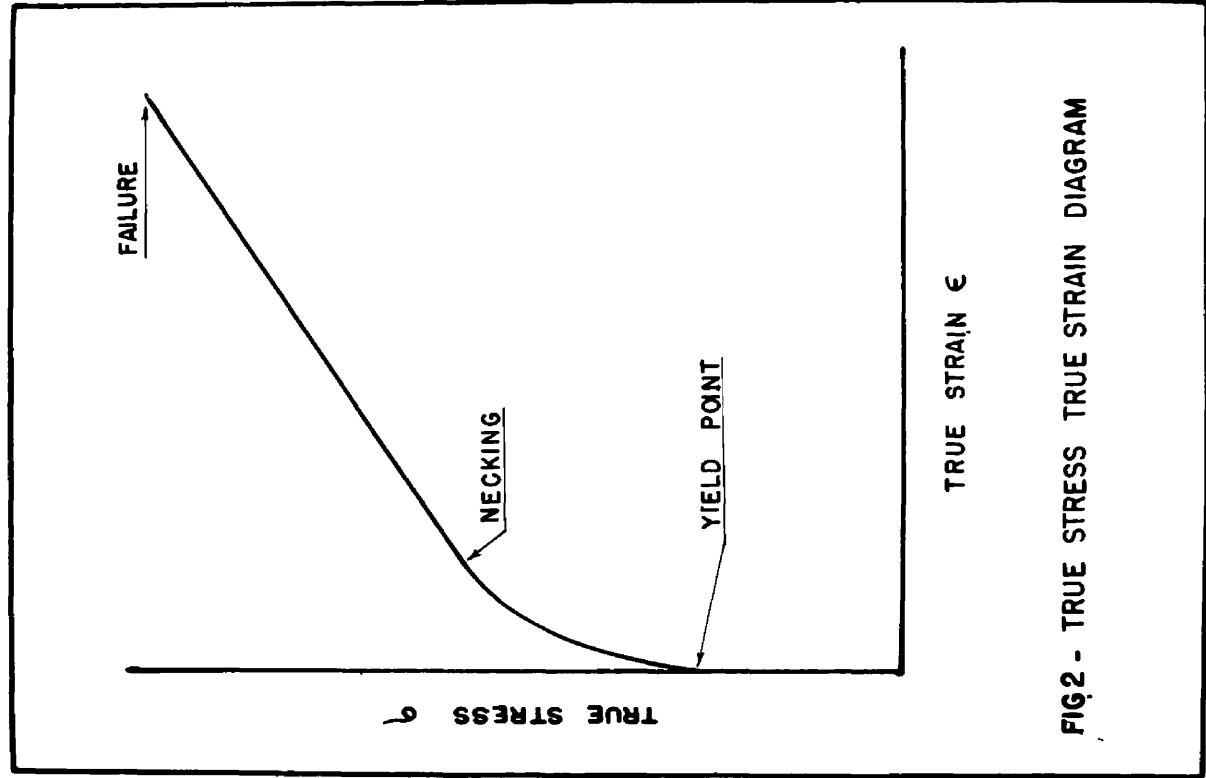


FIG. 2 - TRUE STRESS TRUE STRAIN DIAGRAM

Table 1
Stress-Strain Relationships

| Name of Investigator | Year | Stress-Strain Relationship |
|----------------------|------|--|
| Hooke | 1680 | $\epsilon' = S$ |
| Bulffingeri | 1729 | $\epsilon' = K S^n$ |
| Riccati | 1731 | $S = K e^{-\frac{1}{\epsilon'}}$ $S = (\frac{1}{a})(e^{\frac{a\epsilon'}{1+\epsilon'}} - 1)$ |
| Gerstner | 1831 | $S = \epsilon' + b\epsilon'^2$ |
| Poncelet | 1841 | $\epsilon' = S [1 + \beta(e^{\alpha S} - 1)]$ |
| Wertheim | 1847 | $\epsilon'^2 = \alpha S + \beta S^2$ |
| Hodgkinson | 1849 | $S = \epsilon' + b\epsilon'^2 + c\epsilon'^3 + d\epsilon'^4$ |
| Cox | 1851 | $\epsilon' = S / (1 + \alpha S)$ $\epsilon' = S + \beta S^2 + \gamma S^3$ $S = \epsilon' + b\epsilon'^2 + c\epsilon'^3$ |
| Imbert | 1880 | $\epsilon' = (\frac{1}{\alpha})(e^{\alpha S} - 1)$ |
| Hartig | 1893 | $S = (\frac{1}{a})(e^{a\epsilon'} - 1)$ $S = (\frac{\epsilon'}{1-\epsilon'}) \cdot e^{a\epsilon'}$ |
| Schula | 1898 | $S = a\epsilon'^m + b\epsilon'^2$ |
| Prager | 1939 | $S = a\epsilon' + b \tanh[\frac{1-a}{b}] \cdot \epsilon'$ |
| Holmquist & Nadai | 1939 | $\epsilon' = S$ $\epsilon' = S + K(S - S_p) \quad S \gg S_p$ $\epsilon' = \alpha S + \beta [(e)^{\frac{1-\alpha}{\beta} \cdot S} - 1]$ |
| Ramberg & Osgood | 1943 | $\epsilon' = S + K S^n$ |
| Rao & Leggett | 1946 | $\epsilon' = S + \beta (\cosh \alpha S - 1)$ |

* a, b, c, d, α and β are constants determined experimentally for each material.

$$\epsilon' = \text{ordinary strain} \quad S = \frac{\sigma'}{E}$$

$$\sigma = \text{ordinary stress}$$

E = Modulus of elasticity

In 1944, MacGregor^{7,8} showed that, from yielding of the material in tension up to its failure, the true-stress true-strain diagram shown in Fig. 2 is the diagram which best describes the relationship between stress and strain. The true stress = $\frac{P}{A} = \frac{\text{Load}}{\text{Cross Sec. Area at time of this loading}}$

$$\text{and the true strain} = \sum \frac{\Delta L}{L_i} = \int_{L_0}^L \frac{dL}{L} = \log \frac{L}{L_0} .$$

where L_0 = original length, L = length at time of loading. It is considered that the deformations happen in the plastic region without change in volume, i.e. Poisson's ratio = 0.5. $A_0 L_0 = A \cdot L$

A_0 = original cross sectional area and A = Measured area at time of loading.

$$\text{Therefore} \quad \frac{A_0}{A} = \frac{L}{L_0} .$$

$$\begin{aligned} \text{Then true strain} &= \log \frac{L}{L_0} = \log \frac{A_0}{A} \\ &= 2 \log \frac{D_0}{D} \quad \text{for a circular cross section} \end{aligned}$$

where D_0 = original diameter, D = diameter at time of loading .

Hollomon⁸ stated that the true-stress true-strain relationship, from yield point up to the maximum load just before necking, is in the form of a curve represented by $\sigma = a \cdot e^n$ and this relationship from maximum load (necking) up to failure is a straight line tangent to the previously mentioned curve.

2. Discussion of the Stress-Strain Relationship.

Although most of the previously mentioned equations of stress and strain based on the ordinary stress-strain diagram are not in an easy,

simple form, their use has also been limited by the mathematical difficulties encountered in applying them to specific engineering problems. Besides, these equations tend to show discrepancies from the yield point of the material up to its failure, since they are based on the original cross section and original gage length, both of which change materially in this region. They can be applied to engineering problems in the elastic region only and their application beyond this region is for their historical significance. Consequently the true stress true strain diagram can correctly fill this gap and can be applied in the hyper-elastic region since it is based on the true stress and the true strain.

Then in what form will be the equation which describes the behavior of any material? It is known from experiments and the literature⁹ that a material under tension or compression till failure passes thru the elastic, elastic plastic, and plastic states. The elastic state is the case where the fibers of the material elongate or contract and can return to their original state upon removal of the load. The elastic-plastic state is the case where the material is changed from elastic to plastic, its grains break and slide in different directions. This is an unstable process¹⁰ and the material cannot regain its original shape upon removal of the load. The plastic state is where the crystals resulting from grain fracture slide in one direction due to the dislocation of the atoms.^{9,11,12} If the load is removed, the material possesses distinct deformation.

Therefore the equation of the relationship of stress and strain for a given material should be composed of three equations, each describing

its state--either elastic, elastic plastic, or plastic. In this way the characteristic of the material is accurately defined all over its range of stress up to failure.

3. Proposed Stress-Strain Relationship.

The relationship mentioned above generally will be a straight line equation for the elastic region based on the original stress diagram data, an equation of a curve or equations of a curve and straight line for the elastic plastic region based on the true-stress true-strain diagram, and an equation of a straight line for the plastic region based on the true-stress true-strain diagram as shown in Fig. 3.

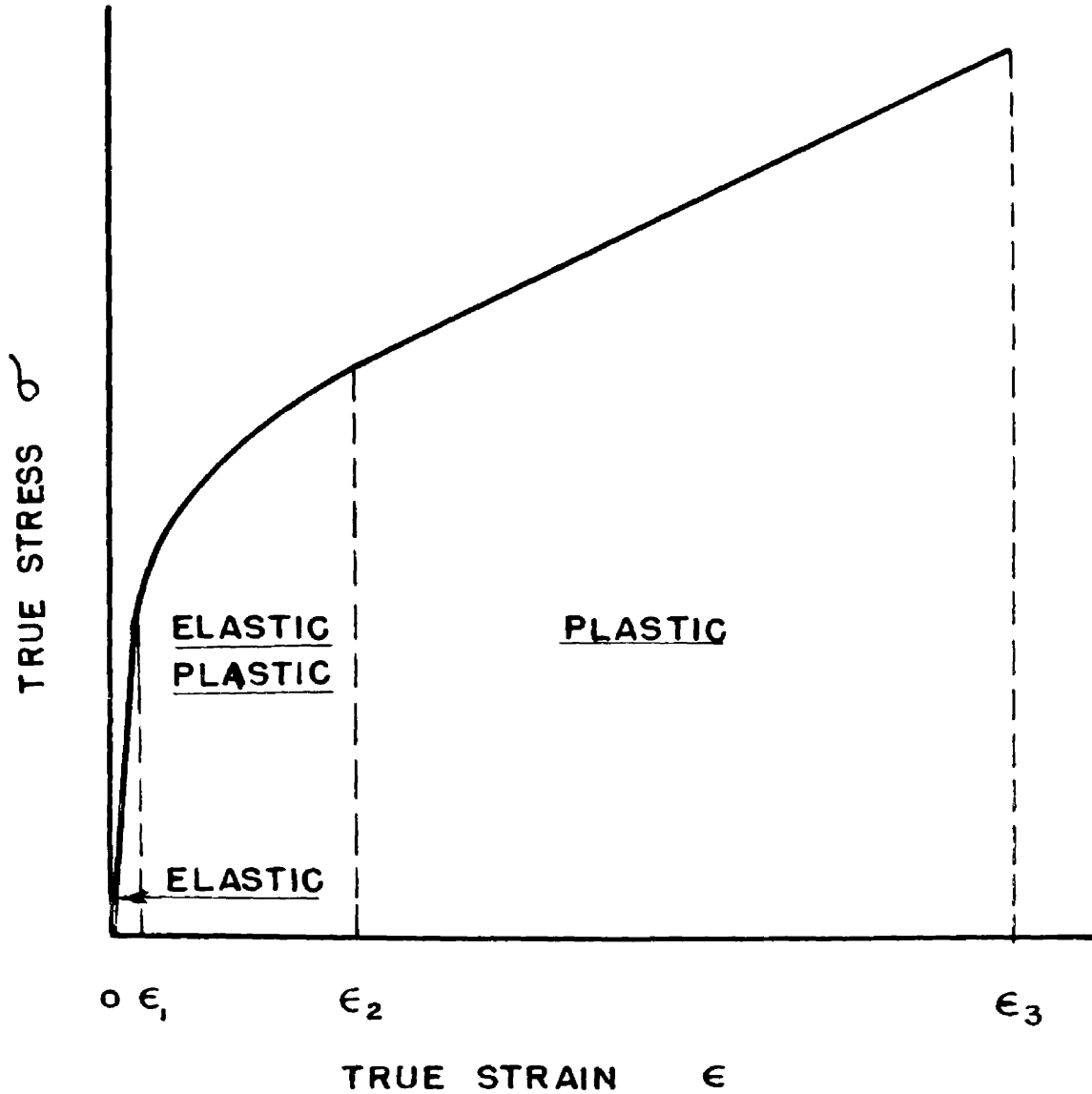
Since we have two variables, stress σ and strain ϵ , what kind of equation should we formulate: stress in terms of strain or strain in terms of stress? The answer is the kind which is of practical use. Since in most engineering problems we are always interested in the load required for a certain structural part and since the strains at the points of transition from elastic to elastic plastic and from elastic plastic to plastic are a characteristic of each material whether for tension or compression (as proved experimentally later), then the stress in terms of the strain is the actual practical type. The proposed new relationship of stress and strain will be:

$$\sigma = \left[a \epsilon \right]_{\epsilon=0}^{\epsilon=\epsilon_1} + \left[b \epsilon^c \right]_{\epsilon=\epsilon_1}^{\epsilon=\epsilon_2} + \left[K \epsilon + m \right]_{\epsilon=\epsilon_2}^{\epsilon=\epsilon_3} \quad (1)$$

as shown in Fig. 3, where:

σ = true stress ϵ = true strain

ϵ_1 = strain at proportional limit which is chosen as the end of the elastic region.



$$\sigma = [a\epsilon]_0^{\epsilon_1} + [b\epsilon^c]_{\epsilon_1}^{\epsilon_2} + [K\epsilon + m]_{\epsilon_2}^{\epsilon_3}$$

FIG. 3- TENSILE OR COMPRESSIVE TRUE STRESS
TRUE STRAIN RELATIONSHIP DIAGRAM

ϵ_2 = strain at the transition from elastic plastic to plastic state

ϵ_3 = strain in the plastic region up to failure .

ϵ_1 and ϵ_2 are to be obtained for each material and they are constant for this material as a part of its character.

a, b, c, k and m are constants determined from the good experimental fit - a to the ordinary stress-strain diagram, and b, c, k and m to the true-stress true-strain diagram. These coefficients are different in tension from compression.

It may be noted that we cannot use the yield point or yield strength to represent the end of elastic region since we lose proportionality between stress and strain when we leave the proportional limit; besides the yield point is affected by several factors and may be subjected to slight errors due to the testing machines, their factors and speeds, and to the investigators too. Moreover the stress strain diagram from the proportional limit to yield point is a curve which indicates that fracture of some grains takes place.

The above proposed equation is in a simple form to describe the behavior of the material. It is also general since it is adaptable to many different materials by varying the value of its parameters a, b, c, k, and m and introducing the corresponding values of ϵ_1 and ϵ_2 for the material. It is also easy to apply, especially in case of hyper-elastic bending and column analysis where it leads to integrals that can be expressed in a closed form.

4. Stress-Strain Relationship in Tension and Compression for Mild Steel, Stainless Steel, Aluminum and Magnesium.

In order to show the deduced equation in its practical form and the ease of comparison between the behavior of different materials in various states of stresses and between the behavior of different specimens from the same cross section of the same material, tension and compression tests for mild steel, stainless steel, aluminum, and magnesium were conducted. Ordinary stress strain diagrams up to the yielding region and true-stress true-strain diagrams were obtained. Then the coefficients required in the previously proposed equation were deduced from the data of these stress-strain diagrams.

A. Tests

The test equipment and procedure are as follows:

- a. Machine. The machine used in the tension and compression experiments is a Riehle machine. It is a lever type, well calibrated, having a capacity of 50,000# and min. reading of 5#. It is shown in Fig. 4.
- b. Specimens. A bar 8 ft. long and approximately 2" x 2" in cross section was sawed into three pieces each 32" long. The central piece was used to prepare the tension and the compression specimens. Two tension specimens were machined from this cross section 2" x 2" one number 3 from inside and the other number 4 from the outside of the cross section. Similarly two compression specimens number 1 from the inside of the cross section and number 2 from the outside as shown in Fig. 5. The tension specimen was of a standard

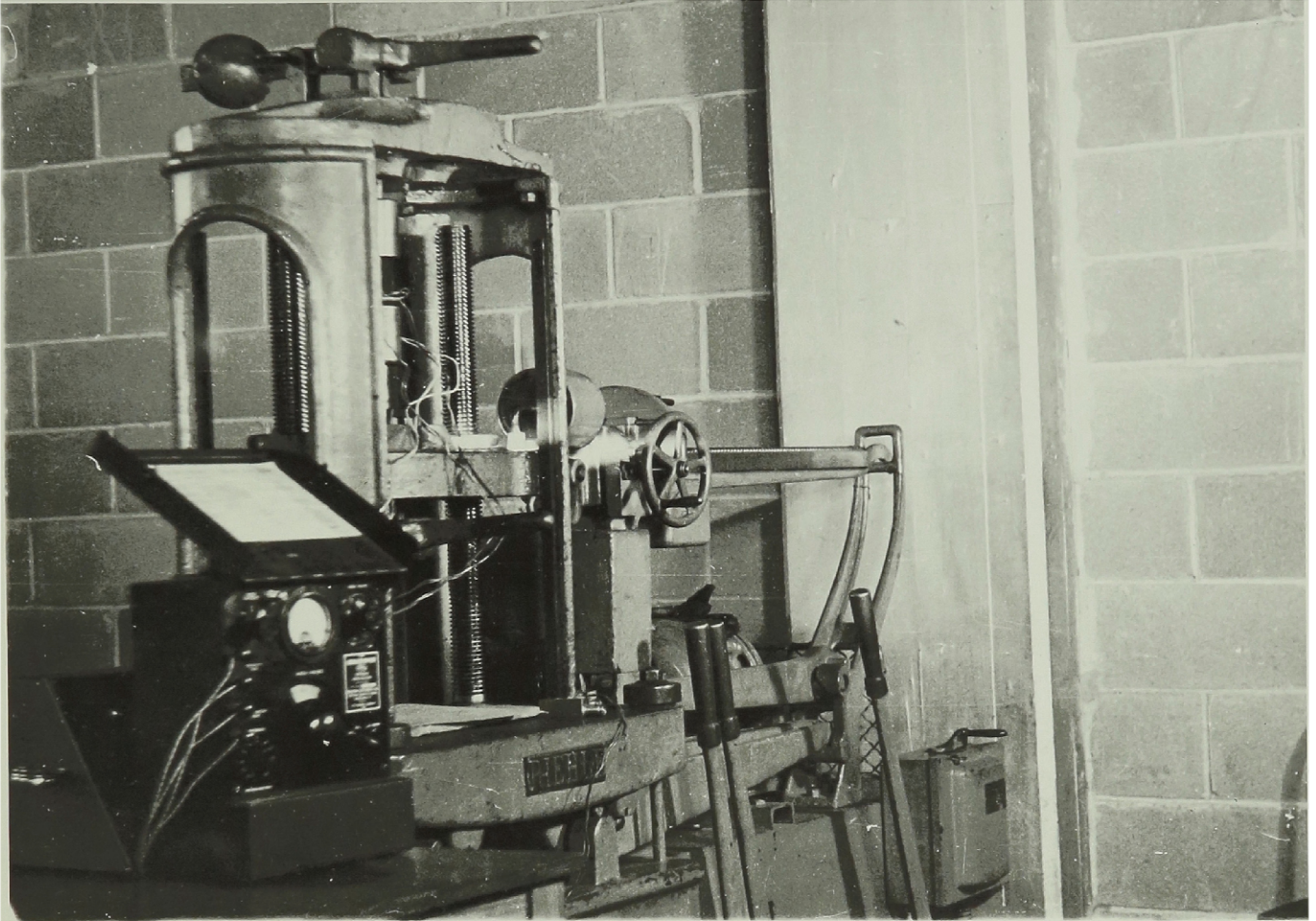


FIG. 4 - RIEHLE TESTING MACHINE

size, 0.505" diameter and 2" gage length. The compression specimen was also of the standard size 0.798" diameter and 2 3/8" long. These specimens are shown in Fig. 6.

c. Materials. The available materials, which were used in the tests, are hot rolled mild steel, stainless steel, 1/4 S-F extruded aluminum, and ZK60A extruded magnesium which was aged after extrusion.

d. Strain Gages. SR-4 electrical strain gages, type A-7, 1/4" gage length, resistance 120 ohms, and gage factors 1.96 and 1.97 were used to measure the strains up to the yielding region. Four gages were placed longitudinally on the circumference of the central section of each tension and compression specimen to measure the strain at four different points on the circumference of the cross section. The lead wires for the gages were mounted on a circular plastic disc made in two parts. The two parts forming the disc were cemented on the tension or compression using Duco household cement. The arrangement of the gages on the tension and compression specimens and the plastic discs for mounting the lead wires are shown in Figures 7 and 8.

e. Strain Indicator. A Baldwin type K strain indicator was used. It has a range up to 30,000 micro-inches and can be read to 10 micro inches. A micro inch and its multiples up to 10 can be approximated by the eye. It is shown with a Baldwin Bridge balancing unit in Fig. 9.

f. Micrometers. The diameter of the tension specimen was measured throughout the plastic region with a micrometer having pointed anvils. It could be read up to 0.001 in. and the readings can be approximated to 0.0005 in. For the compression specimens, a micrometer having flat ends which could be read to 0.0001 in. was used.

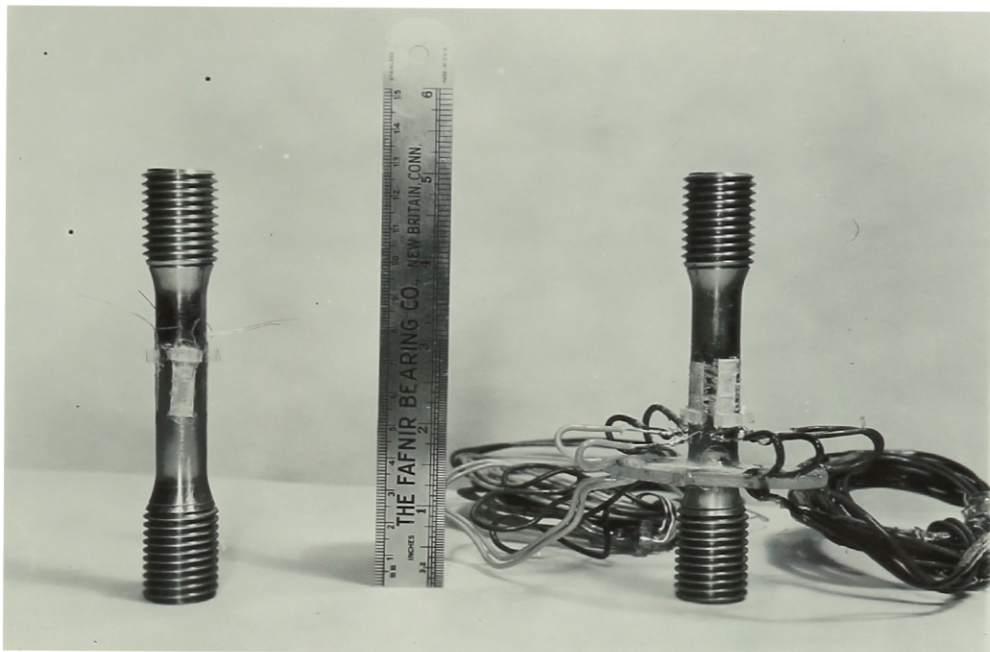


FIG. 7 - TENSILE SPECIMENS

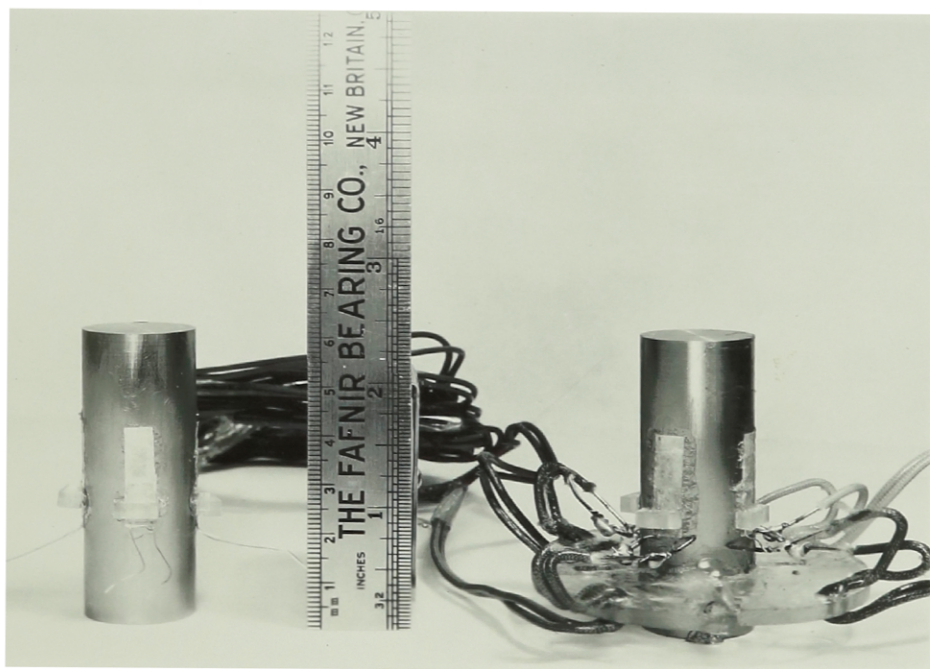


FIG. 8 - COMPRESSIVE SPECIMENS

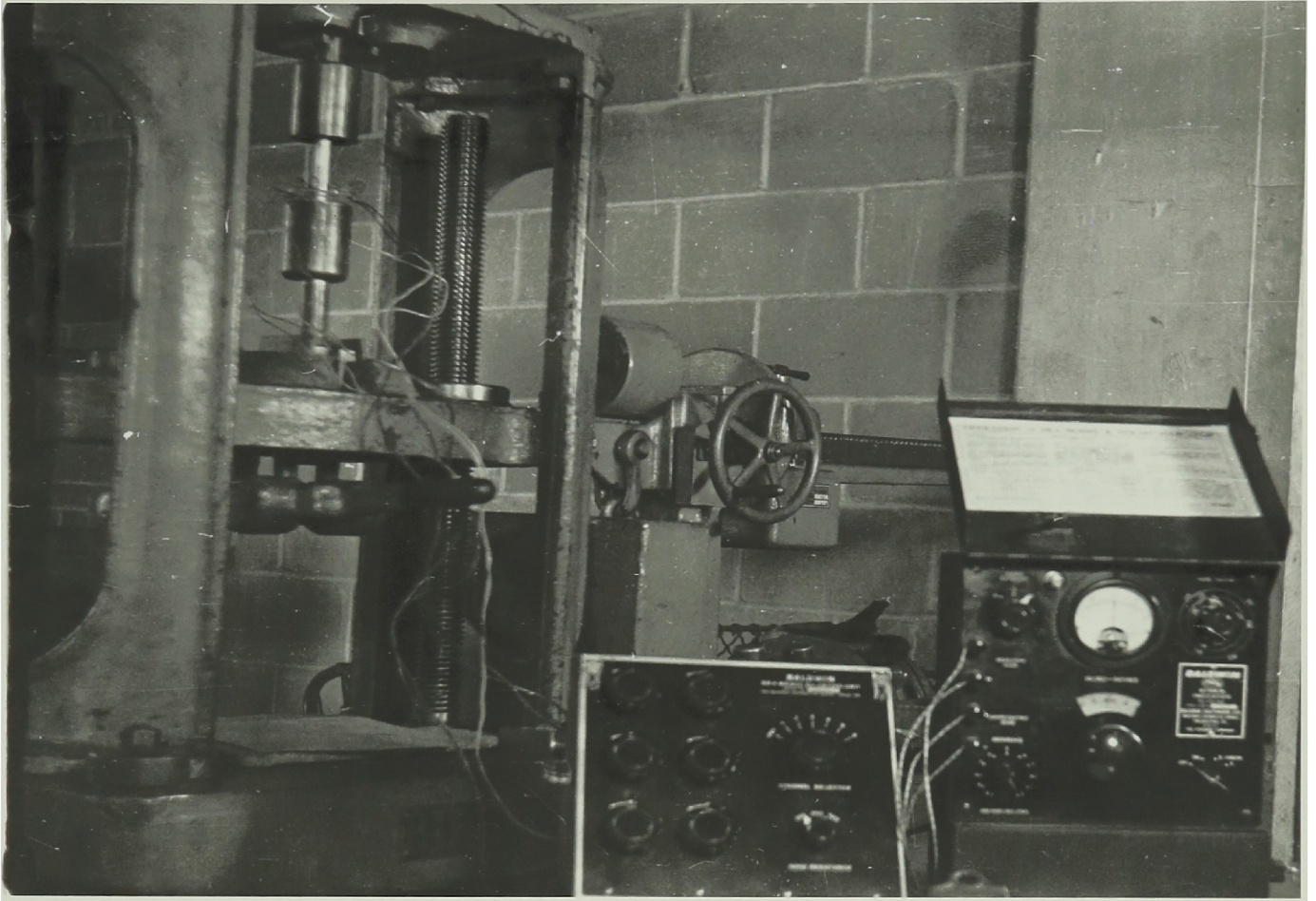


FIG. 9 - STRAIN INDICATOR & BALANCING UNIT

g. Tests procedure. The tension specimen was attached to the grips of the machine; then an initial small load was applied to the specimen to hold it in position. An initial load within the elastic limit of the material was applied cyclically at least four times to stabilize the SR-4 strain gages and to minimize the zero shift. Then the zero reading of each gage was recorded and also the initial diameter of the specimen. The load was applied in increments and each time the readings of the four SR-4 gages, the measurement of the diameter of the specimen, and the machine load were recorded. When the yielding region was passed and the range of the strain indicator exceeded, machine load and the diameter of the specimen only were recorded till the specimen failed.

The same procedure was applied to the compression test, except in this case recording of data was stopped when the full capacity of the machine, 50,000#, was reached. In this test two caps as shown in Fig. 10 were used to assure the centering of the load on the specimen.

The above mentioned tests were run using the slow speed of the testing machine. Also all the readings were taken by the writer only.

B. Test Results

a. Ordinary Stress-Strain Diagrams. These diagrams are plotted using the readings of the four SR-4 gages and the machine load and the original cross sectional area. From these plots shown in Figures 11 and 12 as a sample, and Figures 81 to 94 in the Appendix, we conclude:

1. Yield strength for the specimen machined from the outer part of the cross section is higher than the one for the inner part of

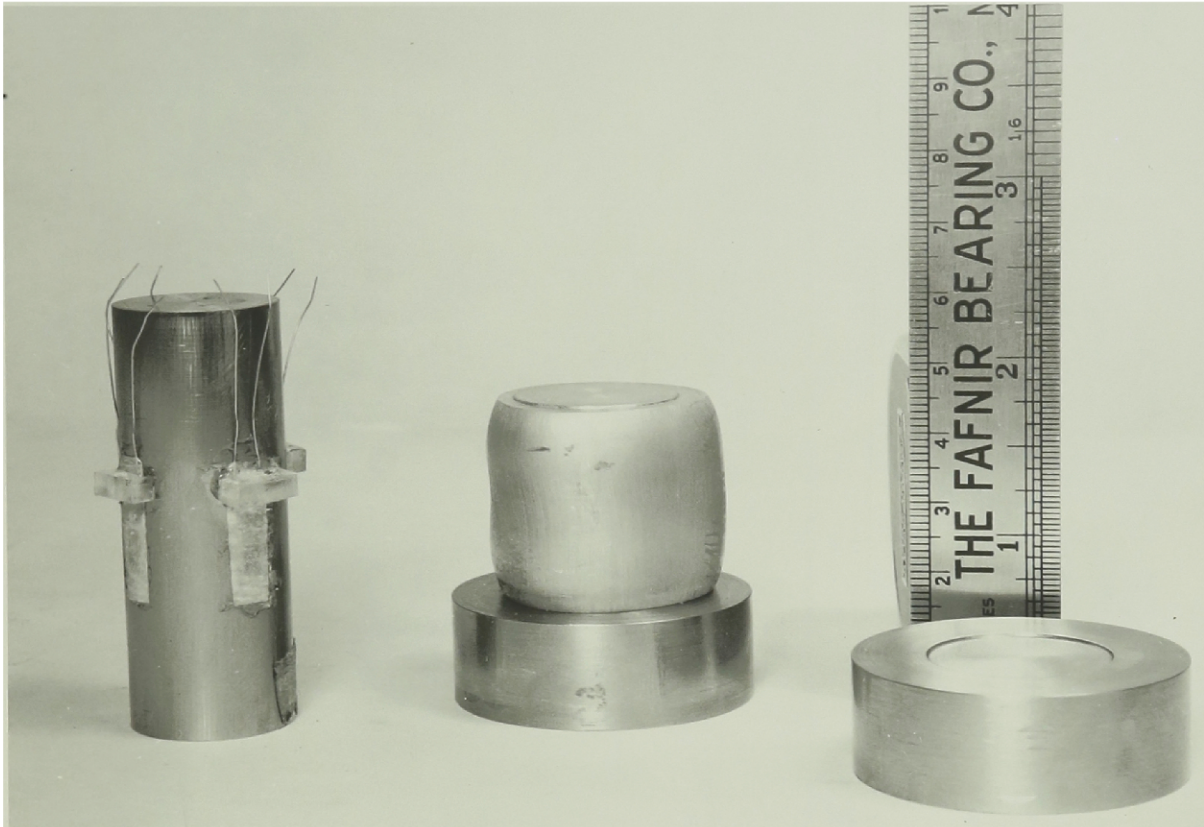


FIG. 10 - CAPS FOR COMPRESSION SPECIMENS

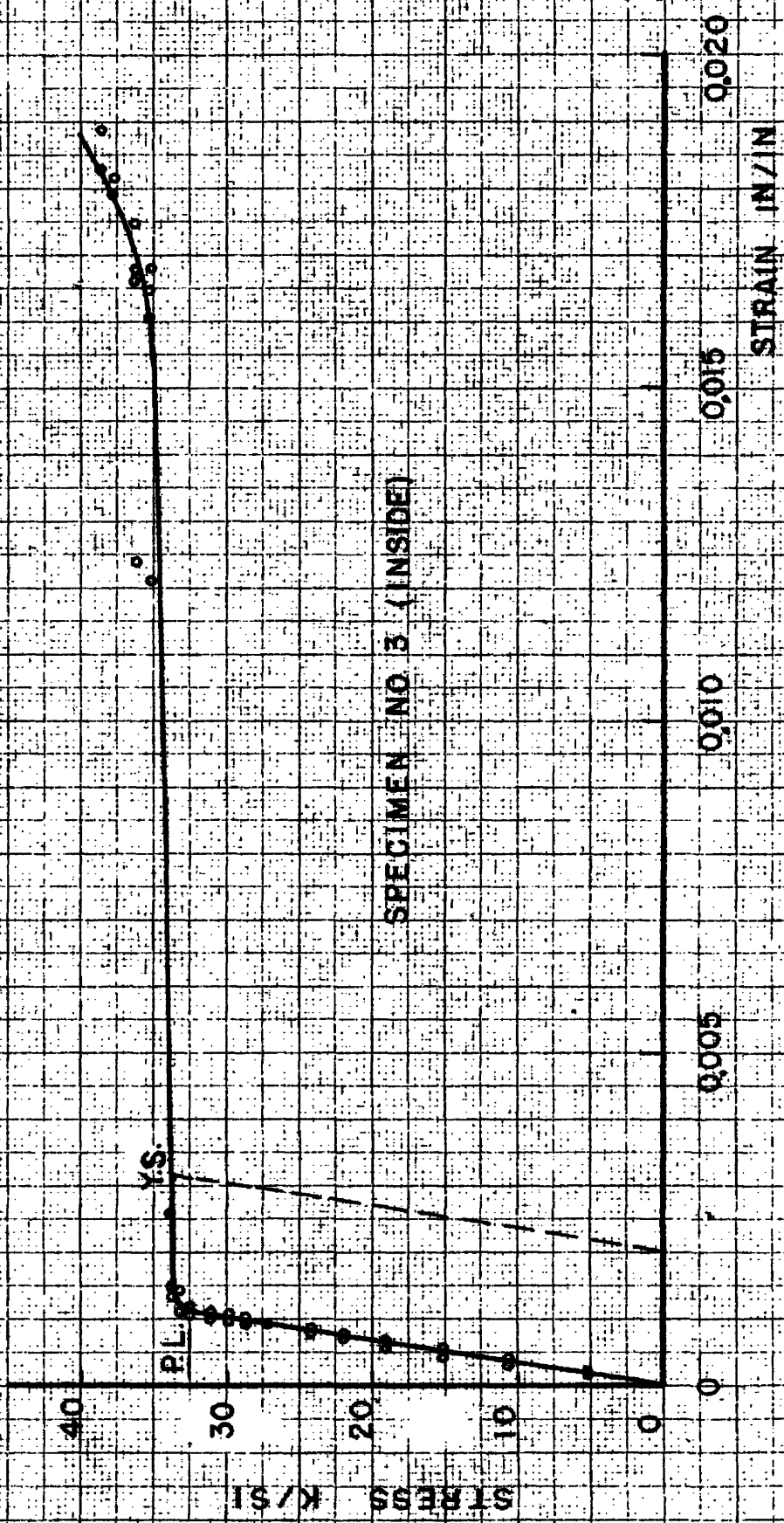


FIG. 11 - ORDINARY STRESS STRAIN DIAGRAM
FOR MILD STEEL IN TENSION

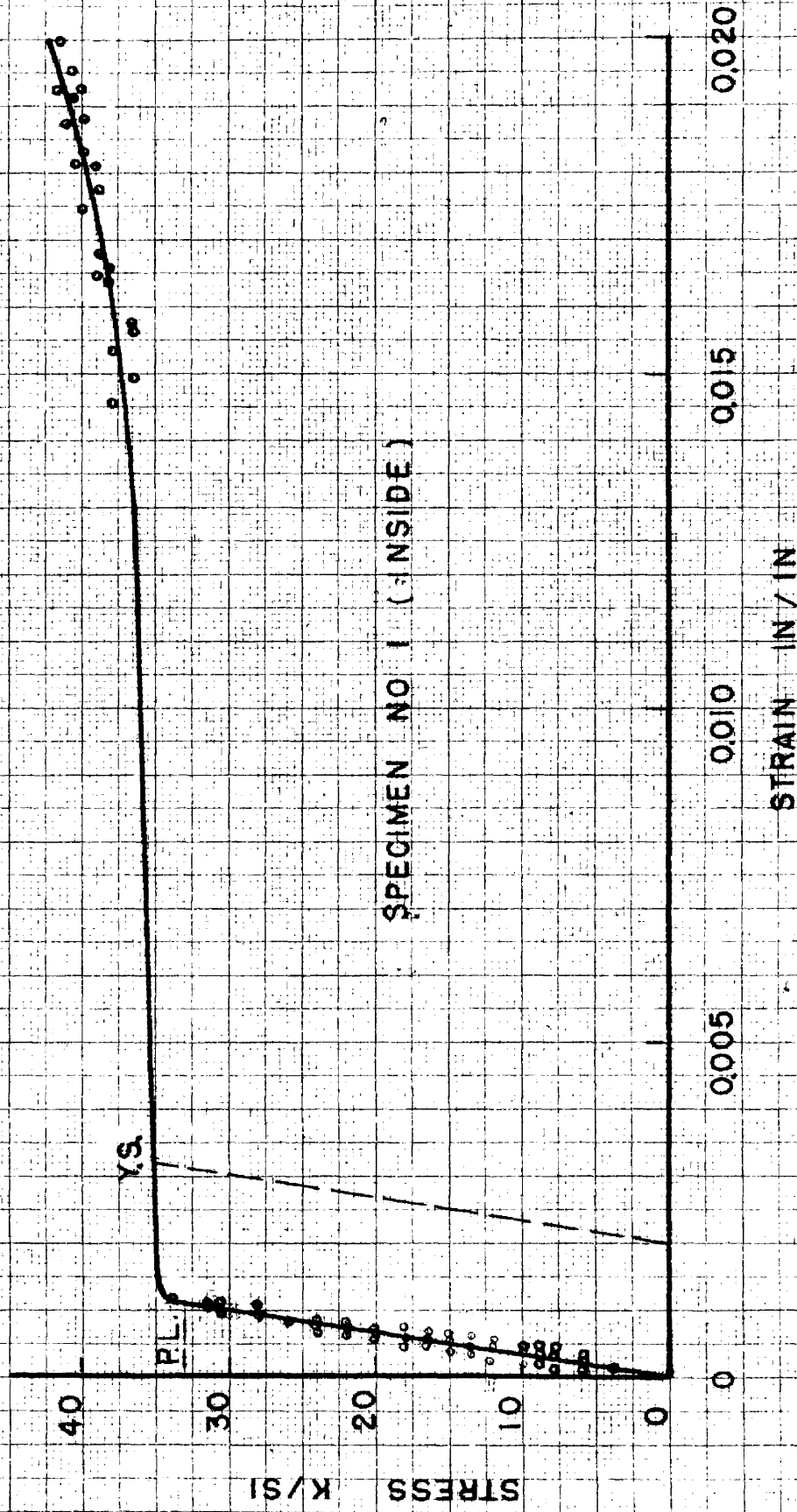


FIG. 12 ORDINARY STRESS STRAIN DIAGRAM FOR MILD STEEL IN COMPRESSION

the cross section for mild steel and stainless steel and the yield strength of the inner specimen is higher than the outer one for aluminum and is equal to the outer in magnesium. This result is the same for both tension and compression tests. The percentage of increase is shown in Table 2.

2. The strain ϵ_1 for the proportional limit for each material is the same for compression as for tension.
3. The modulus of elasticity in tension and compression is practically the same for each material.

b. True stress true strain diagrams. These diagrams are plotted

using the true stress =
$$\frac{\text{Machine load}}{\text{Cross sec. area based on diam. measured at this load}}$$

and the true strain = $2 \log \frac{D_0}{D}$ for tension test and $2 \log \frac{D}{D_0}$

for compression tests where D_0 = original diameter and D = diameter measured at the corresponding load. These curves are shown in Figures 13 and 14 for mild steel, as a sample, and the rest in Figures 95 to 108 in the Appendix. From these diagrams we conclude:

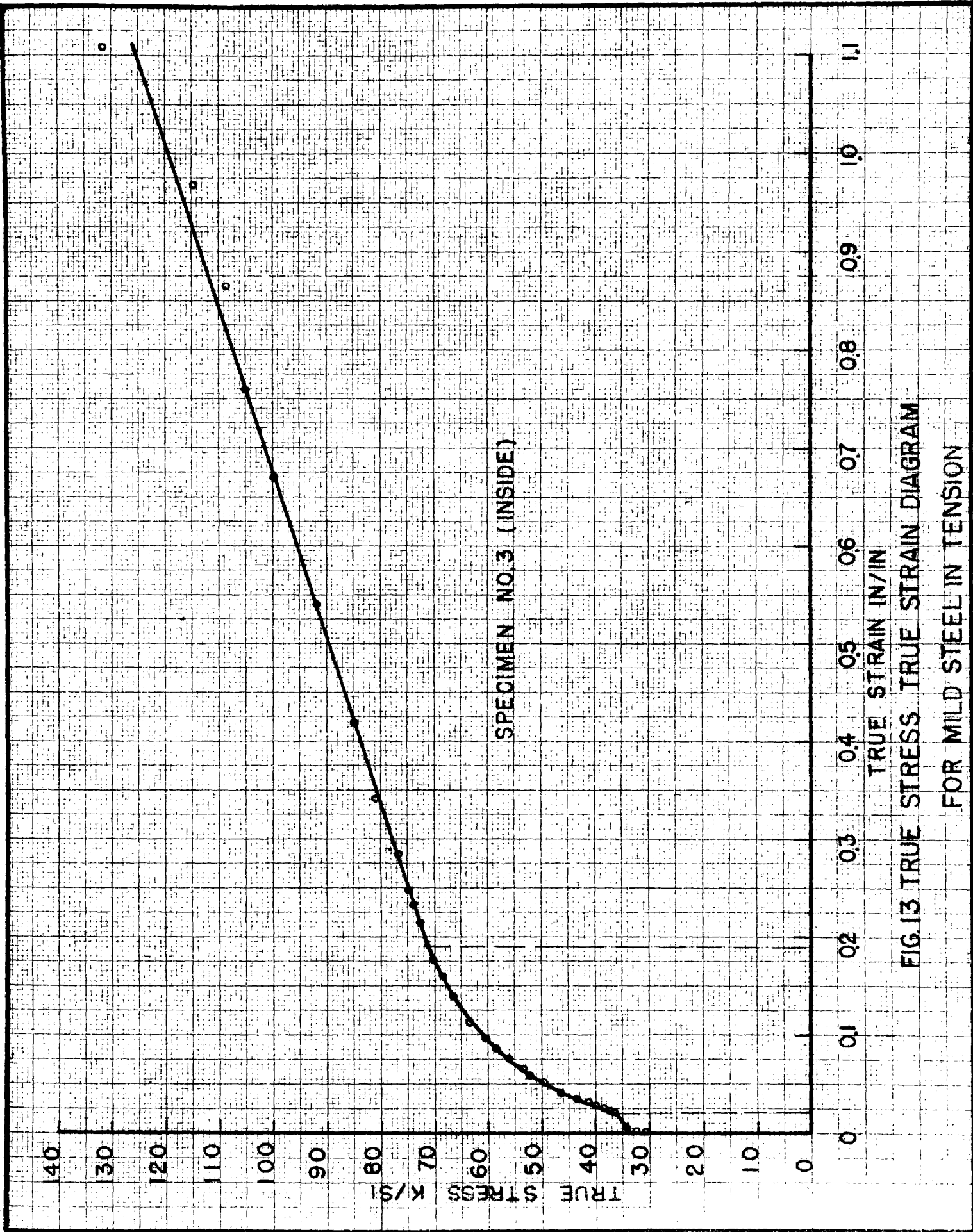
1. The true stress-strain diagrams for outer specimens are different from those of the inner specimens for all the materials. For the mild steel, tension or compression tests, for a certain strain the outside specimen shows higher stress than the inside one. The same happens in the case of stainless steel and magnesium. For the aluminum, the opposite result occurs, since it is found that for a certain strain the inside specimen shows higher stress than the outside.

Table 2

Percentage of Increase of Yield Strength in Outer and Inner Specimens

| Material | Test | Yield Strength psi | | Difference psi | % of Difference |
|-----------------|-------------|--------------------|--------------|-------------------|--------------------|
| | | Outside spec. | Inside Spec. | | |
| Mild Steel | Tension | 36,000 | 33,800 | 2,200 | 5.90 |
| | Compression | 36,000 | 35,000 | 1,000 | 2.86 |
| Stainless Steel | Tension | 42,000 | 40,500 | 1,500 | 3.70 |
| | Compression | 43,000 | 39,000 | 4,000 | 10.25 |
| Aluminum* | Tension | 16,200 | 16,500 | 300 | 1.85 |
| | Compression | 16,900 | 17,200 | 300 | 1.77 |
| Magnesium | Tension | 39,500 | 39,500 | 0 | 0 |
| | Compression | 30,500 | 26,500 | 4,000 | 13 |

* See Point 8, page 29.



SPECIMEN NO.3 (INSIDE)

FIG.13 TRUE STRESS TRUE STRAIN DIAGRAM FOR MILD STEEL IN TENSION

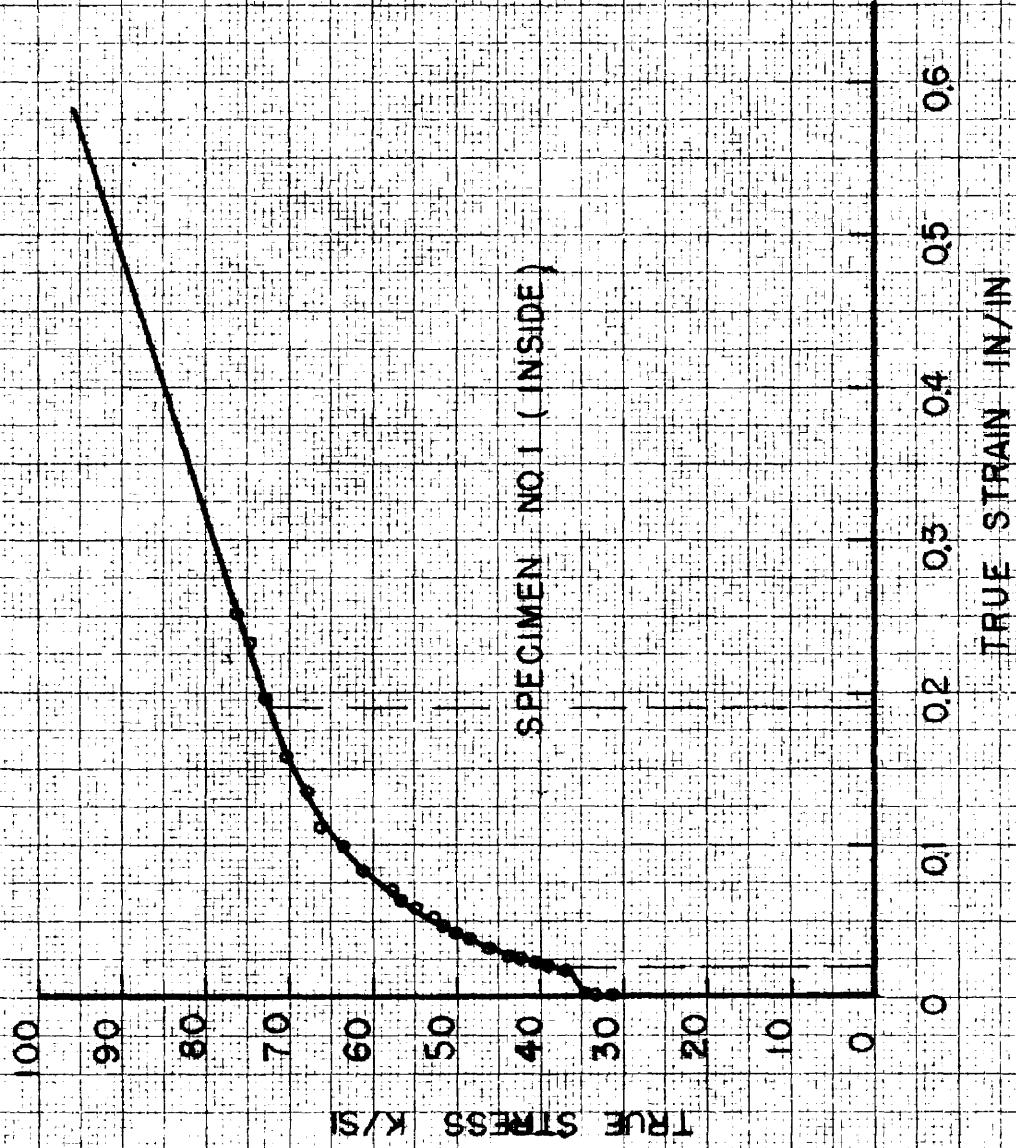


FIG. 14 TRUE STRESS TRUE STRAIN DIAGRAM
FOR MILD STEEL IN COMPRESSION

2. The transition from elastic-plastic to plastic and from one range in the elastic plastic region to another range in it, is accompanied by a certain strain, the same for tension as for compression specimens, irrespective of the varying stress at this strain for different specimens--tension or compression, outside, or inside. This (accompanied by result 2 of part a) means that the strain at the transition from one state to another (ϵ_1 or ϵ_2) is a constant value for each material, whatever the type of stress or position of the specimen from the cross section. The fact that this value acts as a characteristic of this material is a basic assumption used in applying the true stress true-strain relationship to the problem at hand.

3. The stress at necking point in the tension tests (which corresponds to the strain ϵ_2) is greater than the slope of the true stress-true strain diagram at this point in contrast to that given in the literature⁸ which states their equality.

c. Failure of the tested specimens.

1. The mild steel specimens in tension whether inside specimen or outside specimen failed after necking as shown in Fig. 15.
2. The outer specimens of stainless steel in tension failed after gradual necking whereas the inside specimens failed suddenly having a ∇ edge, as shown in Fig. 16.
3. The outside specimens of aluminum in tension as well as the inside specimens failed at a sharp inclined 45° plane without any appreciable necking as shown in Fig. 17.
4. The outside specimen as well as the inside of magnesium failed in tension in a conical necking fracture with sharp edges as shown in Figure 19.

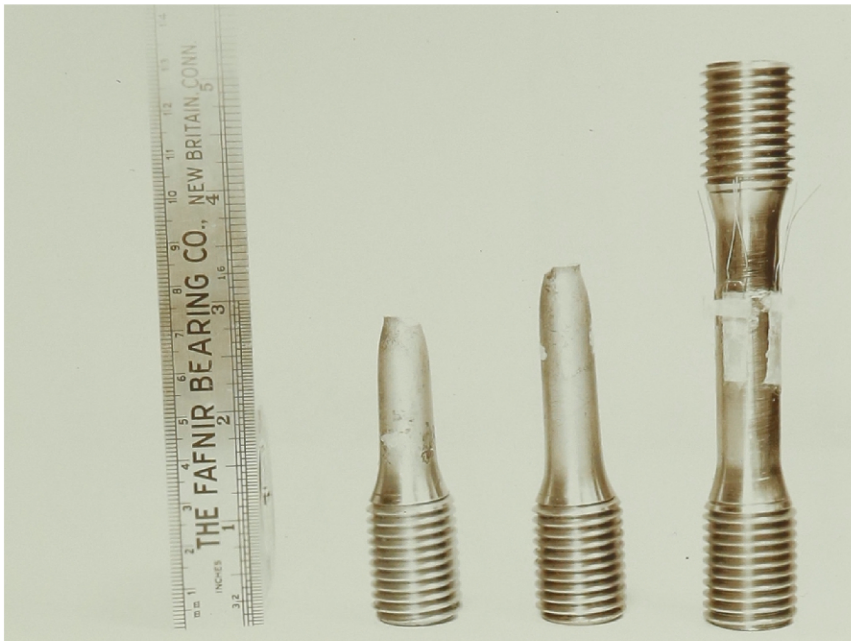


FIG. 15 - MILD STEEL FRACTURE

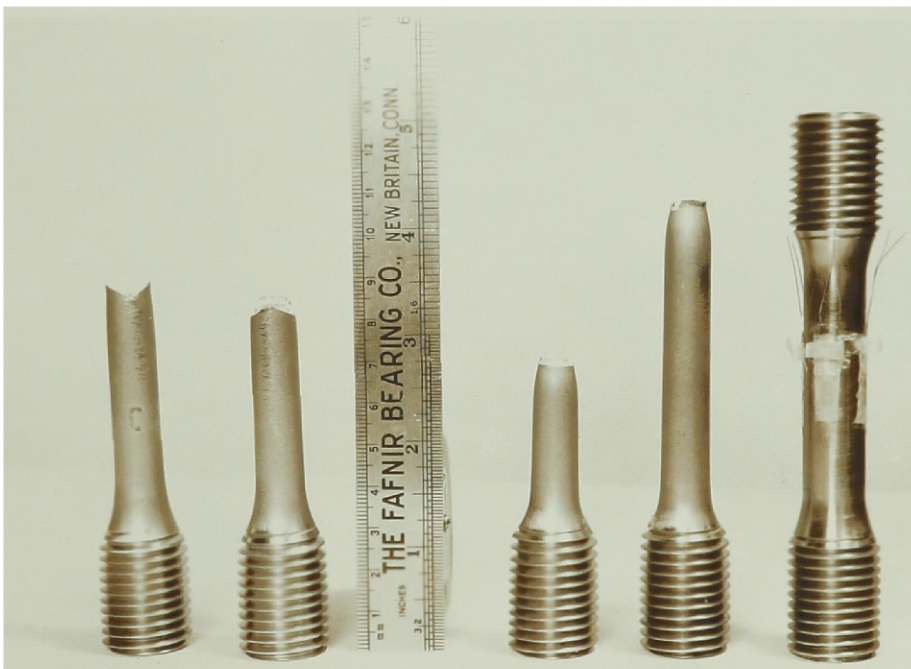


FIG. 16 - STAINLESS STEEL FRACTURE

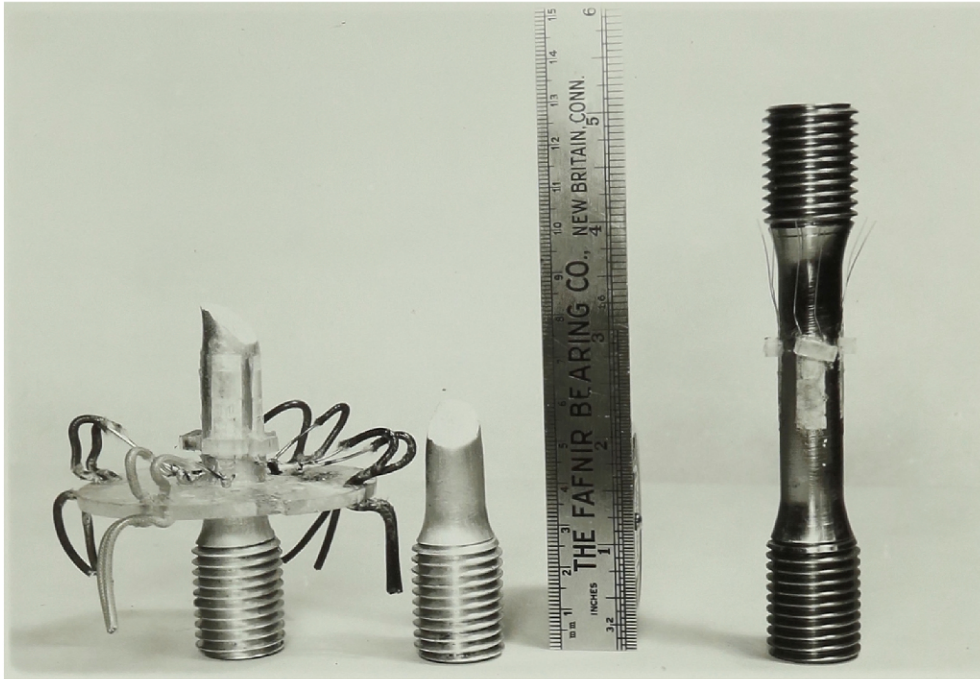


FIG. 17 - ALUMINUM FRACTURE

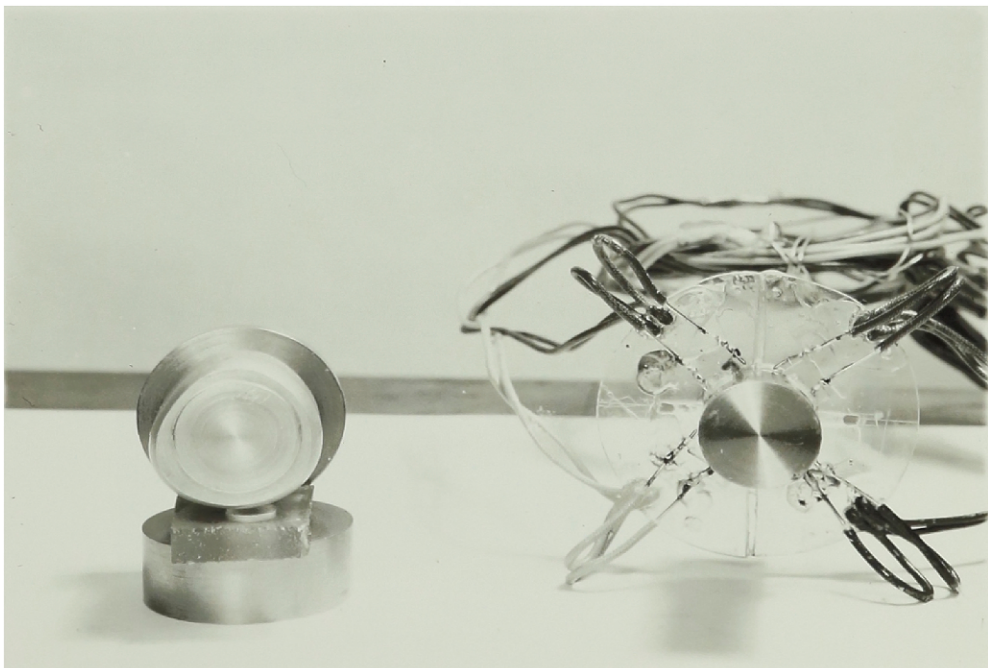


FIG. 18 - ALUMINUM COMPRESSIVE SPECIMENS

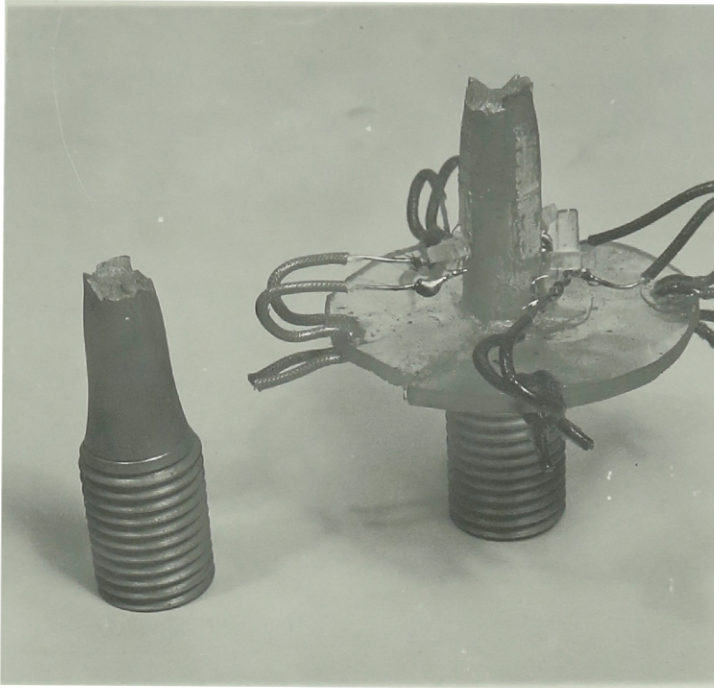


FIG.19 - MAGNESIUM TENSILE FRACTURE

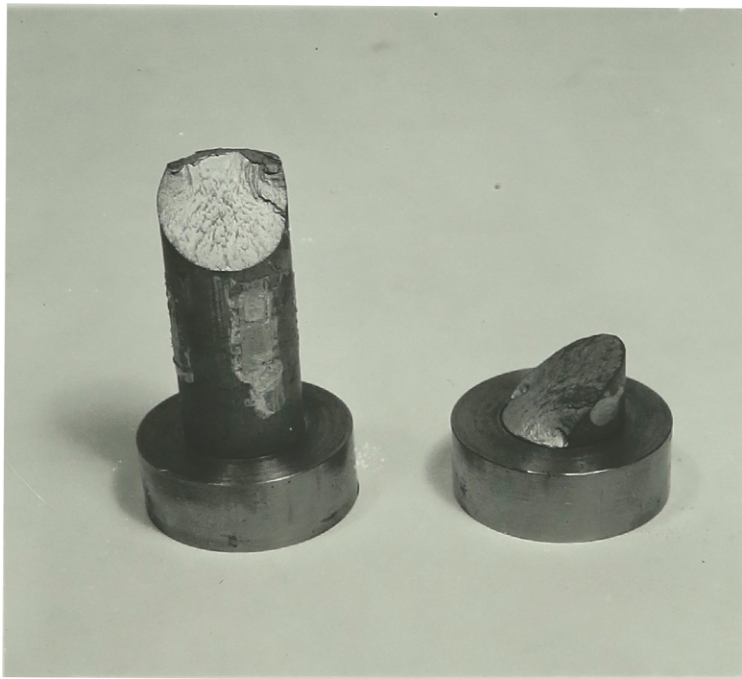


FIG 20 - MAGNESIUM COMPRESSIVE FRACTURE

5. The compression specimens of mild steel and stainless steel after test bulged as usual, decreasing in length and having a circular cross section all over their length.
6. The aluminum specimens after testing in compression showed distinct decrease in length accompanied with the change of their cross section all over their lengths to a triangular form as shown from Figures 10 and 18.
7. The magnesium compression specimens did not show appreciable increase of diameter by increasing the load and they failed and fractured as shown in Fig. 20 at 9 % deformation.
8. The properties of the aluminum rod were not those normally obtained from the structural grade of this material, and should not be considered as typical.

C. Sample of Derivation of the Stress-Strain Relationship Equation From Test Data.

The proposed equation is in the form:

$$\sigma = \left[a\epsilon \right]_{\epsilon=0}^{\epsilon=\epsilon_1} + \left[b\epsilon^c \right]_{\epsilon=\epsilon_1}^{\epsilon=\epsilon_2} + \left[K\epsilon + m \right]_{\epsilon=\epsilon_2}^{\epsilon=\epsilon_3} \quad (1)$$

Elastic Elastic Plastic Plastic

The elastic plastic state also may be represented by a curve and straight line equations or vice versa according to the behavior of the material.

A sample derivation for the inside specimen number 3 of mild steel in tension is as follows:

1. Elastic state. Using the ordinary stress-strain diagram Fig. 11,

Stress at proportional limit = 32,500 psi

Strain at proportional limit $\epsilon_1 = 0.0011$ in/in

$$\sigma = a\epsilon$$

$$a = \frac{\sigma}{\epsilon} = \frac{32,500}{0.0011} = 29.7 \times 10^6 \text{ psi}$$

Therefore the relation will be: $\sigma = \left[29.6 \times 10^6 \epsilon \right]_{\epsilon=0}^{\epsilon=0.0011}$

2. Elastic plastic state. Using the part of the true stress true strain diagram Fig. 13 in the elastic plastic region as shown in Fig. 21, the part of this diagram from $\epsilon = 0.0011$ to $\epsilon = 0.020$ is a straight line. Its intersection with σ axis = 32,000 and its slope = 192,000.

Therefore its equation will be: $\sigma = \left[192,000 \epsilon + 32,000 \right]_{\epsilon=0.0011}^{\epsilon=0.020}$

The other part of the true stress true strain diagram from $\epsilon = 0.020$ to $\epsilon = 0.19$ is a curve whose coordinates as obtained from Fig. 21 are:

| | | | | | | | |
|--------------|-------|-------|-------|--------|-------|-------|-------|
| σ : | 40 | 45 | 50 | 55 | 60 | 65 | 70 |
| ϵ : | 0.029 | 0.040 | 0.053 | 0.0705 | 0.093 | 0.122 | 0.170 |

Plotting these coordinates on log log paper, we get a straight line as shown in Fig. 22. Therefore the equation of this curve is in the form of $\sigma = b \epsilon^c$

$$\text{Log } \sigma = \text{Log } b + c \text{ Log } \epsilon$$

The same result of linearity is obtained when plotting σ vs ϵ on log log paper for all the tested material in tension or in compression as shown in Figures 109 to 116 in the Appendix.

To obtain the constants b and c , we substitute the coordinates of any two points of the straight line shown in Fig. 22. Thus, two equations are obtained which can be solved in b and c .

Take the two points σ :

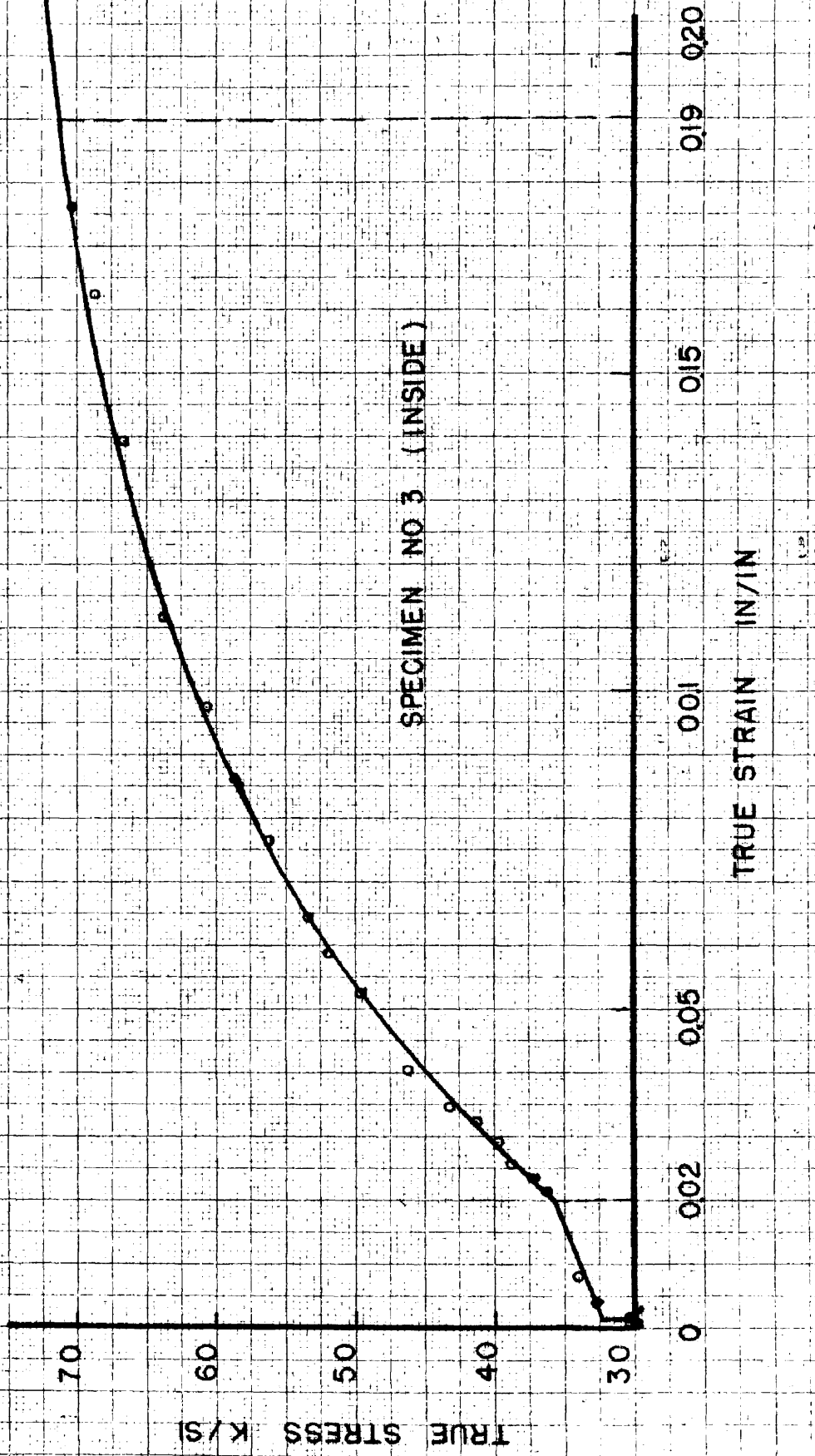
| | | |
|--------------|-------|-------|
| 40 | 60 | |
| ϵ : | 0.029 | 0.093 |

$$\log 40 \times 10^3 = \log b + c \log 0.029$$

$$\log 60 \times 10^3 = \log b + c \log 0.093$$

$$4.0621 = \log b + \bar{2}.4624 c$$

$$4.7782 = \log b + \bar{2}.9685 c$$



SPECIMEN NO 3 (INSIDE)

FIG 21 TRUE STRESS TRUE STRAIN DIAGRAM FOR HYPER-ELASTIC REGION FOR MILD STEEL IN TENSION

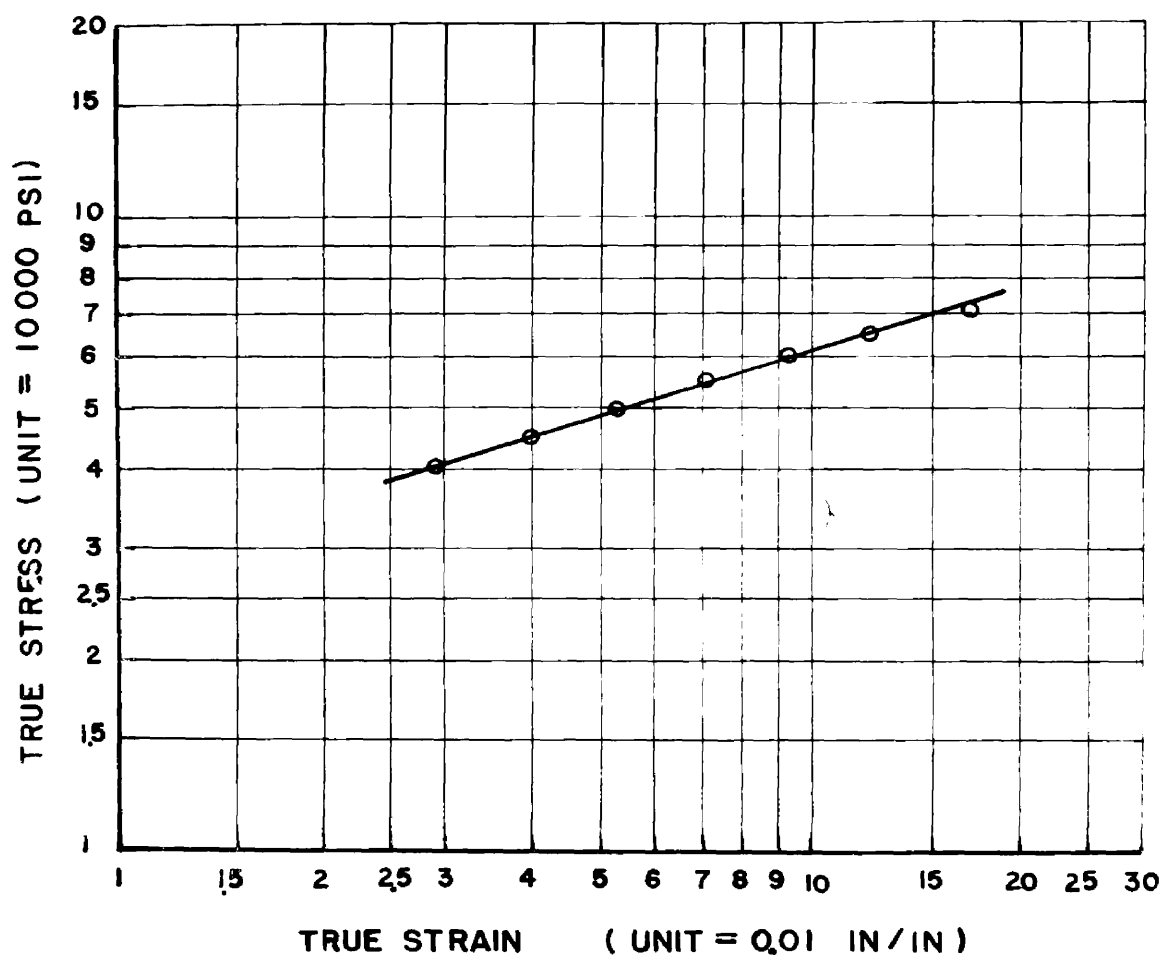


FIG.22 - LOGARITHMIC TRUE STRESS TRUE STRAIN DIAGRAM

Subtracting we get:

$$0.1761 = 0.5051 c, \quad c = \frac{0.1761}{0.5051} = 0.349.$$

Substituting the value of c in one of the above equations we get:

$$\begin{aligned} \log b &= 4.7782 + 1.0315 \times 0.349 = 4.7782 + 0.36 = 5.1382 \\ b &= 137,500. \end{aligned}$$

Therefore the equation of the curve will be:

$$\sigma = \left[137,500 \cdot \epsilon^{0.349} \right]_{\epsilon=0.020}^{\epsilon=0.190}$$

Therefore the elastic plastic relation will be:

$$\sigma = \left[192,000 \epsilon + 32,000 \right]_{\epsilon=0.0011}^{\epsilon=0.020} + \left[137,500 \cdot \epsilon^{0.349} \right]_{\epsilon=0.020}^{\epsilon=0.190}$$

3. Plastic state. Using the true stress strain diagram Fig. 27, the relation is a straight line from $\epsilon = 0.19$ to $\epsilon = 1.13$. The intersection of this line with σ axis = 60,000
Its slope = 60,000

$$\text{The relation will be: } \sigma = \left[60,000 \epsilon + 60,000 \right]_{\epsilon=0.19}^{\epsilon=1.13}$$

Therefore the relation between stress and strain for mild steel in tension is represented by the equation:

$$\begin{aligned} \sigma &= \left[29.6 \times 10^6 \epsilon \right]_{\epsilon=0}^{\epsilon=0.0011} + \left[192,000 \epsilon + 32,000 \right]_{\epsilon=0.0011}^{\epsilon=0.02} + \\ &+ \left[137,500 \epsilon^{0.349} \right]_{\epsilon=0.020}^{\epsilon=0.190} + \left[60,000 \epsilon + 60,000 \right]_{\epsilon=0.19}^{\epsilon=1.13} \quad (2) \end{aligned}$$

| TEST | PROPORTIONAL LIMIT STRESS | YIELD STRENGTH PSI | POSITION OF THE SPECIMEN | ELASTIC STATE | | ELASTIC PLASTIC STATE | | | PLASTIC STATE | | |
|-------------|---------------------------|--------------------|--------------------------|-------------------|----------------------|-----------------------|-----------------|-------------------|-----------------|-------------------|-----------------|
| | | | | STRAIN ϵ | STRESS σ | STRAIN ϵ | STRESS σ | STRAIN ϵ | STRESS σ | STRAIN ϵ | STRESS σ |
| TENSION | 33000 | 36000 | OUTSIDE | 0 | 30.0×10^6 € | 0.0011 | 244000 € | 0.020 | 141000 € | 0.190 | 69000 € |
| | | | | TO 0.0011 | | TO 0.020 | TO 0.190 | TO 0.190 | TO 1.096 | TO 63000 | |
| | 32500 | 33800 | INSIDE | 0 | 29.6×10^6 € | 0.0011 | 192000 € | 0.020 | 137500 € | 0.190 | 60000 € |
| | | | | TO 0.0011 | | TO 0.020 | TO 0.190 | TO 0.190 | TO 1.130 | TO 60000 | |
| COMPRESSION | 34000 | 36000 | OUTSIDE | 0 | 29.6×10^6 € | 0.0011 | 200000 € | 0.020 | 120300 € | 0.190 | 62000 € |
| | | | | TO 0.0011 | | TO 0.020 | TO 0.190 | TO 0.190 | TO ULTIMATE | TO 62000 | |
| | 33000 | 35000 | INSIDE | 0 | 30.0×10^6 € | 0.0011 | 220000 € | 0.020 | 117500 € | 0.190 | 60000 € |
| | | | | TO 0.0011 | | TO 0.020 | TO 0.190 | TO 0.190 | TO ULTIMATE | TO 60000 | |

STRESS PSI STRAIN IN/IN

TABLE 3 - STRESS STRAIN RELATIONS FOR MILD STEEL

| TEST | POSITION OF THE SPECIMEN | PROPORTIONAL LIMIT STRESS | YIELD STRENGTH PSI | ELASTIC STATE | | ELASTIC PLASTIC STATE | | | | PLASTIC STATE | | |
|-------------|--------------------------|---------------------------|--------------------|---------------|----------------------|-----------------------|-----------------|----------------|-----------------|------------------|-------------------|------------------|
| | | | | STRAIN € | STRESS σ | STRAIN € | STRESS σ | STRAIN € | STRESS σ | STRAIN € | STRESS σ | |
| TENSION | OUTSIDE | 32500 | 42000 | 0 TO 0,0011 | $29,6 \times 10^6$ € | 0,0011 TO 0,020 | 162700 € | 0,020 TO 0,500 | $0,350$ € | 260000 € + 46000 | 0,500 TO 0,912 | 190000 € + 86000 |
| | INSIDE | 32500 | 40500 | 0 TO 0,0011 | $29,6 \times 10^6$ € | 0,0011 TO 0,020 | 162600 € | 0,020 TO 0,500 | $0,354$ € | 260000 € + 44000 | 0,500 TO 0,900 | 180000 € + 86000 |
| COMPRESSION | OUTSIDE | 30000 | 43000 | 0 TO 0,0010 | $30,0 \times 10^6$ € | 0,0010 TO 0,020 | 113200 € | 0,020 TO 0,500 | $0,181$ € | 355000 € + 46000 | 0,500 TO ULTIMATE | |
| | INSIDE | 27500 | 39000 | 0 TO 0,0010 | $27,5 \times 10^6$ € | 0,0010 TO 0,020 | 100800 € | 0,020 TO 0,500 | $0,183$ € | 360000 € + 41500 | 0,500 TO ULTIMATE | |

STRESS PSI STRAIN IN/IN

TABLE 4 - STRESS STRAIN RELATIONS FOR STAINLESS STEEL

| TEST | POSITION OF THE SPECIMEN | PROPORTIONAL LIMIT STRESS | YIELD STRENGTH PSI | ELASTIC STATE | | ELASTIC PLASTIC STATE | | PLASTIC STATE | |
|-------------|--------------------------|---------------------------|--------------------|---------------|-----------------------|-----------------------|----------|---------------|----------|
| | | | | STRAIN € | STRESS € | STRAIN € | STRESS € | STRAIN € | STRESS € |
| TENSION | OUTSIDE | 11600 | 16200 | 0 | 10.52×10^6 € | 0.0011 | 0.283 | 0.140 | 30000 € |
| | | | | TO | | TO | 72000 € | TO | + 34000 |
| | INSIDE | 11000 | 16500 | 0.0011 | | 0.140 | | 0.380 | |
| | | | | 0 | 10.50×10^6 € | 0.00105 | 0.249 | 0.140 | 32000 € |
| COMPRESSION | OUTSIDE | 12400 | 16900 | 0 | 10.50×10^6 € | 0.00118 | 0.248 | 0.140 | 12500 € |
| | | | | TO | | TO | 69760 € | TO | + 36500 |
| | INSIDE | 12000 | 17200 | 0.00118 | | 0.140 | | ULTIMATE | |
| | | | | 0 | 10.90×10^6 € | 0.0011 | 0.243 | 0.140 | 12500 € |
| | | | | 0.0011 | | 0.140 | | TO | + 38000 |
| | | | | 0.140 | | | | ULTIMATE | |

STRESS PSI STRAIN IN/IN

TABLE 5 - STRESS STRAIN RELATIONS FOR ALUMINUM

| TEST | POSITION OF THE SPECIMEN | PROPORTIONAL LIMIT STRESS | YIELD STRENGTH PSI | ELASTIC STATE | | ELASTIC PLASTIC STATE | | PLASTIC STATE | |
|-------------|--------------------------|---------------------------|--------------------|---------------|----------------------|-----------------------|------------------|---------------|---------------------|
| | | | | STRAIN € | STRESS σ | STRAIN € | STRESS σ | STRAIN € | STRESS σ |
| TENSION | OUTSIDE | 25000 | 39500 | 0 | 6.75×10^6 € | 0.0037 | Q14 73650 € | 0.04 | 31250 € + 43500 |
| | | | | TO | | TO | | TO | |
| | | | | 0.0037 | | 0.04 | | 0.52 | |
| TENSION | INSIDE | 25000 | 39500 | 0 | 6.75×10^6 € | 0.0037 | Q193 98550 € | 0.04 | 26250 € + 43000 |
| | | | | TO | | TO | | TO | |
| | | | | 0.0037 | | 0.04 | | 0.54 | |
| COMPRESSION | OUTSIDE | 25000 | 30500 | 0 | 6.75×10^6 € | 0.0037 | Q142 35750 € | 0.04 | 140000 € + 25000 |
| | | | | TO | | TO | | TO | |
| | | | | 0.0037 | | 0.04 | | 0.06 | |
| COMPRESSION | INSIDE | 25000 | 26500 | 0 | 6.75×10^6 € | 0.0037 | Q0474 33770 € | 0.04 | 220000 € + 20000 |
| | | | | TO | | TO | | TO | |
| | | | | 0.0037 | | 0.04 | | 0.06 | |

STRESS PSI

STRAIN IN/IN

TABLE 6 - STRESS STRAIN RELATIONS FOR MAGNESIUM

The same procedures were applied to all the other specimens tension or compression of mild steel, stainless steel, aluminum and magnesium. The resulting equations showing the relation between stress and strain are shown in Tables 3, 4, 5 and 6.

5. The Relation Between the Stress and the Slope of the True Stress True Strain Diagram for the Tensile Specimen at Necking.

A. Theoretical Derivation.

It is noted in the literature⁸ that the condition for the initiation of localized deformation in a tensile specimen (necking) may be expressed in the form

$$dP = 0 \quad (3)$$

where P = load applied to the specimen of cross section A .

Since the load is equal to the stress σ times the area A ,

then: $P = \sigma \cdot A$, (4)

$$dP = d(\sigma \cdot A) = A d\sigma + \sigma dA = 0 \quad (5)$$

$$\text{Therefore } \sigma = \frac{d\sigma}{-\frac{dA}{A}} \quad (6)$$

During the plastic deformation (up to necking) the volume remains essentially constant and therefore:

$$d(A \cdot L) = AdL + LdA = 0 \quad (7)$$

$$\text{i.e. } -\frac{dA}{A} = \frac{dL}{L} = d\epsilon \quad (8)$$

where L is the length of a small section of the specimen and

$d\epsilon$ is the increment of the true strain .

Substituting equation 8 in equation 6, the following equation results:

$$\sigma_{\text{necking}} = \left(\frac{d\sigma}{d\epsilon} \right)_{\text{necking}} \quad (9)$$

i.e. Stress at necking equals the slope of the true stress true strain diagram at this point.

One may conclude from the previous derivation that the result

$$\sigma_{\text{necking}} = \left(\frac{d\sigma}{d\epsilon} \right)_{\text{necking}} \quad \text{is based on the assumptions:}$$

1. The volume remains constant during the plastic deformation.
2. dP at necking equals to zero.

The first assumption describing the plastic deformation can be made safely since it is based on experimental evidence. The second assumption describing the increment of the load at necking seems to have nothing to substantiate it. Also, it is realized that the load begins to decrease at the first initiation of necking and therefore dP can not equal zero but should be equal to a negative quantity. The following derivation, based on the first assumption only and on the fact that dP has a value, seems to hold at necking:

$$\begin{aligned} P &= \sigma \cdot A \\ dP &= A d\sigma + \sigma dA \\ \text{or } \sigma &= \frac{d\sigma}{-\frac{dA}{A}} + \frac{dP}{dA} \end{aligned} \quad (10)$$

Introducing $-\frac{dA}{A} = d\epsilon$, then:

$$\sigma = \frac{d\sigma}{d\epsilon} + \frac{dP}{dA} \quad (11)$$

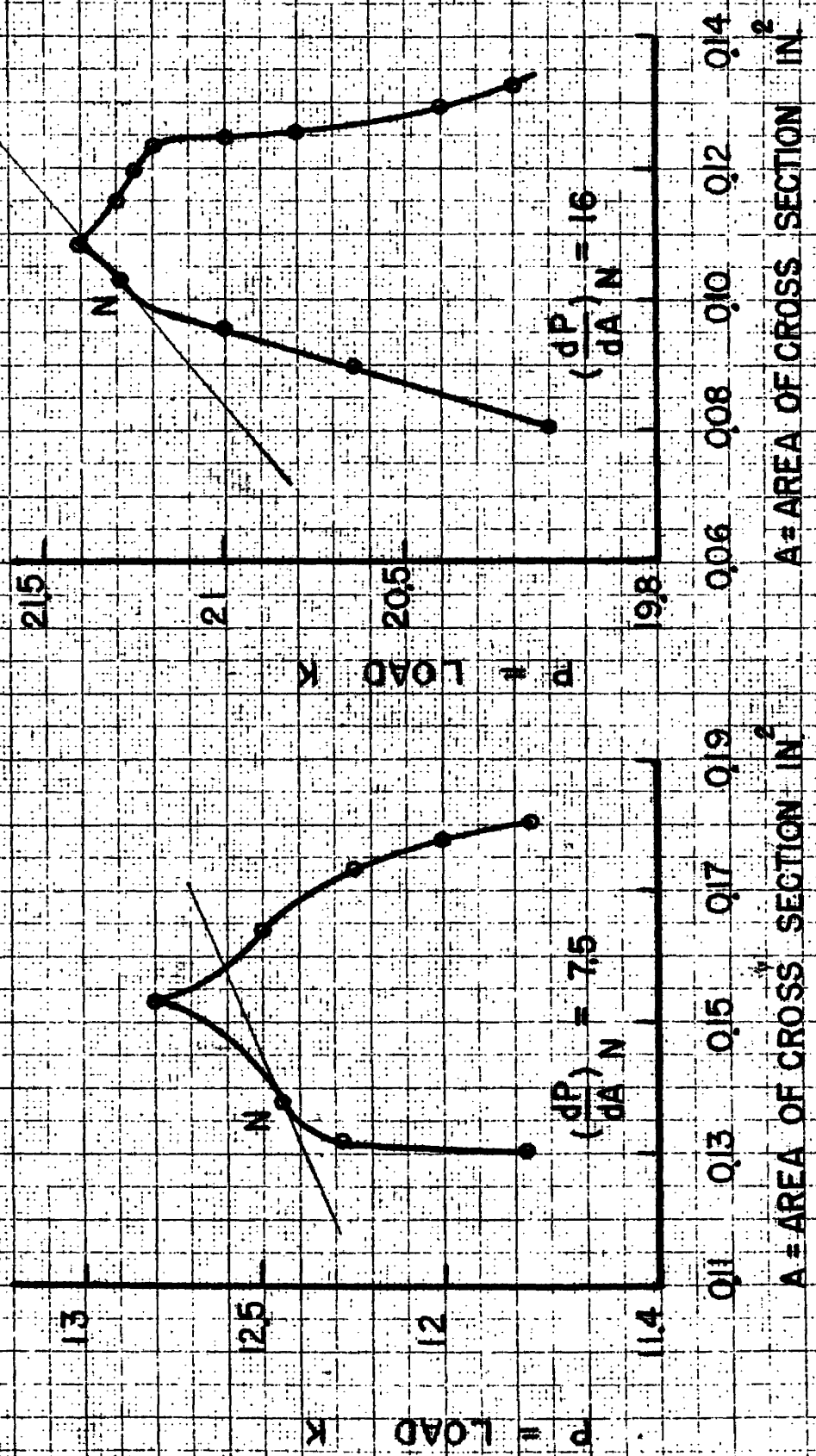
This relation holds over the entire range of the true stress true strain diagram and therefore:

$$\sigma_{\text{necking}} = \left(\frac{d\sigma}{d\epsilon} \right)_{\text{necking}} + \left(\frac{dP}{dA} \right)_{\text{necking}} \quad (12)$$

i.e. The stress at necking for a tension specimen equals the slope of the true stress true strain diagram at this point plus the rate of change of the load with respect to the cross sectional area at necking.

It is worthy to note that dP and dA at necking are both negative quantities (since the area of the cross section is decreasing in the tensile test); therefore $\frac{dP}{dA}$ is a positive quantity, which means that the stress at necking is larger than the slope at necking by the value of $\frac{dP}{dA}$. The difference between our derivation shown in equation 12 and that of the literature shown in equation 9, is in the value of $\frac{dP}{dA}$, which we assume to have a positive value; the literature assumes it to be zero since dP equals zero. To clear this point experimentally, the results of P and A of the previous tensile tests carried out on mild steel, stainless steel, aluminum, and magnesium were plotted in curves of P vs A . These curves are shown in Figures 23 and 24. The plots show discontinuous curves between P and A , of such form that $\frac{dP}{dA}$ cannot equal zero anywhere since no horizontal tangent can be drawn.

Further, we assumed that $\frac{dP}{dA}$ is a positive quantity. The following experimental observations will prove this and will define

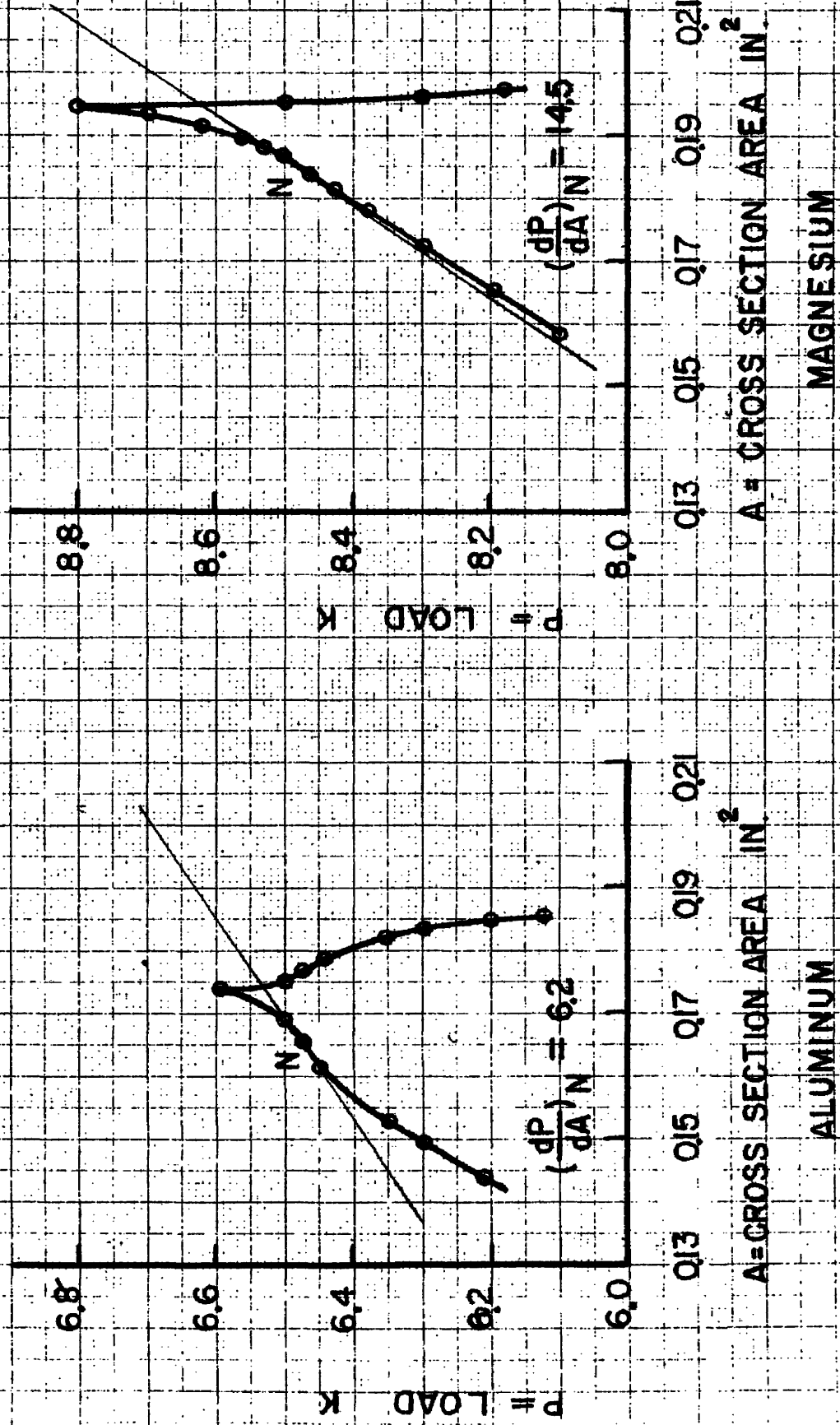


MILD STEEL

STAINLESS STEEL

N = POINT OF CONTRAFLEXURE OF P & A CURVE = NECKING POINT

FIG23 - LOAD VS CROSS SECTION AREA FOR OUTSIDE TENSION SPECIMENS



N = NECKING POINT = POINT OF CONTRAFLEXURE OF P & A CURVE

FIG24- LOAD VS CROSS SECTION AREA FOR OUTSIDE TENSION SPECIMENS

the value of $\frac{dP}{dA}$. It is observed that necking begins when the machine load and strains correspond to the point where the true stress, true strain curve just leaves the elastic plastic state and enters the plastic state, i.e. load P necking and strain ϵ_2 . Referring to Figures 23 and 24, this load corresponds to the point "N" where the discontinuous curve of P and A begins to decrease from its highest peak and where the curvature of this curve changes its sign. The slope at this point "N" is a positive quantity for the four materials previously mentioned as shown in the Figures 23 and 24. Also the value of $\frac{dP}{dA}$ necking equals the value of the slope at the point of contraflexure of the P and A diagram after the highest load is reached. This means that necking does not occur when the maximum load is reached but occurs at point "N" defined previously after this load has been passed.

B. Experimental Verification.

The previous tests made on mild steel, stainless steel, aluminum, and magnesium give the values of stress at necking and the slope of the true stress strain diagram at necking as shown in Table 7. These show that σ_{necking} is not equal to $(\frac{d\sigma}{d\epsilon})_{\text{necking}}$ but is greater than this value. This means that the equation: $\sigma = (\frac{d\sigma}{d\epsilon})_{\text{necking}}$ (9)

does not hold and the equation: $\sigma = \frac{d\sigma}{d\epsilon} + \frac{dP}{dA}$ (12) at necking,

where $\frac{dP}{dA}$ is a positive value agrees with the experiments. Using the value of $\frac{dP}{dA}$ as previously explained and as shown in Figures 23 and 24, the agreement of this relation with the experimental results is very close as shown in Table 8.

Table 7

Values of Stress and Slope of True Stress True Strain Diagram at Necking
for Tension Specimens

| Material | Position of Specimen | Stress psi | Slope psi |
|-----------------|----------------------|---------------|--------------|
| Mild Steel | Outside | 75,000 | 69,000 |
| | Inside | 71,000 | 60,000 |
| Stainless Steel | Outside | 206,900 | 190,000 |
| | Inside | 203,800 | 180,000 |
| Aluminum | Outside | 36,000 | 30,000 |
| | Inside | 39,000 | 32,000 |
| Magnesium | Outside | 45,000 | 31,250 |
| | Inside | 44,000 | 26,250 |

Table 8

Values of the Stress at Necking for Tensile Specimens

| Material | $\frac{d\sigma}{d\epsilon}$ psi | $\frac{dP}{dA}$ psi | Stress at Necking psi | |
|-----------------|------------------------------------|------------------------|---|--|
| | | | Computed $\frac{d\sigma}{d\epsilon} + \frac{dP}{dA}$ | Experimentally (From true stress true strain diagram) |
| Mild Steel | 69,000 | 7,500 | 76,500 | 75,000 |
| Stainless Steel | 190,000 | 16,000 | 206,000 | 206,900 |
| Aluminum | 30,000 | 6,200 | 36,200 | 36,000 |
| Magnesium | 31,250 | 14,500 | 45,750 | 45,000 |

C. Value of Strain at Necking for a Tensile Specimen.

It is shown in the literature⁸, assuming $(\frac{dP}{dA})_{\text{necking}} = 0$, that the strain at necking equals the strain hardening exponent as follows:

$$\sigma = b \cdot \epsilon^c \quad (13)$$

where σ = true stress ϵ = true strain b = constant
 c = strain hardening exponent (constant)

$$\frac{d\sigma}{d\epsilon} = c b \cdot \epsilon^{c-1} \quad (14)$$

$$\text{For } \frac{dP}{dA} = 0, \quad \sigma = \frac{d\sigma}{d\epsilon}, \quad b \cdot \epsilon^c = c b \cdot \epsilon^{c-1} \quad (15)$$

$$\text{Therefore: } \epsilon = c \quad \text{at necking.} \quad (16)$$

Since the value of $\frac{dP}{dA}$ is not equal to zero as previously shown, then the above result does not hold.

Using our derivation equation (12) that:

$$\sigma_{\text{necking}} = \left(\frac{d\sigma}{d\epsilon}\right)_{\text{necking}} + \left(\frac{dP}{dA}\right)_{\text{necking}} \quad (12)$$

and since the necking point falls on the true stress true strain diagram which is defined by the equation (1) as shown in Fig. 3

$$\sigma = k \epsilon + m$$

where k = slope of true stress strain diagram = $\frac{d\sigma}{d\epsilon}$,

m = intercept of the straight line portion of the true stress true strain diagram extrapolated to the σ axis .

$$\text{Therefore } \sigma_{\text{necking}} = \frac{d\sigma}{d\epsilon}_{\text{necking}} \times \epsilon_{\text{necking}} + m \quad (17)$$

Equating equation (12) and (17) then:

$$\epsilon_{\text{necking}} = 1 - \frac{m - \left(\frac{dP}{dA}\right)_{\text{necking}}}{\left(\frac{d\sigma}{d\epsilon}\right)_{\text{necking}}} \quad (18)$$

The experimental results shown in Table 9 verify that $\epsilon_{\text{necking}}$ is not equal to the strain hardening exponent. Applying the previous result shown in equation (18) for the mild steel in tension as a sample, the strain at necking is found to be 0.208 where as it is 0.19 as obtained from the true stress true strain diagram, Fig. 13. The experimental value of 0.19, the strain at which necking begins, was determined by selecting the point on the true stress true strain diagram Fig. 13, at which the graph changed from a curve to a straight line, this choice being correlated and compared with the experimental observations of the behavior of the load as applied by the machine as the test progressed.

This shows close agreement between the computed and experimental value of the strain at necking. It is worthy to note that the difference between the two cases may be due to the experimental location of the point of necking, which is taken as the end of the elastic plastic state curve given by the equation $\sigma = b \cdot \epsilon^c$ and the beginning of the plastic straight line given by the equation $\sigma = k\epsilon + m$. The point of intersection of the curve and the straight line (necking point) may vary according to personal judgment. This judgment will vary the strain value but produce negligible corresponding change in the value of the stress at necking.

It may be valuable to note that the same experimental results, obtained for tensile tests with respect to the stress and the slope of the true stress true strain diagram and with respect to the true strain and the strain hardening, holds again for the compressive tests as shown in Table 10.

Table 9
Values of Strain at Necking of Tension Specimens and
the Values of Their Strain Hardening Exponent

| Material | Position of Spec. | Strain at Necking | Strain Hardening Exponent |
|-----------------|-------------------|----------------------|------------------------------|
| Mild Steel | Outside | 0.19 | 0.343 |
| | Inside | 0.19 | 0.349 |
| Aluminum | Outside | 0.14 | 0.283 |
| | Inside | 0.14 | 0.249 |
| Magnesium | Outside | 0.04 | 0.140 |
| | Inside | 0.04 | 0.193 |
| Stainless Steel | Outside | 0.05 | 0.350 |
| | Inside | 0.05 | 0.354 |

Table 10

Values of Stress, Strain, Slope of True Stress True Strain Diagram and Strain Hardening Exponent for Compression Specimens at Transition from Elastic Plastic to Elastic Region

| Material | Position of Spec. | Stress | Slope | Strain | Strain Hardening Exponent |
|------------|-------------------|--------|---------|--------|---------------------------|
| Mild Steel | Outside | 73,000 | 62,000 | 0.19 | 0.278 |
| | Inside | 72,000 | 60,000 | 0.19 | 0.283 |
| Aluminum | Outside | 38,000 | 12,500 | 0.14 | 0.248 |
| | Inside | 39,500 | 12,500 | 0.14 | 0.243 |
| Magnesium | Outside | 31,000 | 140,000 | 0.04 | 0.0474 |
| | Inside | 29,000 | 220,000 | 0.04 | 0.0442 |

CHAPTER II

Hyper-elastic Pure Bending

1. Introduction.

The classic theory of pure bending in which the bending stress is calculated by the formula $\sigma_i = \frac{MC}{I}$ (σ_i = Bending stress, M = Bending Moment, C = Extreme fiber distance from N.A., I = Moment of inertia of the cross section about axis of flexure) was developed on the basis of two assumptions:

- (1) Plane transverse cross sections of a beam before bending remain plane after bending, i.e. the elongation and contraction of the longitudinal fibers are proportional to the distance from the neutral axis.
- (2) Hooke's law is valid, which means that there is a linear variation of normal stress distribution along the depth of the cross section of the beam varying from zero at the neutral axis to a maximum at the extreme fiber.

For bending of beams the theoretical equation $\sigma_i = \frac{MC}{I}$ can be applied within the elastic limit where the stress and the strain are linearly related. However, when the extreme fiber stress of beams in pure bending exceeds the proportional limit, this theory can no longer be applied because the stress distribution over the cross section is no longer linear but tends to follow the stress-strain characteristic of the material. Therefore other theories were derived to treat this case as will be explained later.

2. Review of Literature.

Many authors have attacked the hyper-elastic pure bending problem either analytically or semi-graphically.^{13,14,15,16,17,18,19,20,21,22,23,24,25} All these solutions are based on the two following equations of equilibrium:

$$(a) \text{ Tensile force} = \text{Compressive force} \quad \text{i.e.} \quad \sum F_H = 0$$

$$(b) \text{ External Moment} = \text{Internal moment} \quad \text{i.e.} \quad \sum M_o = 0$$

These equations apply for any cross section at any stage of hyper-elastic bending. It is also assumed that a plane transverse cross section remains plane after hyper-elastic bending i.e. the elongation and contraction of the longitudinal fibers are proportional to their distances from the neutral axis. This assumption is backed by the results of various experiments. Consider two parallel sections of a beam close to one another. After bending these sections are no longer parallel but make an angle $d\alpha$ with each other.

Referring to Fig. 25, assuming $dx = ds$ then:

$$\frac{\epsilon dx}{y} = \tan d\alpha = d\alpha \quad (19)$$

$$\epsilon dx = yd\alpha \quad \text{but} \quad dx = \rho d\alpha .$$

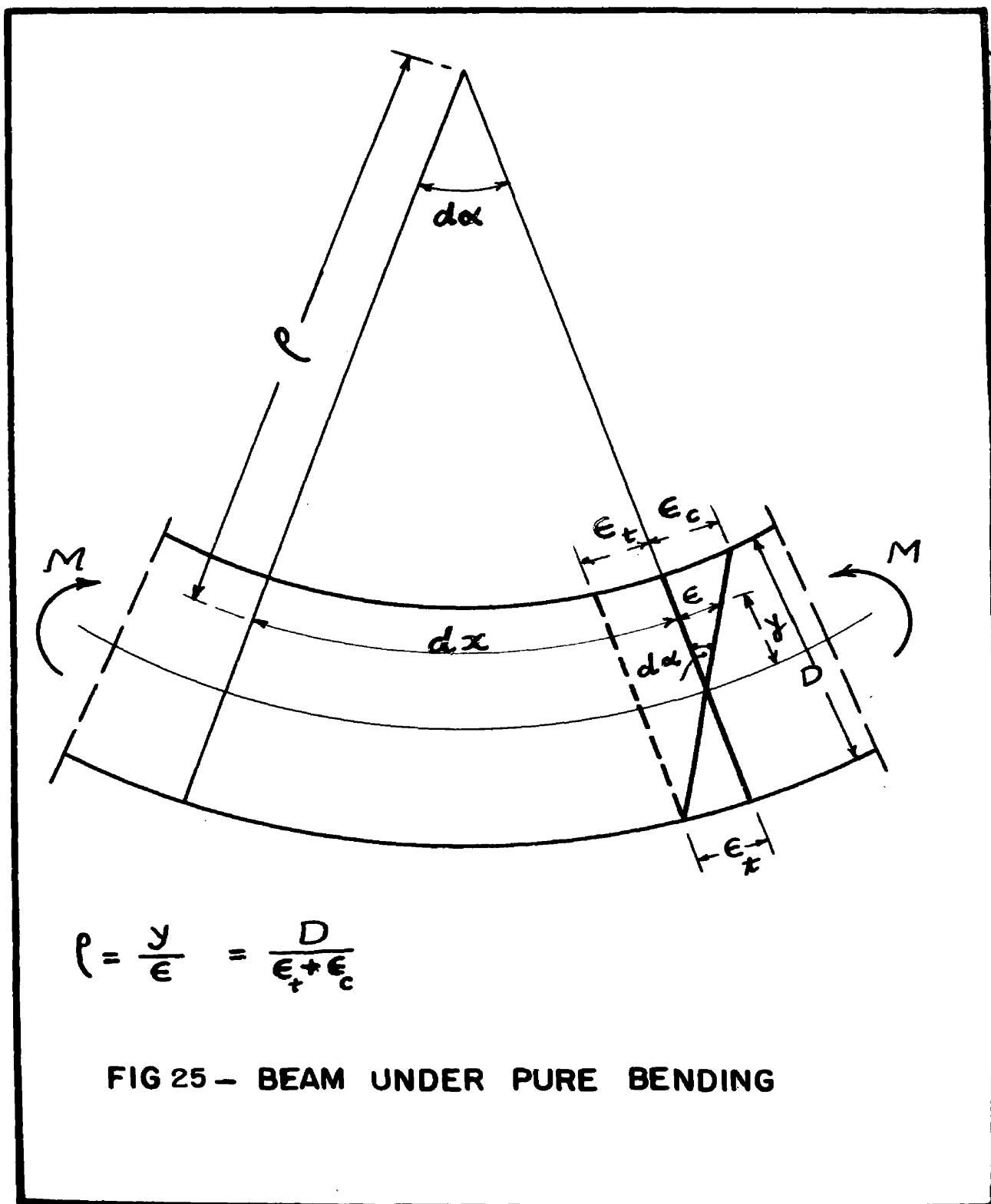
$$\epsilon = \frac{y}{\rho} , \quad (20)$$

where $\epsilon =$ strain

$y =$ distance of strained fiber from N.A.

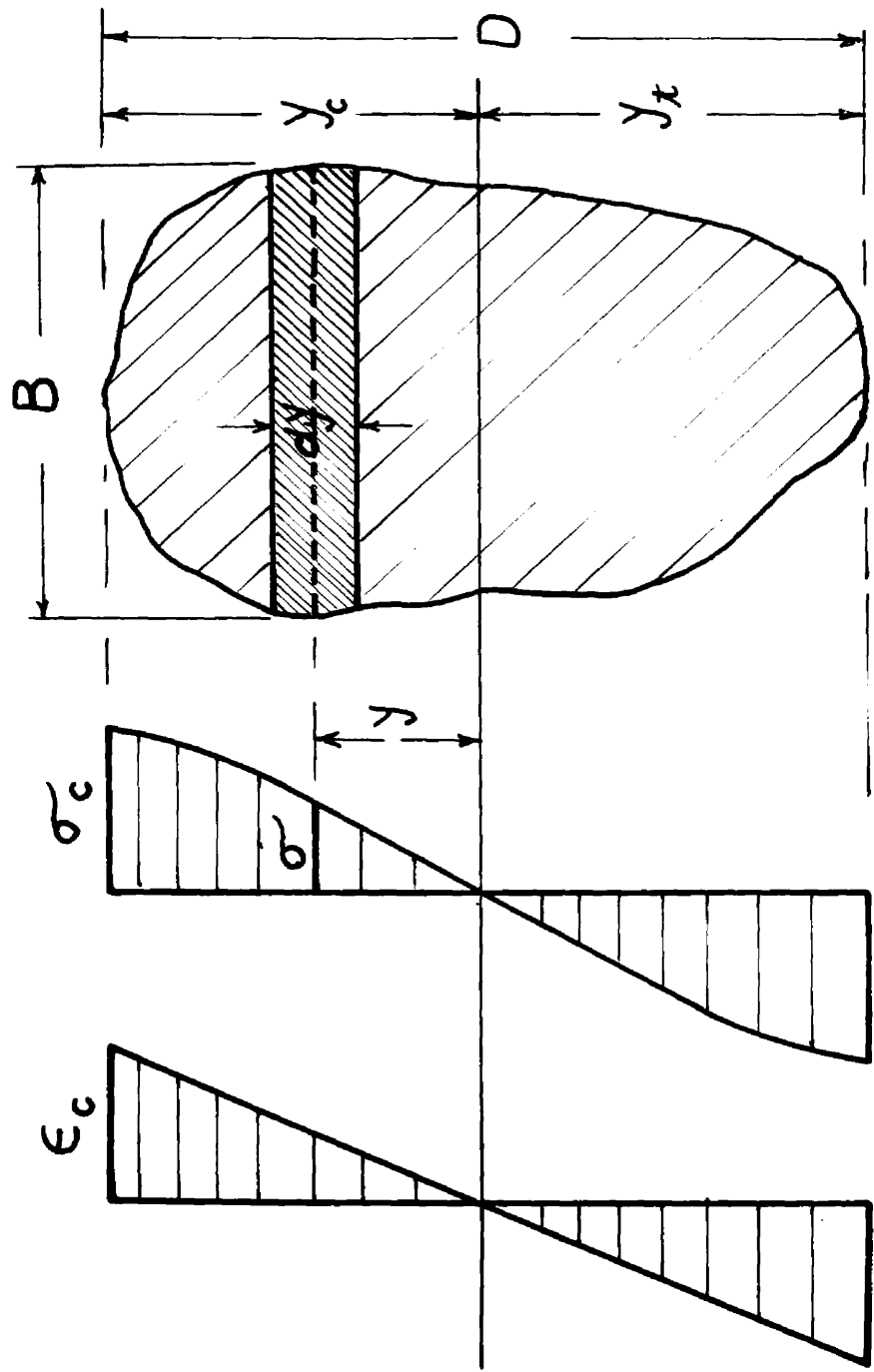
$\rho =$ radius of curvature .

$$y = \rho \epsilon \quad \text{and} \quad dy = \rho d\epsilon . \quad (21)$$



$$\rho = \frac{y}{\epsilon} = \frac{D}{\epsilon_t + \epsilon_c}$$

FIG 25 - BEAM UNDER PURE BENDING



CROSS SECTION

STRESS

STRAIN

FIG26- STRESS & STRAIN DISTRIBUTION OVER CROSS SECTION IN PURE BENDING

Similarly $D = \rho (\epsilon_t + \epsilon_c)$ where $\epsilon_t =$ Extreme tension strain
and $\epsilon_c =$ Extreme compression strain

$$\text{i.e. } \rho = \frac{D}{\epsilon_t + \epsilon_c} \quad (22)$$

Applying the previously mentioned equations of equilibrium and referring to Fig. 26 then:

(i) Tensile force = Compressive force

$$\begin{aligned} \text{i.e. } \int_0^{y_t} b \sigma dy &= \int_0^{y_c} b \sigma dy \\ \int_0^{\epsilon_t} b \sigma d\epsilon &= \int_0^{\epsilon_c} b \sigma d\epsilon \end{aligned} \quad (23)$$

(ii) External moment = Internal moment

$$\begin{aligned} M_t &= \int_{y_c}^{y_t} b \sigma dy \cdot y = \int_{\epsilon_c}^{\epsilon_t} b \rho^2 \sigma \epsilon d\epsilon \\ M_t &= \frac{D^2}{(\epsilon_t + \epsilon_c)^2} \left[\int_0^{\epsilon_t} b \sigma \epsilon d\epsilon + \int_0^{\epsilon_c} b \sigma \epsilon d\epsilon \right] \end{aligned} \quad (24)$$

The integrations of the equilibrium equations (23) and (24) are solved by using the relation between σ and ϵ either as obtained from the ordinary stress strain diagram or from approximation of this diagram as follows:

A. Solutions Based on Ordinary Stress Strain Diagram.

Solution 1.¹³ This solution assumes identical diagrams of stress and strain for tension and compression as obtained from the data of a tensile specimen. Also it neglects the effect of lateral deformations, and considers no shift in the position of the neutral axis. Applied for a rectangular cross section, having depth = D and width = b the neutral axis is still at the center of the depth D and ϵ_t the extreme tensile strain, will be equal to ϵ_c , the extreme compressive strain.

Assume $\epsilon_t = \epsilon_c = \epsilon$ then equation (24) will be:

$$M_t = \frac{2bD^2}{(\epsilon_t + \epsilon_c)^2} \cdot \int_0^{\epsilon} \sigma \epsilon d\epsilon$$

$$= \frac{2bD^3}{\rho (\epsilon_t + \epsilon_c)^3} \cdot \int_0^{\epsilon} \sigma \epsilon d\epsilon \quad \text{by multiplying and}$$

dividing by $\frac{D}{\rho} = (\epsilon_t + \epsilon_c)$

$$M_t = \frac{I}{\rho} \cdot \frac{24}{(\epsilon_t + \epsilon_c)^3} \cdot \int_0^{\epsilon} \sigma \epsilon d\epsilon = \frac{I}{\rho} \cdot E_r \quad (25)$$

where $E_r = \frac{24}{(\epsilon_t + \epsilon_c)^3} \cdot \int_0^{\epsilon} \sigma \epsilon d\epsilon$

E_r is called the reduced modulus and can be calculated applying the graphical integration to the ordinary stress-strain diagram in tension. $I =$ Moment of inertia of the cross section about axis of flexure $= \frac{bD^3}{12}$

$\rho =$ Radius of Curvature

This form of $M_t = \frac{I}{\rho} \cdot E_r$ for the hyper-elastic moment is similar to that of the elastic bending where $M_t = \frac{I}{\rho} \cdot E$ where $E =$ Young's modulus.

Solution 2.²⁶ This solution is based on solution 1, but is put into a practical form as follows:

$$M_t = \frac{2bD^2}{(\epsilon_t + \epsilon_c)^2} \cdot \int_0^{\epsilon} \sigma \epsilon d\epsilon = \frac{2bD^2}{4\epsilon_t^2} \cdot \int_0^{\epsilon_t} \sigma \epsilon d\epsilon$$

$$= \frac{bD^2}{2} \cdot \frac{\int_0^{\epsilon_t} \sigma \epsilon d\epsilon}{\epsilon_t^2} = \frac{bD^2}{2} \cdot K = 3\left(\frac{I}{C}\right) \cdot K \quad (26)$$

where $I = \frac{bD^3}{12}$, $C = D/2$

$K =$ Moment of area under stress strain diagram divided by the square of the strain in the outer fiber which can be obtained graphically for any stress in the outer fiber as shown on Fig. 27. K is called the plastic bending factor.

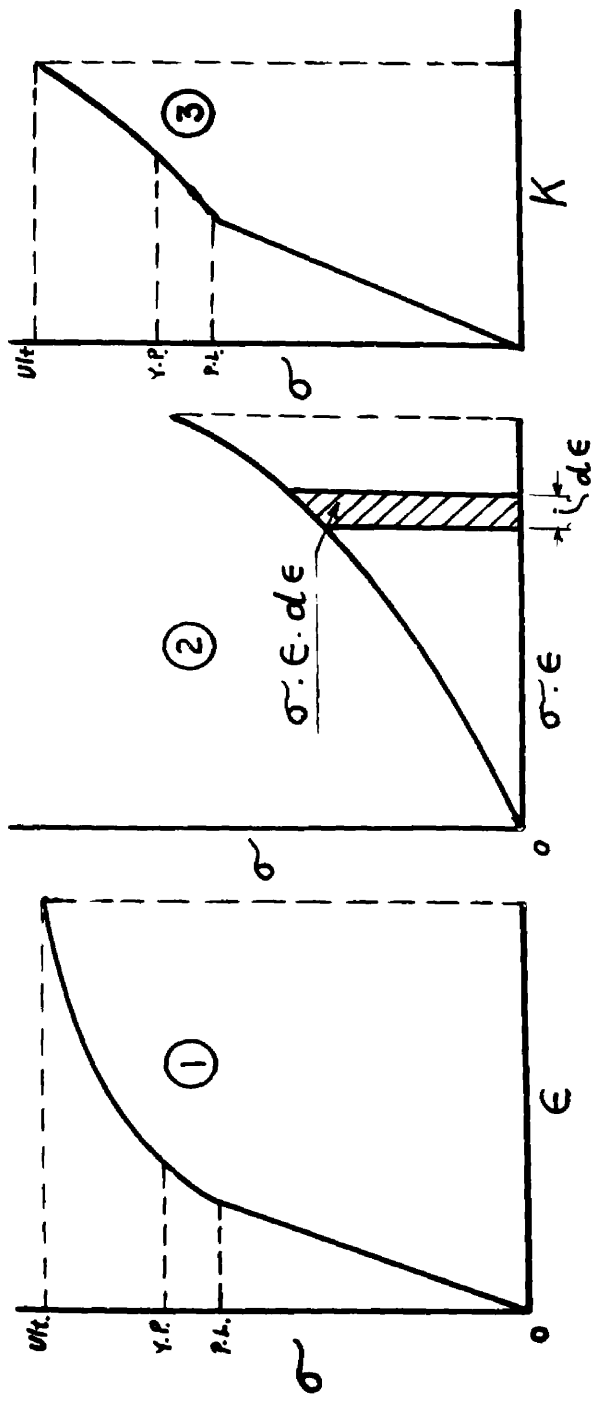


DIAGRAM ① ORDINARY STRESS STRAIN DIAGRAM σ vs ϵ

DIAGRAM ② σ vs $\sigma \cdot \epsilon$ USING DIAGRAM ①

DIAGRAM ③ σ vs K USING DIAGRAMS ① & ②

FOR GIVEN σ $\therefore M = 3 \left(\frac{I}{C} \right) \cdot K$

FROM DIAGRAM ① ϵ IS KNOWN

FROM DIAGRAM ② $\int_0^{\epsilon} \sigma \cdot \epsilon \cdot d\epsilon = \sum_0^{\epsilon} \sigma \cdot \epsilon \cdot d\epsilon$ IS KNOWN

FROM DIAGRAM ③ $K = \frac{\int_0^{\epsilon} \sigma \cdot \epsilon \cdot d\epsilon}{\epsilon^2}$ IS KNOWN

FIG 27 - PLASTIC BENDING FACTOR K

Solution 3.¹⁸ The moment of resistance M_t is obtained from the equilibrium equations using the analytical relation between σ and ϵ for the ordinary stress strain diagram as illustrated in Table 1, Chapter I. This solution has been limited by the mathematical difficulties encountered in applying it to a specific problem.

B. Solutions Based on Approximating the Ordinary Stress Strain Diagram. (Assuming identical stress strain diagram in tension and compression).

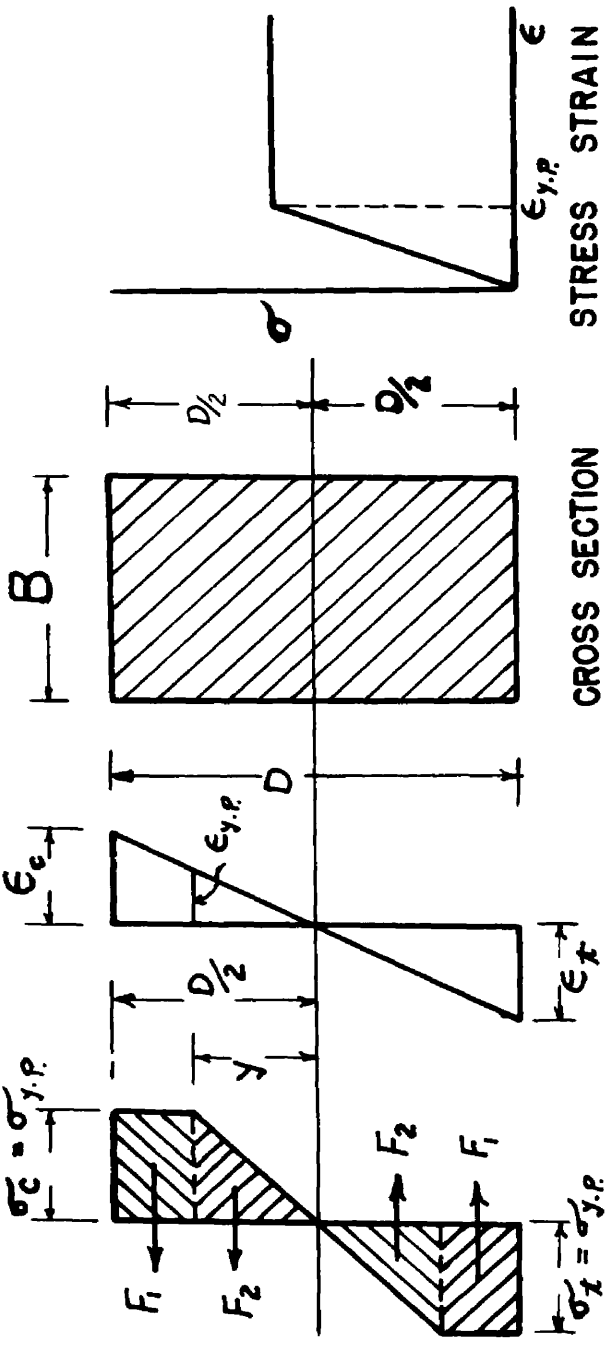
Solution 1. Rectangular distribution.²⁷ The stress strain diagram is approximated by the shape shown on Fig. 28, in which it is assumed that no increase of stress occurs with the increase of strain after reaching the yield point. Applying this to a rectangular cross section under pure bending as shown in Fig. 25 we can get:

$$M_t = \frac{bD^2}{12} \cdot \sigma_{\text{Yield Point}} \left[3 - \left(\frac{\epsilon_{y.p.}}{\epsilon_t} \right)^2 \right], \quad (27)$$

$$\frac{M_t}{M_{y.p.}} = \frac{1}{2} \left[3 - \left(\frac{\epsilon_{y.p.}}{\epsilon_t} \right)^2 \right], \quad (28)$$

with a limiting value of 1.5 .

Using this approximation for the stress strain diagram, the curve showing relations between $\frac{M}{M_{\text{yield Pt}}}$ vs $\frac{\epsilon}{\epsilon_{\text{yield Pt}}}$ for different sections is as shown in Fig. 29.

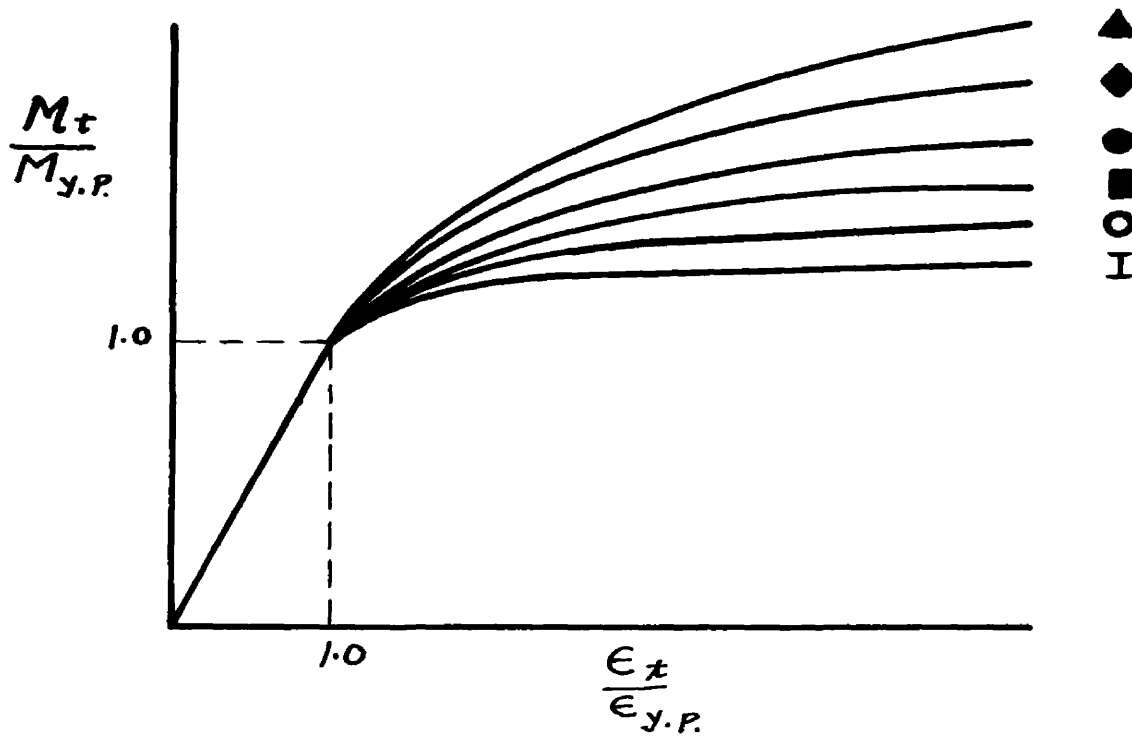


STRESS STRAIN IN PURE BENDING CROSS SECTION STRESS STRAIN DIAGRAM

$$\begin{aligned}
 M_t &= 2 \left\{ B \sigma_{y.p} \left[\frac{D}{2} - y \right] \left[\frac{1}{2} (D - y) + y \right] \right\} + \left\{ 2 B \frac{\sigma_{y.p} \cdot y}{2} \cdot \frac{2}{3} y \right\} \\
 &= B \sigma_{y.p} \left[\frac{D^2}{4} - \frac{y^2}{3} \right] \\
 &= \frac{B D^2}{12} \cdot \sigma_{y.p} \left[3 - \left(\frac{\epsilon_{y.p}}{\epsilon_t} \right)^2 \right]
 \end{aligned}$$

INTRODUCING $y = \frac{\epsilon_{y.p}}{\epsilon_t} \cdot \frac{D}{2}$

FIG28- MOMENT OF RESISTANCE USING APPROXIMATE STRESS STRAIN DISTRIBUTION



LIMITING VALUE OF $\frac{M_t}{M_{y.P}}$ FOR DIFFERENT CROSS SECTIONS:

▲ 2.37

◆ 2.00

● 1.70

■ 1.50

○ 1.27

I 1.08

FIG 29- $\frac{M_t}{M_{y.P}}$ & $\frac{\epsilon_t}{\epsilon_{y.P}}$ DIAGRAM FOR DIFFERENT
CROSS SECTIONS

Solution 2. Modified Form of Distribution.²⁸

The stress strain diagram is assumed to have the slope shown in Fig. 30. Applying this distribution to a rectangular cross section we obtain

$$\frac{M_t}{M} \text{ yield pt} = \frac{3}{2} (1-n) - \frac{1-n}{2 \cdot \left(\frac{\epsilon_t}{\epsilon_{y,p}} \right)^2} + n \cdot \frac{\epsilon_t}{\epsilon \text{ yield pt}} \quad (29)$$

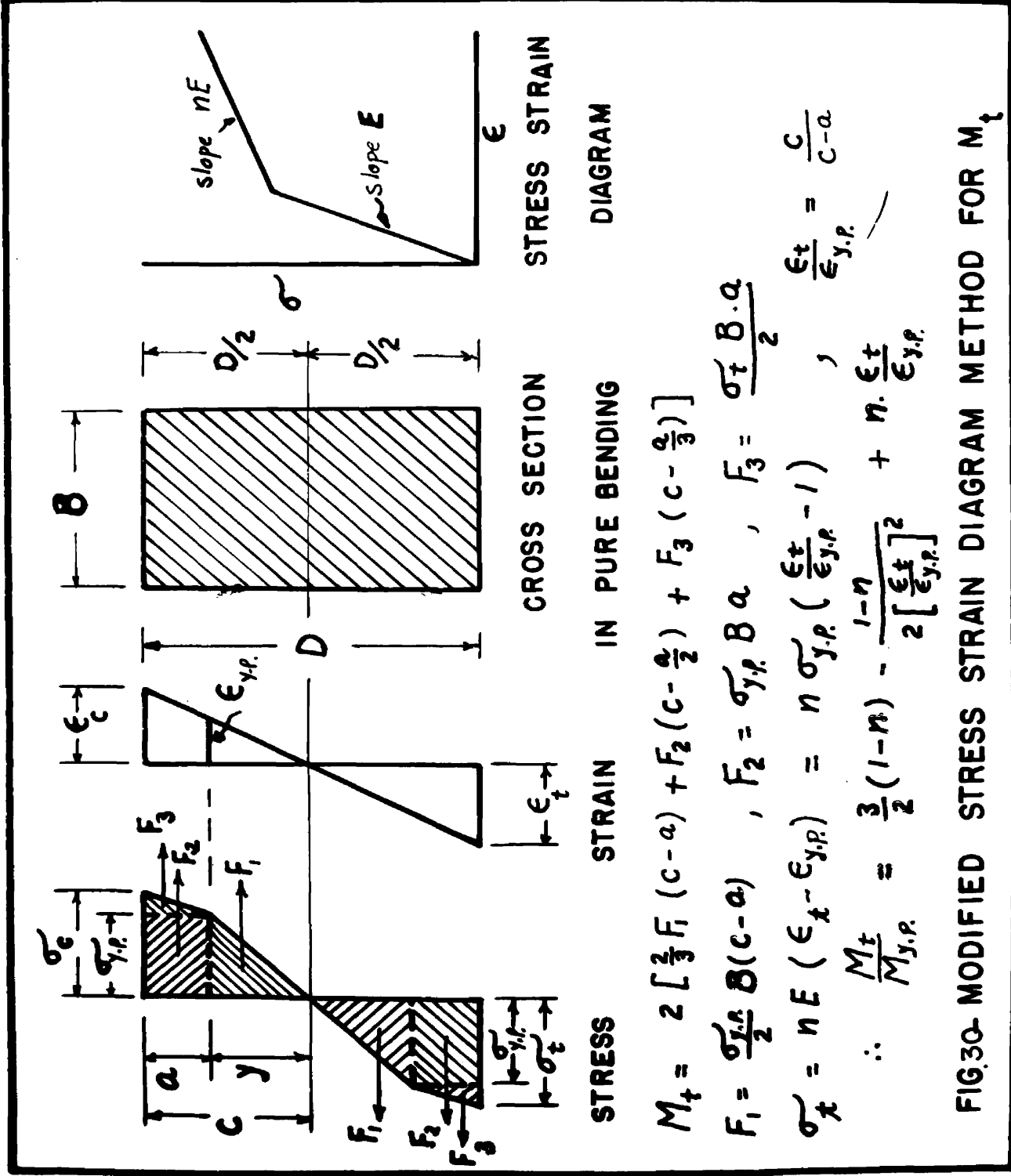
where n is the slope of the line representing stress strain relation after the yield point, which is constant for given material.

Solution 3. Triangular Distribution "Kuntze's Theory".²⁹

This theory contends that in pure bending the yield point is higher than that of tension and when the yield point is reached in the extreme fiber in pure bending the yielding occurs suddenly for the entire cross section of the beam, having a limiting moment of resistance $M_t = 1.4114 M_{y.p.}$ and assuming the triangular distribution of stress all over the cross section. See Fig. 31. It is noted also that the outer fiber yields when the tensile yield limit has been attained in a certain layer in the interior of the cross section such that it divides the triangular stress distribution from the N.A. to the outer fiber into two equal areas. This theory while it gives reasonable results in isolated cases, cannot be claimed to have any fundamental basis.

Solution 4. Stress-Strain Distribution Taking into Account Upper and Lower Yield Points.³⁰

The same treatment as the rectangular distribution is to be followed to obtain the moment of resistance except the distribution of stress is as shown in Fig. 32.



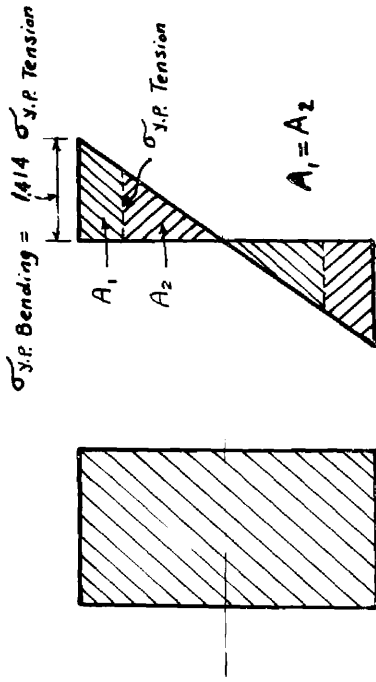
$$M_t = 2 \left[\frac{2}{3} F_1 (c-a) + F_2 (c - \frac{a}{2}) + F_3 (c - \frac{D}{3}) \right]$$

$$F_1 = \frac{\sigma_{y.p.}}{2} B (c-a), \quad F_2 = \sigma_{y.p.} B a, \quad F_3 = \frac{\sigma_t B \cdot a}{2}$$

$$\sigma_x = nE (\epsilon_x - \epsilon_{y.p.}) = n \sigma_{y.p.} \left(\frac{\epsilon_t}{\epsilon_{y.p.}} - 1 \right), \quad \frac{\epsilon_t}{\epsilon_{y.p.}} = \frac{c}{c-a}$$

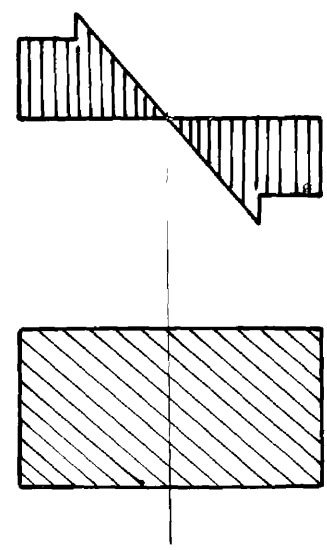
$$\therefore \frac{M_t}{M_{y.p.}} = \frac{3}{2} (1-n) - \frac{1-n}{2} \left[\frac{\epsilon_t}{\epsilon_{y.p.}} \right]^2 + n \frac{\epsilon_t}{\epsilon_{y.p.}}$$

FIG.30- MODIFIED STRESS STRAIN DIAGRAM METHOD FOR M_t



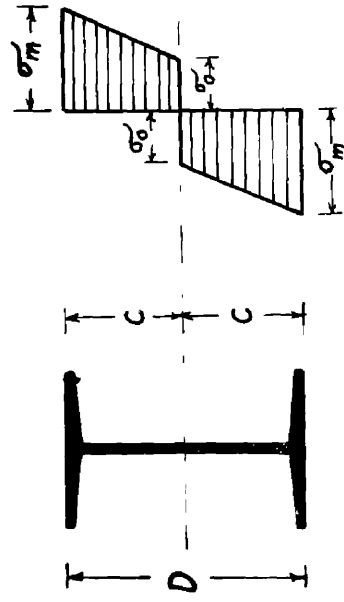
CROSS SECTION STRESS DISTRIBUTION

FIG.31 - KUNTZE'S THEORY



CROSS SECTION STRESS DISTRIBUTION

FIG.32 THEORY TAKING CARE OF UPPER AND LOWER YIELD POINTS



CROSS SECTION STRESS DISTRIBUTION

$$\frac{M_c C}{I} = \sigma_m + \sigma_0 [K-1]$$

$$K = 0.85 C \sqrt{\frac{R}{I}}$$

I & A_c = MOMENT OF INERTIA & AREA OF CROSS SECTION

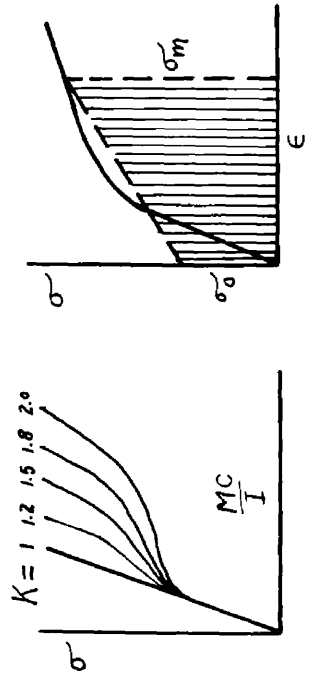


FIG.33- TRAPEZOIDAL DISTRIBUTION METHOD

Solution 5. Trapezoidal Distribution.³¹

The moment of resistance for any cross section can be computed using the trapezoid as an approximation to the stress strain diagram as shown in Fig. 33 by the following relation:

$$\frac{M_t C}{I} = \sigma_m + \sigma_0 \quad \times (K - 1) \quad (30)$$

where M_t = moment of resistance of the cross section for the extreme bending stress σ_m

C = Distance of extreme fiber from N.A. = $D/2$

I = Moment of inertia of the cross section

$$\sigma_0 = \frac{6 \int_0^{\sigma_m} \sigma \epsilon d\epsilon}{\epsilon_m^2} - 2\sigma_m \quad \text{where } \sigma \ \& \ \epsilon \text{ are the}$$

stress and strain and σ_m, ϵ_m are stress and strain in the extreme fibers.

$K = 0.85 C \sqrt{\frac{I}{A}}$ where A = area of the cross section of the beam under bending.

This method can be put in a tabulated form to make the computation easy and leads to a relation between σ_m and M_t as shown in Fig. 33.

3. Discussion of the Previous Methods.

The methods previously shown for calculation of moment of resistance of a beam under pure bending - whether they are based on the stress-strain diagram or its approximation are dependent on the following assumptions:

- (1) The ordinary stress-strain diagram represents the true relation between the stress and the strain in the elastic plastic and the plastic states.
- (2) The neutral axis of the cross section under pure bending of any material at any stage of bending remains at the centroid of the cross section (center in case of symmetrical sections which are mostly treated).
- (3) The stress-strain curve of tension is the same as that of compression for any material.
- (4) The lateral deformations are neglected, so that the width of the cross section at any place is considered still to be unchanged whatever the bending moment may be.

It seems that all these assumptions ought to be avoided in the computation since they are all on the side of discrepancy. As was explained before in Chapter I, the ordinary stress-strain diagram does not represent the actual relation between the stress and the strain in the elastic plastic or plastic state. Also the stress strain curves in tension and compression are not the same for all materials but they are completely different with a very distinct variation in some materials. These curves are dependent on the characteristic of each material and such an assumption of equality is not based on fact. Besides, the assumption of neglecting lateral deformations ignores an action which has an effect on the value of the moment of resistance. Moreover, the neutral axis should not remain at the centroid of the cross section but should shift due to (a) difference of the stress-strain diagrams in tension and compression,

(b) change of the shape of the cross section as a result of lateral deformation with an increase of the width of the cross section on the compression side and a decrease on the tension side.

4. New Method for Computing Moment of Resistance in Hyper-Elastic State.

A new method is now proposed to obtain the value of moment of resistance of a beam in pure bending having the following basis:

- (1) The true stress-true strain is considered as representing the relation between stress and strain in the elastic plastic and the plastic states, using the equation of relationship between the stress and the strain which was previously deduced in Tables 3, 4, 5, and 6 of Chapter I.
- (2) Separate relations between stress and strain in tension and in compression as given by the true stress-true strain curves for tension and compression are introduced.
- (3) Shift of neutral axis of varying amount at different stages of bending is taken into account.
- (4) The effect of lateral deformation on the shape of the cross section is considered.

This method is based on the following assumptions which are backed by the results of experiment:

- (1) Plane sections remain plane after bending in elastic plastic and plastic states.
- (2) The behavior of the tension side and the compression side in pure bending follow the corresponding pure tension and pure compression behaviors.

Procedure of the Method.

In this method, the moment of resistance of a cross section of a given beam under pure bending is computed in terms of a given extreme fiber stress either in tension or in compression. The relation between the stress and the strain

$$\sigma = \left[a\epsilon \right]_{\epsilon_1}^{\epsilon_2} + \left[b\epsilon^c \right]_{\epsilon_1}^{\epsilon_2} + \left[K\epsilon + m \right]_{\epsilon_2}^{\epsilon_3}$$

is used where the values of a , b , c , k , m , ϵ_1 & ϵ_2 are characteristics for each material which are known experimentally for tension as well as for compression as explained previously in Chapter I. These relations are shown in Tables 3, 4, 5 and 6. The relations for pure bending, considering lateral deformations, will be as follows:

A. Effect of Lateral Deformation on Relation between Stress and Strain.

For any material considering the tension or compression side in the elastic state (where the longitudinal strains $\epsilon = 0$ to ϵ_1) the effect of lateral deformation can be neglected since the longitudinal strain ϵ_1 is very small and consequently the lateral elongation or contraction is negligible. The width of the cross section "B" from $\epsilon = 0$ to ϵ_1 will still be practically constant. For longitudinal strains $\epsilon = \epsilon_1$ to ϵ_2 - assuming Poisson's ratio = 0.50 - the lateral elongation on the compression side and the lateral contraction on the tension side can be taken constant all over the region from ϵ_1 to ϵ_2 . Therefore the width "B" of the cross section between the longitudinal strains ϵ_1 to ϵ_2 becomes for the compression side $B \left[1 + 0.5 \times \frac{\epsilon_{1c} + \epsilon_{2c}}{2} \right]$ and for the tension side

$B \left[1 - 0.5 \times \frac{\epsilon_{1t} + \epsilon_{2t}}{2} \right]$. The assumption that Poisson's ratio = 0.50

is close to its actual value and small changes in this quantity will not affect materially the value of width of the cross section after elongation or contraction as previously stated. For the longitudinal strains,

$\epsilon = \epsilon_2$ to ϵ_3 , following the same procedure as for $\epsilon = \epsilon_1$ to ϵ_2 , the width of the cross section "B" will be changed to $B \left[1 + 0.5 \cdot \frac{\epsilon_{2c} + \epsilon_{3c}}{2} \right]$ on the compression side and $B \left[1 - 0.5 \cdot \frac{\epsilon_{2t} + \epsilon_{3t}}{2} \right]$ on the tension side.

Therefore for any cross section in pure bending where the extreme tensile strain is ϵ_{3t} and the extreme compressive strain ϵ_{3c} the value of "B" using the proposed relation between the stress and the strain and taking the effect of lateral deformation into consideration will be

1. For the compression side:

$$B\sigma = B \left[a\epsilon \right]_0^{\epsilon_1} + B \left[1 + \frac{\epsilon_1 + \epsilon_2}{4} \right] \left[b\epsilon^c \right]_{\epsilon_1}^{\epsilon_2} + B \left[1 + \frac{\epsilon_2 + \epsilon_3}{4} \right] \left[K\epsilon + m \right]_{\epsilon_2}^{\epsilon_3}$$

$$= B \left\{ \left[a\epsilon \right]_0^{\epsilon_1} + \left[1 + \frac{\epsilon_1 + \epsilon_2}{4} \right] \left[b\epsilon^c \right]_{\epsilon_1}^{\epsilon_2} + \left[1 + \frac{\epsilon_2 + \epsilon_3}{4} \right] \left[K\epsilon + m \right]_{\epsilon_2}^{\epsilon_3} \right\}. \quad (31)$$

2. For the tension side:

$$B\sigma = B \left\{ \left[a\epsilon \right]_0^{\epsilon_1} + \left[1 - \frac{\epsilon_1 + \epsilon_2}{4} \right] \left[b\epsilon^c \right]_{\epsilon_1}^{\epsilon_2} + \left[1 - \frac{\epsilon_2 + \epsilon_3}{4} \right] \left[K\epsilon + m \right]_{\epsilon_2}^{\epsilon_3} \right\}. \quad (32)$$

This means that to take the effect of lateral deformation into account assume the width of the section at any layer whether inside or outside

unchanged and multiply the value of stresses from longitudinal strains ϵ_1 to ϵ_2 by the factor $\left[1 + \frac{\epsilon_1 + \epsilon_2}{4}\right]$ for the compression side and $\left[1 - \frac{\epsilon_1 + \epsilon_2}{4}\right]$ for the tension side, and also from $\epsilon = \epsilon_2$ to ϵ_3 the factors will be: $\left[1 + \frac{\epsilon_2 + \epsilon_3}{4}\right]$ and $\left[1 - \frac{\epsilon_2 + \epsilon_3}{4}\right]$ respectively.

Thus

$$\sigma_t = \left[a\epsilon \right]_0^{\epsilon_1} + \left[1 - \frac{\epsilon_1 + \epsilon_2}{4} \right] \left[b\epsilon^c \right]_{\epsilon_1}^{\epsilon_2} + \left[1 - \frac{\epsilon_2 + \epsilon_3}{4} \right] \left[K\epsilon + m \right]_{\epsilon_2}^{\epsilon_3} \quad (33)$$

$$\sigma_c = \left[a\epsilon \right]_0^{\epsilon_1} + \left[1 + \frac{\epsilon_1 + \epsilon_2}{4} \right] \left[b\epsilon^c \right]_{\epsilon_1}^{\epsilon_2} + \left[1 + \frac{\epsilon_2 + \epsilon_3}{4} \right] \left[K\epsilon + m \right]_{\epsilon_2}^{\epsilon_3}, \quad (34)$$

Knowing the effect of lateral deformation on the relation between the stress and the strain, the position of neutral axis and the moment of resistance for the cross section of a beam under pure bending can be known.

B. Position of the Neutral Axis.

For a given value of extreme fiber tensile stress σ_t , the corresponding strain ϵ_t equals ϵ_{3t} can be obtained using the true stress true strain diagram. Then, using the fundamental relation that the tensile force = the compressive force in pure bending i.e. $\int_0^{\epsilon_{3t}} \sigma_t dA = \int_0^{\epsilon_{3c}} \sigma_c \cdot dA$ and substituting $dA = Bdy = B\rho d\epsilon$ as shown

previously

$$\int_0^{\epsilon_t} B\rho\sigma_t d\epsilon = \int_0^{\epsilon_c} B\rho\sigma_c d\epsilon \quad (35)$$

Substituting the value of σ_t and σ_c as given in equations (33) and (34) to take care of the lateral deformation

$$\int B \rho \left[(a\epsilon)_0^{\epsilon_{1t}} + \left(1 - \frac{\epsilon_{1t} + \epsilon_{2t}}{4}\right) (b\epsilon^c)_{\epsilon_{1t}}^{\epsilon_{2t}} + \left(1 - \frac{\epsilon_{2t} + \epsilon_{3t}}{4}\right) (K\epsilon + m)_{\epsilon_{2t}}^{\epsilon_{3t}} \right] d\epsilon$$

$$= \int B \rho \left[(a\epsilon)_0^{\epsilon_{1c}} + \left(1 + \frac{\epsilon_{1c} + \epsilon_{2c}}{4}\right) (b\epsilon^c)_{\epsilon_{1c}}^{\epsilon_{2c}} + \left(1 + \frac{\epsilon_{2c} + \epsilon_{3c}}{4}\right) (K\epsilon + m)_{\epsilon_{2c}}^{\epsilon_{3c}} \right] d\epsilon \quad (36)$$

In the above equation ρ cancelled from both sides since the curvature is the same practically for the tension and compression sides. Also B cancelled for constant width section or its value in terms of ρ , ϵ_3 and ϵ can be substituted for variable width cross section as shown later where ϵ = longitudinal strain at the layer whose width is considered, $\epsilon_3 = \epsilon_{3t}$ which is known from the given stress σ_{3t} for the tension side or $\epsilon_3 = \epsilon_{3c}$ required on the compression side. The values a , b , c , k , m , ϵ_1 , and ϵ_2 are known as properties of the material.

Assume for simplicity of computation with negligible error that the

value of the factor $\left[1 + \frac{\epsilon_{2c} + \epsilon_{3c}}{4} \right] = \left[1 + \frac{\epsilon_{2c} + \epsilon_{3t}}{4} \right]$; this will not change the factor materially. Then from the above equation (36)

the value of ϵ_{3c} the unknown can be easily determined and consequently

$$\text{the value } y_t = D \times \frac{\epsilon_{3t}}{\epsilon_{3t} + \epsilon_{3c}} \quad (37)$$

where y_t = distance of neutral axis from extreme tension surface,

D = depth of the cross section. Therefore the position of the neutral

axis can be determined. The same procedure can be applied to get the

position of the neutral axis for any given fiber in tensile strain

whose value lies between ϵ_1 up to the longitudinal strain at the

failure of the material in tension.

C. The Moment of Resistance.

Since the internal moment = the external moment then the value of moment of resistance as derived before is:

$$M_t = \frac{D^2}{(\epsilon_t + \epsilon_c)^2} \cdot \left[\int_0^{\epsilon_t} B \sigma_t \epsilon d\epsilon + \int_0^{\epsilon_c} B \sigma_c \epsilon d\epsilon \right] \quad (38)$$

For any given extreme tensile stress σ_{3t} , the value ϵ_{3t} is known from the true stress-true strain diagram and the position of the neutral axis is known as previously discussed; therefore ϵ_{3c} is known. Introducing the values of σ_t and σ_c where the effect of lateral deformations are considered as shown in equations (33) and (34) in the above equation (38) then the moment of resistance will be:

$$M_t = \frac{D^2}{(\epsilon_t + \epsilon_c)^2} \left\{ \int B \epsilon \left[(a\epsilon)_0^{\epsilon_{1t}} + \left(1 - \frac{\epsilon_{1t} + \epsilon_{2t}}{4}\right) (b\epsilon^c)_{\epsilon_{1t}}^{\epsilon_{2t}} + \left(1 - \frac{\epsilon_{2t} + \epsilon_{3t}}{4}\right) (K\epsilon + m)_{\epsilon_{2t}}^{\epsilon_{3t}} \right] d\epsilon \right. \\ \left. + \int B \epsilon \left[(a\epsilon)_0^{\epsilon_{1c}} + \left(1 + \frac{\epsilon_{1c} + \epsilon_{2c}}{4}\right) (b\epsilon^c)_{\epsilon_{1c}}^{\epsilon_{2c}} + \left(1 + \frac{\epsilon_{2c} + \epsilon_{3c}}{4}\right) (K\epsilon + m)_{\epsilon_{2c}}^{\epsilon_{3c}} \right] d\epsilon \right\}. \quad (39)$$

In the right hand side of this equation every term is known therefore the moment of resistance can easily be obtained noting that the integrations needed in the computation are of a very simple type.

5. Application of the New Method for Various Cross Sections.

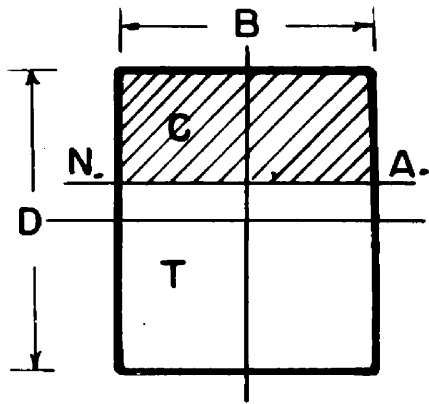
The values of σ_t and σ_c in the following discussions are the values of σ where the effect of lateral deformation is taken into consideration, as given by equations (33) and (34) as follows:

$$\sigma_t = \left[a\epsilon \right]_0^{\epsilon_1} + \left[1 - \frac{\epsilon_1 + \epsilon_2}{4} \right] \left[b\epsilon^c \right]_{\epsilon_1}^{\epsilon_2} + \left[1 - \frac{\epsilon_2 + \epsilon_3}{4} \right] \left[K\epsilon + m \right]_{\epsilon_2}^{\epsilon_3} \\ \sigma_c = \left[a\epsilon \right]_0^{\epsilon_1} + \left[1 + \frac{\epsilon_1 + \epsilon_2}{4} \right] \left[b\epsilon^c \right]_{\epsilon_1}^{\epsilon_2} + \left[1 + \frac{\epsilon_2 + \epsilon_3}{4} \right] \left[K\epsilon + m \right]_{\epsilon_2}^{\epsilon_3}.$$

A. Rectangular Cross Section (Fig. 34)

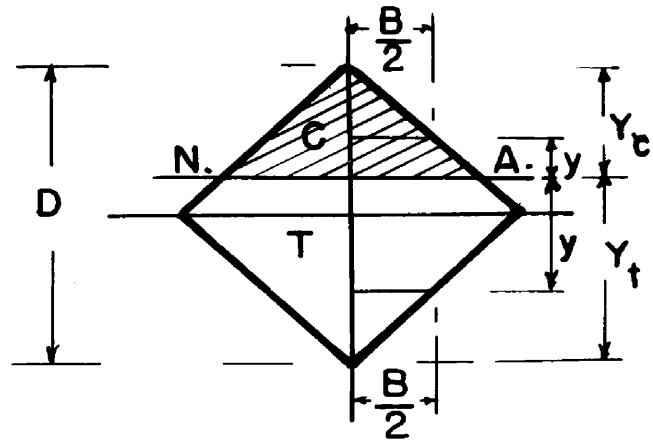
a. Position of Neutral Axis:

$$\int_0^{\epsilon_t} \sigma_t \cdot dA = \int_0^{\epsilon_c} \sigma_c \cdot dA, \\ \int \sigma dA = \int \sigma B dy = \int \sigma B \rho d\epsilon, \\ B \rho \int_0^{\epsilon_t} \sigma_t d\epsilon = B \rho \int_0^{\epsilon_c} \sigma_c d\epsilon, \\ \int_0^{\epsilon_t} \sigma_t \cdot d\epsilon = \int_0^{\epsilon_c} \sigma_c \cdot d\epsilon. \quad (40)$$



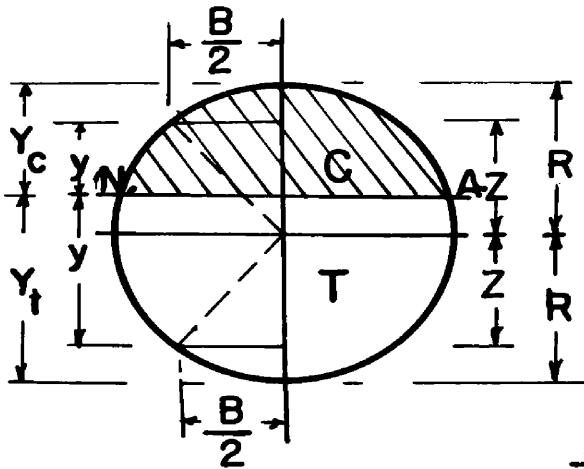
RECTANGLE

C = COMPRESSION

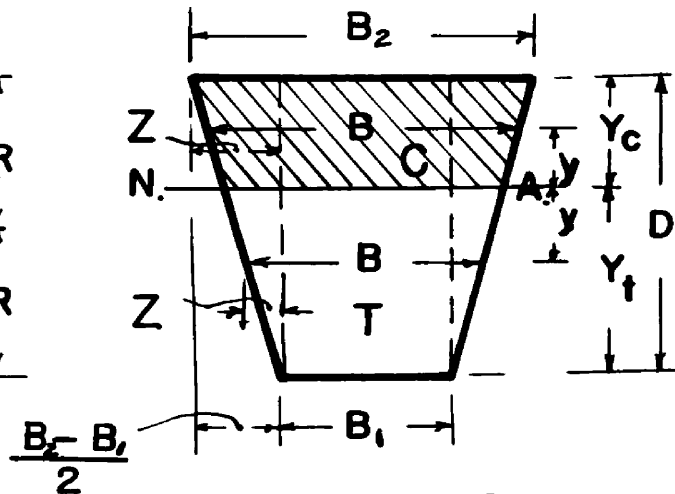


SQUARE ON EDGE

T = TENSION



CIRCLE



TRAPEZOID

FIG.34- CROSS SECTIONS IN PURE BENDING

Therefore for given σ_t i.e. ϵ_t , the value ϵ_c is known and the position of neutral axis can be located.

b. Moment of Resistance

The value of moment of resistance as shown before equals:

$$M_t = \frac{D^2}{(\epsilon_t + \epsilon_c)^2} \cdot \left[\int_0^{\epsilon_t} B \sigma_t \epsilon d\epsilon + \int_0^{\epsilon_c} B \sigma_c \epsilon d\epsilon \right] .$$

Since $B = \text{constant}$

$$M_t = \frac{BD^2}{(\epsilon_t + \epsilon_c)^2} \cdot \left[\int_0^{\epsilon_t} \sigma_t \epsilon d\epsilon + \int_0^{\epsilon_c} \sigma_c \epsilon d\epsilon \right] . \quad (41)$$

For a given σ_t , ϵ_t is known from the true stress-true strain diagram and ϵ_c is known from equation (40), therefore the value of moment of resistance is known by substituting the values of the terms of the right hand side of the above equation and computing the shown simple integration. As a special case of the rectangle, the moment of resistance of a square cross section will be:

$$M_t = \frac{D^3}{(\epsilon_t + \epsilon_c)^2} \cdot \left[\int_0^{\epsilon_t} \sigma_t \epsilon d\epsilon + \int_0^{\epsilon_c} \sigma_c \epsilon d\epsilon \right] . \quad (42)$$

B. Square on Edge. (Fig. 34)

a. Position of neutral axis:

Referring to Fig. 34 we have: for the tension side

$$\begin{aligned} \frac{B}{2} &= (y_t - y) \\ B &= 2(y_t - y) = 2(\epsilon_t - \epsilon) . \end{aligned} \quad (43)$$

Similarly for the compression side:

$$B = 2(\epsilon_c - \epsilon) . \quad (44)$$

$$\int \sigma \cdot dA = \int B \rho \sigma \cdot d\epsilon = 2\rho^2 \left[\epsilon_c \text{ or } t \int \sigma \cdot d\epsilon - \int \sigma \epsilon \cdot d\epsilon \right].$$

$$\text{Since } \int_0^{\epsilon_t} \sigma_t \cdot dA = \int_0^{\epsilon_c} \sigma_c \cdot dA$$

$$\text{Therefore } \epsilon_t \int_0^{\epsilon_t} \sigma_t \cdot d\epsilon - \int_0^{\epsilon_t} \sigma_t \epsilon \cdot d\epsilon = \epsilon_c \int_0^{\epsilon_c} \sigma_c \cdot d\epsilon - \int_0^{\epsilon_c} \sigma_c \epsilon \cdot d\epsilon. \quad (45)$$

For a given σ_t i.e. ϵ_t , then ϵ_c is known and the position of the neutral axis is determined.

b. Moment of Resistance

$$M_t = \frac{D^2}{(\epsilon_t + \epsilon_c)^2} \cdot \left[\int_0^{\epsilon_t} B \sigma_t \epsilon \cdot d\epsilon + \int_0^{\epsilon_c} B \sigma_c \epsilon \cdot d\epsilon \right].$$

$$\text{Since } B = 2\rho (\epsilon_t \text{ or } c - \epsilon) = \frac{2D}{(\epsilon_t + \epsilon_c)} \cdot (\epsilon_t \text{ or } c - \epsilon), \quad (46)$$

$$M_t = \frac{2D^3}{(\epsilon_t + \epsilon_c)^3} \cdot \left\{ \left[\epsilon_t \int_0^{\epsilon_t} \sigma_t \epsilon \cdot d\epsilon - \int_0^{\epsilon_t} \sigma_t \epsilon^2 \cdot d\epsilon \right] + \left[\epsilon_c \int_0^{\epsilon_c} \sigma_c \epsilon \cdot d\epsilon - \int_0^{\epsilon_c} \sigma_c \epsilon^2 \cdot d\epsilon \right] \right\}. \quad (47)$$

Since for a given σ_t , every term on the right side is known; $\therefore M_t$ can be determined.

C. Trapezoidal Cross Section.

a. Position of the neutral axis

Referring to Fig. 3/4 we have:

$$Z_t = \frac{B_2 - B_1}{2} \cdot \frac{Y_t - y}{D}$$

$$2Z_t = \frac{B_2 - B_1}{(\epsilon_t + \epsilon_c)} \cdot (\epsilon_t - \epsilon)$$

$$B_t = B_1 + 2Z_t = B_1 + \frac{B_2 - B_1}{(\epsilon_t + \epsilon_c)} \cdot (\epsilon_t - \epsilon)$$

$$B_t = \frac{I}{(\epsilon_t + \epsilon_c)} \cdot [B_1 \epsilon_t + B_1 \epsilon_c + B_2 \epsilon_t - B_1 \epsilon_t - (B_2 - B_1) \epsilon]$$

$$B_t = \frac{I}{(\epsilon_t + \epsilon_c)} \cdot [(B_1 \epsilon_c + B_2 \epsilon_t) - (B_2 - B_1) \cdot \epsilon] \quad (48)$$

Also $B_c = B_1 + 2Z_c$ where $Z_c = \frac{B_2 - B_1}{2} \cdot \frac{y_t + y}{D} = \frac{B_2 - B_1}{2(\epsilon_t + \epsilon_c)} (\epsilon_t + \epsilon)$

$$B_c = B_1 + \frac{B_2 - B_1}{\epsilon_t + \epsilon_c} \cdot (\epsilon_t + \epsilon)$$

And similarly to B_t , B_c will be:

$$B_c = \frac{I}{(\epsilon_t + \epsilon_c)} \cdot [(B_1 \epsilon_c + B_2 \epsilon_t) + (B_2 - B_1) \cdot \epsilon] \quad (49)$$

$$\begin{aligned} \int_0^{\epsilon_t} \sigma_x dA &= \int_0^{\epsilon_t} B_x \cdot \rho \cdot \sigma_t d\epsilon \\ &= \frac{\rho}{(\epsilon_t + \epsilon_c)} \cdot \left[(B_1 \epsilon_c + B_2 \epsilon_t) \cdot \int_0^{\epsilon_t} \sigma_t d\epsilon - (B_2 - B_1) \cdot \int_0^{\epsilon_t} \sigma_t \cdot \epsilon d\epsilon \right] \end{aligned}$$

Therefore the position of the neutral axis can be obtained from the

equation: $\int_0^{\epsilon_t} \sigma_x \cdot dA = \int_0^{\epsilon_c} \sigma_c \cdot dA$, or

$$\begin{aligned} &(B_1 \epsilon_c + B_2 \epsilon_t) \cdot \int_0^{\epsilon_t} \sigma_t d\epsilon - (B_2 - B_1) \cdot \int_0^{\epsilon_t} \sigma_t \cdot \epsilon d\epsilon \\ &= (B_1 \epsilon_c + B_2 \epsilon_t) \cdot \int_0^{\epsilon_c} \sigma_c d\epsilon + (B_2 - B_1) \int_0^{\epsilon_c} \sigma_c \cdot \epsilon d\epsilon \end{aligned} \quad (50)$$

For a given σ_t , the value of ϵ_c can be obtained from the equation

which determine the position of the neutral axis.

b. Moment of Resistance

We have

$$M_t = \frac{D^2}{(\epsilon_t + \epsilon_c)^2} \cdot \left[\int_0^{\epsilon_t} B_t \sigma_t \epsilon d\epsilon + \int_0^{\epsilon_c} B_c \sigma_c \epsilon d\epsilon \right]$$

$$B_t = \frac{I}{(\epsilon_t + \epsilon_c)} \cdot [(B_1 \epsilon_c + B_2 \epsilon_t) - (B_2 - B_1) \cdot \epsilon]$$

$$\text{Also } B_c = \frac{1}{(\epsilon_t + \epsilon_c)} \cdot [(B_1 \epsilon_c + B_2 \epsilon_t) + (B_2 - B_1) \cdot \epsilon]$$

$$M_t = \frac{D^2}{(\epsilon_t + \epsilon_c)^3} \cdot \left\{ \left[(B_1 \epsilon_c + B_2 \epsilon_t) \cdot \int_0^{\epsilon_t} \sigma_t \cdot \epsilon \, d\epsilon - (B_2 - B_1) \cdot \int_0^{\epsilon_t} \sigma_t \cdot \epsilon^2 \cdot d\epsilon \right] + \right. \\ \left. + \left[(B_1 \epsilon_c + B_2 \epsilon_t) \cdot \int_0^{\epsilon_c} \sigma_c \cdot \epsilon \, d\epsilon + (B_2 - B_1) \cdot \int_0^{\epsilon_c} \sigma_c \cdot \epsilon^2 \cdot d\epsilon \right] \right\}, \quad (51)$$

For a given σ_t , ϵ_t and ϵ_c are known and also all the terms of the right side of the above equation can be easily computed; therefore moment of resistance is determined.

D. Circular Cross Section.

a. Position of the neutral axis

Referring to Fig. 34 we have for the tension side: $Z = (R + y - y_t)$

$$\frac{B}{2} = \sqrt{R^2 - Z^2} = \sqrt{R^2 - (R + y - y_t)^2} \\ = \sqrt{2Ry_t + 2yy_t - 2Ry - y^2 - y_t^2}.$$

$$B_t = 2 \sqrt{2R(y_t - y) - (y_t^2 - 2yy_t + y^2)} \\ = 2 \sqrt{2R(y_t - y) - (y_t - y)^2} = 2\sqrt{(y_t - y)(2R - y_t + y)}$$

$$= 2 \sqrt{\rho(\epsilon_t - \epsilon) \cdot \rho[(\epsilon_t + \epsilon_c) - \epsilon_t + \epsilon]}$$

$$= 2 \rho \sqrt{(\epsilon_t - \epsilon)(\epsilon_c + \epsilon)}$$

$$= 2 \rho \sqrt{\epsilon_t \epsilon_c + \epsilon(\epsilon_t - \epsilon_c) - \epsilon^2},$$

$$B_t = 2 \rho \sqrt{\epsilon_t \epsilon_c} \left\{ 1 - \left[\frac{\epsilon^2 - \epsilon(\epsilon_t - \epsilon_c)}{\epsilon_t \epsilon_c} \right] \right\}^{\frac{1}{2}}, \quad (52)$$

Using the Binomial theorem then:

$$B_t = 2l \sqrt{\epsilon_t \epsilon_c} \left\{ 1 - \frac{\frac{1}{2}}{1!} \left[\frac{\epsilon^2 - \epsilon(\epsilon_t - \epsilon_c)}{\epsilon_t \epsilon_c} \right] + \frac{\frac{1}{2}(\frac{1}{2}-1)}{2!} \left[\frac{\epsilon^2 - \epsilon(\epsilon_t - \epsilon_c)}{\epsilon_t \epsilon_c} \right]^2 - \dots \right\}.$$

Neglecting the 3rd term of the binomial and over

$$B_t = 2l \sqrt{\epsilon_t \epsilon_c} \left\{ 1 - \left[\frac{\epsilon^2 - \epsilon(\epsilon_t - \epsilon_c)}{2 \epsilon_t \epsilon_c} \right] \right\}. \quad (53)$$

Similarly for the compression side:

$$B_c = 2l \sqrt{\epsilon_t \epsilon_c} \left\{ 1 - \left[\frac{\epsilon^2 - \epsilon(\epsilon_c - \epsilon_t)}{2 \epsilon_t \epsilon_c} \right] \right\}. \quad (54)$$

Using the relation $\int_0^{\epsilon_t} \sigma_t \cdot dA = \int_0^{\epsilon_c} \sigma_c \cdot dA$

to get position of the neutral axis we have:

$$\int_0^{\epsilon_t} \sigma_t \cdot dA = \int_0^{\epsilon_t} B \rho \sigma_t d\epsilon = 2l^2 \sqrt{\epsilon_t \epsilon_c} \cdot \left[\int_0^{\epsilon_t} \sigma_t \cdot d\epsilon - \frac{1}{2\epsilon_t \epsilon_c} \int_0^{\epsilon_t} \sigma_t \cdot \epsilon^2 d\epsilon + \frac{(\epsilon_t - \epsilon_c)}{2\epsilon_t \epsilon_c} \int_0^{\epsilon_t} \sigma_t \cdot \epsilon \cdot d\epsilon \right].$$

Therefore:

$$\begin{aligned} & \int_0^{\epsilon_t} \sigma_t d\epsilon + \frac{(\epsilon_t - \epsilon_c)}{2\epsilon_t \epsilon_c} \int_0^{\epsilon_t} \sigma_t \cdot \epsilon d\epsilon - \frac{1}{2\epsilon_t \epsilon_c} \int_0^{\epsilon_t} \sigma_t \cdot \epsilon^2 d\epsilon \\ &= \int_0^{\epsilon_c} \sigma_c d\epsilon + \frac{(\epsilon_c - \epsilon_t)}{2\epsilon_t \epsilon_c} \int_0^{\epsilon_c} \sigma_c \cdot \epsilon d\epsilon - \frac{1}{2\epsilon_t \epsilon_c} \int_0^{\epsilon_c} \sigma_c \cdot \epsilon^2 d\epsilon. \end{aligned} \quad (55)$$

For a given σ_t , ϵ_t is known, therefore ϵ_c can be computed from the above equation. Then the position of the neutral axis is determined.

b. Moment of Resistance

$$M_t = \frac{D^2}{(\epsilon_t + \epsilon_c)^2} \cdot \left[\int_0^{\epsilon_t} B_t \sigma_t \epsilon d\epsilon + \int_0^{\epsilon_c} B_c \sigma_c \epsilon d\epsilon \right].$$

The values of B_t and B_c having the form shown in equations (53) and (54)

$$\begin{aligned}
\int_0^{\epsilon_t} B_x \sigma_t \epsilon d\epsilon &= 2\rho \left\{ \sqrt{\epsilon_t \epsilon_c} \cdot \int_0^{\epsilon_t} \sigma_t \epsilon d\epsilon + \frac{\epsilon_t - \epsilon_c}{2\sqrt{\epsilon_t \epsilon_c}} \cdot \int_0^{\epsilon_t} \sigma_t \cdot \epsilon^2 d\epsilon - \right. \\
&\quad \left. - \frac{1}{2\sqrt{\epsilon_t \epsilon_c}} \cdot \int_0^{\epsilon_t} \sigma_t \cdot \epsilon^3 d\epsilon \right\} \\
&= \frac{2D}{(\epsilon_t + \epsilon_c)} \times \left[\text{same above expression} \right] \\
M_t &= \frac{2D^3}{(\epsilon_t + \epsilon_c)^3} \cdot \left\{ \left[\sqrt{\epsilon_t \epsilon_c} \cdot \int_0^{\epsilon_t} \sigma_t \epsilon d\epsilon + \frac{\epsilon_t - \epsilon_c}{2\sqrt{\epsilon_t \epsilon_c}} \cdot \int_0^{\epsilon_t} \sigma_t \cdot \epsilon^2 d\epsilon - \right. \right. \\
&\quad \left. \left. - \frac{1}{2\sqrt{\epsilon_t \epsilon_c}} \cdot \int_0^{\epsilon_t} \sigma_t \cdot \epsilon^3 d\epsilon \right] + \left[\sqrt{\epsilon_t \epsilon_c} \cdot \int_0^{\epsilon_c} \sigma_c \epsilon d\epsilon + \right. \right. \\
&\quad \left. \left. + \frac{\epsilon_c - \epsilon_t}{2\sqrt{\epsilon_t \epsilon_c}} \cdot \int_0^{\epsilon_c} \sigma_c \cdot \epsilon^2 d\epsilon - \frac{1}{2\sqrt{\epsilon_t \epsilon_c}} \cdot \int_0^{\epsilon_c} \sigma_c \cdot \epsilon^3 d\epsilon \right] \right\}. \quad (56)
\end{aligned}$$

For a given value of σ_t , ϵ_t , and ϵ_c are known as before; then introducing the value of σ_t and σ_c in terms of ϵ where the effect of lateral deformation is taken into account as previously shown, the integrals can be computed and moment of resistance can be determined.

6. Theoretical Application of the New Method to Beams of Square Cross Sections in Pure Bending for Different Materials.

Computations for the position of the neutral axis and the moment of resistance for beams of square cross sections of different materials in pure bending were carried out using the new method to show its validity and the behavior of these materials in the pure bending. The materials discussed are: (1) Mild steel (2) Stainless steel (3) Aluminum and (4) Magnesium. A sample computation for one material will be given, then followed by the result of computations for the four materials using the data of tension and compression tests from the outside specimens and the inside specimens for the relations between the stress σ and the strain ϵ shown in Tables 3, 4, 5 and 6.

A. Sample Computation for Mild Steel.

The relation between the stress and the strain is taken for this sample as obtained experimentally for the inside tension and the inside compression specimens using Figures 11, 12, 13 and 14 as shown in Table 3. The expression used in computation for each state of stress--elastic, elastic plastic, and plastic--will be shown, and calculations will be given for one point in each state.

a. Position of neutral axis

1. Elastic state , $\epsilon_t = 0$ to $\epsilon_t = 0.0011$,

$$\sigma_t = 29.6 \times 10^6 \cdot \epsilon \quad , \quad \sigma_c = 30 \times 10^6 \cdot \epsilon$$

$$\int_0^{\epsilon_t} \sigma_t \cdot d\epsilon = \int_0^{\epsilon_c} \sigma_c \cdot d\epsilon$$

Practically, the shift of the neutral axis is very small and can be neglected. Therefore there is no appreciable change in position of the neutral axis in the elastic state, and the neutral axis remains at the centroid of the cross section.

2. Elastic plastic state (i) $\epsilon_t = 0.0011$ to $\epsilon_t = 0.020$,

$$\int_{0.0011}^{\epsilon_t} \left(1 - \frac{0.0011 + \epsilon_t}{4}\right) \sigma_t \, d\epsilon = \int_{0.0011}^{\epsilon_c} \left(1 + \frac{0.0011 + \epsilon_t}{4}\right) \cdot \sigma_c \, d\epsilon$$

$$\sigma_t = 192000 \, \epsilon + 32000$$

$$\sigma_c = 220000 \, \epsilon + 32500$$

$$\int_{0.0011}^{\epsilon_t} \left(1 - \frac{0.0011 + \epsilon_t}{4}\right) (192000 \, \epsilon + 32000) \cdot d\epsilon$$

$$= \int_{0.0011}^{\epsilon_c} \left(1 - \frac{0.0011 + \epsilon_t}{4}\right) (220000 \, \epsilon + 32500) \cdot d\epsilon$$

$$\left(1 - \frac{0.0011 + \epsilon_t}{4}\right) (9.6 \, \epsilon_t^2 + 3.2 \, \epsilon_t - 0.003532)$$

$$= \left(1 + \frac{0.0011 + \epsilon_t}{4}\right) (11 \, \epsilon_c^2 + 3.25 \, \epsilon_c - 0.003588)$$

Using the above equation, for any given value of ϵ_t --which corresponds to a certain value of the σ_t , extreme tensile stress,--the value of ϵ_c the extreme compressive strain can be calculated.

Take the extreme tensile strain $\epsilon_t = 0.010$ which corresponds to σ_t from the true stress true strain diagram to $\sigma_t = 33,000$ psi.

Then:

$$\left(1 - \frac{0.0011 + \epsilon_t}{4}\right) = \left(1 - \frac{0.0011 + 0.010}{4}\right) = 0.9972$$

$$\left(1 + \frac{0.0011 + \epsilon_t}{4}\right) = \left(1 + \frac{0.0011 + 0.010}{4}\right) = 1.0028$$

$$0.9972 (9.6 \times 0.01^2 + 3.2 \times 0.01 - 0.003532) = 1.0028 (11 \epsilon_c^2 + 3.25 \epsilon_c - 0.003588)$$

$$11.02 \epsilon_c^2 + 3.26 \epsilon_c - (0.000957 + 0.0319 - 0.003525 + 0.0036) = 0$$

$$11.02 \epsilon_c^2 + 3.26 \epsilon_c - 0.032932 = 0$$

$$\epsilon_c = \frac{-3.26 + \sqrt{(3.26)^2 - 4 \times 11.02 \times 0.032932}}{2 \times 11.02}$$

$$= \frac{-3.26 + 3.4799}{22.04}$$

$$\epsilon_c = 0.00995.$$

$$Y_t = \text{distance of neutral axis from the tension side} = \frac{\epsilon_t}{\epsilon_c + \epsilon_t} \cdot D$$

$$= \frac{0.010}{0.00995 + 0.010} \cdot D = 0.502 D \quad \text{where } D = \text{depth of cross section}$$

$$\text{Shift of neutral axis towards compression side} = 0.002 D$$

3. Elastic plastic state (ii) $\epsilon_t = 0.02$ to $\epsilon_t = 0.19$

$$\sigma_t = 137.5 \times 10^3 \cdot \epsilon^{0.349}$$

$$\sigma_c = 117.5 \times 10^3 \cdot \epsilon^{0.283}$$

$$\int_{0.0011}^{0.02} \left(1 - \frac{0.0011 + 0.02}{4}\right) (192000 \epsilon + 32000) d\epsilon + \int_{0.02}^{\epsilon_t} \left(1 - \frac{0.02 + \epsilon_t}{4}\right) (137.5 \times 10^3 \cdot \epsilon^{0.349}) d\epsilon$$

$$= \int_{0.0011}^{0.02} \left(1 + \frac{0.0011 + 0.02}{4}\right) (220000 \epsilon + 32500) d\epsilon + \int_{0.02}^{\epsilon_c} \left(1 + \frac{0.02 + \epsilon_t}{4}\right) (117.5 \times 10^3 \cdot \epsilon^{0.283}) d\epsilon$$

$$\left(1 - \frac{0.0011 + 0.02}{4}\right) = 0.9947 \quad \& \quad \left(1 + \frac{0.0011 + 0.02}{4}\right) = 1.0053$$

$$\therefore 0.9947 \left(\frac{192000}{2} \epsilon^2 + 32000 \epsilon \right)_{0.0011}^{0.02} + \left(1 - \frac{0.02 + \epsilon_t}{4}\right) \left(\frac{137.5}{1.349} \cdot \epsilon^{1.349} \times 10^3 \right)_{0.02}^{\epsilon_t}$$

$$= 1.0053 \left(\frac{220000}{2} \epsilon^2 + 32500 \epsilon \right)_{0.0011}^{0.02} + \left(1 + \frac{0.02 + \epsilon_t}{4}\right) \left(\frac{117.5}{1.283} \epsilon^{1.283} \times 10^3 \right)_{0.02}^{\epsilon_c}$$

$$\therefore 0.9947 (96 \times 0.00039879 + 32 \times 0.0189) + \left(1 - \frac{0.02 + \epsilon_t}{4}\right) (102 \epsilon_t^{1.349} - 0.523)$$

$$= 1.0053 (110 \times 0.00039879 + 32.5 \times 0.0189) + \left(1 + \frac{0.02 + \epsilon_t}{4}\right) (91.6 \epsilon_c^{1.283} - 0.615)$$

Therefore :

$$0.64 + \left(1 - \frac{0.02 + \epsilon_t}{4}\right) (102 \epsilon_t^{1.349} - 0.523)$$

$$= 0.662 + \left(1 + \frac{0.02 + \epsilon_t}{4}\right) (91.6 \epsilon_c^{1.283} - 0.615)$$

For $\epsilon_t = 0.14$ which corresponds to $\sigma_t = 67,000$ psi.

$$\left(1 - \frac{0.02 + 0.14}{4}\right) = (1 - 0.04) = 0.96$$

$$\left(1 + \frac{0.02 + 0.14}{4}\right) = (1 + 0.04) = 1.04$$

$$102 \times 0.14^{1.349} = 7.2.$$

$$\text{Therefore: } 0.64 + 0.96 (7.2 - 0.523) = 0.662 + 1.04 (91.6 \epsilon_c^{1.283} - 0.615)$$

$$0.64 + 0.96 \times 6.677 - 0.662 - 0.64 = 95.3 \epsilon_c^{1.283} = 7.028$$

$$\epsilon_c^{1.283} = \frac{7.028}{95.3} = 0.0738$$

$$\log \epsilon_c = \frac{\log 0.0738}{1.283} = \frac{\bar{2}.8681}{1.283} = \frac{-1.1319}{1.283} = -0.884 = \bar{1}.116$$

$$\epsilon_c = 0.1306$$

$$Y_t = \frac{\epsilon_t}{\epsilon_t + \epsilon_c} \cdot D = \frac{0.14}{0.14 + 0.1306} \cdot D = \frac{0.14}{0.2706} \cdot D = 0.518 D.$$

∴ Shift of neutral axis towards compression side = 0.018 D.

4. Plastic state $\epsilon_t = 0.19$ $\epsilon_c = 1.13$

$$\sigma_t = 60,000 \epsilon + 60,000$$

$$\sigma_c = 60,000 \epsilon + 60,000$$

$$\begin{aligned} & \int_{0.0011}^{0.02} \left(1 - \frac{0.0011 + 0.02}{4}\right) (192000 \epsilon + 32000) d\epsilon + \int_{0.02}^{0.19} \left(1 - \frac{0.02 + 0.19}{4}\right) (137.5 \times 10^3 \epsilon^{0.349}) d\epsilon + \\ & \quad + \int_{0.19}^{\epsilon_c} \left(1 - \frac{0.19 + \epsilon_t}{4}\right) (60000 \epsilon + 60000) d\epsilon \\ & = \int_{0.0011}^{0.02} \left(1 + \frac{0.0011 + 0.02}{4}\right) (220000 \epsilon + 32500) d\epsilon + \int_{0.02}^{0.19} \left(1 + \frac{0.02 + 0.19}{4}\right) (117.5 \times 10^3 \epsilon^{0.283}) d\epsilon + \\ & \quad + \int_{0.19}^{\epsilon_c} \left(1 + \frac{0.19 + \epsilon_t}{4}\right) (60000 \epsilon + 60000) d\epsilon. \end{aligned}$$

Therefore

$$\begin{aligned} & 0.64 + 9.8 + \left(1 - \frac{0.19 + \epsilon_t}{4}\right)(30 \epsilon_t^2 + 60 \epsilon_t - 12.48) \\ &= 0.662 + 10.8 + \left(1 + \frac{0.19 + \epsilon_t}{4}\right)(30 \epsilon_c^2 + 60 \epsilon_c - 12.48) \end{aligned}$$

i.e.

$$\begin{aligned} & \left(1 - \frac{0.19 + \epsilon_t}{4}\right)(30 \epsilon_t^2 + 60 \epsilon_t - 12.48) \\ &= \left(1 + \frac{0.19 + \epsilon_t}{4}\right)(30 \epsilon_c^2 + 60 \epsilon_c - 12.48) + 1.022. \end{aligned}$$

For $\epsilon_t = 0.6$ which corresponds to $\sigma_t = 95,000$ psi

$$\left(1 - \frac{0.19 + 0.6}{4}\right) = 0.8025 \quad \text{and} \quad \left(1 + \frac{0.09 + 0.6}{4}\right) = 1.1975.$$

Therefore

$$0.8025(30 \times 0.6^2 + 60 \times 0.6 - 12.48) = 1.1975(30 \epsilon_c^2 + 60 \epsilon_c - 12.48) + 1.022$$

$$34.32 = 35.92 \epsilon_c^2 + 71.85 \epsilon_c - 14.95 + 1.022$$

$$35.92 \epsilon_c^2 + 71.85 \epsilon_c - 41.478 = 0$$

$$\epsilon_c = -1 + \sqrt{1 + \frac{2 \times 41.478}{71.85}} = -1 + 1.468 = 0.468.$$

$$Y_t = \text{distance of the neutral axis from the tension side} = \frac{\epsilon_t}{\epsilon_t + \epsilon_c} \cdot D$$

$$= \frac{0.6}{0.6 + 0.468} \cdot D = 0.562 D.$$

∴ Shift of the neutral axis towards compression side = 0.062 D.

b. Moment of Resistance

1. Elastic state $\epsilon_t = 0$ to $\epsilon_t = 0.0011$

$$\sigma_t = 29.6 \times 10^6 \cdot \epsilon \quad \text{and} \quad \sigma_c = 30 \times 10^6 \cdot \epsilon.$$

Since σ_t and σ_c are about the same in the elastic state, take

$$\sigma_t = \sigma_c = 29.8 \times 10^6 \cdot \epsilon \quad \text{and therefore} \quad \epsilon_t = \epsilon_c = \epsilon$$

$$M = \frac{D^3}{(\epsilon_t + \epsilon_c)^2} \cdot \left[\int_0^{\epsilon_t} \sigma_t \cdot \epsilon \, d\epsilon + \int_0^{\epsilon_c} \sigma_c \cdot \epsilon \, d\epsilon \right]$$

$$M = \frac{D^3}{(2\epsilon)^2} \cdot 2 \cdot \int_0^{\epsilon} 29.8 \cdot \epsilon^2 \cdot d\epsilon \times 10^6 = \frac{D^3}{2\epsilon^2} \times \frac{29.8 \epsilon^3}{3} \times 10^6$$

$$M = 4.965 \times 10^6 \cdot \epsilon \cdot D^3$$

where D = side of the square cross section

For $\epsilon_t = 0.0011$, $\epsilon_t = \epsilon_c = \epsilon$, $\sigma_t = 32,500$ psi.

Therefore $M = 4.965 \times 10^6 \times 0.0011 \cdot D^3 = 5462 D^3$.

2. Elastic Plastic State (i) $\epsilon_t = 0.0011$ to 0.02

$$\sigma_t = 192,000 \epsilon + 32,000$$

$$\sigma_c = 220,000 \epsilon + 32,500$$

$$M = \frac{D^3}{(\epsilon_t + \epsilon_c)^2} \times 2 \int_0^{0.0011} \sigma \cdot \epsilon \, d\epsilon + \frac{D^3}{(\epsilon_t + \epsilon_c)^2} \left[\int_{0.0011}^{\epsilon_t} \sigma_t \cdot \epsilon \, d\epsilon + \int_{0.0011}^{\epsilon_c} \sigma_c \cdot \epsilon \, d\epsilon \right]$$

$$M = \frac{26.45 \times 10^{-3}}{(\epsilon_t + \epsilon_c)^2} \cdot D^3 + \frac{D^3}{(\epsilon_t + \epsilon_c)^2} \left[\left(1 - \frac{0.0011 + \epsilon_t}{4}\right) \left(\frac{192000}{3} \epsilon_t^3 + \frac{32000}{2} \epsilon_t^2 - 1.9435\right) + \left(1 + \frac{0.0011 + \epsilon_c}{4}\right) \left(\frac{220000}{3} \epsilon_c^3 + \frac{32500}{2} \epsilon_c^2 - 1.9747\right) \right]$$

For $\epsilon_t = 0.010$, $\epsilon_c = 0.00995$ and $\sigma_t = 33,000$ psi, then

$$M = \frac{26.45 \times 10^{-3}}{(0.010 + 0.00995)^2} \cdot D^3 + \frac{D^3}{(0.010 + 0.00995)^2} \left[0.9972 (64000 \times 0.01^3 + 16000 \times 0.01^2 - 1.9435) + 1.0028 (73.3 \times 10^3 \times 0.00995^3 + 16.25 \times 10^3 \times 0.00995^2 - 1.9747) \right]$$

$$M = 66.6 D^3 + \frac{D^3}{3.97} (16400 + 16720) = 66.6 D^3 + 8350 D^3$$

$$M = 8416.6 D^3.$$

3. Elastic Plastic State (ii) $\epsilon_t = 0.02$ to 0.19

$$\sigma_t = 137.5 \times 10^3 \cdot \epsilon^{0.349}$$

$$\sigma_c = 117.5 \times 10^3 \cdot \epsilon^{0.283}$$

$$M = \frac{D^3}{(\epsilon_t + \epsilon_c)^2} \cdot 2 \int_0^{0.011} \sigma \epsilon d\epsilon + \frac{D^3}{(\epsilon_t + \epsilon_c)^2} \left[\int_{0.011}^{0.02} \sigma_t \epsilon d\epsilon + \int_{0.011}^{0.02} \sigma_c \epsilon d\epsilon \right] + \frac{D^3}{(\epsilon_t + \epsilon_c)^2} \left[\int_{0.020}^{\epsilon_t} \sigma_t \epsilon d\epsilon + \int_{0.020}^{\epsilon_c} \sigma_c \epsilon d\epsilon \right]$$

$$M = \frac{26.45 \times 10^{-3}}{(\epsilon_t + \epsilon_c)^2} \cdot D^3 + \frac{13.53}{(\epsilon_t + \epsilon_c)^2} \cdot D^3 + \frac{D^3}{(\epsilon_t + \epsilon_c)^2} \left[\left(1 - \frac{0.02 + \epsilon_t}{4}\right) \times \left(\frac{137.5 \times 10^3}{2.349} \epsilon_t^{2.349} - 5.85\right) + \left(1 + \frac{0.02 + \epsilon_c}{4}\right) \left(\frac{117.5 \times 10^3}{2.283} \epsilon_c^{2.283} - 6.77\right) \right].$$

For $\epsilon_t = 0.10$, $\epsilon_c = 0.0933$ and $\sigma_t = 61,000$ psi

$$M = \frac{26.45 \times 10^{-3}}{(0.10 + 0.0933)^2} \cdot D^3 + \frac{13.53}{(0.10 + 0.0933)^2} \cdot D^3 + \frac{D^3}{(0.10 + 0.0933)^2} \left[0.97 \times \left(58.5 \times 10^3 \times 0.1^{2.349} - 5.85\right) + 1.0284 \left(51.4 \times 10^3 \times 0.0933^{2.283} - 6.77\right) \right]$$

$$M = 0.708 D^3 + 362 D^3 + 12,800 D^3 = 13,162.7 D^3.$$

4. Plastic State $\epsilon_t = 0.19$ to 1.13

$$\sigma_t = 60,000 \epsilon + 60,000 \quad \text{and} \quad \sigma_c = 60,000 \epsilon + 60,000$$

$$\begin{aligned} M &= \frac{D^3}{(\epsilon_t + \epsilon_c)^2} \cdot 2 \cdot \int_0^{0.0011} \sigma \epsilon d\epsilon + \frac{D^3}{(\epsilon_t + \epsilon_c)^2} \cdot \left[\int_{0.0011}^{0.02} \sigma_t \epsilon d\epsilon + \int_{0.0011}^{0.02} \sigma_c \epsilon d\epsilon \right] + \\ &+ \frac{D^3}{(\epsilon_t + \epsilon_c)^2} \cdot \left[\int_{0.02}^{0.19} \sigma_{II_t} \epsilon d\epsilon + \int_{0.02}^{0.19} \sigma_{II_c} \epsilon d\epsilon \right] \\ &+ \frac{D^3}{(\epsilon_t + \epsilon_c)^2} \cdot \left[\int_{0.19}^{\epsilon_t} \sigma_{III_t} \epsilon d\epsilon + \int_{0.19}^{\epsilon_c} \sigma_{III_c} \epsilon d\epsilon \right] \\ M &= \frac{26.45 \times 10^{-3}}{(\epsilon_t + \epsilon_c)^2} \cdot D^3 + \frac{13.53}{(\epsilon_t + \epsilon_c)^2} \cdot D^3 + \frac{2133}{(\epsilon_t + \epsilon_c)^2} \cdot D^3 + \\ &+ \frac{D^3}{(\epsilon_t + \epsilon_c)^2} \cdot \left[\left(1 - \frac{0.19 + \epsilon_t}{4}\right) \left(\frac{60000}{3} \epsilon_t^3 + \frac{60000}{2} \epsilon_t^2 - 1222 \right) + \right. \\ &\quad \left. + \left(1 + \frac{0.19 + \epsilon_c}{4}\right) \left(\frac{60000}{3} \epsilon_c^3 + \frac{60000}{2} \epsilon_c^2 - 1222 \right) \right]. \end{aligned}$$

For $\epsilon_t = 0.8$, $\epsilon_c = 0.578$ and $\sigma_t = 107,000$ psi

$$\begin{aligned} M &= \frac{26.45 \times 10^{-3}}{(0.8 + 0.578)^2} \cdot D^3 + \frac{13.53}{(0.8 + 0.578)^2} \cdot D^3 + \frac{2133}{(0.8 + 0.578)^2} \cdot D^3 + \\ &+ \frac{D^3}{(0.8 + 0.578)^2} \cdot \left[0.7525 (20000 \times 0.8^3 + 30000 \times 0.8^2 - 1222) + \right. \\ &\quad \left. + 1.122 (20000 \times 0.578^3 + 30000 \times 0.578^2 - 1222) \right] \\ M &= 0.014 D^3 + 7.16 D^3 + 1130 D^3 + 19200 D^3 \\ M &= 20337 D^3. \end{aligned}$$

B. Results

Computations as shown in the sample discussed before in (A) were carried out for the four materials: mild steel, stainless steel,

aluminum and magnesium. These were made for different points in each state: elastic, elastic plastic and plastic states using the data of the tension and compression tests shown previously for outside specimens and inside specimens as given in Tables 3, 4, 5 and 6. The results of these computations and the Figure numbers of the graphs showing the relations between σ_t vs M_t , σ_t vs shift of neutral axis, ϵ_t vs M_t , and ϵ_t vs ϵ_c are shown as follows:

| | Figures of the Results | | | |
|------------------------------|------------------------|-----------------|----------|-----------|
| | Mild Steel | Stainless Steel | Aluminum | Magnesium |
| σ_t vs M_t | 35 | 39 | 43 | 47 |
| ϵ_t vs M_t | 36 | 40 | 44 | 48 |
| σ_t vs shift of N.A. | 37 | 41 | 45 | 49 |
| ϵ_t vs ϵ_c | 38 | 42 | 46 | 50 |

7. Experimental Verification of the New Theory.

To verify the new theory, tests were made on beams with square cross sections of mild steel, stainless steel, aluminum and magnesium. These beams were subjected to pure bending by equal loading at two symmetrical points from their center. The test equipment, procedure and test results follow.

A. Test Equipment and Procedure

a. Loading system

The same Riehle machine, Fig. 4, which was used for compression and tension tests, was used for the bending tests to give the load at one point. This load was transferred to the specimen at two points to obtain pure bending by the set up shown in Fig. 51.

EXTREME FIBER TENSILE STRESS
 KSI

THEORETICAL CURVES:

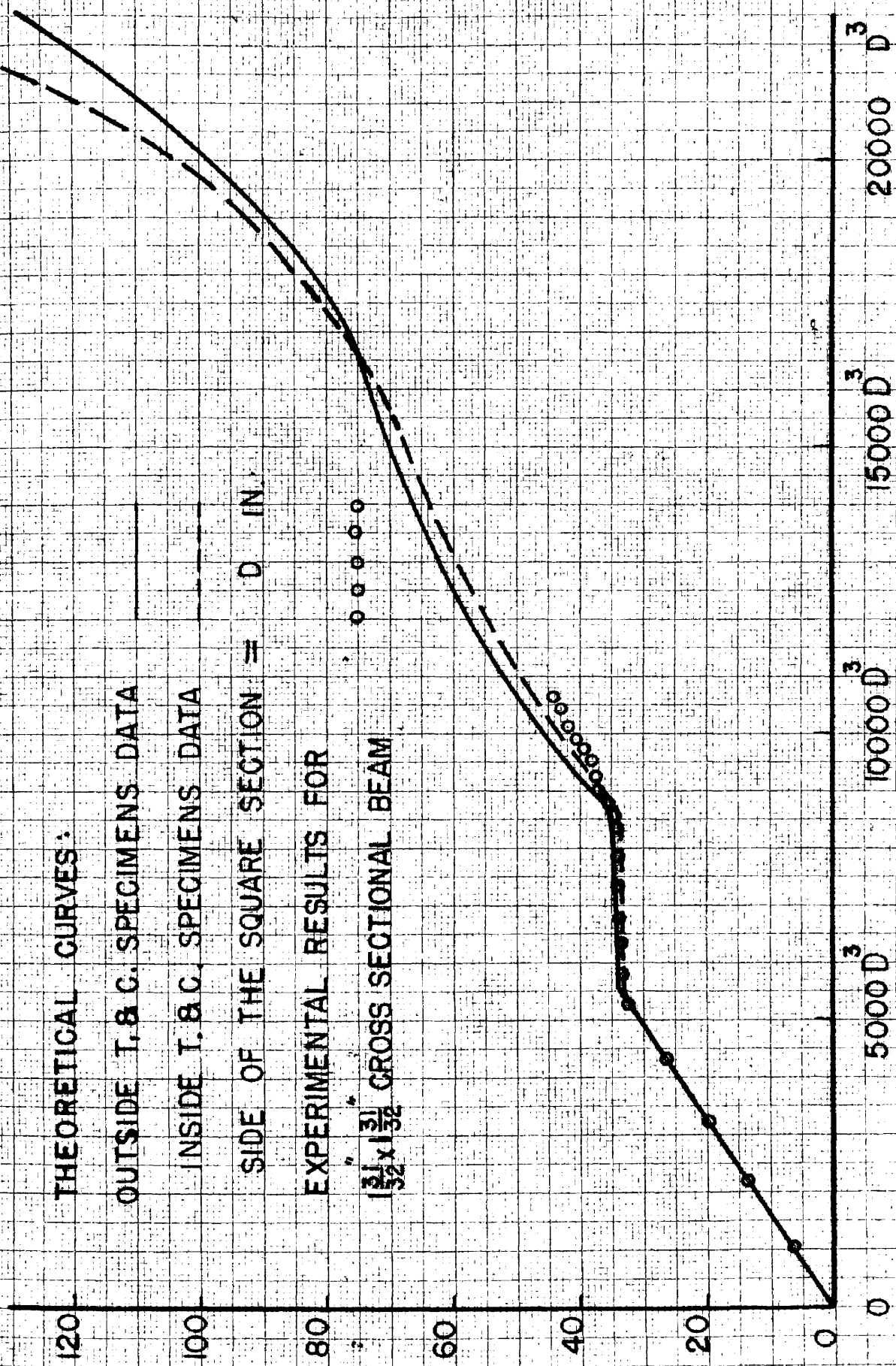
OUTSIDE T. & C. SPECIMENS DATA

INSIDE T. & C. SPECIMENS DATA

SIDE OF THE SQUARE SECTION = D IN.

EXPERIMENTAL RESULTS FOR

$1\frac{31}{32}$ " x $1\frac{31}{32}$ " CROSS SECTIONAL BEAM



MOMENT OF RESISTANCE LB-INS

FIG35— MOMENT OF RESISTANCE VS MAXIMUM TENSILE STRESS
 SQUARE CROSS SECTION OF MILD STEEL

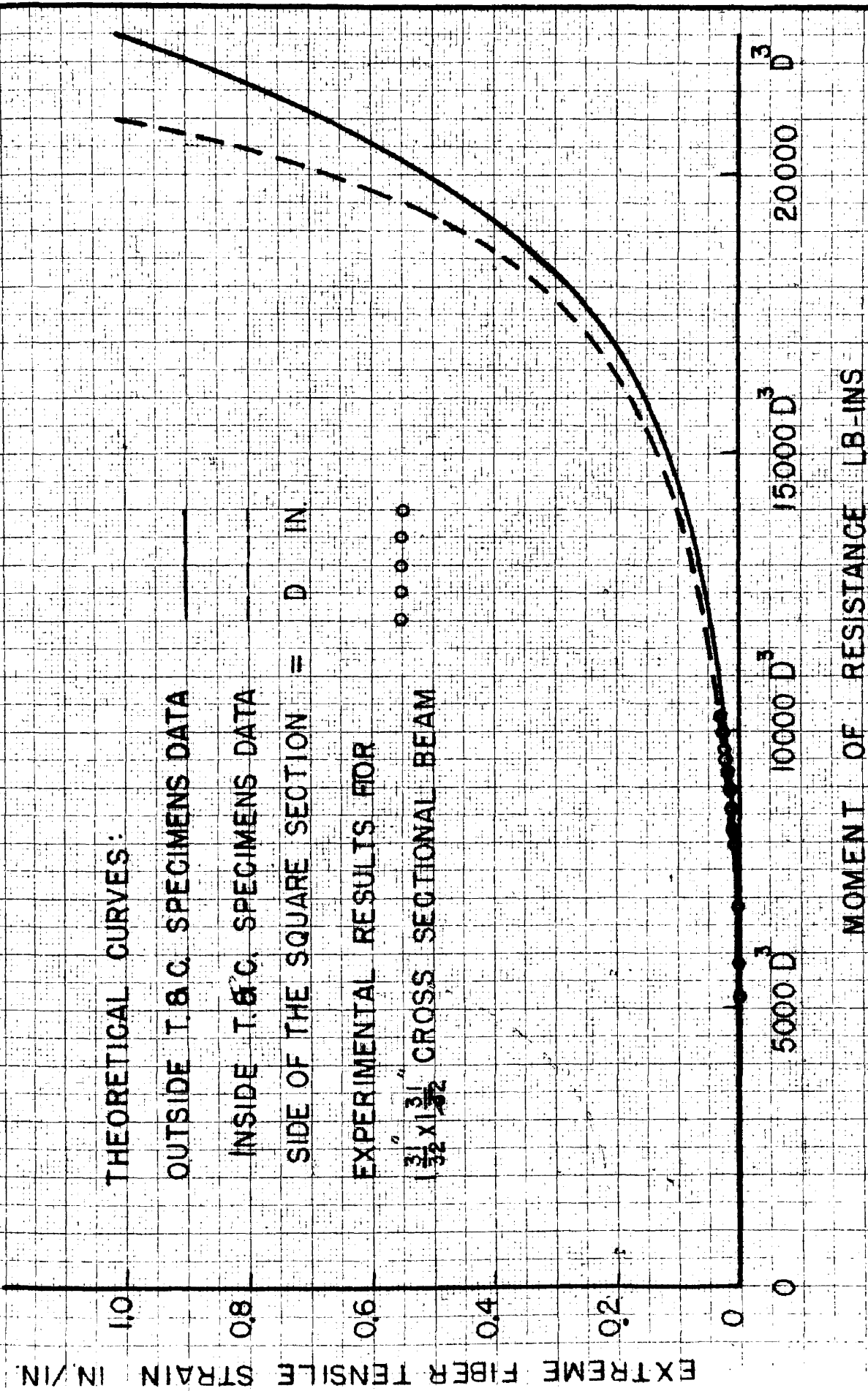


FIG.36-- MOMENT OF RESISTANCE VS MAXIMUM TENSILE STRAIN
 SQUARE CROSS SECTION OF MILD STEEL

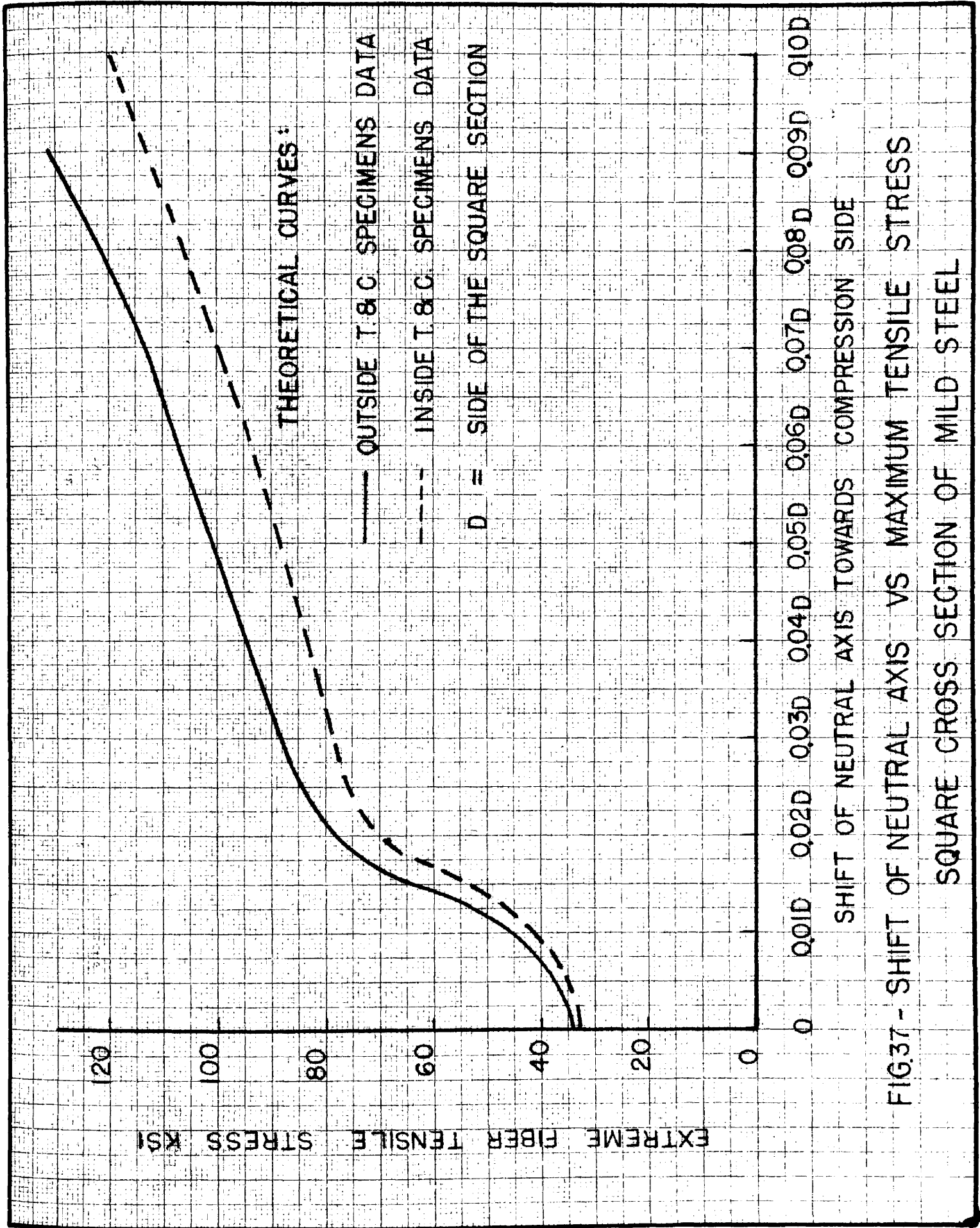


FIG.37 - SHIFT OF NEUTRAL AXIS VS MAXIMUM TENSILE STRESS
 SQUARE CROSS SECTION OF MILD STEEL

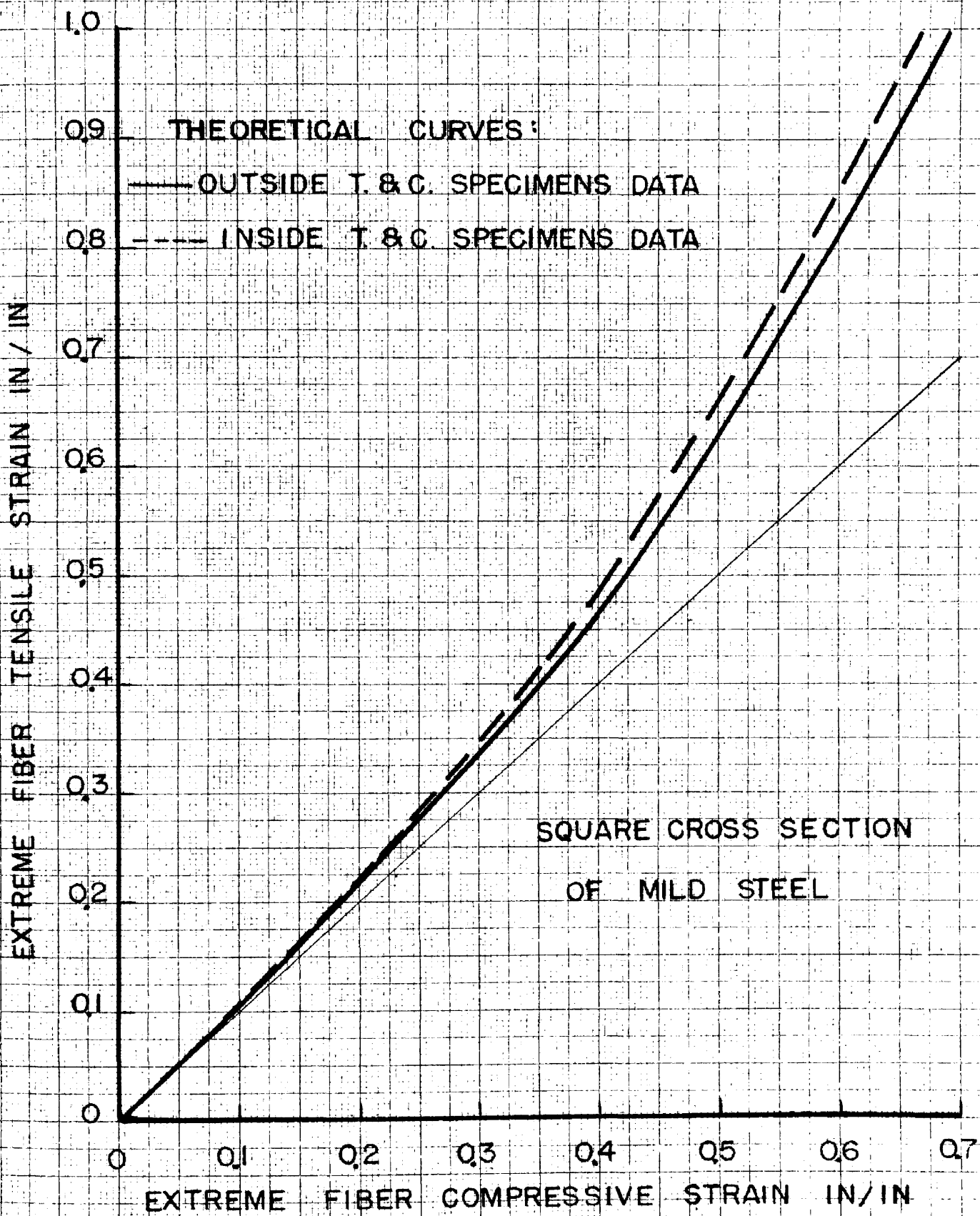


FIG.38- MAXIMUM TENSILE VS MAXIMUM COMPRESSIVE STRAINS

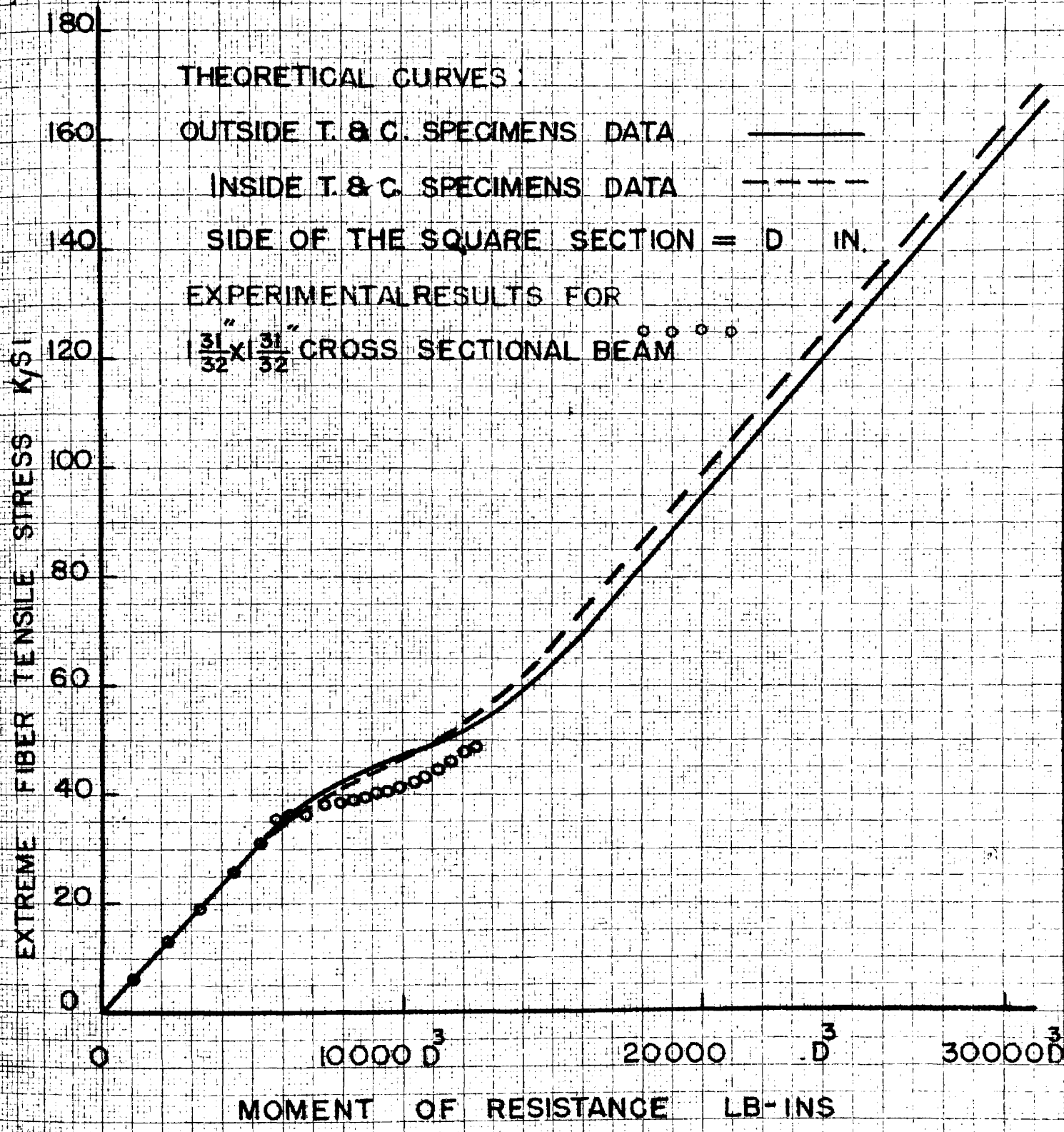


FIG.39- MOMENT OF RESISTANCE VS MAX. TENSILE STRESS
 SQUARE CROSS SECTION OF STAINLESS STEEL

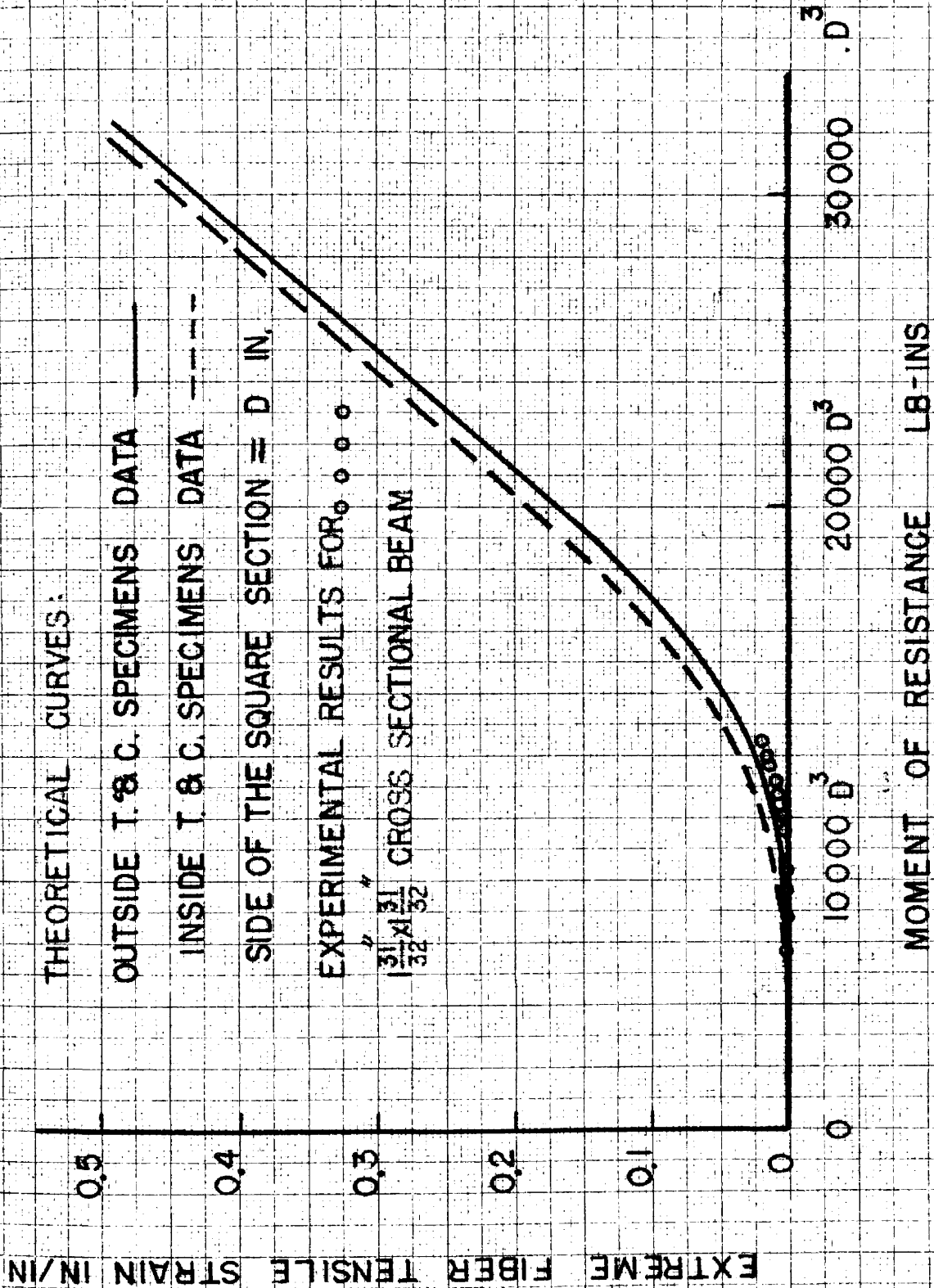
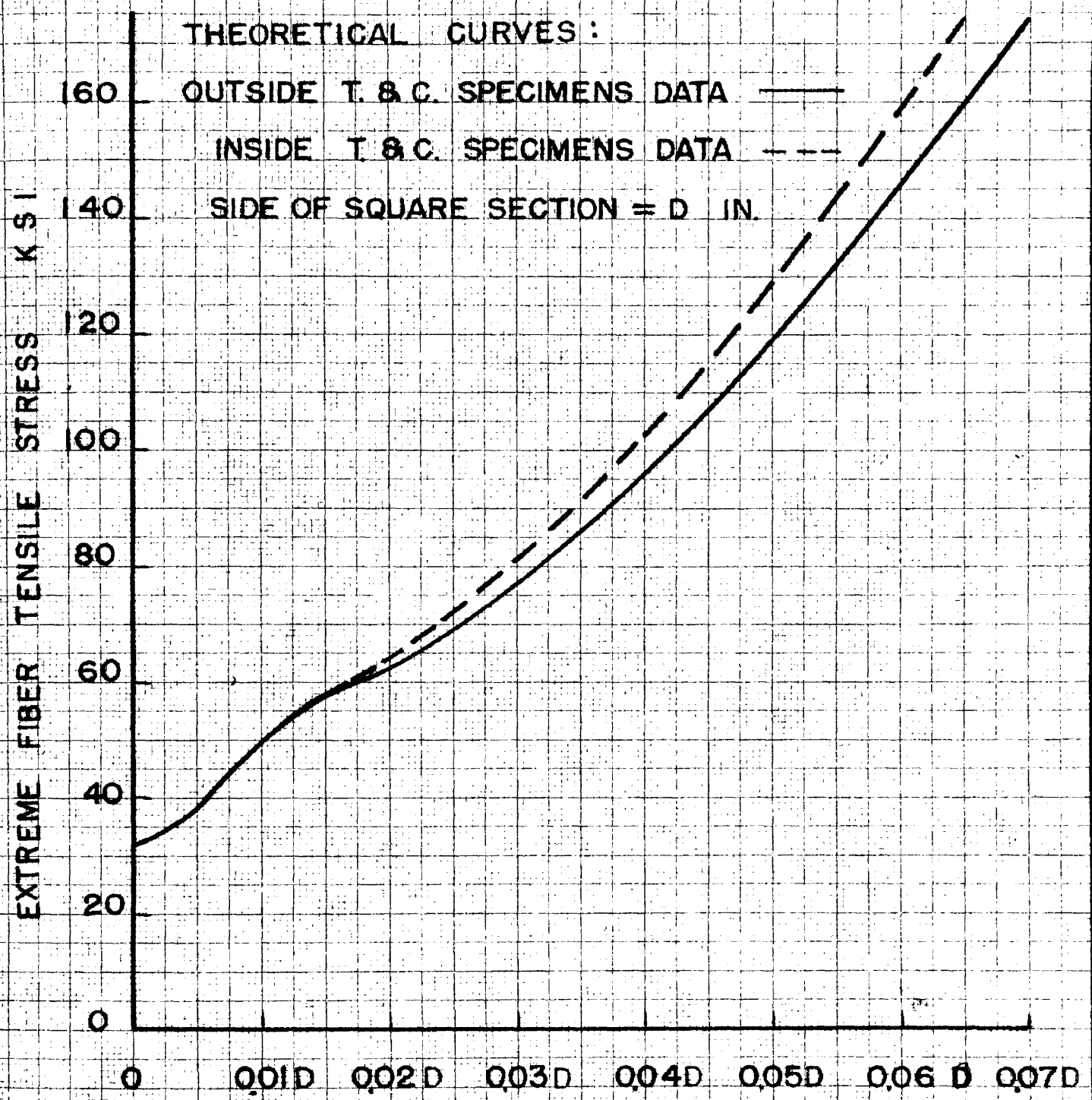


FIG.40- MOMENT OF RESISTANCE VS MAXIMUM TENSILE STRAIN
SQUARE CROSS SECTION OF STAINLESS STEEL



SHIFT OF NEUTRAL AXIS TOWARDS COMPRESSION SIDE

FIG.41 - SHIFT OF NEUTRAL AXIS VS MAX. TENSILE STRESS
SQUARE CROSS SECTION OF STAINLESS STEEL

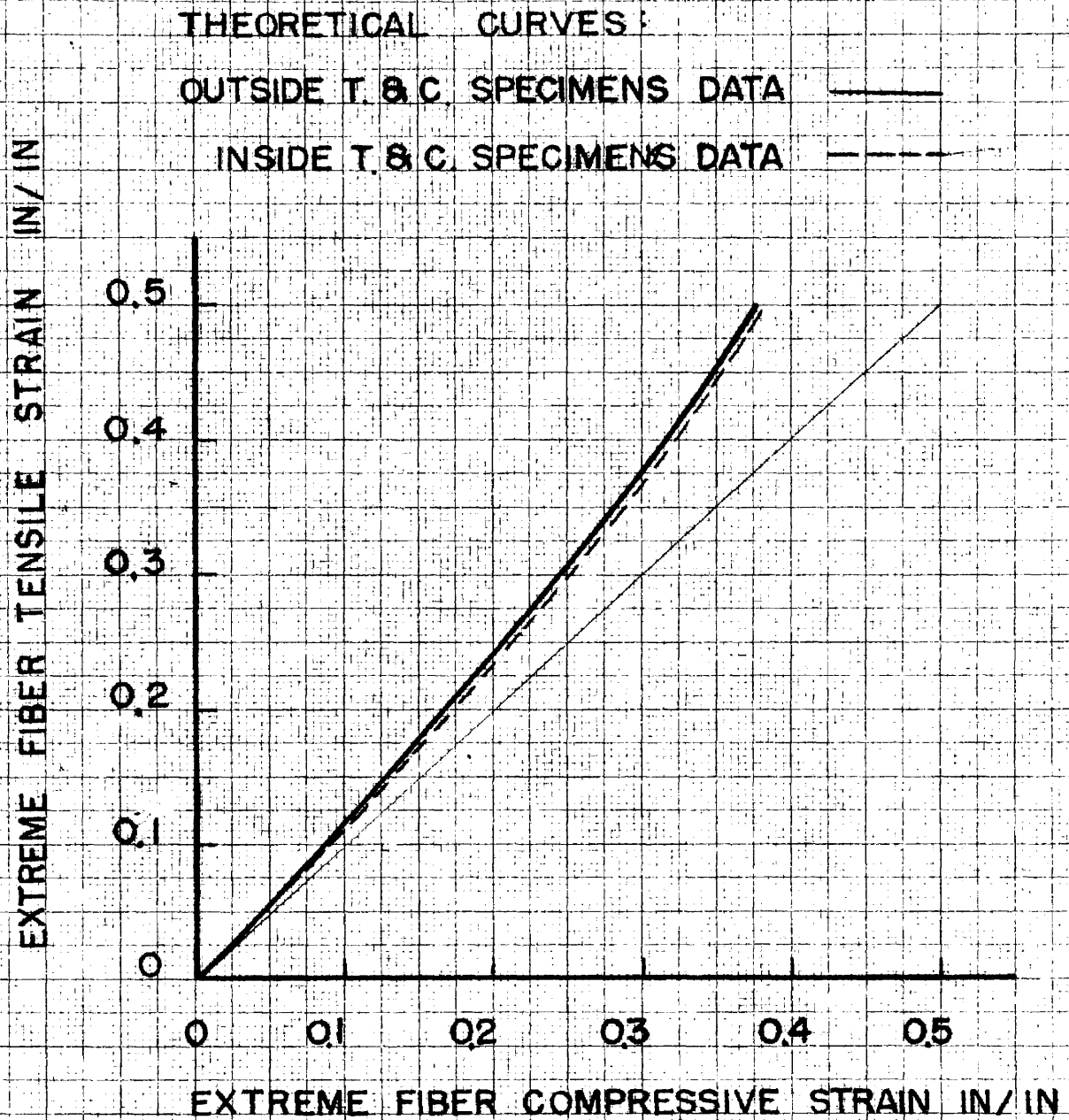


FIG.42 - MAXIMUM TENSILE VS MAX COMPRESSIVE STRAINS

SQUARE CROSS SECTION OF STAINLESS STEEL

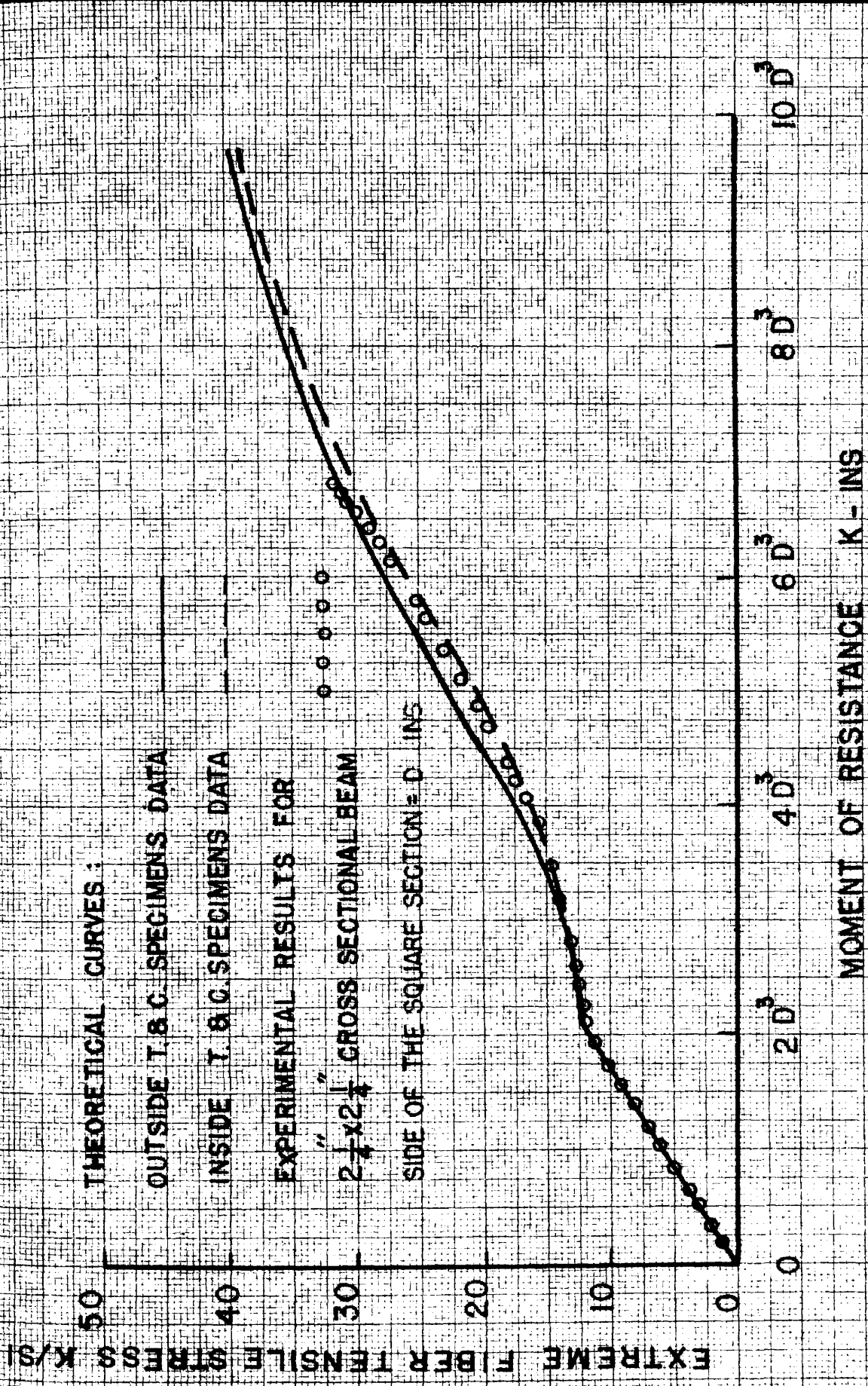


FIG.43 - MOMENT OF RESISTANCE VS MAXIMUM TENSILE STRESS
SQUARE CROSS SECTION OF ALUMINUM

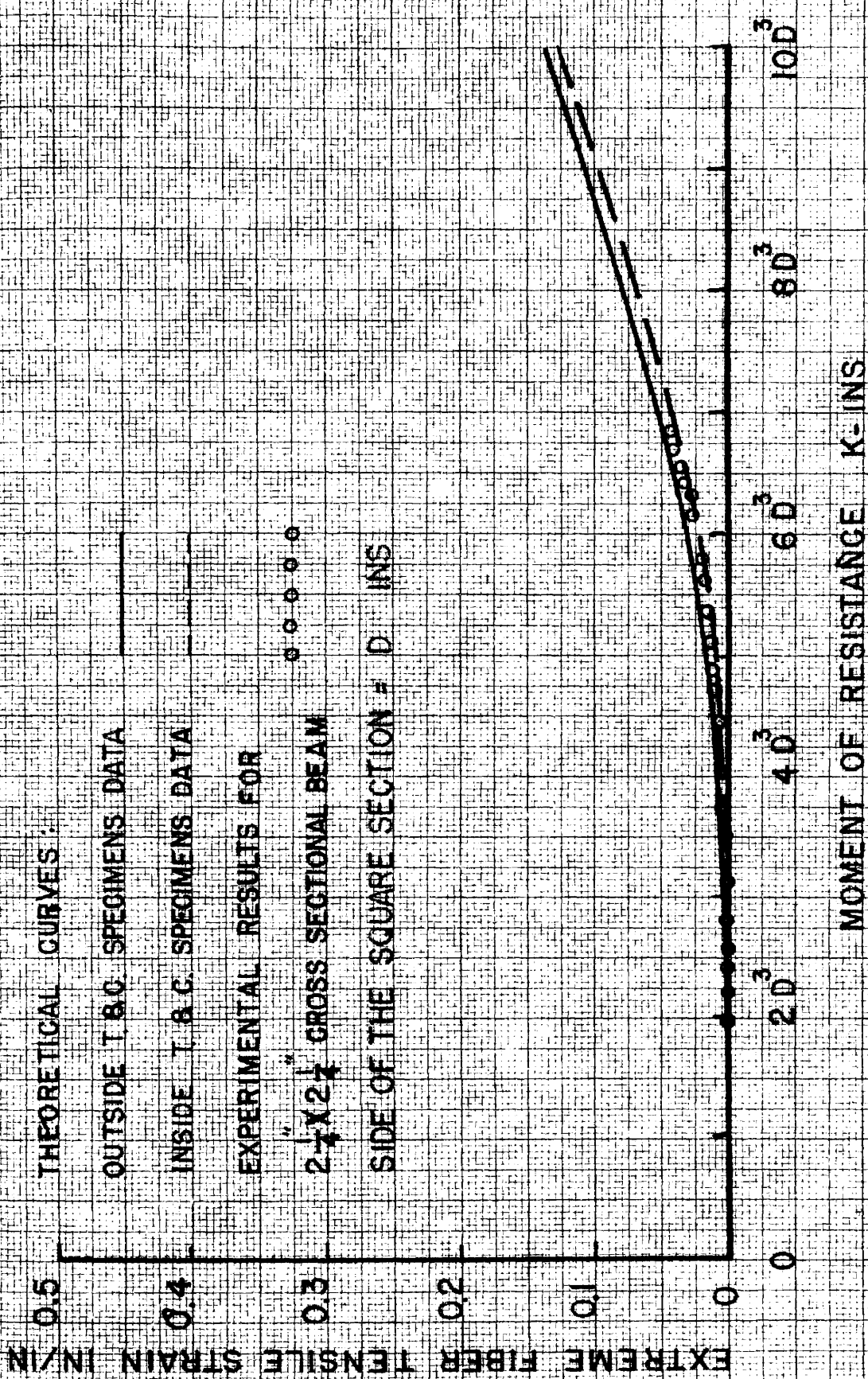
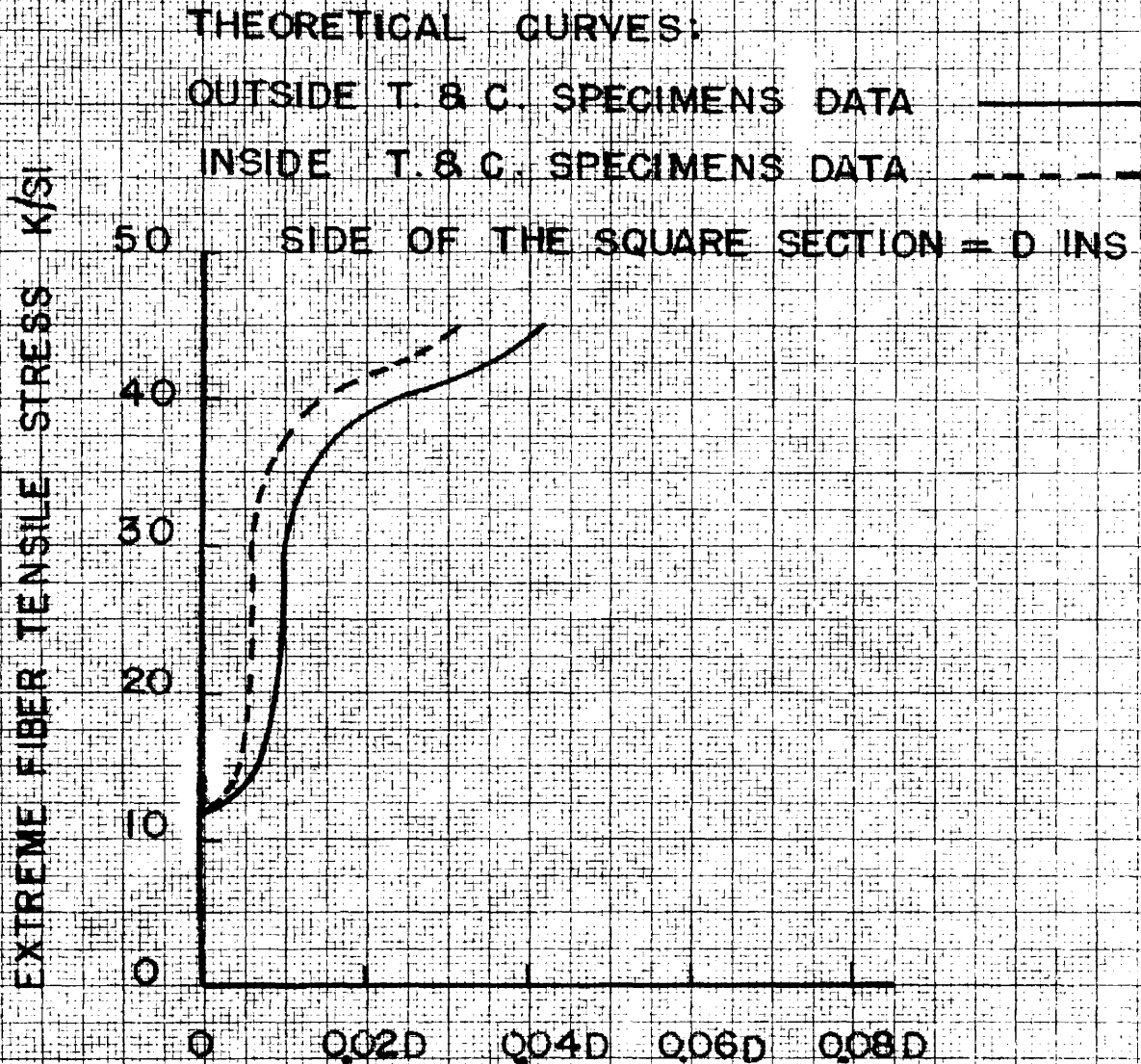


FIG. 4.4 - MOMENT OF RESISTANCE VS MAXIMUM TENSILE STRAIN
SQUARE CROSS SECTION OF ALUMINUM



SHIFT OF NEUTRAL AXIS TOWARDS COMPRESSION SIDE

FIG.45 SHIFT OF NEUTRAL AXIS VS MAX. TENSILE STRESS
 SQUARE CROSS SECTION OF ALUMINUM

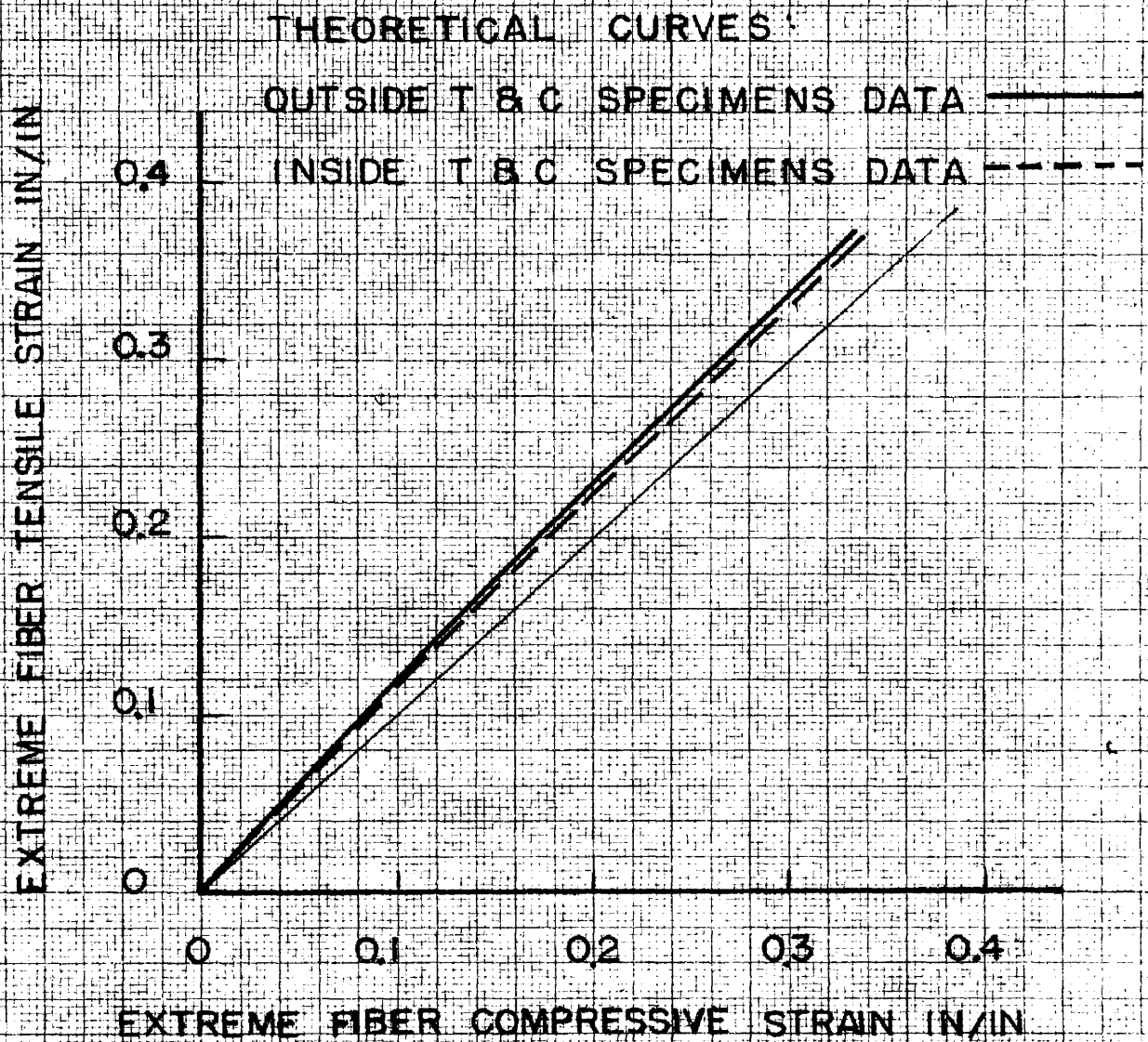


FIG 46 - MAX TENSILE VS MAX COMPRESSIVE STRAINS
SQUARE CROSS SECTION OF ALUMINUM

THEORETICAL CURVES :

OUTSIDE T.&C. SPECIMENS DATA

INSIDE T.&C. SPECIMENS DATA

SIDE OF THE SQUARE SECTION = D IN

EXPERIMENTAL RESULTS

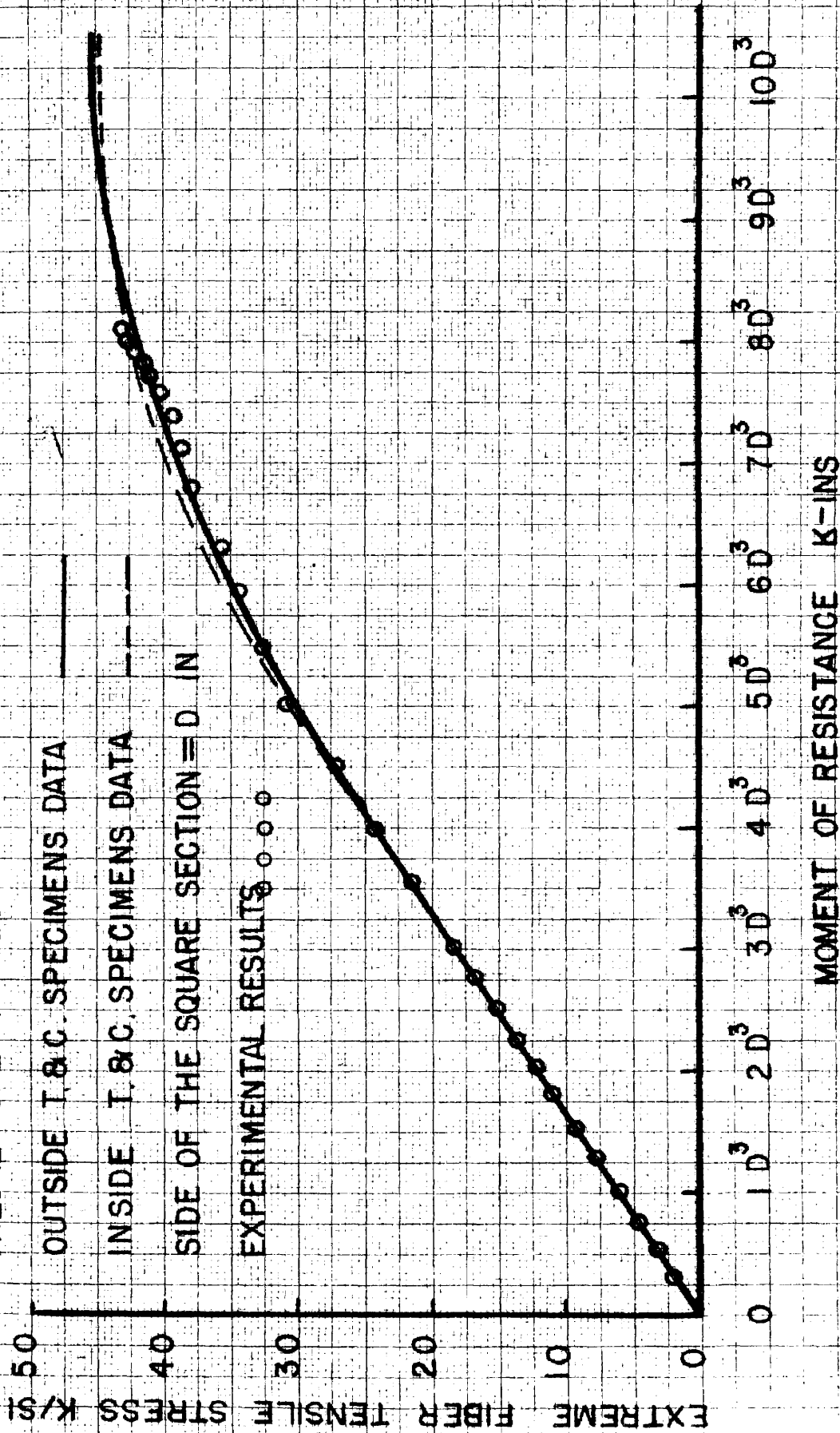


FIG.47 - MOMENT OF RESISTANCE VS MAX. TENSILE STRESS
SQUARE CROSS SECTION OF MAGNESIUM

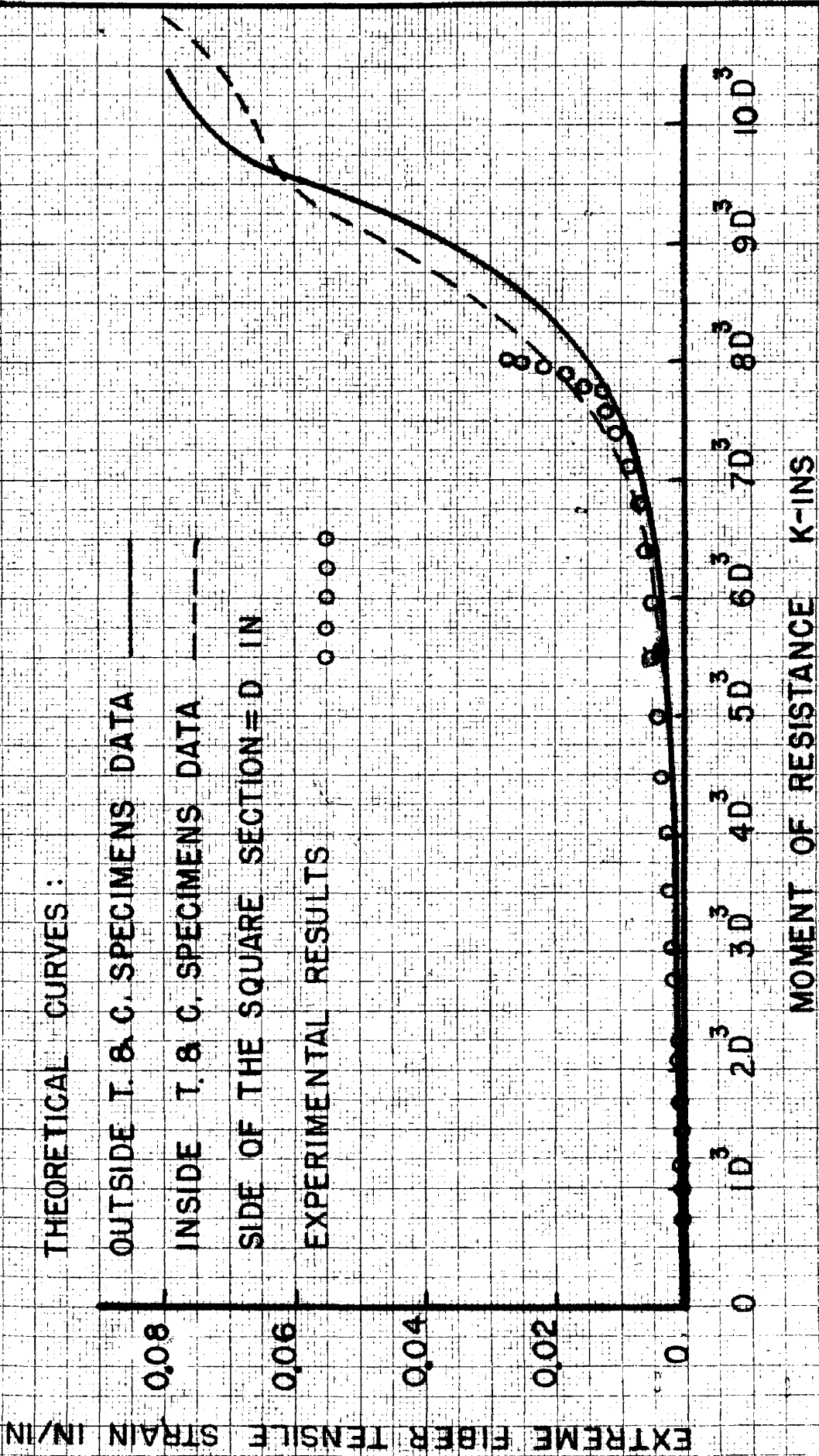


FIG.48 - MOMENT OF RESISTANCE VS MAX TENSILE STRAIN
 SQUARE CROSS SECTION OF MAGNESIUM

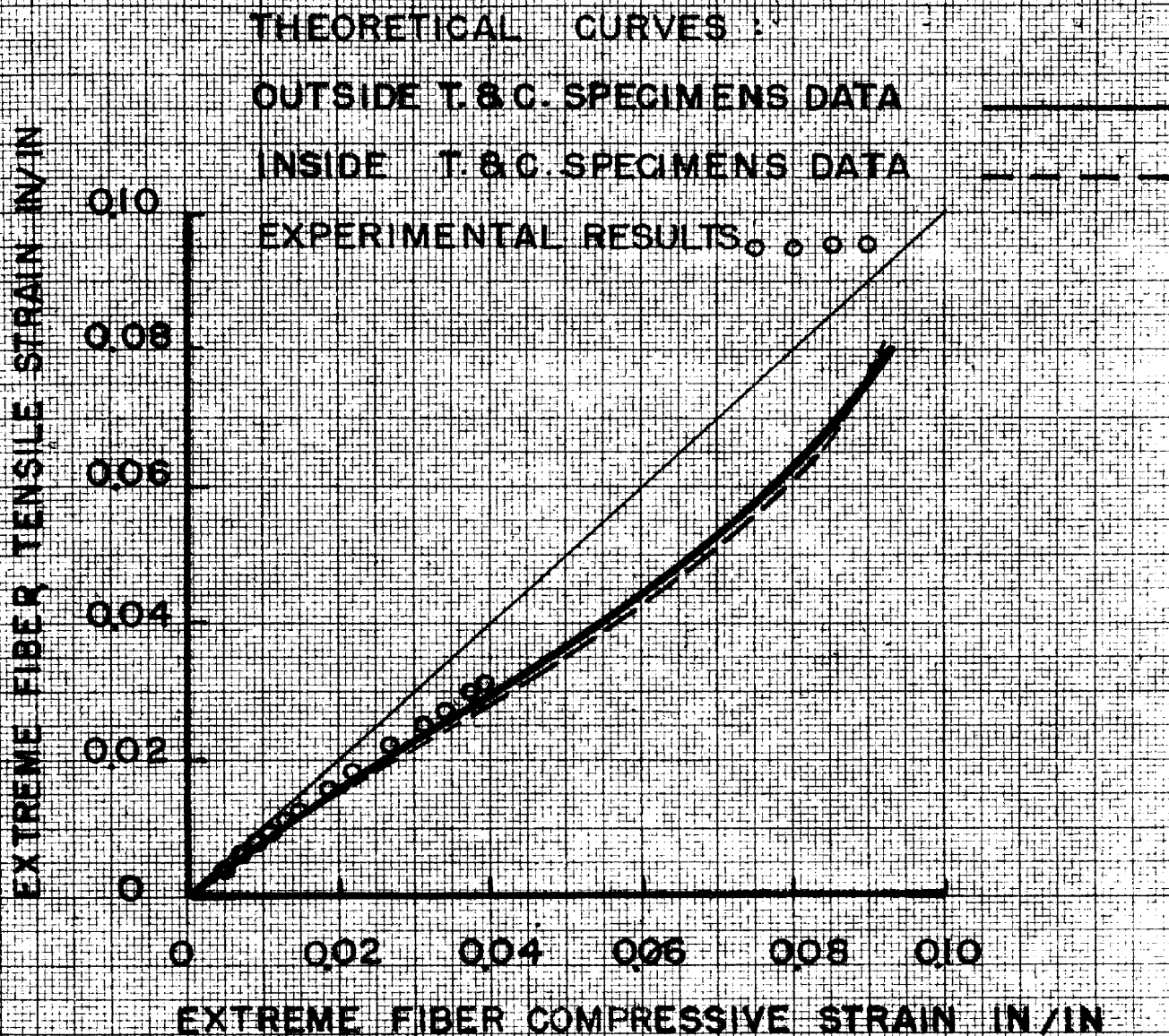


FIG50 - MAX TENSILE VS MAX COMPRESSIVE STRAINS

SQUARE CROSS SECTION OF MAGNESIUM

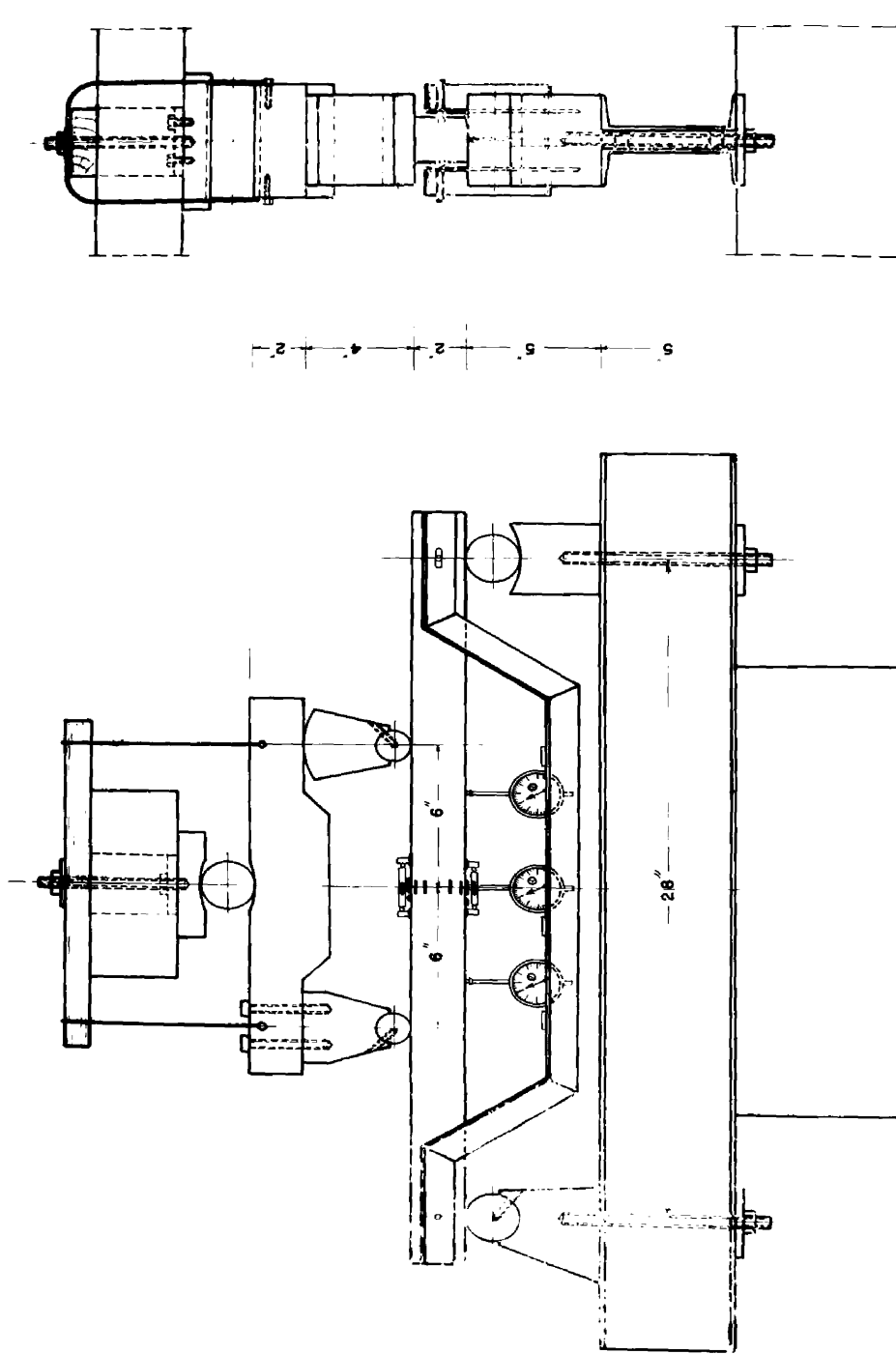


FIG. 51 - BENDING APPARATUS

| | |
|---------------------------------------|----------------|
| DESIGNED & DRAWN : <i>A. M. J. R.</i> | DATE : MAY-12- |
| CHECKED : <i>P. O. J. J.</i> | C-88- |
| APPROVED : <i>A. B. C.</i> | |

b. Specimens

Square cross sectional beams 32" long and about 2" x 2" in cross section were sawed from bars 8 ft. long as shown in Fig. 5. The beam was supported on two free supports with a span of 28" and the loads were applied by free supports at the two points each 6" distant from the center line as shown in Fig. 51.

c. Strain gages

Three types of gages were used:

1. Baldwin SR-4 electrical gages, type A-7, of gage length $\frac{1}{4}$ ", 120 ohms resistance, and gage factor 1.97. Four gages were located on the vertical surface of the central cross section of the beam. Two gages were located on the upper surface of the central cross section one longitudinally and the other laterally. Two gages were located symmetrically on the lower surface of the central section.
2. 17-4 post yield strain gages of 120 ohms resistance. One was located on the upper and the other on the lower surfaces of the central cross section. Both were located longitudinally.
3. Clip gages for measuring high strains as explained in the Appendix, page 203. One gage was placed on the upper surface of the central cross section to measure the longitudinal compressive strains, the other on the lower surface for the longitudinal tensile strains.

The location of gages on the specimen is shown in Fig. 51.

d. Strain Indicator

Two strain indicators were used. One was a Baldwin type K with a range of 30,000 micro inches used for all gages except the clip gages. The other was a Baldwin type K of older design with a range of 10,000 micro inches, used for the clip gages only.

e. Strain Range Extender

This was a system of resistances, made by Baldwin, which could be attached to the strain indicator to divide the readings by five. Therefore the range of measuring strains is extended five times i.e. strains can be measured up to 15 % deformation. This range extender, the strain indicator and the specimen under load in the machine are shown in Fig. 52.

f. Ames Dials

Three dials were used to measure the deflections at the central point and at two points each 4 inches distant from the center. Each dial had a minimum reading of 0.001 inch and maximum reading of about 1.00 inch. A reading of 0.0001 inch can be read approximately. These dials were fixed on a frame which rested freely on pins through the center of the cross sections of the beam at its supporting points as shown in Fig. 51.

g. Test Procedure

The gages were attached to the surfaces of the beams at the location previously mentioned, following the usual techniques. The gages were allowed to dry five days and four nights i.e. about 110 hours. Then the specimen and its supporting and loading equipment were placed in the testing machine. An initial load within the elastic limit of the material was applied cyclically at least four times to stabilize the

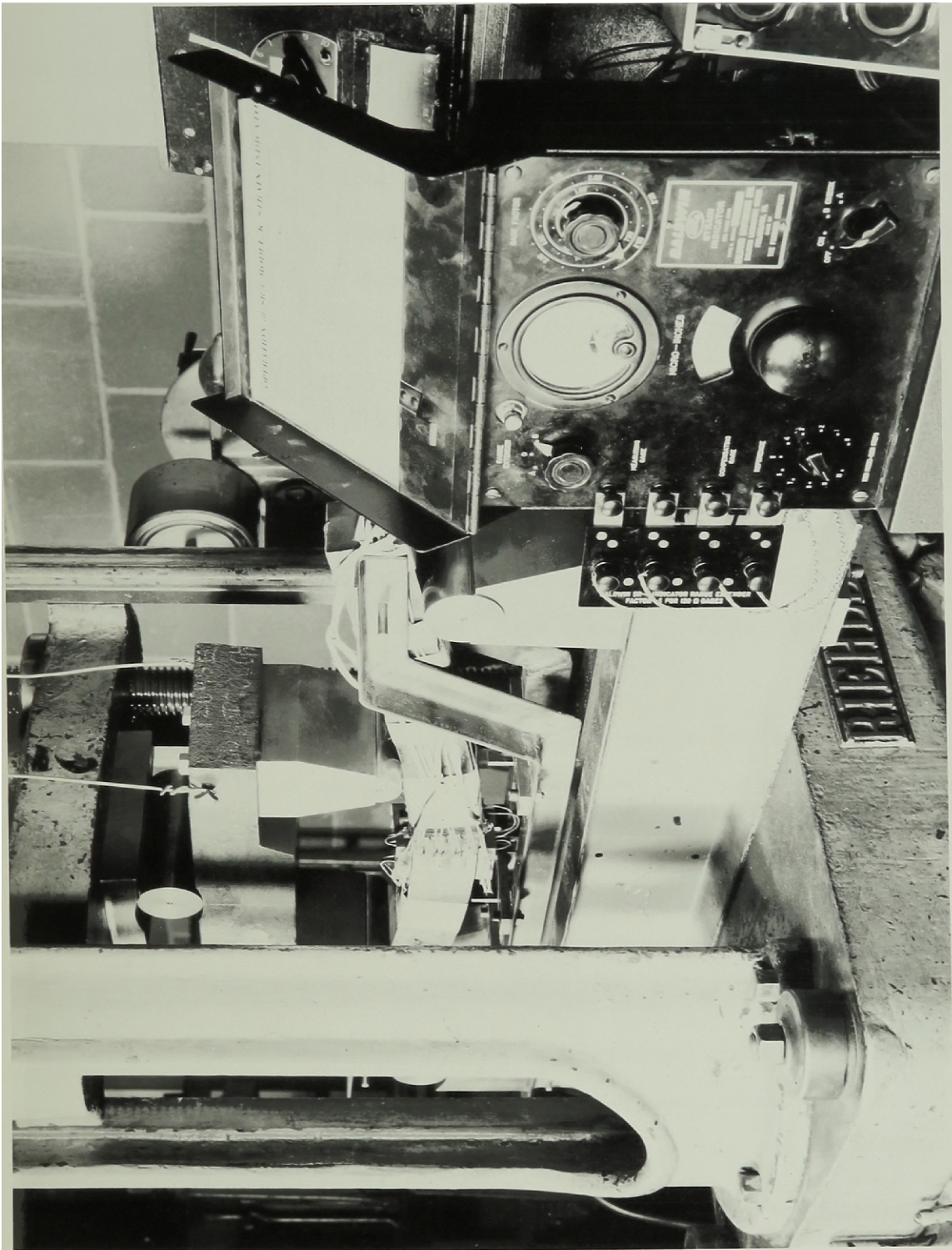


FIG. 52 - RANGE EXTENDER ON STRAIN INDICATOR

electrical gages and to minimize the zero shift. Then the zero reading of each gage and the zero deflection reading of each Ames dial were recorded. The load was applied in increments and each time the readings of the strains and deflections were recorded. The loading stopped when enough deflection (with corresponding curvature of the specimen) was reached such that no further deflection could be safely handled with this testing equipment. Then the beam was unloaded also in increments till the zero loading was reached; this was followed by loading and unloading again. Strains were recorded throughout these cycles of loading and unloading.

The above mentioned tests were run using the slow speed of the testing machine and all the readings made were taken by the writer only.

The mild steel beam in the testing machine is shown in Figures 52 and 53. This specimen is shown in Figure 54-A after testing. The specimens of tested beams after bending are shown in Fig. 54-B.

B. Test Results

The previously mentioned pure bending tests for beams of square cross sections of mild steel, stainless steel, aluminum, and magnesium show the following results:

- (1) The experimental data of the value of the moment of resistance of the central section shows close agreement with the theoretical values obtained by the new theory derived on pages 71 and 73. This agreement is illustrated by the theoretical curves drawn between σ_t vs M_t and ϵ_t vs M_t and the experimental results given in Figures 35, 39, 43, 47, 36, 40, 44, and 48. It may be noted that the tests were carried up to a maximum strain of about 4 % deformation which is the maximum value obtained by the test set-up used.

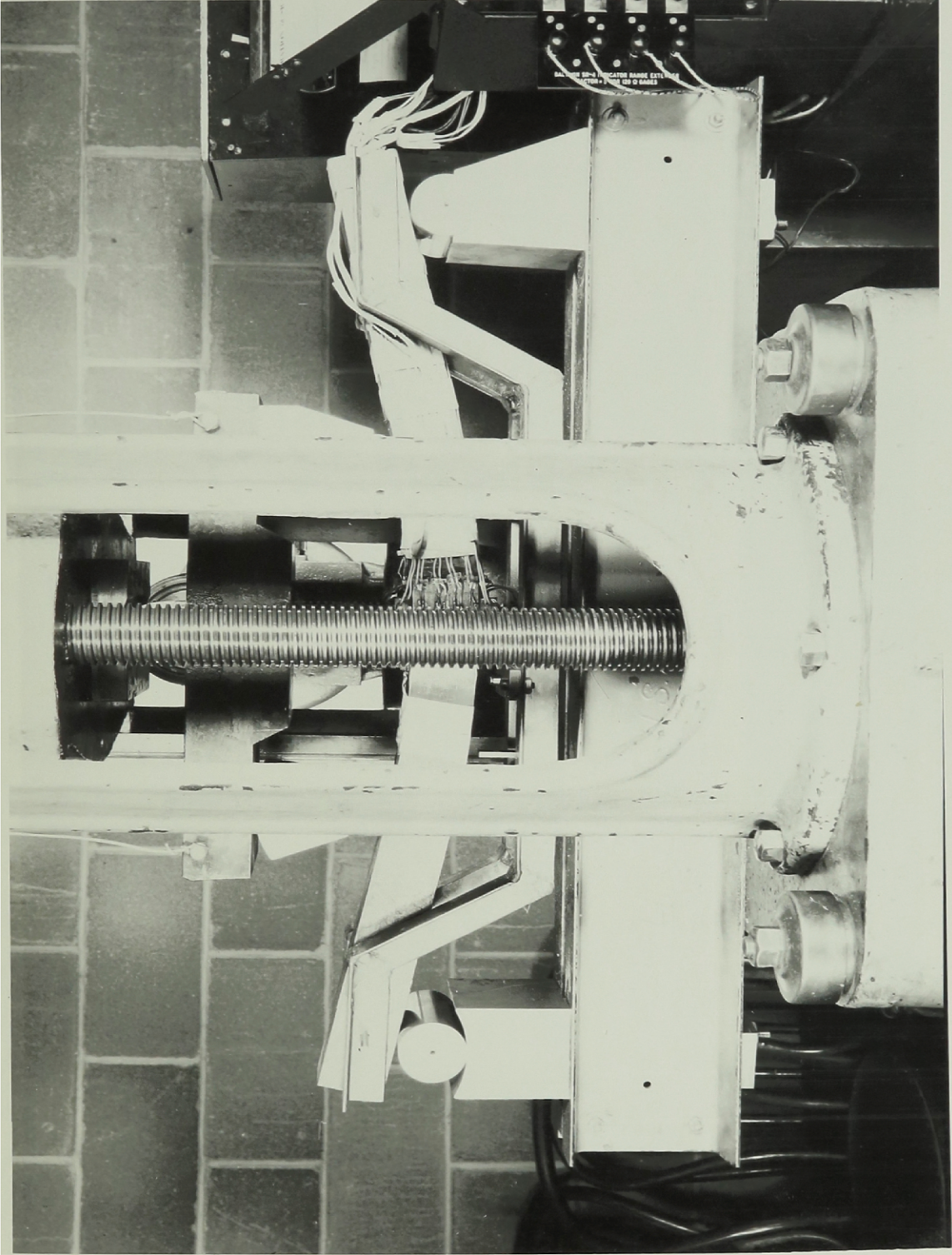


FIG 53 - MILD STEEL BEAM DURING TEST



FIG 54-A - MILD STEEL BEAM AFTER TEST

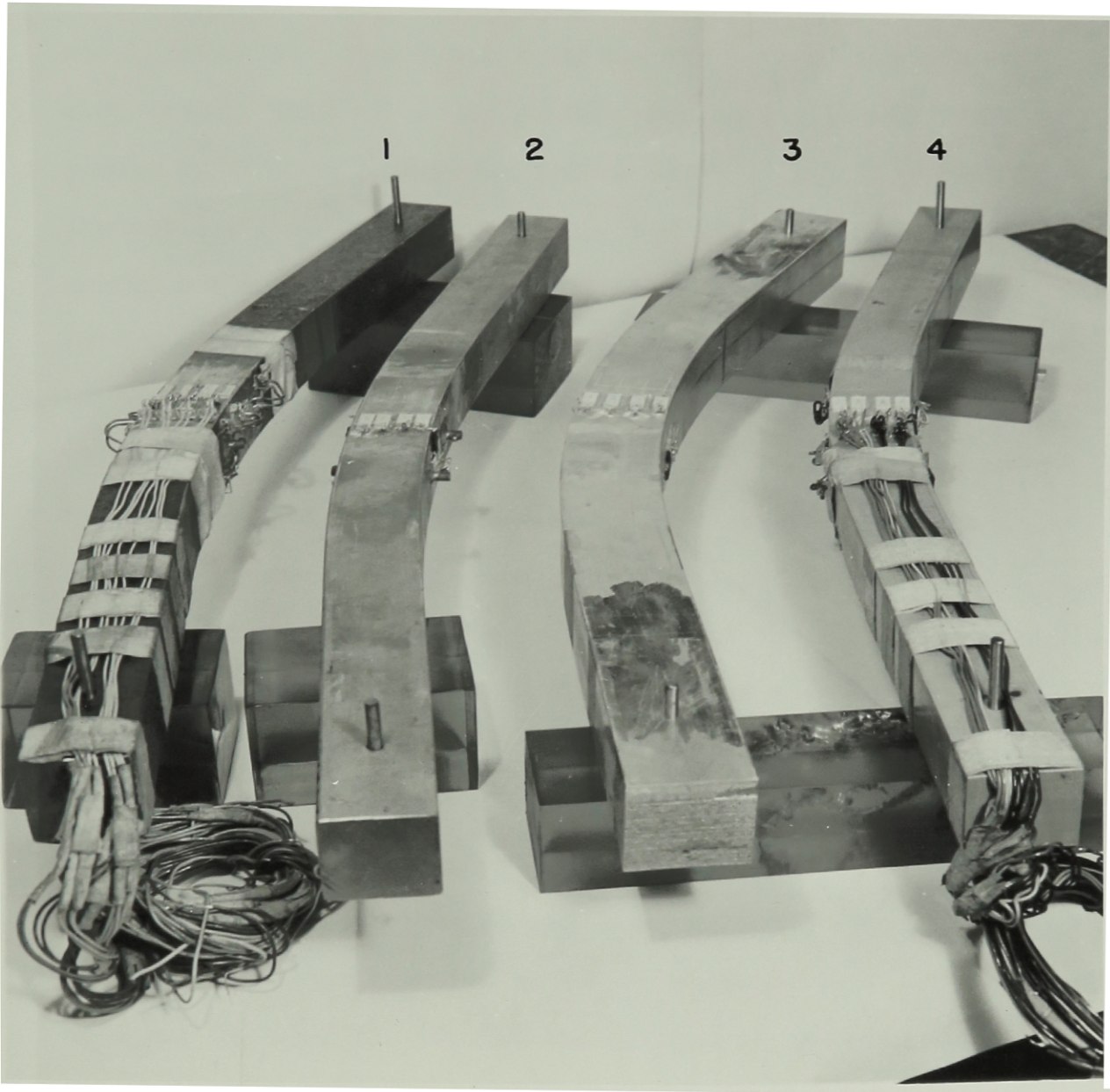


FIG.54-B - BEAMS AFTER TEST

1-MILD STEEL

2 - STAINLESS STEEL

3- ALUMINUM

4 - MAGNESIUM

(2) The shift of the neutral axis for the central section of mild steel, stainless steel, and aluminum was towards the compression side whereas that of magnesium was towards the tension side as expected by the new theory derived on pages 70 and 71. This is shown theoretically in Figs. 37, 41, 45, and 49; experimentally this shift is clear from Figs. 55, 56, 57, and 58.

(3) The theoretical values of the shift of the neutral axis for the case of magnesium agree with the experimental results as shown in Fig. 49. The shift of the neutral axis for the other materials is so small that it did not show up well experimentally with a value to be compared with the theoretical but in the case of magnesium a larger shift up to 0.072 depth of the section was reached.

(4) Figs. 55, 56, 57, and 58 show that the strain distribution over the central cross section of all the materials tested is linear up to the maximum strain of 4%. This verifies one of the assumptions made for the new theory.

(5) Poisson's ratio changed gradually from its original constant value in the elastic region up to the value of 0.5. It was noted as shown in Figs. 59, 60, 61, and 62 that in the elastic state Poisson's ratio for the tension side equals that of the compression side of the bent beams but it began to differ for tension and compression at the end of the elastic region tending however to reach the value of 0.5 in the limit. It was also realized that the maximum value obtained for mild steel on the compression side was 0.55 whereas it was 0.45 for the tension side; this gives an average of 0.50 for both sides. These values may be influenced in part by the transverse sensitivity of the SR-4 strain gages, a

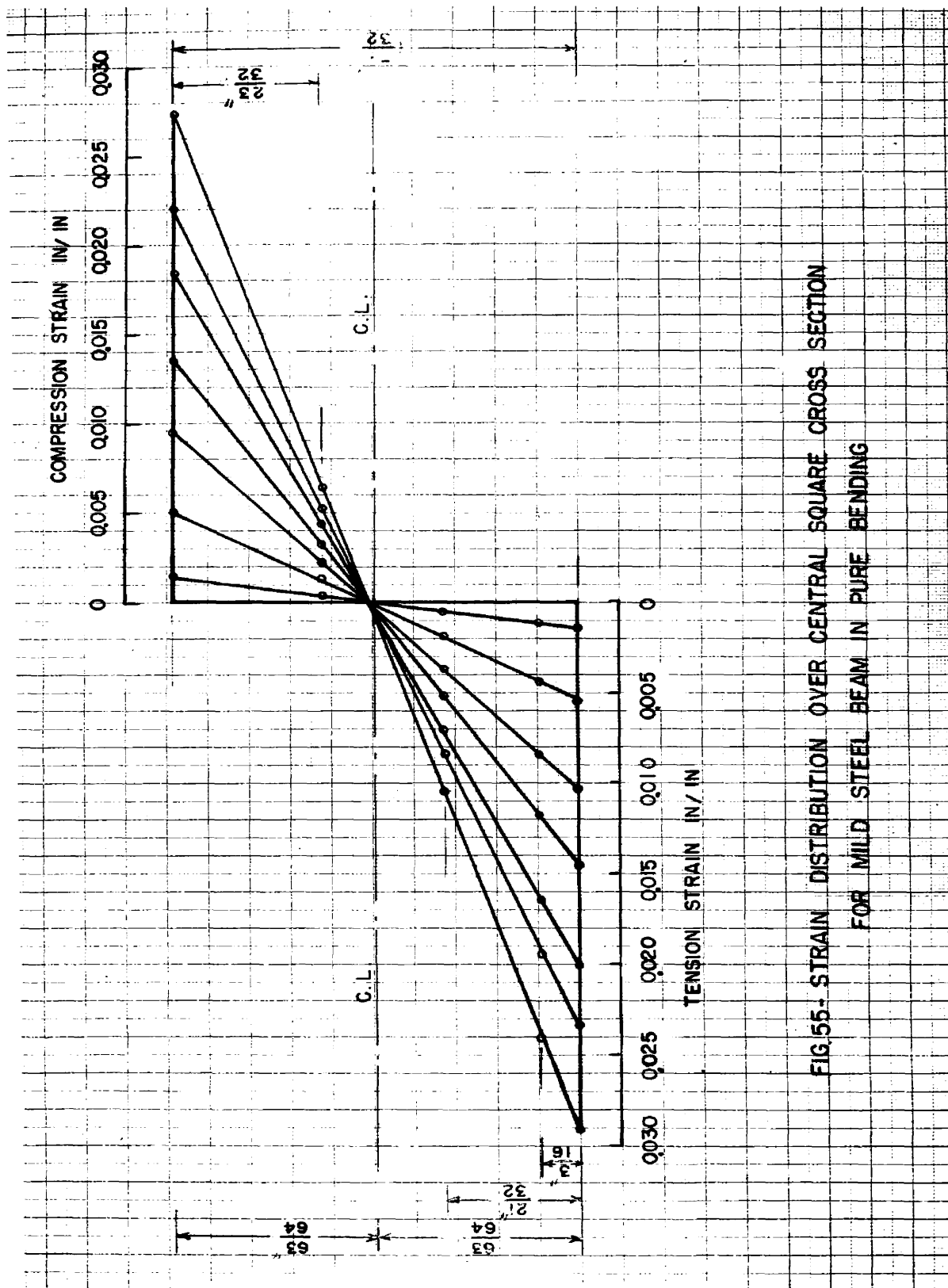


FIG. 55- STRAIN DISTRIBUTION OVER CENTRAL SQUARE CROSS SECTION FOR MILD STEEL BEAM IN PURE BENDING

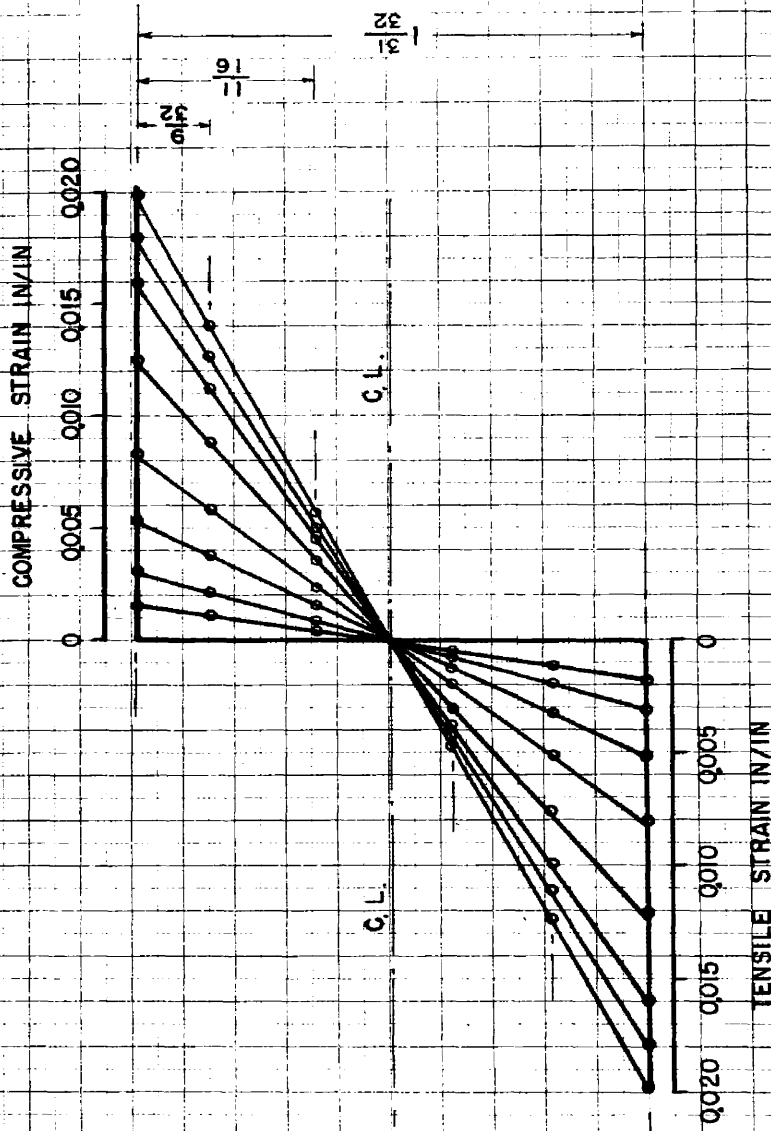


FIG.56 - STRAIN DISTRIBUTION OVER CENTRAL SQUARE CROSS SECTION
FOR STAINLESS STEEL BEAM IN PURE BENDING

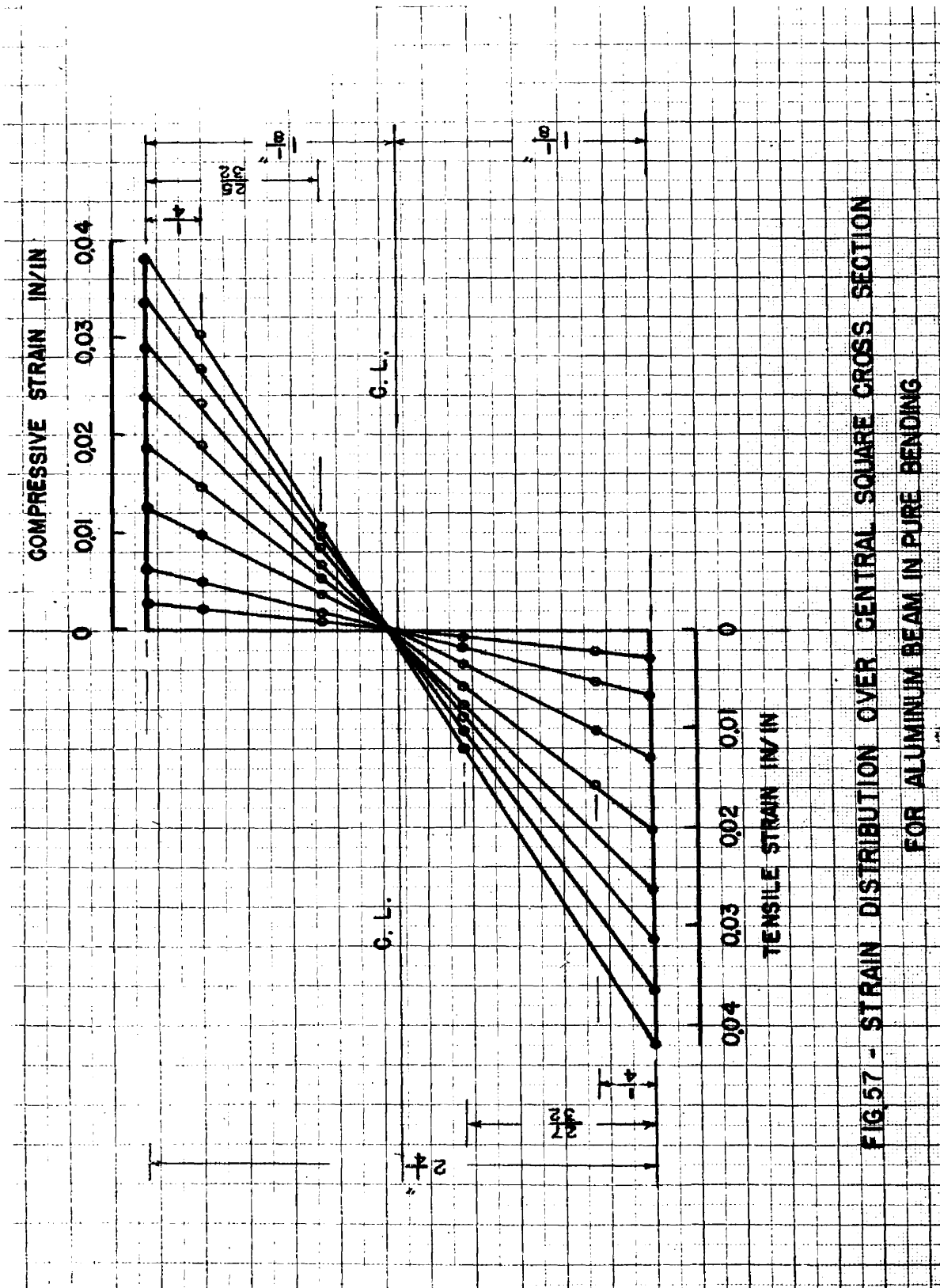


FIG.57 - STRAIN DISTRIBUTION OVER CENTRAL SQUARE CROSS SECTION FOR ALUMINUM BEAM IN PURE BENDING

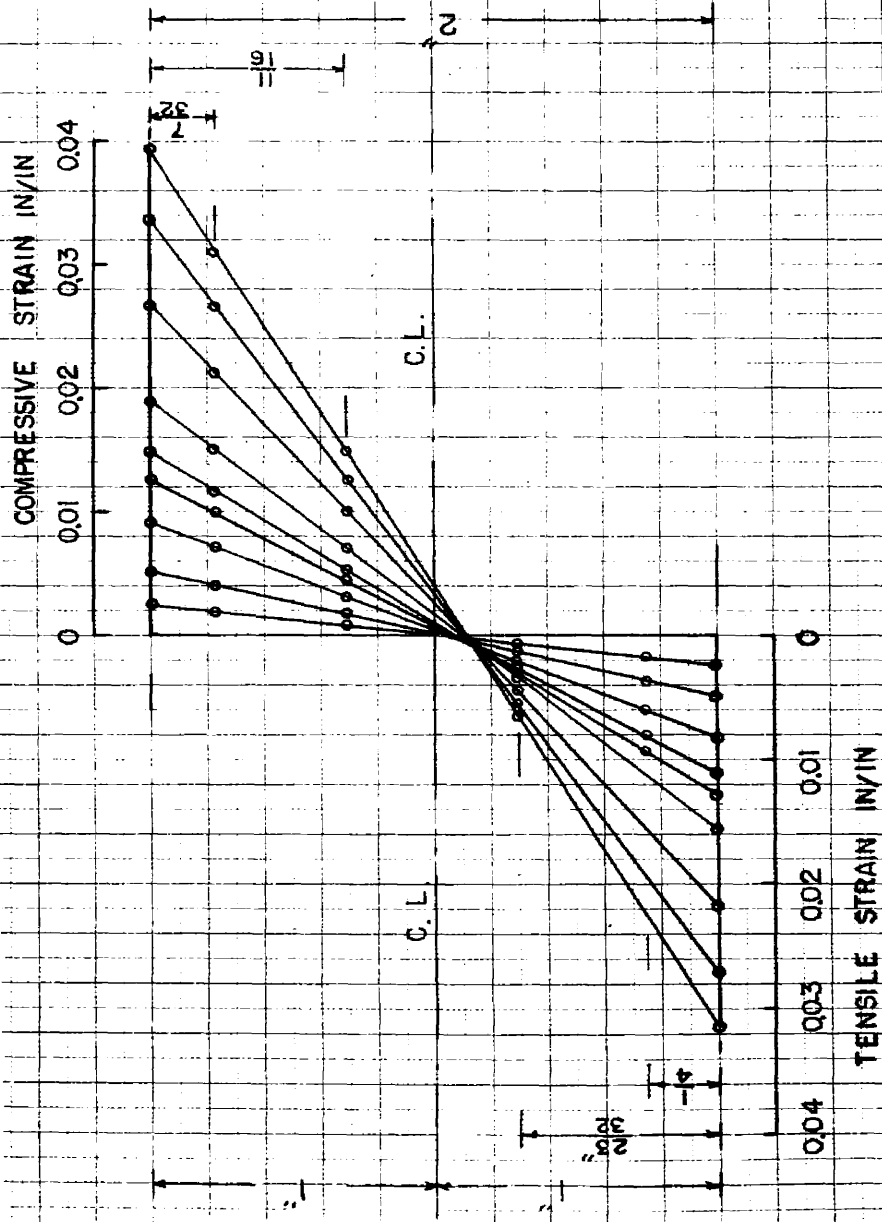


FIG.58 - STRAIN DISTRIBUTION OVER CENTRAL SQUARE CROSS SECTION FOR MAGNESIUM BEAM IN PURE BENDING

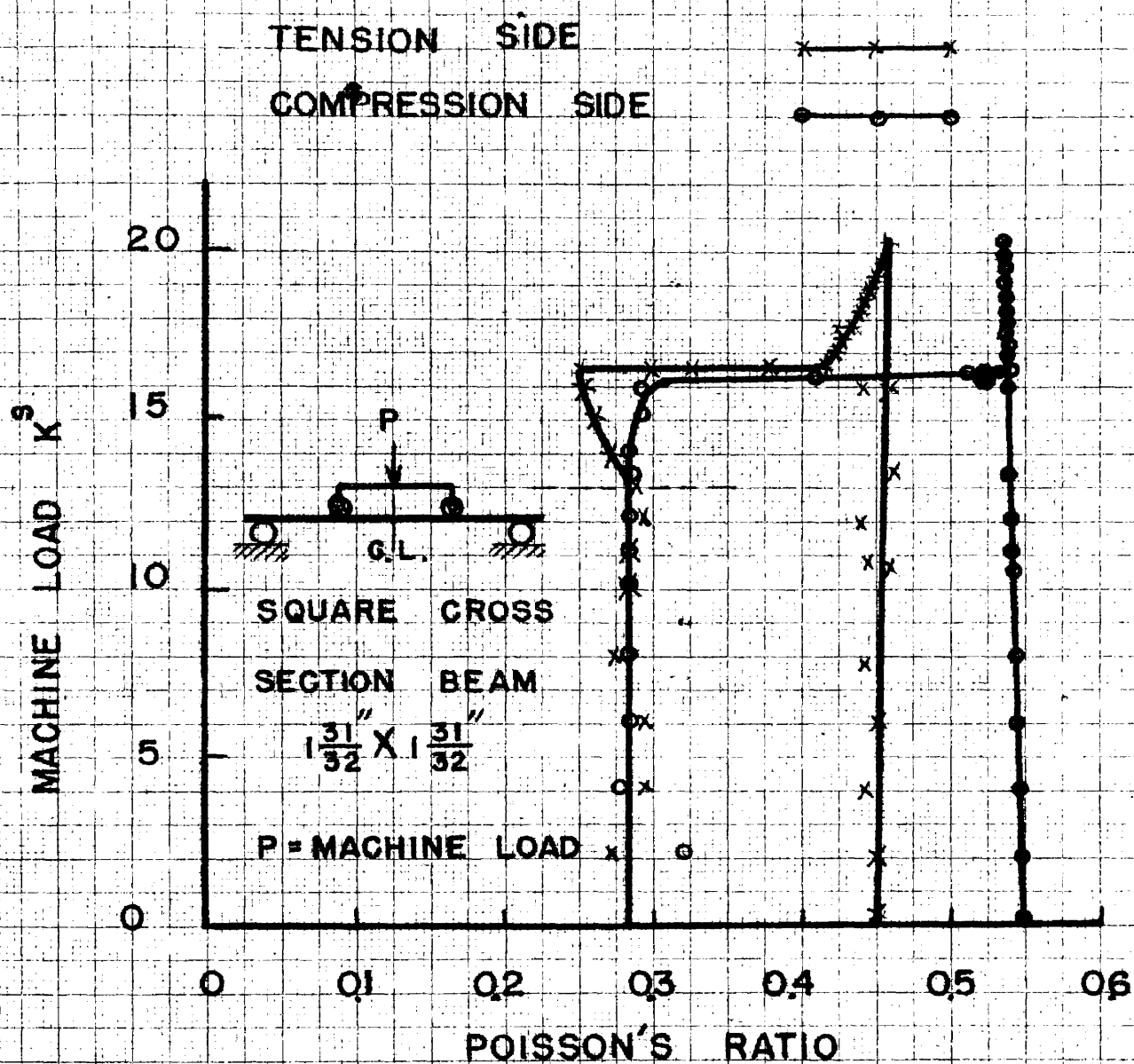


FIG.59 - POISSON'S RATIO OF CENTRAL EXTREME FIBERS VS MACHINE LOAD FOR MILD STEEL BEAM IN PURE BENDING

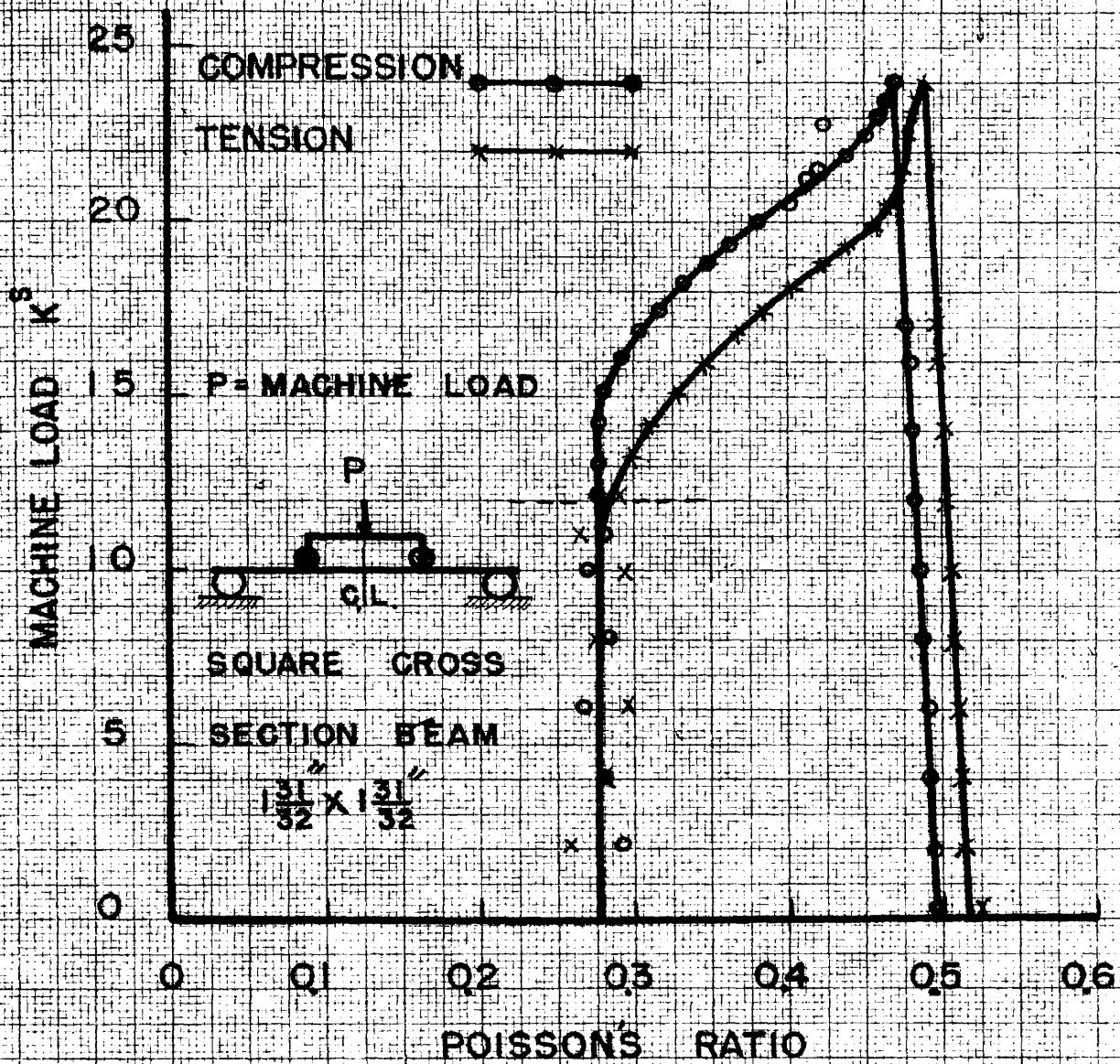


FIG. 60 - POISSON'S RATIO OF CENTRAL EXTREME FIBERS VS MACHINE LOAD FOR STAINLESS STEEL BEAM IN PURE BENDING

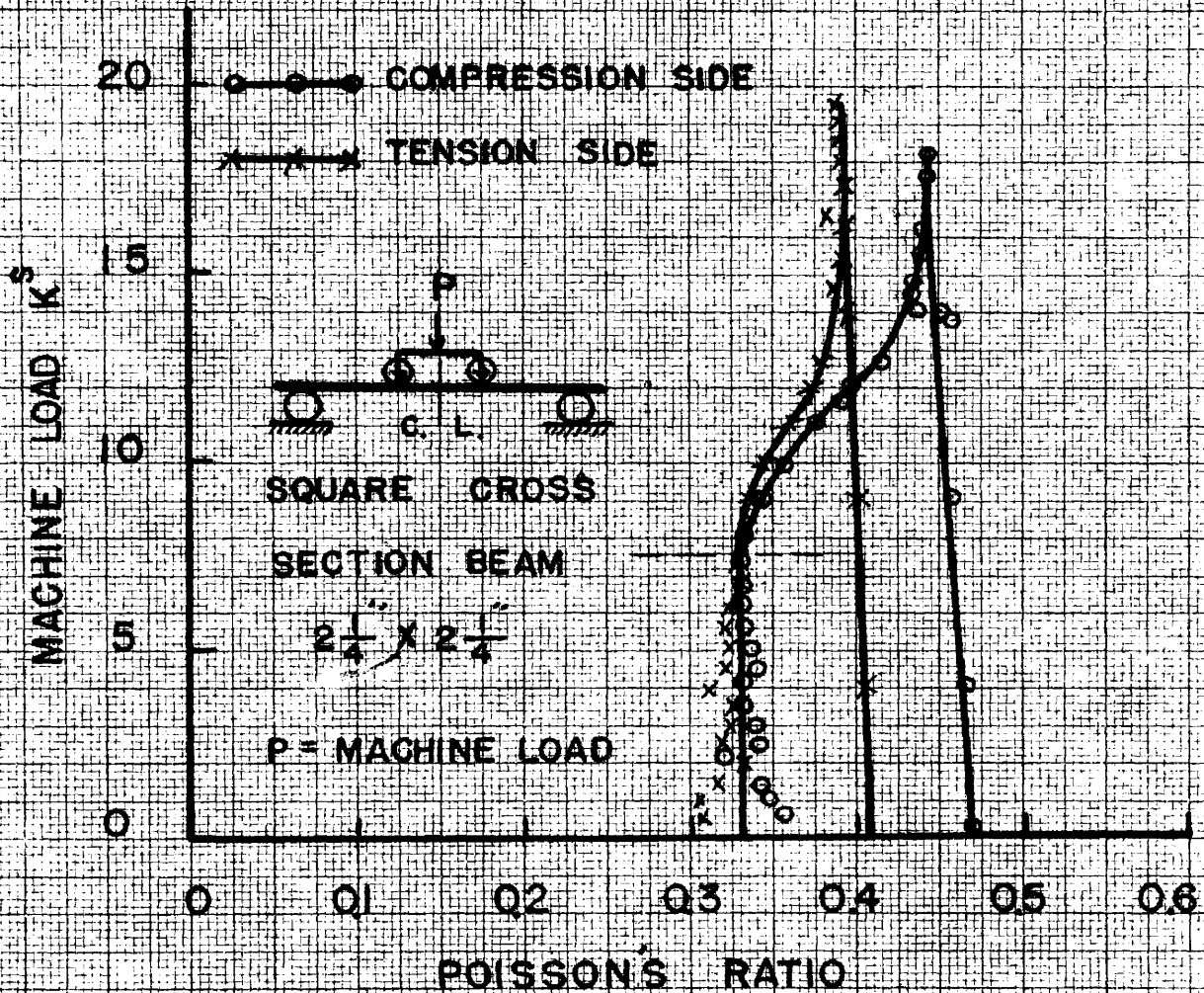


FIG. 61 - POISSON'S RATIO OF CENTRAL EXTREME FIBERS VS MACHINE LOAD FOR ALUMINUM BEAM IN PURE BENDING

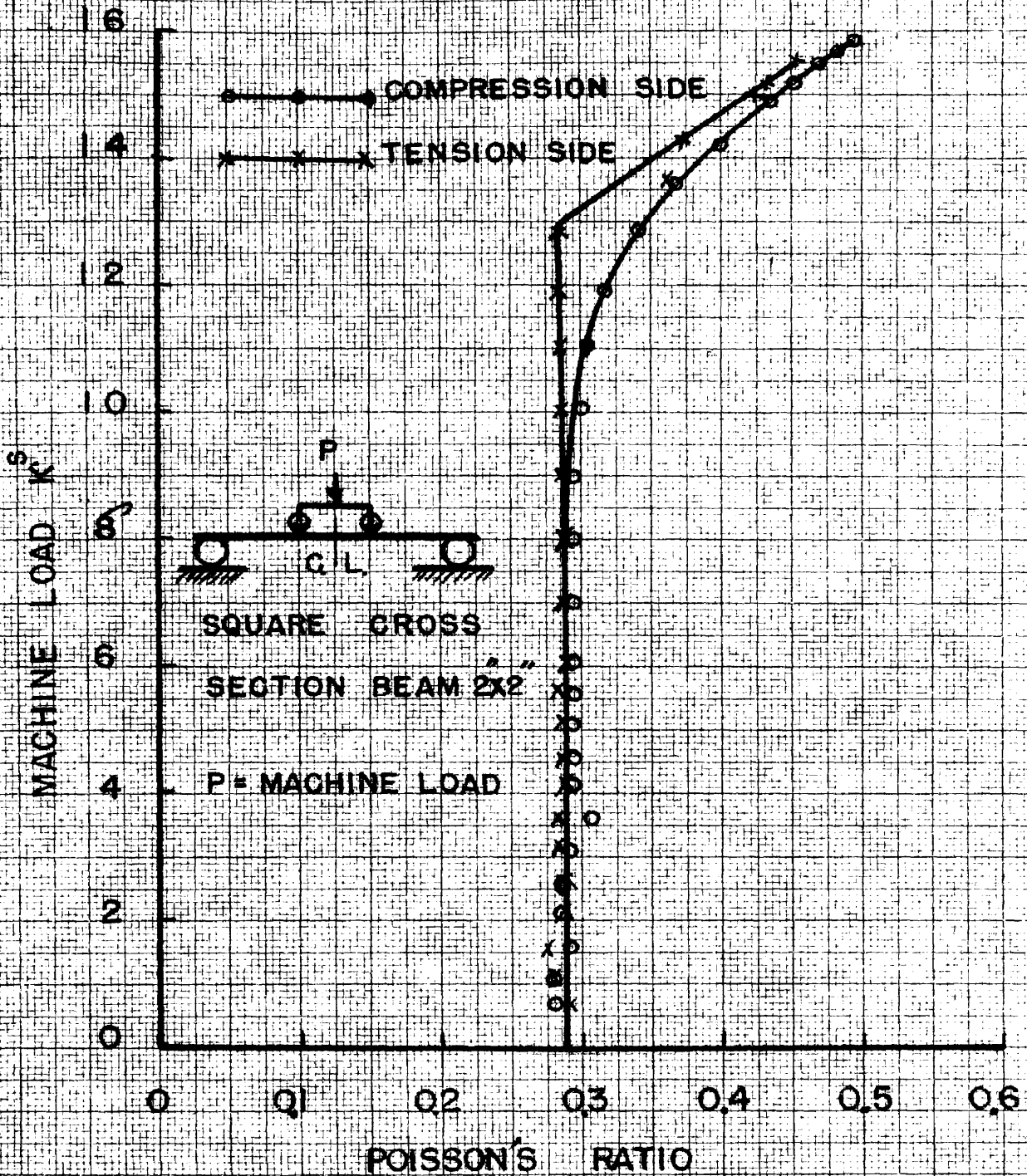


FIG. 62 - POISSON'S RATIO OF CENTRAL EXTREME FIBERS VS MACHINE LOAD FOR MAGNESIUM BEAM IN PURE BENDING

factor which was not taken into account in the calculations. This shows that the assumption in the new theory of the value of the Poisson's ratio of 0.5 is valid around 3 to 4 % deformation, but this assumption is an approximation from the beginning of the elastic plastic region up to 3 % deformation. The assumption in this mentioned region has a negligible effect on the new theory for determining the moment of resistance and the shift of the neutral axis as shown on page 68.

(6) The widths of the compression and the tension sides of aluminum and magnesium beams were measured for the maximum strain reached in the test and their values were compared to those mentioned by the new theory shown on pages 67 and 68. The comparison shows close agreement as follows:

a. Aluminum

$$\begin{aligned} & \text{For the Tension Side} \quad \text{Theoretically} \\ \text{Width} &= B \left(1 - 0.5 \cdot \frac{\epsilon_t + \epsilon_r}{2} \right) = 2.25 \left(1 - \frac{0.0011 + 0.0415}{4} \right) \\ &= 2.226 \text{ inches.} \end{aligned}$$

$$\text{Experimentally Width} = 2.228 \text{ inches.}$$


$$\begin{aligned} & \text{For the Compression Side} \quad \text{Theoretically} \\ \text{Width} &= B \left(1 + 0.5 \cdot \frac{\epsilon_c + \epsilon_t}{2} \right) = 2.25 \left(1 + \frac{0.0011 + 0.0383}{4} \right) \\ &= 2.27 \text{ inches.} \end{aligned}$$

$$\text{Experimental Value} = 2.30 \text{ inches.}$$

b. Magnesium Following the above similar way we get:

| | Theoretically | Experimentally |
|------------------|---------------|----------------|
| Tension side | 1.978 | 1.980 |
| Compression side | 2.021 | 2.025 |

(7) It was observed that the tension side after bending was laterally convex but the compression side was laterally concave

i.e.  This is similar to the theoretical result shown on page 225 of "Timoshenko, Theory of Elasticity."

(8) It was observed during the tests that the magnesium beam in pure bending showed a greater spring back than the aluminum, stainless steel, or mild steel beams as shown in Fig. 54-B. This is in the same sense as the theoretical curves given later in Fig. 74.

(9) The SR-4 gages (A-7 type) failed in tension around 2 % elongation but those in compression did not fail up to the maximum strain of 4 % .

(10) The 17-4 post-yield strain gages and the clip gages showed consistent readings with those of the SR-4 gages placed on the upper and lower surfaces where these gages were located.

(11) The beginning of yielding of the tested beams in pure bending occurred at the following stresses which correspond to the point where the load deflection diagrams and the load strain diagrams deviated from linearity as shown in Figs. 63, 64, 65, 66, 67, 68, 69, and 70. These points correspond also to the points where Poisson's ratio in tension and compression began to deviate from each other, Figs. 59, 60, 61, and 62. The stresses at the beginning of yielding are in psi:

| Mild Steel | Stainless Steel | Aluminum | Magnesium |
|------------|-----------------|----------|-----------|
| 37,620 | 37,620 | 15,900 | 36,000 |

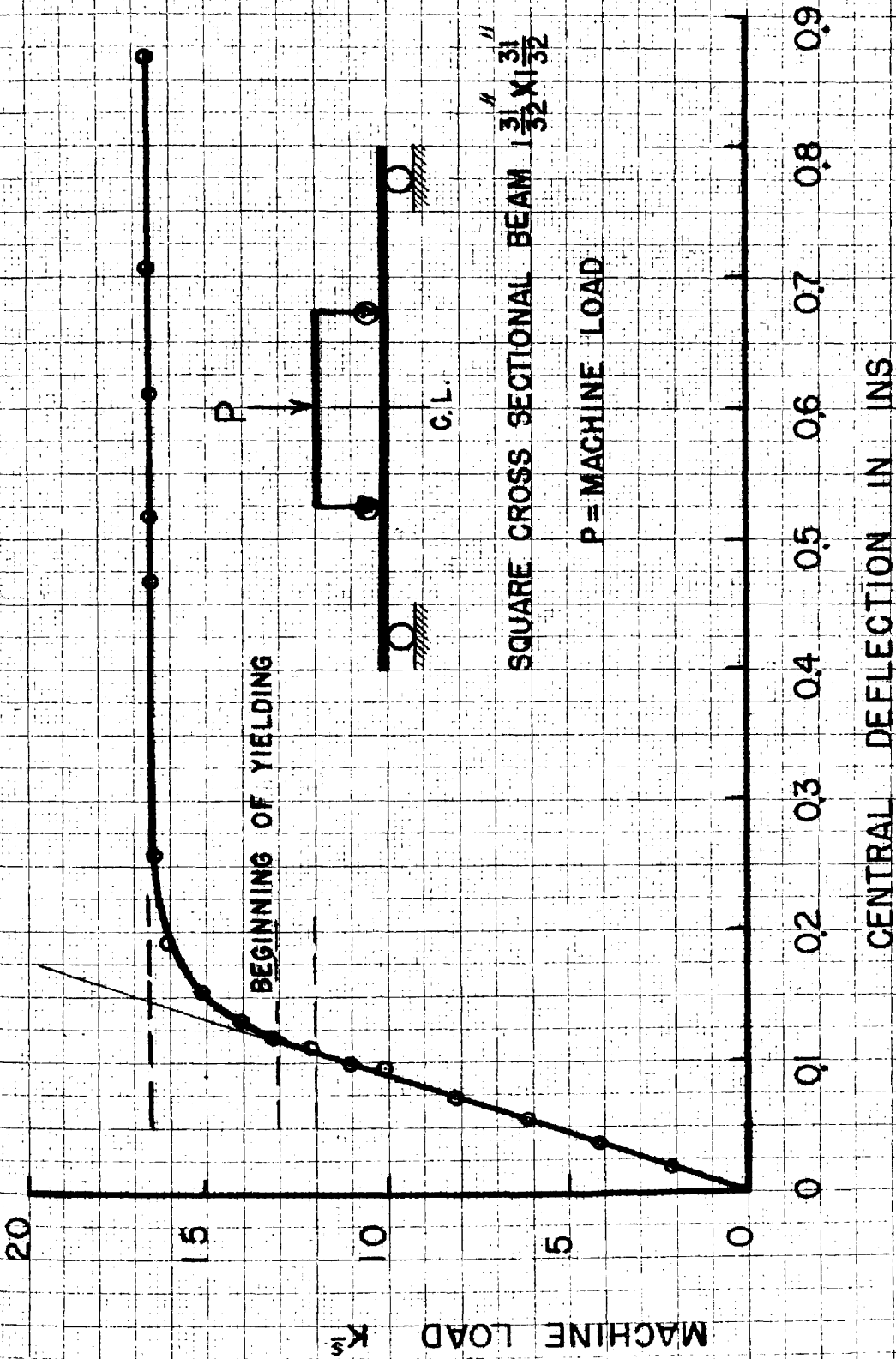


FIG.63 - CENTRAL DEFLECTION VS MACHINE LOAD
FOR MILD STEEL BEAM IN PURE BENDING

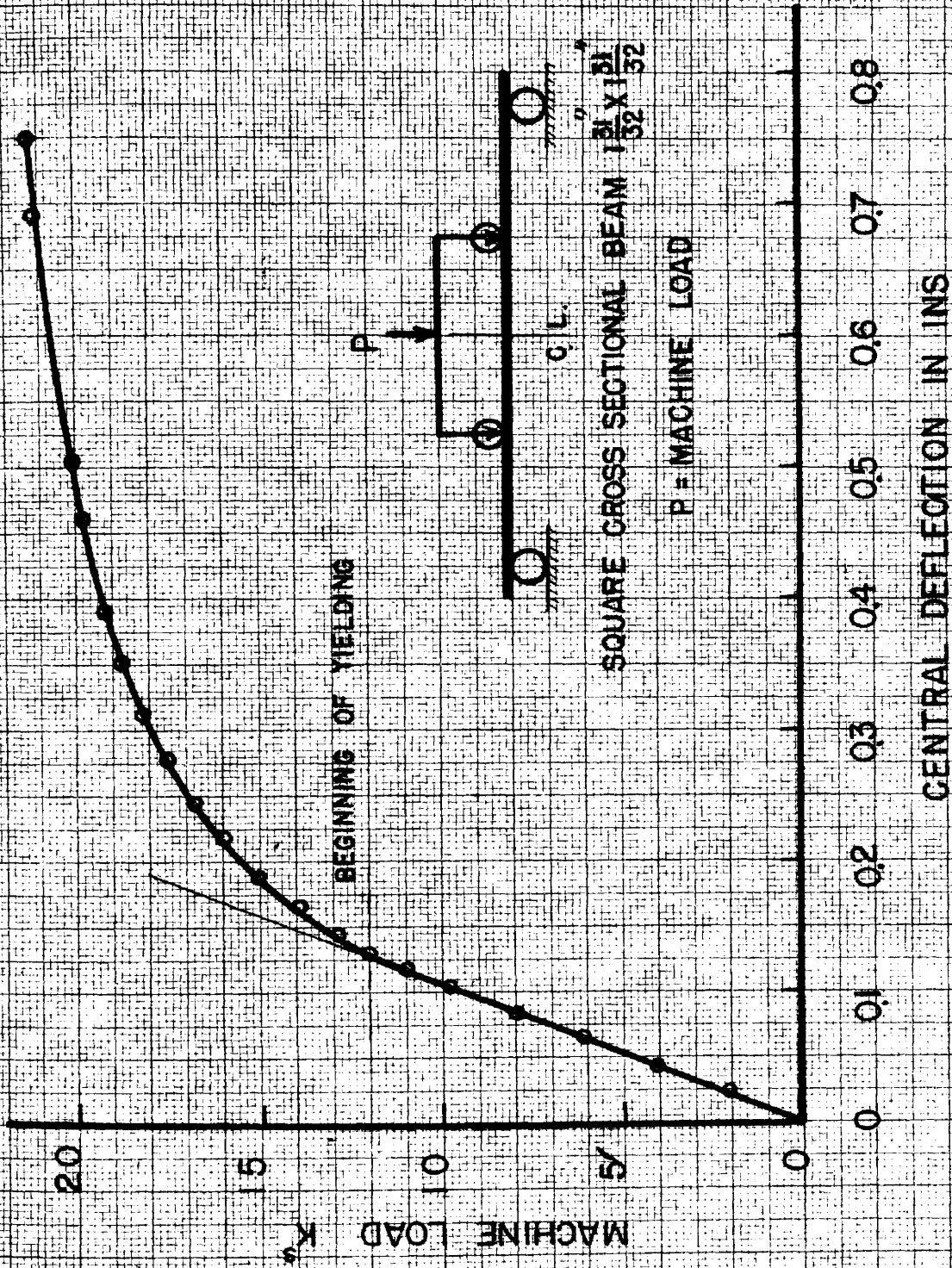


FIG.64 - CENTRAL DEFLECTION VS MACHINE LOAD FOR STAINLESS STEEL BEAM IN PURE BENDING

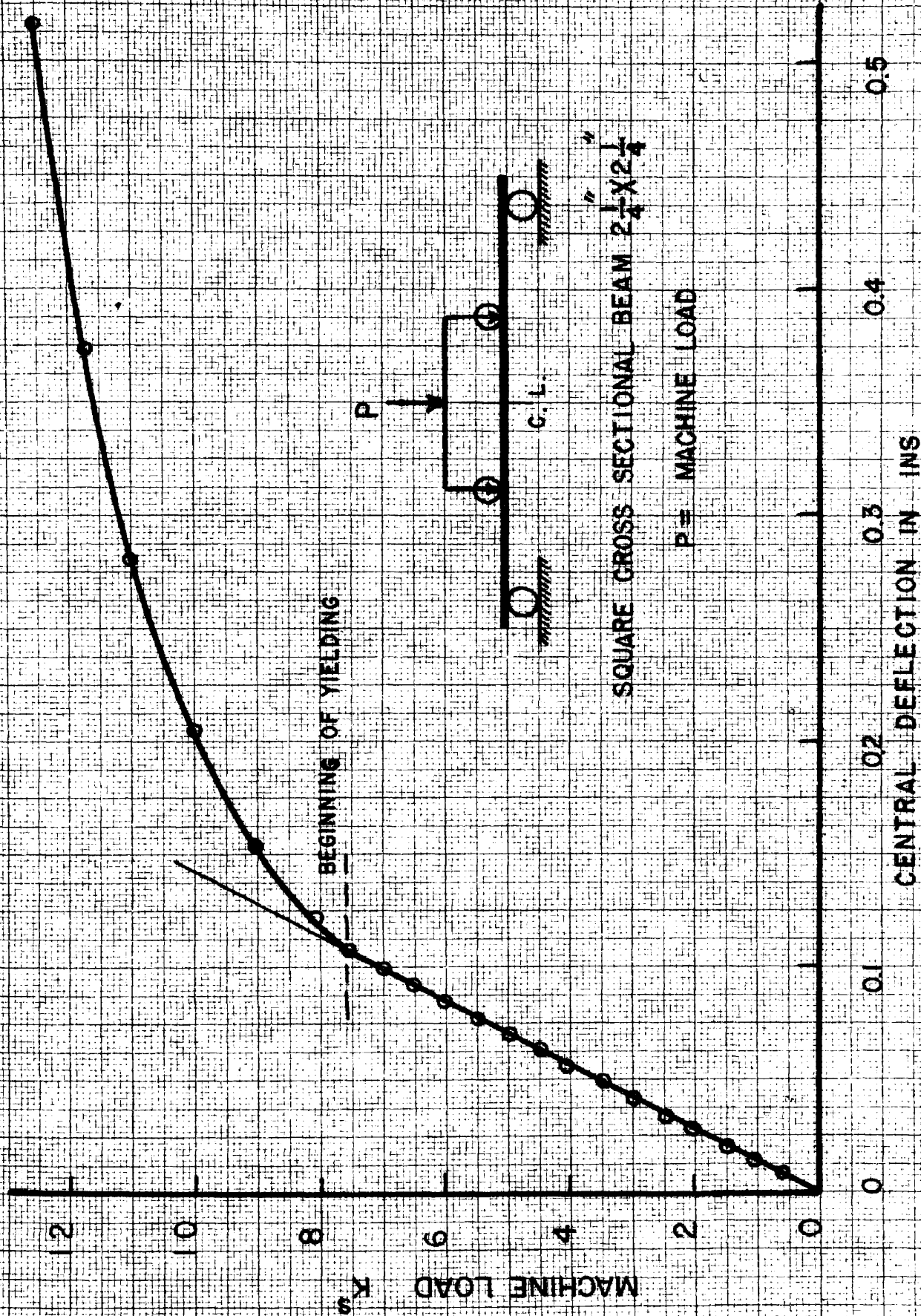


FIG. 65 - CENTRAL DEFLECTION VS MACHINE LOAD FOR ALUMINUM BEAM IN PURE BENDING

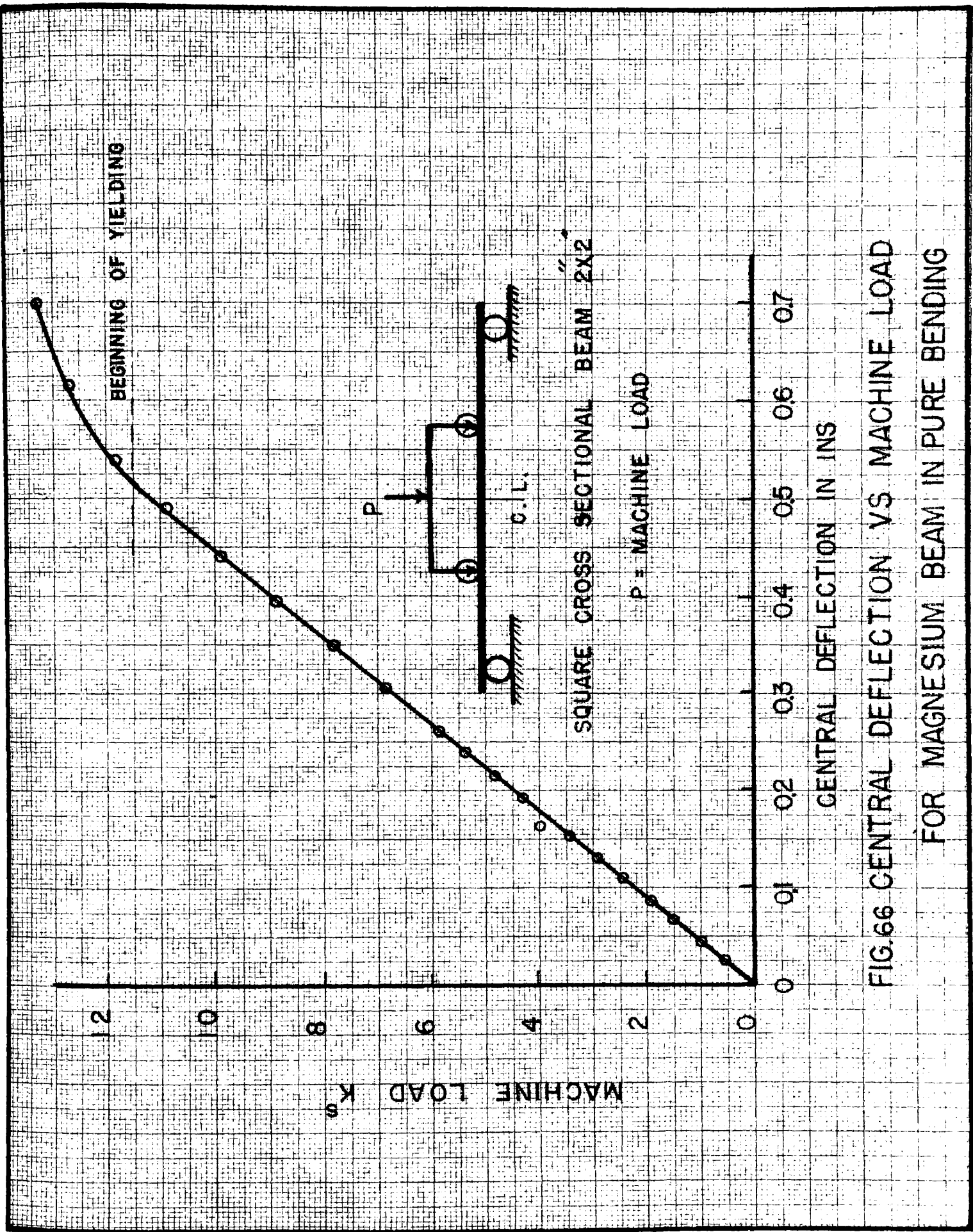


FIG.66 CENTRAL DEFLECTION VS MACHINE LOAD
FOR MAGNESIUM BEAM IN PURE BENDING

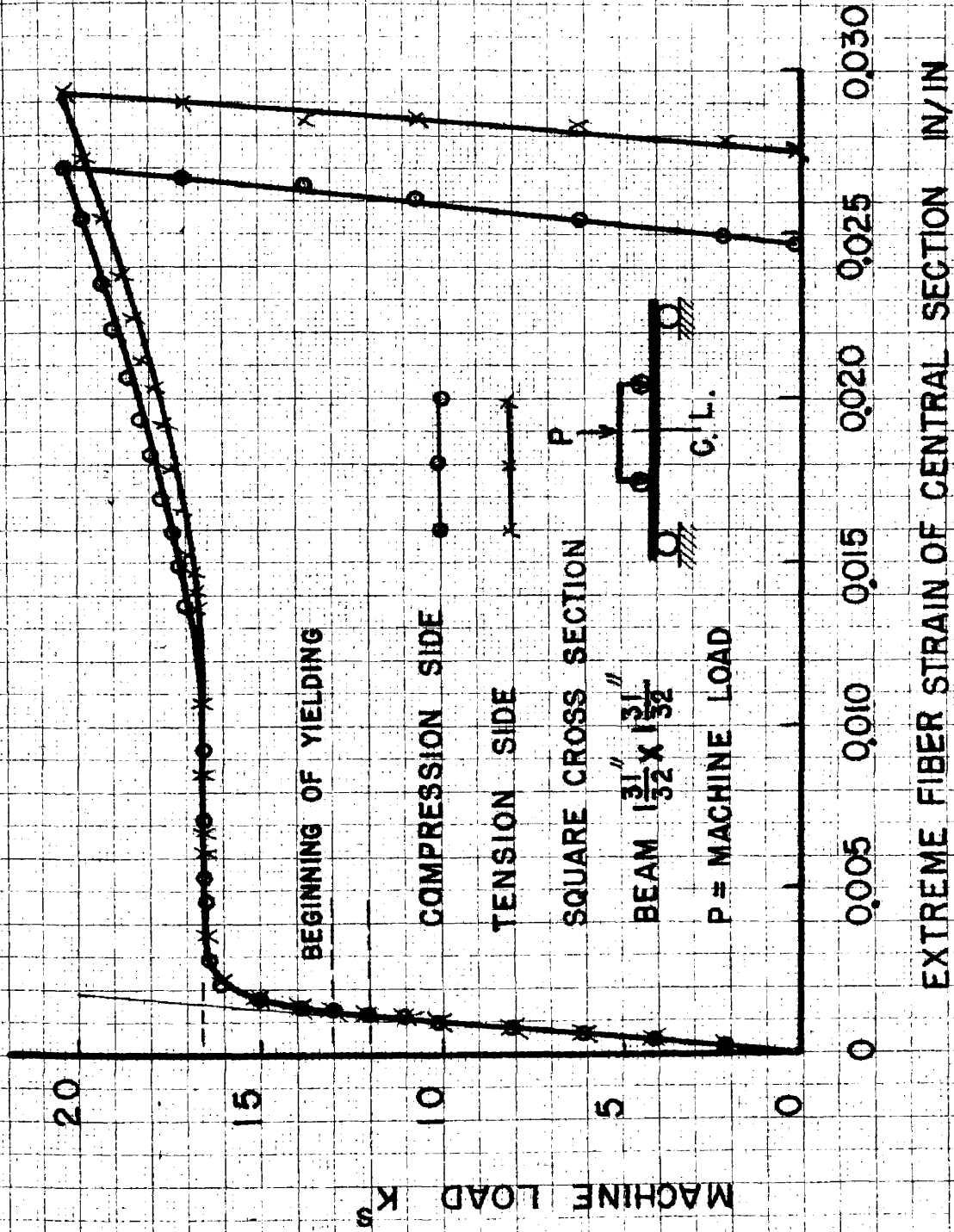


FIG.67 - CENTRAL EXTREME FIBER STRAIN VS MACHINE LOAD FOR MILD STEEL BEAM IN PURE BENDING

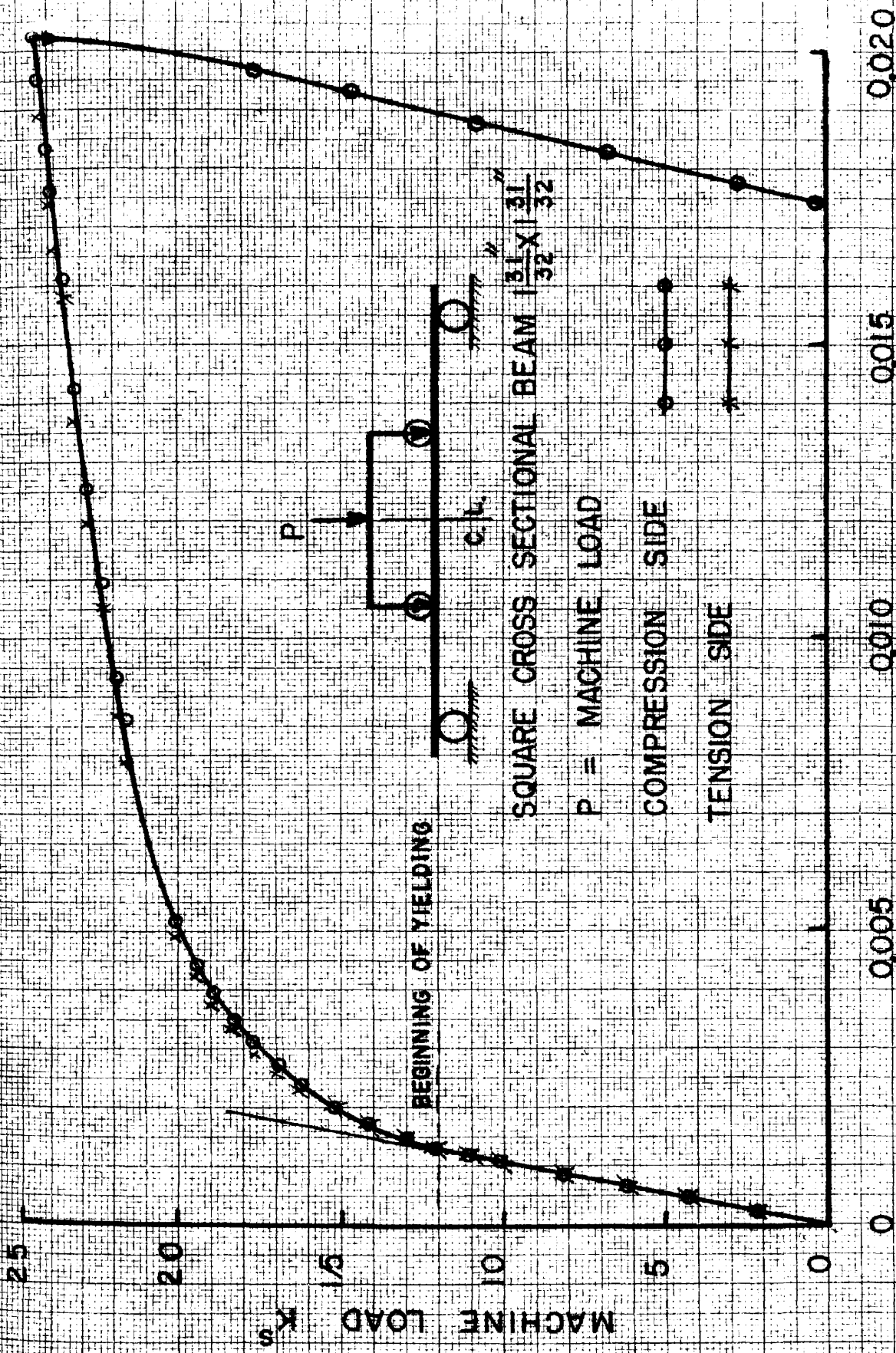


FIG.68- EXTREM FIBER STRAIN OF CENTRAL SECTION VS MACHINE LOAD FOR STAINLESS STEEL BEAM IN PURE BENDING

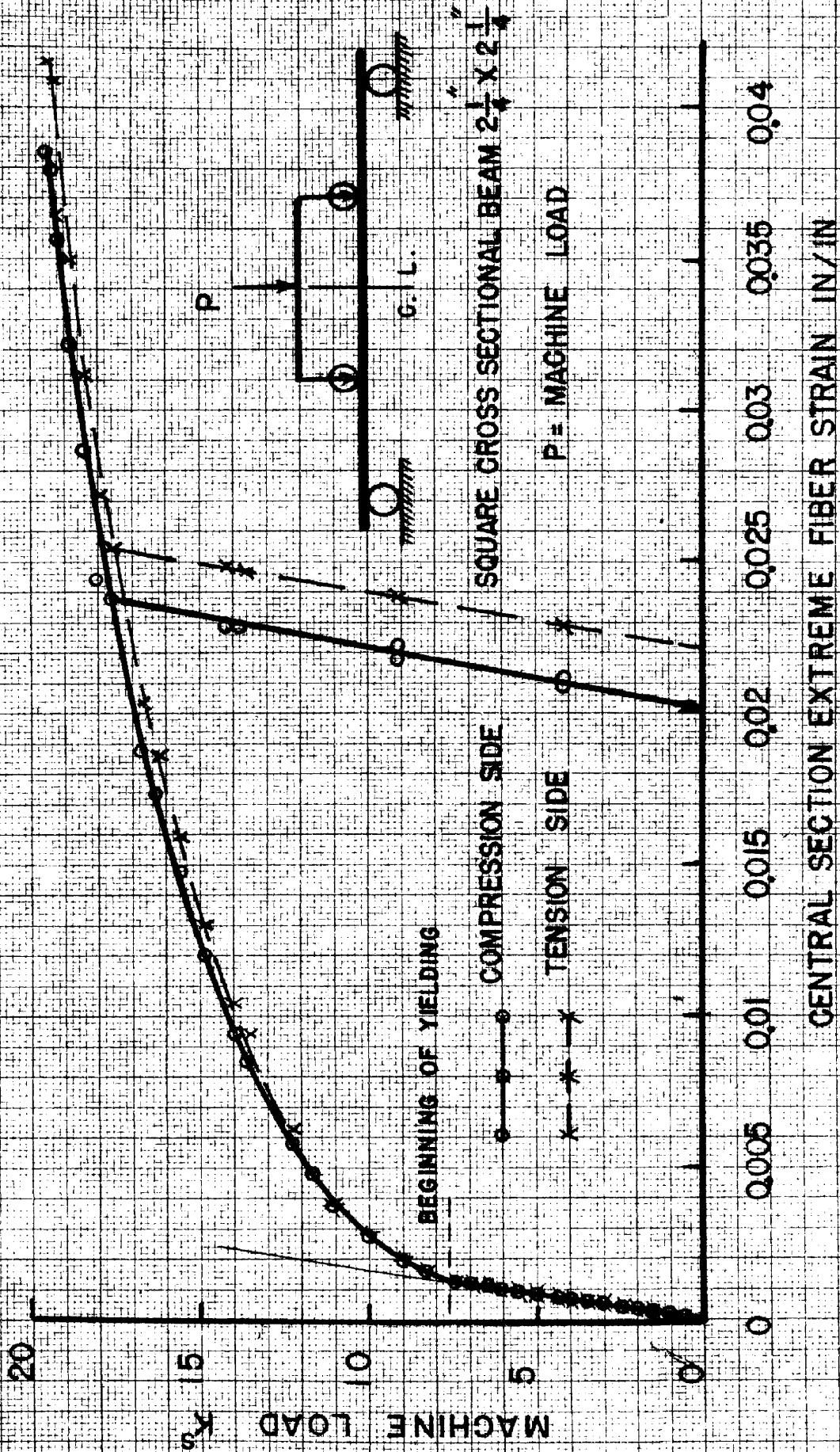


FIG.69 - EXTREME FIBER STRAIN OF CENTRAL SECTION VS MACHINE LOAD FOR ALUMINUM BEAM IN PURE BENDING

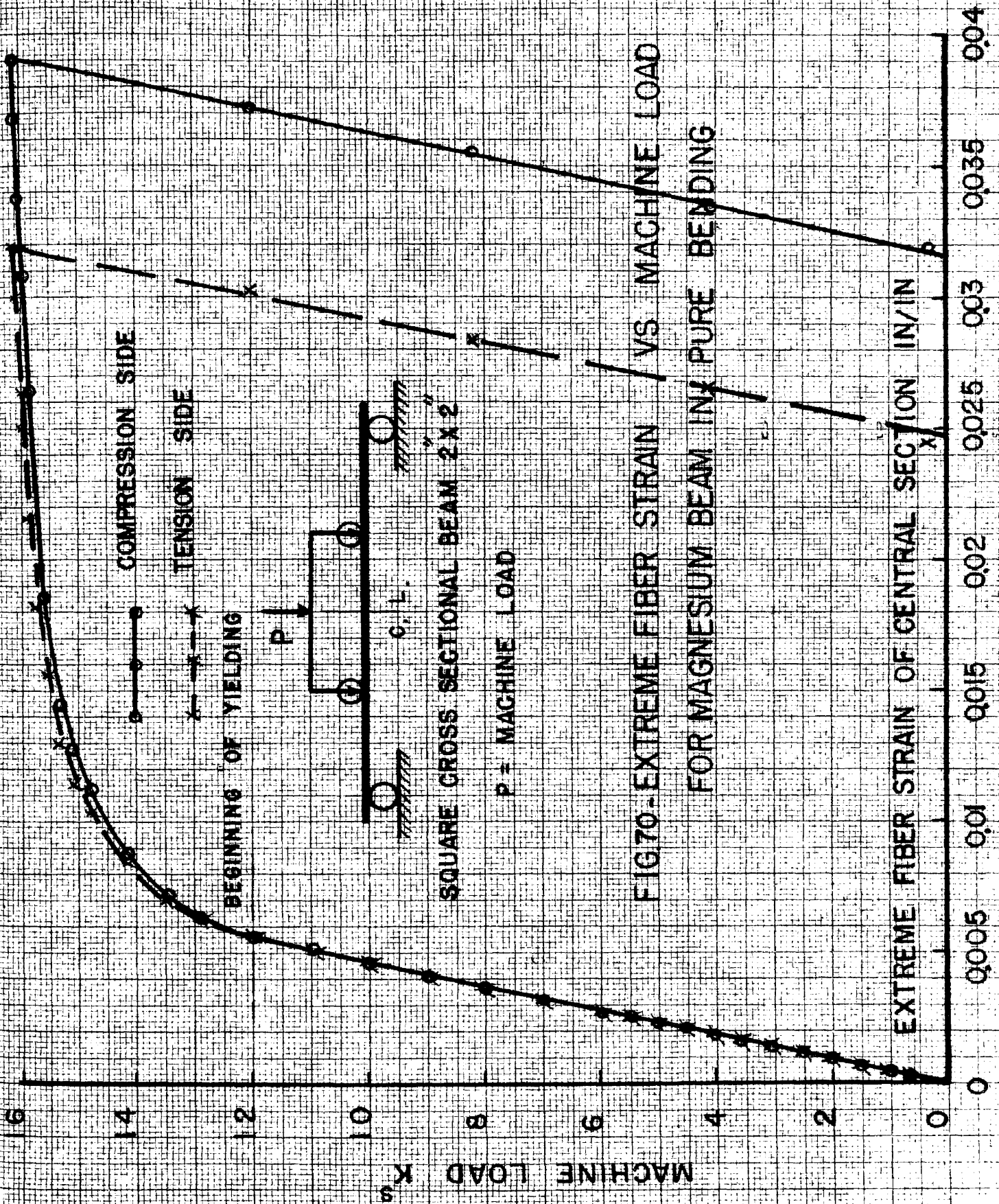


FIG70- EXTREME FIBER STRAIN / VS MACHINE LOAD
FOR MAGNESIUM BEAM IN PURE BENDING

SQUARE CROSS SECTIONAL BEAM 2 X 2

P = MACHINE LOAD

EXTREME FIBER STRAIN OF CENTRAL SECTION IN/IN

CHAPTER III

Springback Curvature

1. Review of Literature

The fabrication of metal structures frequently involves the bending of individual members to a prescribed contour. The member is bent so that the neutral axis assumes the curvature R_1 (see Fig. 71) and the extreme fibers of the member are stressed beyond the elastic limit. When the bending forces are released the member tends to straighten out or "spring back" so that the neutral axis assumes a new curvature R_2 . The following methods were derived to compute the value of R_1 such that the final radius after springback will be a certain given value R_2 .

A. General Method³²

As the member is bent as shown in Fig. 71, the amount of lengthening of a length ds of the extreme tensile fiber will be:

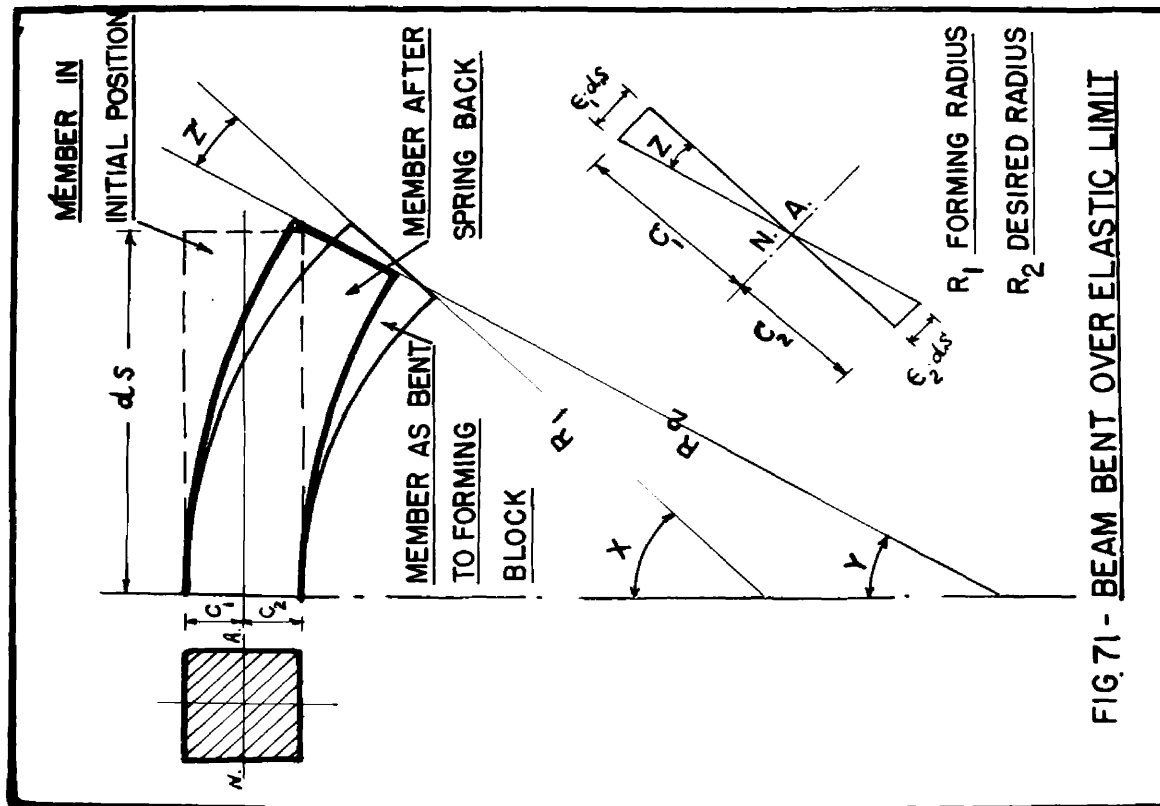
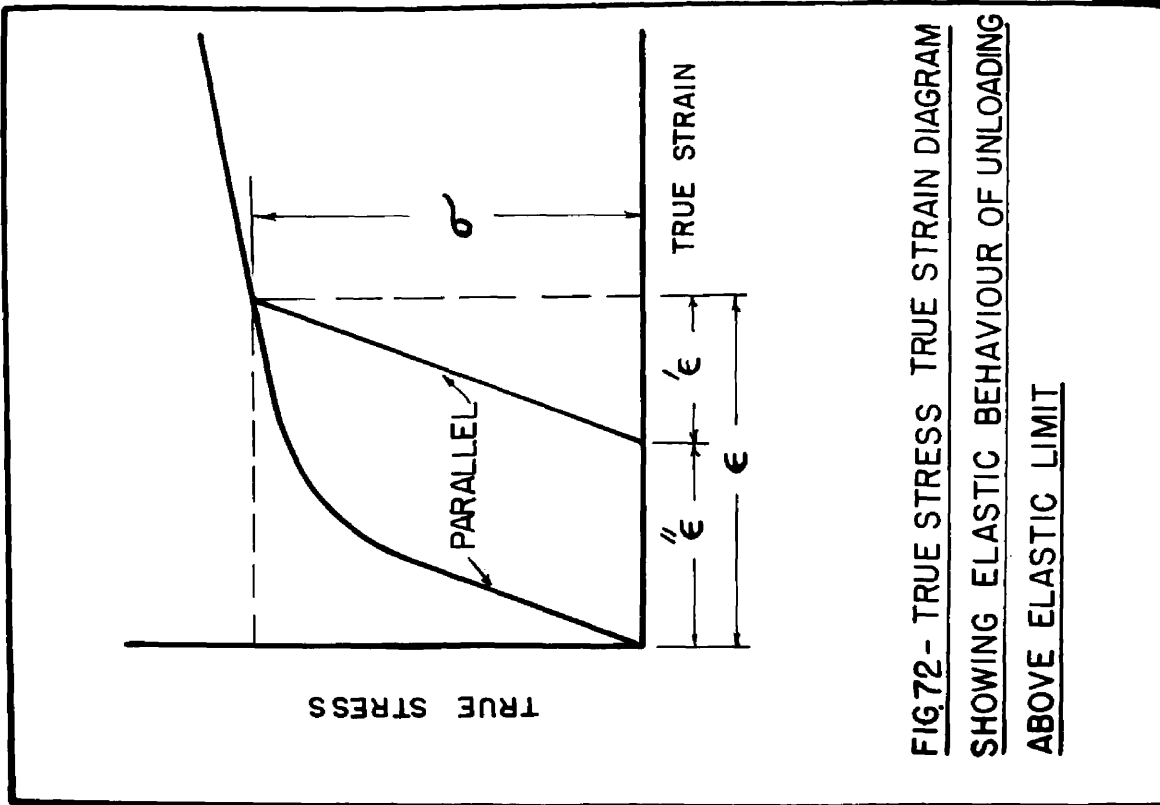
$$\epsilon_1 ds \quad \text{where } \epsilon_1 = \text{units tensile strain in/in}$$

The amount of shortening of a length ds of the extreme compressive fiber = $\epsilon_2 ds$ where $\epsilon_2 = \text{unit compressive strain in/in}$

When the bending forces are released and the member springs back, the elastic recovery of the tension and compression fibers may be expressed as: $\epsilon'_1 ds$ and $\epsilon'_2 ds$, where ϵ'_1 and ϵ'_2 are the elastic recovery in tension and compression unit strains respectively. (See Fig. 72).

Referring to Fig. 71, the angle change Z resulting from the springback

$$\text{is: } Z = \frac{\epsilon'_1 ds}{c_1} \quad \text{or} \quad Z = \frac{\epsilon'_2 ds}{c_2} .$$



It follows that $Z = X - Y = \frac{ds}{R_1} - \frac{ds}{R_2} = \frac{\epsilon'_1 ds}{C_1}$.

Therefore $\frac{1}{R_1} - \frac{1}{R_2} = \frac{\epsilon'_1}{C_1} = \frac{\epsilon'_2}{C_2}$.

The elastic recovery ϵ' can be expressed in terms of an equivalent stress and modulus of elasticity of the material: $\epsilon' = \frac{\sigma}{E}$.

When the bending forces are removed, the total internal moment produced in the member by these forces must become zero and the stress released behaves elastically. Therefore when the moment M resulting from the bending forces is released the corresponding elastic stress release may be computed by the ordinary flexural formula $\sigma = \frac{MC}{I}$.

Therefore $\epsilon' = \frac{\sigma}{E} = \frac{MC}{EI}$.

Consequently: $\frac{1}{R_1} - \frac{1}{R_2} = \frac{M}{EI}$ or $\frac{1}{R_1} = \frac{1}{R_2} + \frac{M}{EI}$.

Where R_1 = the forming radius of curvature

R_2 = the final radius of curvature

M = Total internal moment resulting from bending forces

E = Modulus of elasticity

I = Moment of inertia of the cross section.

In this method for a desired known value R_2 , the position of the neutral axis is assumed and the total internal moment resulting from bending moment M is computed using the tensile and compressive ordinary stress-strain diagrams and assuming a reasonable value for R_1 : $M = \sum(\sigma \cdot dA \cdot C)$,

Where dA = elemental area of the cross section.

Then this relation should hold: $\frac{1}{R_1} = \frac{1}{R_2} + \frac{M}{EI}$.

It is probable that the assumed value of R_1 is not exactly correct to give the desired value of R_2 ; then a new value of R_1 must be chosen and another trial made. Two or three trials may be sufficient to reach the correct value.

B. Approximate Method³²

In this method the actual area of the cross section of the member is considered to be replaced by two hypothetical areas A_1 and A_2 such that $A_1 C_1 = A_2 C_2$ and $A_1 + A_2 = \text{Area of the cross section}$.

$$M = A_1 \sigma_1 C_1 + A_2 \sigma_2 C_2 = A_1 C_1 (\sigma_1 + \sigma_2) ,$$

$$I = A_1 C_1^2 + A_2 C_2^2 = A_1 C_1 (C_1 + C_2) .$$

Substituting in the formula: $\frac{1}{R_1} = \frac{1}{R_2} + \frac{M}{EI}$ then:

$$\frac{1}{R_1} = \frac{1}{R_2} + \frac{1}{E} \left(\frac{\sigma_1 + \sigma_2}{C_1 + C_2} \right) = \frac{1}{R_2} + \frac{\sigma_1 + \sigma_2}{E \cdot D} \quad D = \text{depth of section .}$$

Therefore using the ordinary stress-strain diagrams and the relations:

$$\epsilon_1'' = \frac{C_1}{R_2} \quad \text{and} \quad \epsilon_2'' = \frac{C_2}{R_2} .$$

Since the value of C_1 and C_2 are known at the beginning due to the condition $A_1 C_1 = A_2 C_2$ and the value of R_2 is given, then the values of ϵ_1'' and ϵ_2'' are known and their corresponding values of σ_1 and σ_2 can be obtained from the ordinary stress-strain diagrams of tension and compression. Therefore the value of R_1 can be obtained by substitution in the formula:

$$\frac{1}{R_1} = \frac{1}{R_2} + \frac{1}{E} \left(\frac{\sigma_1 + \sigma_2}{C_1 + C_2} \right) ,$$

2. Discussion

It is shown from the previous illustrations that the general method for determining the spring back is based on:

- (1) The use of the ordinary stress-strain diagram of tension and compression.
- (2) The assumption of the position of the neutral axis for the material stressed beyond the elastic limit.
- (3) The assumptions of the forming radius of curvature R_1 using the approximate method for the first assumption.
- (4) The necessity for two or more trials.
- (5) The computation of internal moment resulting from bending forces using the formula $M = \sum \sigma \cdot dA \cdot C$.

The use of the ordinary stress-strain diagram above the elastic limit does not describe the behavior of the material as shown in Chapter I. Besides, assumptions of position of neutral axis and the forming radius R_1 may be in error so that more trials are required. Moreover, the computation of the internal moment M by the formula $M = \sum \sigma \cdot dA \cdot C$ is laborious.

Therefore some method of computation is required to determine the forming radius for a desired radius of curvature R_2 through use of the stress-strain diagram describing the behavior of the material above the elastic limit. Any assumption either in position of the neutral axis or the forming radius should be avoided and only one direct calculation of internal moment should be required.

3. Proposed Method

Referring to the previously shown illustration in Chapters I and II, the true stress-true strain diagrams describe the behavior of the material in tension and compression. Also the moment M and the position of the

neutral axis can be easily obtained for a given outer tensile stress σ_t using the graphs shown there based on the previously proposed theory discussed in Chapter II.

The proposed method based on that mentioned above is as follows: Assume that the member is bent so that the tensile stress in the outer fiber is a known value σ_t which corresponds to the case of forming radius R_1 . Then, the position of neutral axis, i.e. C_1 and C_2 , will be known using the graphs of σ_t vs shift of neutral axis shown in Chapter II. Also, the value of ϵ_1'' can be obtained from the true stress-true strain diagram using the given value σ_t as shown in Fig. 72. Since the value of C_1 is already known from the position of the neutral axis and ϵ_1'' is obtained, then:

$$\epsilon_1'' = \frac{C_1}{R_2} .$$

Therefore
$$R_2 = \frac{C_1}{\epsilon_1''} .$$

The value of R_2 is known for the given σ_t . The value of the bending moment M of the forming radius R_1 for the given σ_t can be obtained using curves of M vs σ_t previously mentioned in Chapter II. Then the value of M and the corresponding value of R_2 can be obtained for a certain tensile stress σ_t . A curve showing the relation between M and R_2 can easily be made from which we can obtain the moment required for a desired radius R_2 .

Therefore to determine the value of forming radius R_1 for a known desired radius R_2 the following two steps are to be followed:

(1) From the curve of M vs R_2 the value of the moment M can be known

(2) Using the relation:

$$\frac{1}{R_1} = \frac{1}{R_2} + \frac{M}{EI} .$$

R_2 is given; E and I are known properties of the material and the bent cross section; M is obtained as above mentioned in (1) then the value of R_1 can easily be obtained from the above relation and a curve can be constructed to show the relation between R_1 and R_2 .

4. Application of the New Method to Beams of Square Cross Sections of Different Materials

Using the curves of the true stress-true strain diagrams shown in Chapter I and Appendix, the curves of tensile stress vs moment of resistance and the curves of tensile stress vs shift in neutral axis as given in Chapter II, and using the procedure of the new method of finding forming radius, the curves of M vs R_2 and the curves of R_1 vs R_2 can be established for a square cross section of mild steel, stainless steel, aluminum and magnesium as shown in Figs. 73 and 74. A sample of steps and computation will be given as follows for a point on the curve of the mild steel:

- (1) For a tensile stress $\sigma_t = 45$ Ksi
- (2) Tensile strain $\epsilon = 0.035$ in/in using true stress true strain diagram of mild steel in tension Fig. 13 (Chapter I)
- (3) Then $\epsilon' = \sigma_t \frac{x \cdot 0.0011}{33} = 0.00150$ in/in where 33 is the stress at the proportional limit in Ksi and 0.0011 is the corresponding strain in/in as shown in Fig. 11 (Chapter I).
- (4) Then $\epsilon'' = \epsilon - \epsilon' = 0.0350 - 0.00150 = 0.03350$ in/in Fig. 72 (Chapter III).
- (5) The shift of neutral axis corresponds to the tensile stress σ_t and $= 45$ Ksi, is equal to $0.0100 D$ inches (where D is the side of the square section in inches) using Fig. 37 (Chapter II).

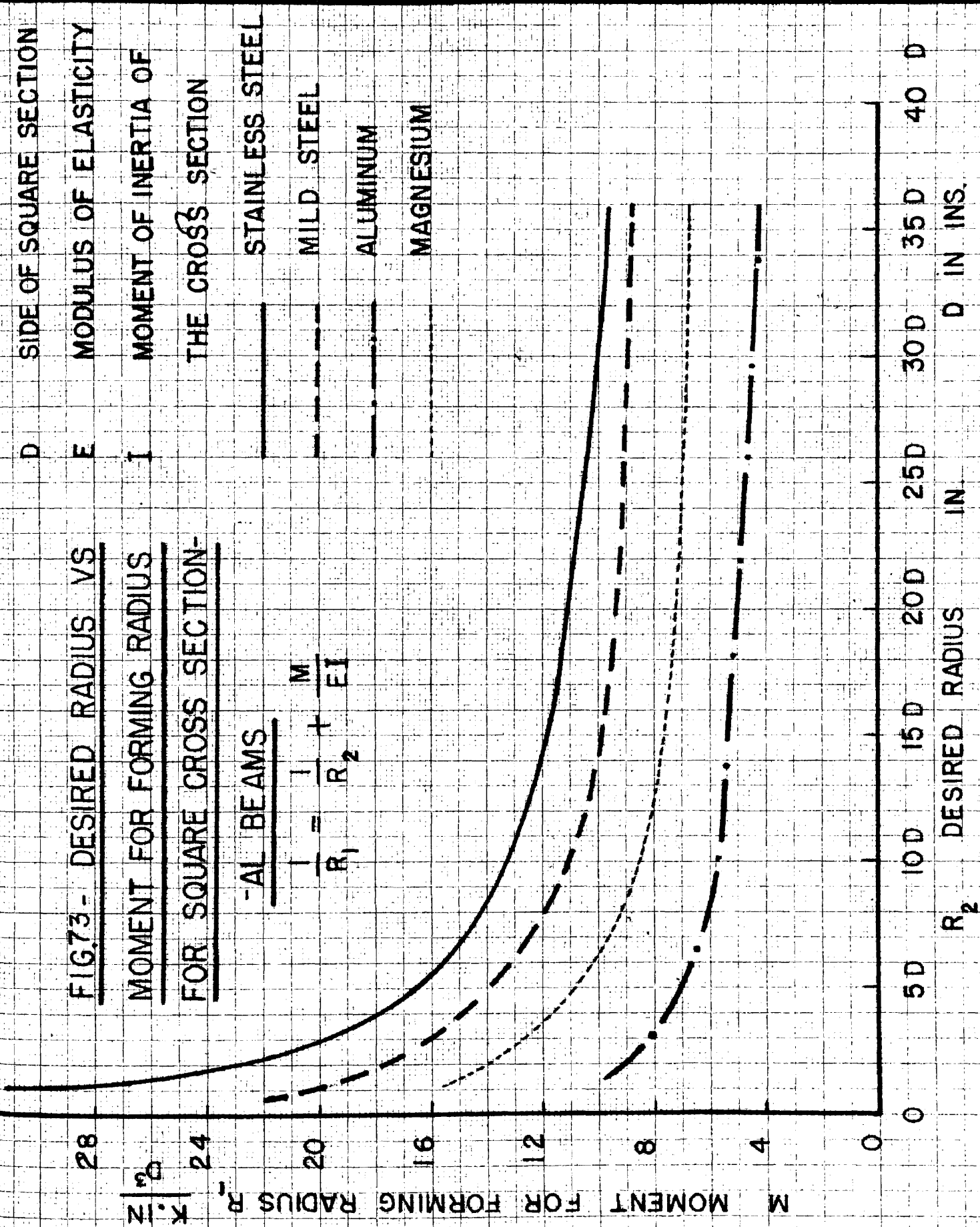
- (6) The value of the distance C_1 of the neutral axis from the tensile extreme fiber is then $= 0.5 D + 0.0100 D = 0.5100 D$ inches.
- (7) The value of the desired radius $R_2 = \frac{C_1}{\epsilon''}$ as previously shown in page 136 (Chapter III). Then $R_2 = \frac{0.5100 D}{0.03350} = 15.20 D$ inches ($D =$ side of square section in inches).
- (8) The value of the moment M for the forming radius R_1 and corresponding extreme tensile stress σ_t is obtained using Fig. 35 (Chapter II) $M = 10.0 \times 10^3 \times D^3$ lb. in (D in inches)
- (9) The value of $\frac{M}{EI}$ can then be computed, since E as given in Table 3 equals 30×10^6 psi and $I = \frac{D^4}{12}$; therefore
- $$\frac{1}{EI} = \frac{1}{2.5 \times 10^6 D^4} \quad \text{and} \quad \frac{M}{EI} = \frac{10 \times 10^3 \times D^3}{2.5 \times 10^6 \times D^4} = \frac{0.004}{D} .$$
- (10) The value $\frac{1}{R_2} = \frac{\epsilon''}{C_1} = \frac{1}{15.20 D} = \frac{0.0657}{D} .$
- (11) Using the relation $\frac{1}{R_1} = \frac{1}{R_2} + \frac{M}{EI}$, then $\frac{1}{R_1} = \frac{0.0657}{D} + \frac{0.004}{D}$, $\therefore \frac{1}{R_1} = \frac{0.0697}{D} .$
- (12) Therefore $R_1 = \frac{D}{0.0697} = 14.35 D .$

Therefore for the desired radius $R_2 = 15.20 D$ inches, the forming radius $R_1 = 14.35 D$ inches and the moment required to obtain this radius R_1 is $M = 10 \times 10^3 D^3$ lb. in (where $D =$ side of the square cross section of mild steel in inches). Repeating the previously mentioned 12 steps for different values of σ_t , we obtain values of R_2 and corresponding R_1 and M at different points and the curves of M vs R_2 and R_1 vs R_2 as shown in Fig. 73 and Fig. 74 can be established for mild steel. The same procedure can then be applied to the stainless steel, aluminum, and magnesium.

**FIG.73 - DESIRED RADIUS VS
MOMENT FOR FORMING RADIUS
FOR SQUARE CROSS SECTION-**

-AL BEAMS

$$\frac{1}{R_1} = \frac{1}{R_2} + \frac{M}{EI}$$



D SIDE OF SQUARE SECTION
E MODULUS OF ELASTICITY
I MOMENT OF INERTIA OF THE CROSS SECTION

STAINLESS STEEL
MILD STEEL
ALUMINUM
MAGNESIUM

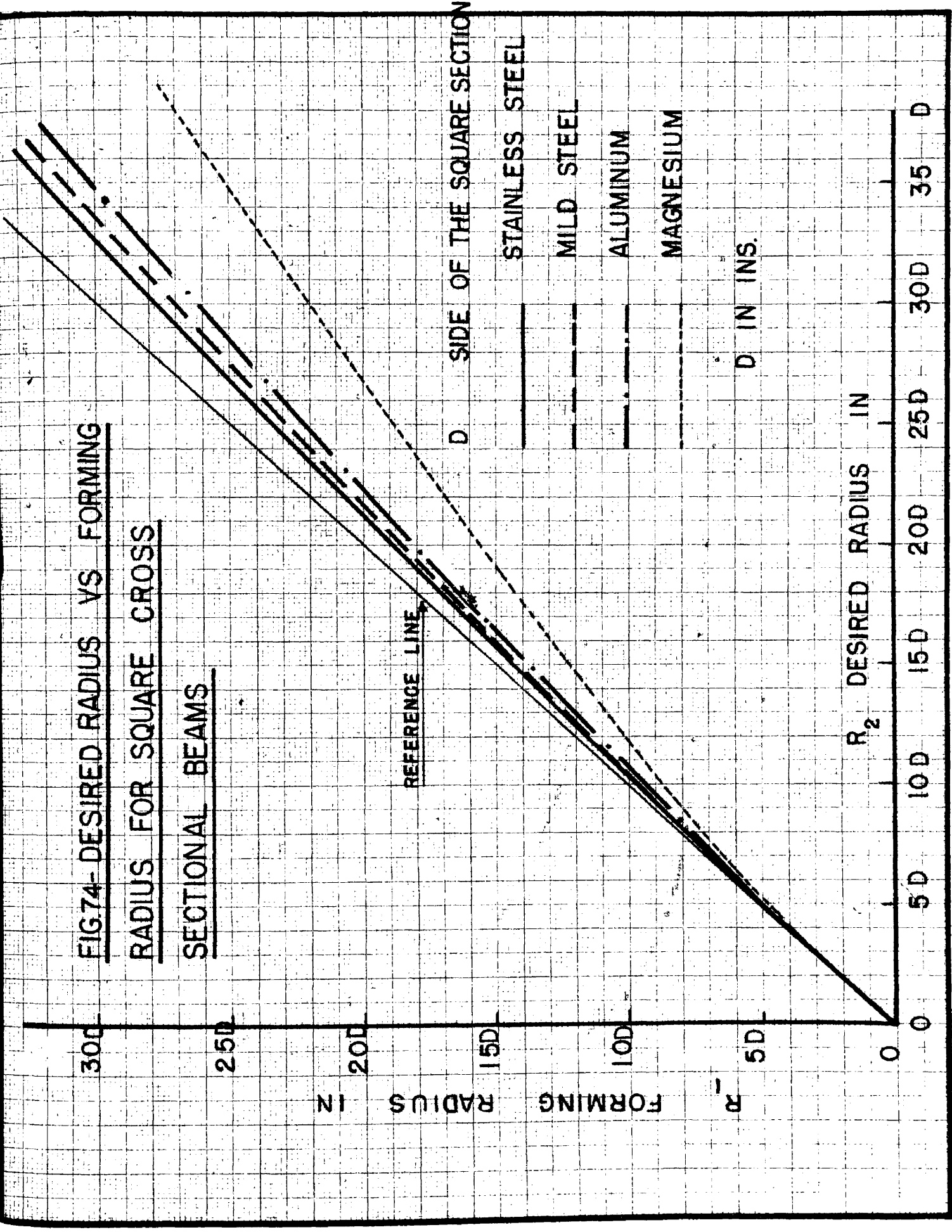
28
24
20
16
12
8
4
0

MOMENT FOR FORMING RADIUS R_2 K-IN

0 5D 10D 15D 20D 25D 30D 35D 40 D

R_2 DESIRED RADIUS IN IN.

FIG.74- DESIRED RADIUS VS FORMING
RADIUS FOR SQUARE CROSS
SECTIONAL BEAMS



CHAPTER IV

Yield Strength in Tension, Compression and Bending

1. Introduction

In the last 25 years various investigators have observed marked increase in the yield point of steel under non-uniform stress distribution, e.g. bending, above that obtained under uniform stress distribution as in tension. Others found that the yield point is the same in both cases. The attempts of these two contradicting groups of investigators to clear up this problem has not produced an entirely satisfactory solution. Therefore, further experimental investigations are required to get additional information.

2. Review of Some Previous Tests

(1) F. Nakanishi³³(1931) tested beams of different cross sections in pure bending and he found that when the outer fibers yielded the stress reached a value 1.26 to 1.70 times the yield stress as obtained by a standard tensile test from the same material.

(2) A. Thum and F. Wunderlich³⁴(1932) also tested beams in pure bending and found an increase of yield point stress in bending over the tension one, by 35-45 %.

(3) H. Moller and J. Barbers³⁵ (1934) found that the increase of the bending yield stress was 40% more than the tensile and repeating the tests in (1935) using X-rays for detecting yielding they obtained only 13% increase.

(4) E. Siebel and F. H. Vieregge³⁶ (1934) found increase of 28% of bending over tension yield stress.

- (5) F. Rinagl²⁷ (1936) found that bending yield stress equaled the tension yield stress and no increase was marked.
- (6) F. Bollenrath and J. Shmied³⁵ (1938) reached same conclusion as Rinagl.
- (7) N. Zhudin³⁷ (1939) tested steel whose upper yield stress in tension equals 1.04 to 1.38 lower yield stress in the same test. He found that the bending yield stress agrees with the lower tensile yield stress.
- (8) Peterson³⁸ (1946) detected for a steel beam of rectangular cross section under pure bending, an increase of bending yield stress of 40% over the tension yield stress.
- (9) Morkovin²⁸ (1947) found that steel which did not exhibit an upper yield point in the tension test, has equal yield stress in bending and tension. But there was an increase detected for yielding stress of bending over tension for the steel which exhibited an upper and lower yield points.
- (10) A. K. Ata³⁹ (1947) tested steel whose upper yield stress equals 1.02 lower yield stress in tension. He found that the bending yield stress agrees with the upper tensile yield stress.

3. Discussion of the Factors Tending to Produce Different Results

- (1) Rate of loading⁴⁰. Most of the tests made, were carried out without considering the effect of rate of loading which, if changed in tension from the bending tests, will affect the yield stress and consequently fair comparison cannot be attained.
- (2) Tensile Test Specimens. Specimens used for tension tests were obtained in three following ways; this lead to variation of results in comparison with bending tests.

(a) Tension specimens were cut from bending bars after they had been stressed above the yield point.

(b) Tension specimens were obtained from the same material as the bending specimens.

(c) Tension specimens were cut from the same bar of material adjacent to the bending specimen to obtain as much homogeneity as possible between tension and bending specimens.

(3) Strain Gages. The use of various mechanical gages besides the SR-4 gages might lead under different conditions of experiments to the variation of results.

(4) Accidental Eccentricity in Tensile Test. This might occur and therefore yielding was produced on one side of the tension specimen before the average stress in the cross section reached the yield limit. The yield stress obtained in this case will be smaller than the actual one and consequently there was a marked increase between tension and bending yield stresses.

(5) Determination of yield stress in the bending tests. The yield stress in bending was detected for the different tests by various methods which might have had an effect on varying its value.

(a) The appearance of Leuders Lines was taken as a sign of the start of yielding in bending. This may not lead to an exact value since Leuders Lines may appear when the plastic phenomenon has reached an important stage after yielding. If this result were used to compare with those in tension, there might be a marked increase of bending yield point over that ⁱⁿ tension.

(b) The Load Deflection Diagrams. The point where this curve tends to become horizontal was taken as the point where the bending yield stress occurred. This may vary for different investigators.

(c) Permanent Deformation. The yield stress in bending was determined by loading and unloading the bending specimens with increasing increment of load each time till the first detection of a permanent deflection and strain. The yield limit may not be safely determined by this method because the plastic deformation set up in a small zone may be entirely cancelled by the strong elastic reactions of the remaining portions of the tested specimen.

(6) Existence of Upper and Lower Yield Points for the Tension Specimens. Some of the previous results were obtained by comparing the bending yielding stress with the upper yield point stress in tension. Other results used the lower yield point stress in tension to compare it with bending. Another test made a comparison between bending and tension where there was no upper yield point stress detected in tension. This may lead to a confusion in comparing different results. Besides, the tensile lower yield point is remarkably constant but the upper yield point is variable and unpredictable and depends upon: (a) Rigidity of testing machine (b) Alignment of the specimens in the grips (c) Radius of fillets in the specimens (d) Inherent stress raisers as surface roughness, residual stresses, and discontinuities in the material.

(7) State of Yielding Bending Stress. The theory⁴¹ shows that the pure bending stress is a uniaxial state of stress. Is that experimentally true or not? This may throw a light on the variation of the results and the increase of the yielding bending stress over the tensile if any. Also, the position of the bending specimens in some of the previous tests

might not have been well aligned and torsion occurred beside the bending causing a complexed state of stress.

(8) Machine Factor. Some of the tension tests were made on one machine and the bending tests on another machine. This might lead to the possibility of the varying machine factor in obtaining different results.

4. Elements to be Considered in the Experiments to Obtain Sound Comparison Between Tension, Compression and Bending Results: To eliminate the factors discussed in III which may affect the result the following points were observed in the present tests:

(1) The rate of loading of tension, compression, and bending tests was the same i.e. the speed of the machine all over these tests was constant.

(2) SR-4 gages on four opposite sides of tension and compression specimens were used to detect the yield point.

(3) Tension and compression specimens were cut from the same bar adjacent to bending specimens as shown in Fig. 5.

(4) Detection of yield point in bending was obtained from the load strain diagram where the strain was measured by three different gages: SR-4 gage, 17-4 post yield strain gage, and clip gage. A check using the load deflection diagram was made.

(5) To reach a general conclusion--instead of working with steel alone as most of the previous experiments were done--tension, compression, and bending tests were carried out for the following materials: (a) mild steel, (b) stainless steel, (c) aluminum, (d) magnesium.

(6) Photoelastic bending test of a square cross sectional beam was made with care in alignment to know whether the elastic bending stress is a uniaxial stress as theoretically developed or not.

5. Tests

A. Description

(1) Tension and Compression Tests. These tests are carried out as previously described in Chapter I for the four materials: mild steel, stainless steel, aluminum, and magnesium.

(2) Bending Tests. They were done as explained before in Chapter I for the four mentioned materials.

(3) Photoelastic Bending Test. A Fosterite beam $8\frac{1}{2}$ " length of square cross section $15/16$ " x $15/16$ " was cut from a cylinder $3\frac{1}{2}$ " diam., 12" length. It was annealed up to 130°F to remove any residual stresses. Then it was supported in the frame as shown in Fig. 75 to be ready for a bending test. The frame having the beam attached was put in an oil bath and was heated up to 162°F . The beam was now subjected to pure bending, a moment of 12 in. lb. being applied to the central section. With the load applied the beam was allowed to cool slowly in the oil to room temperature. Then the load was removed and the beam having frozen in stresses of pure bending remained in a deformed shape as shown in Fig. 76. The oil bath, the heater, the frame and the polariscope to detect frozen in stresses during operation is shown in Fig. 77. The beam put in its longitudinal direction was subjected to polarized light and a picture as shown in Fig. 78 was taken to determine the distribution of the fringes (i.e. stresses) in the longitudinal direction. A slice $\frac{1}{4}$ " thick was cut at 90° to the longitudinal axis. This slice was subjected to polarized light where the rays are perpendicular to the surface of the slice to determine the stresses in the transverse direction.

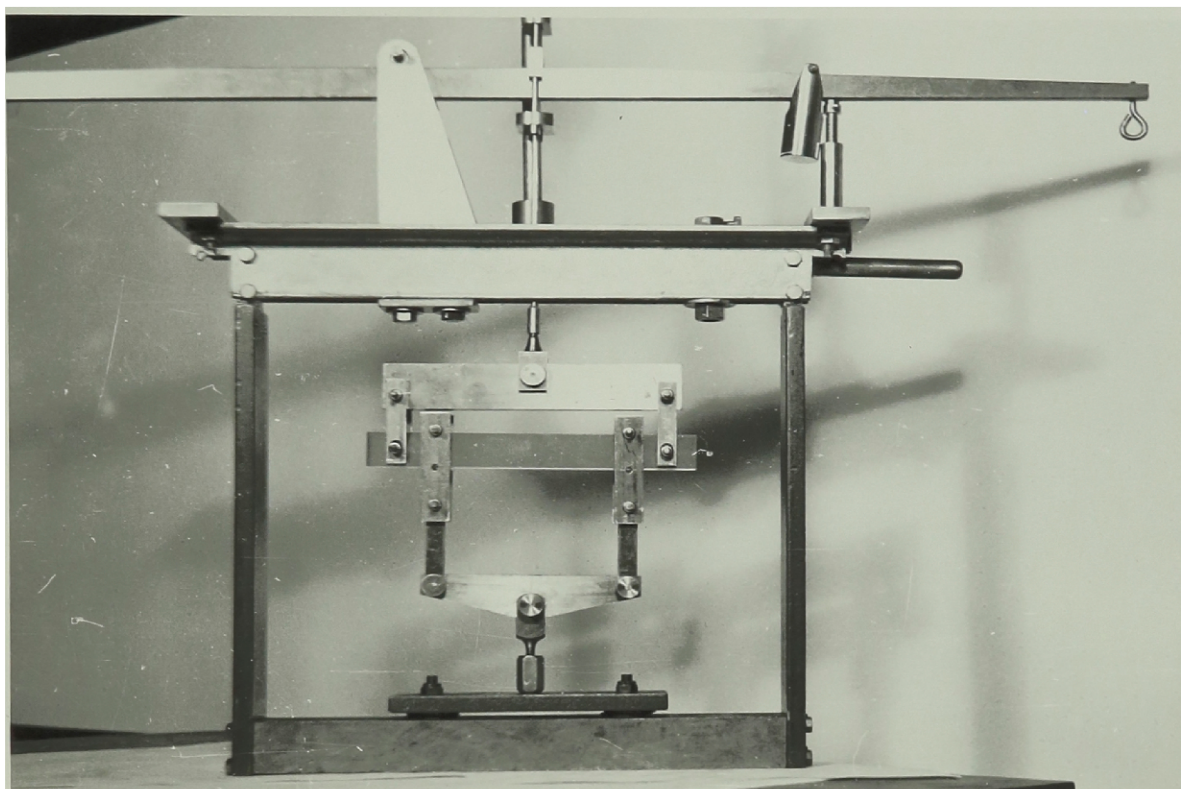


FIG 75 - FOSTERITE BEAM BEFORE BENDING

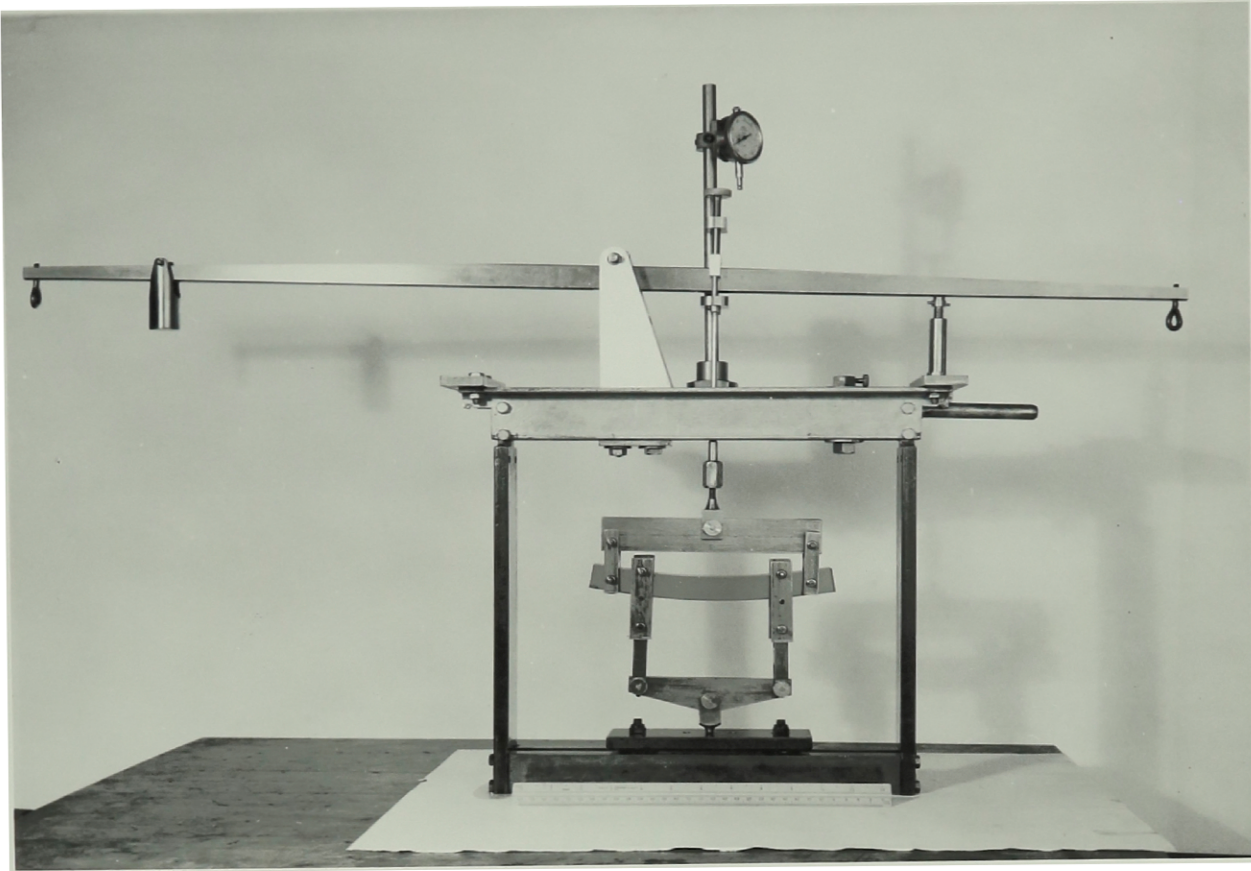


FIG. 76 - FOSTERITE BEAM. AFTER BENDING

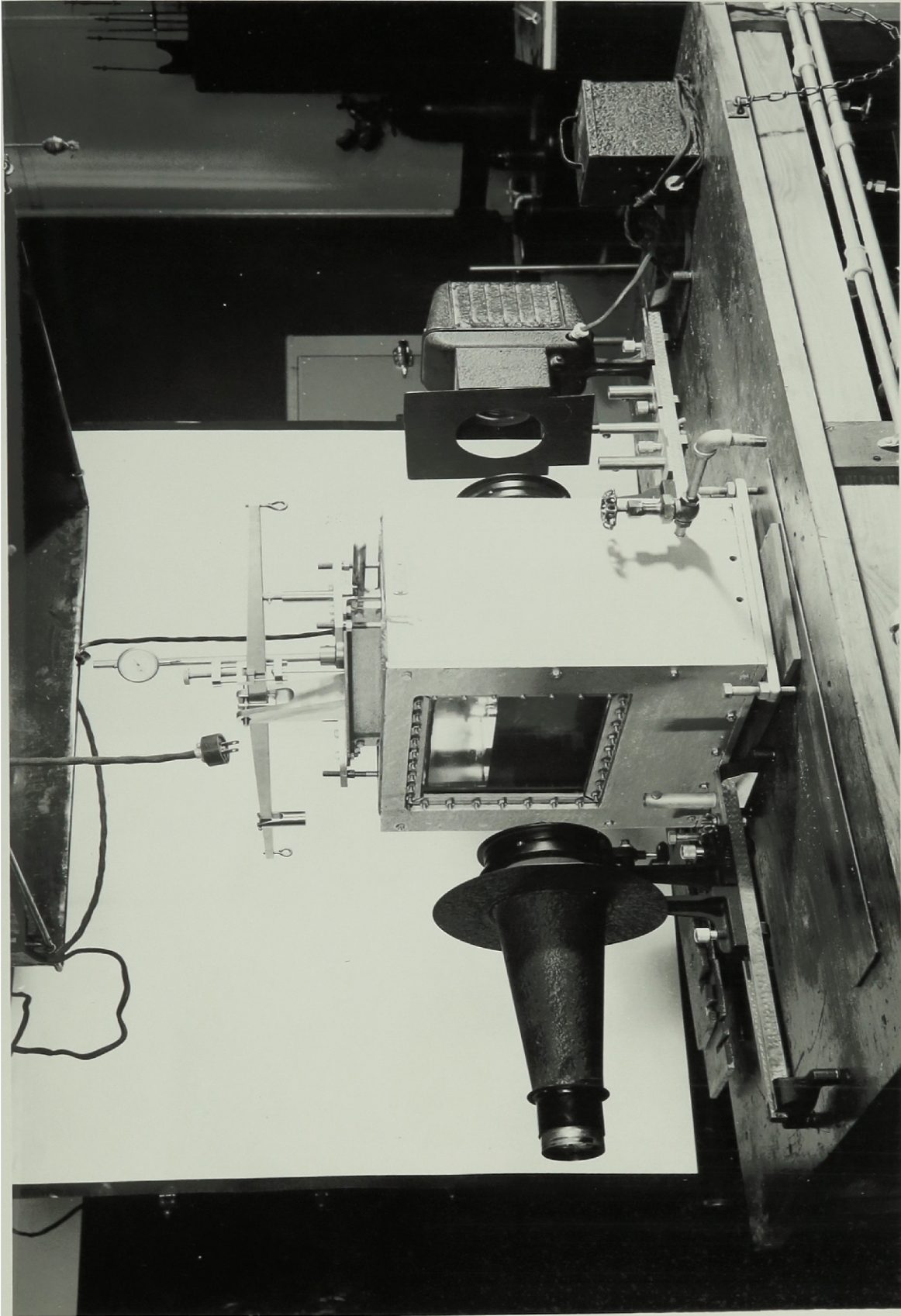


FIG. 77 - PHOTOELASTIC SET - UP

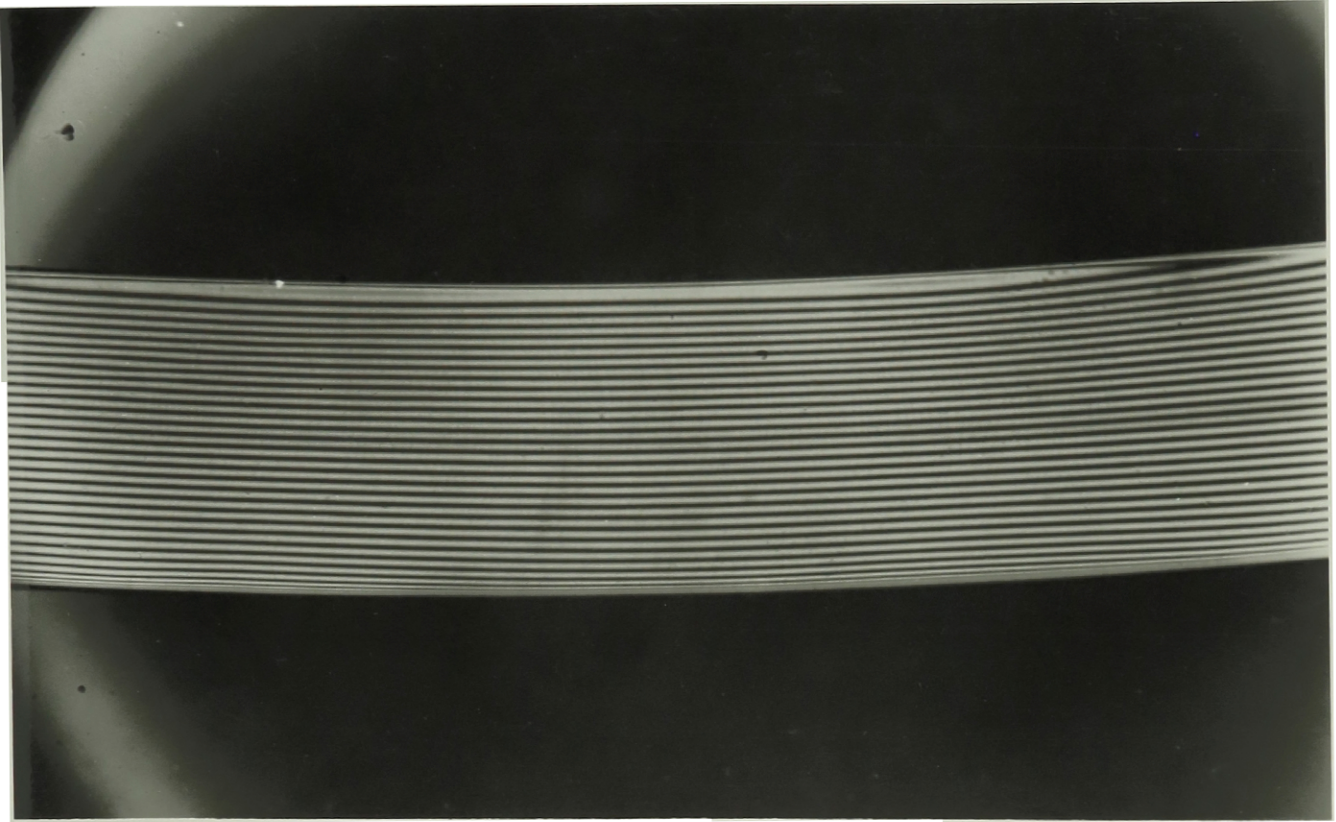


FIG. 78 - FRINGE PATTERN OF FOSTERITE BEAM

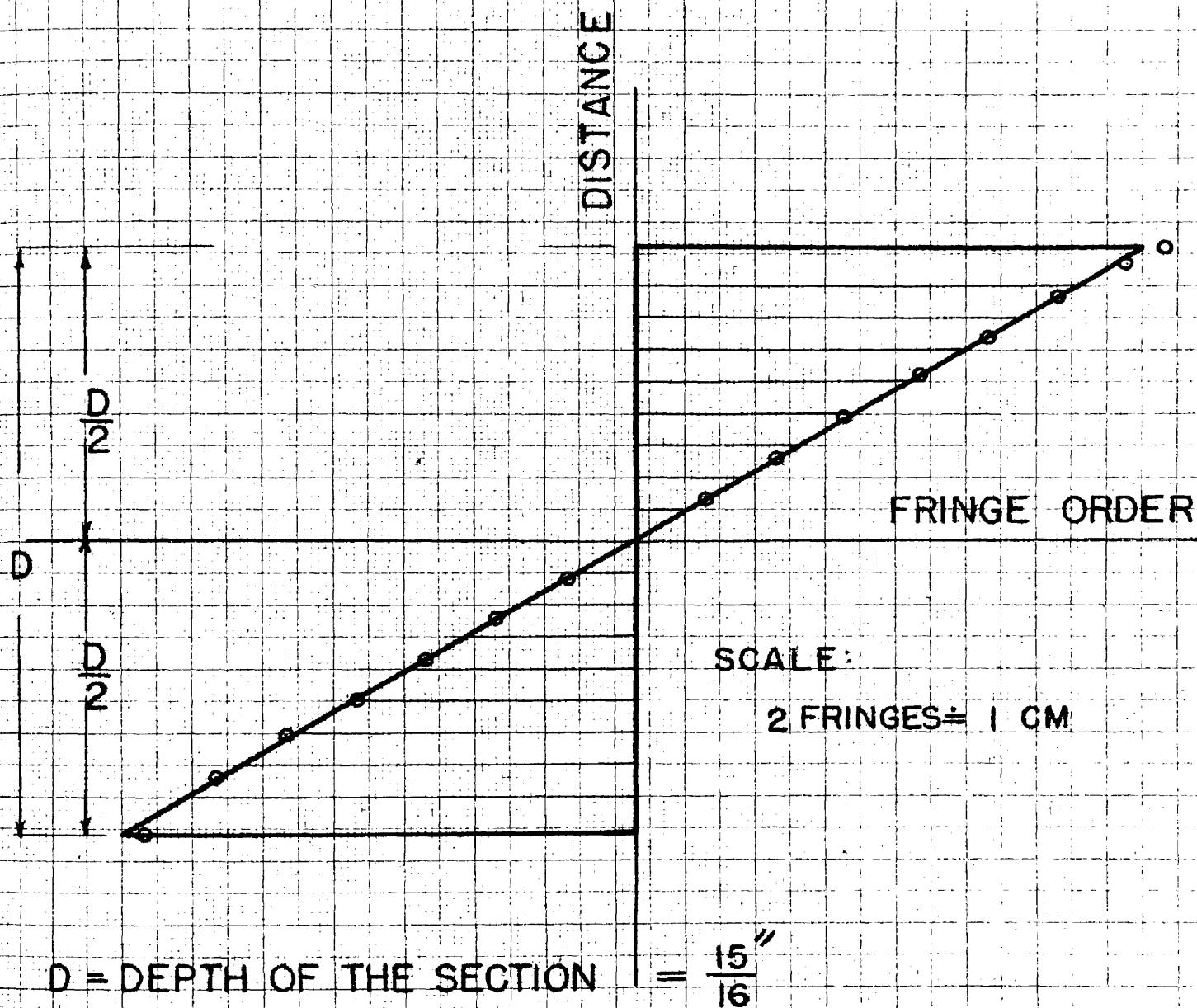


FIG.79 - FRINGE ORDER DISTRIBUTION OVER SQUARE CROSS SECTION OF FOSTERITE BEAM IN PURE BENDING

B. Results

(1) The Photoelastic Bending Test. The lateral slice of the Fosterite beam with bending stresses frozen in did not show any light in the dark field of the polariscope. This means that there is no transverse stress. The longitudinal picture of the tested beam Fig. 78, shows well spaced fringes whose distribution is linear as given in Fig. 79. This denotes that the stresses in the longitudinal direction behave as those predicted by the theory. These previous observations show that the pure bending is a uniaxial state of stress if the test is done in the proper way.

(2) Tension and Compression Tests. The values of yield strength for the tested materials: mild steel, stainless steel, aluminum and magnesium are given previously in Tables 2, 3, 4, 5 and 6.

(3) Bending Tests. The values of the beginning of yielding in bending for the tested beams--which will be compared with tension and compression yield strength--are given on page 122.

6. Comparison Between Yield Strength in Tension and Compression, and the Beginning of Yielding in Bending. The comparison is shown in Table 11. This shows that yield strength in tension or compression for all the tested materials has a maximum deviation of $\pm 10\%$ from the stress at the beginning of yielding in pure bending. This deviation may be mostly due to the experimental work especially in detecting the beginning of yielding in bending tests. Therefore we conclude, since the deviation is sometimes positive and *Sometimes negative*, that the yield strength in tension or compression for any material can be considered practically equal to the stress at the beginning of yielding in pure bending.

Table 11

Comparison between Tension and Compression Yield Strength and the Beginning of Yielding in Bending.

| Material | Tension Yield Strength Psi | Beginning of Yielding in Bending psi | % of Difference | Compression Yield Strength psi | Beginning of Yielding in Bending Psi | % of Difference |
|-----------------|-------------------------------|--------------------------------------|-----------------|-----------------------------------|--------------------------------------|-----------------|
| Mild steel | 36,000 | 37,620 | + 4.5% | 36,000 | 37,620 | + 4.5% |
| | 33,800 | | + 11.3% | 35,000 | | + 7.5% |
| Stainless steel | 42,000 | | -10.4% | 43,000 | 37,620 | -12.5% |
| | 40,500 | 37,620 | -7.1% | 39,000 | | -3.55% |
| Aluminum | 16,200 | | -1.85% | 16,500 | 15,900 | -3.64% |
| | 16,500 | 15,900 | -3.64% | 17,200 | | -7.6% |
| Magnesium | 39,500 | | -8.86% | 30,500 | 36,000 | + 18.1% |
| | 39,500 | 36,000 | -8.86% | 26,500 | | + 35.8% |

CHAPTER V

Summary and Significance of the Results

The results of the investigation previously reported in Chapters I, II, III and IV show the following conclusions:

(1) The relation between the stress and the strain in tension and in compression for any material is proposed to be in the form:

$$\sigma = \left[a\epsilon \right]_{\epsilon=0}^{\epsilon=\epsilon_1} + \left[b\epsilon^c \right]_{\epsilon=\epsilon_1}^{\epsilon=\epsilon_2} + \left[K\epsilon + m \right]_{\epsilon=\epsilon_2}^{\epsilon=\epsilon_3}$$

elastic elastic-plastic plastic

where:

σ = True stress ϵ = True strain

ϵ_1 = strain at proportional limit

ϵ_2 = strain at the transition from elastic-plastic to plastic state

ϵ_3 = strain in the plastic region up to failure

a = constant obtained from the ordinary stress strain diagram

b, c, k and m = constants determined from the true stress-true strain diagram. ϵ_1 and ϵ_2 are constant for each material having the same values in tension as in compression.

The constant "a" is practically the same in tension as in compression. The constants b, c, k and m are different in tension from compression according to the characteristic of the material. The relation between the stress and the strain in this form is simple, adaptable, and easy to apply as shown previously.

(2) The proposed relation between the stress and the strain is established for mild steel, stainless steel, aluminum, and magnesium in

tension as well as in compression as shown in Tables 3, 4, 5, and 6.

(3) It is shown from the experimental data of the true stress true strain diagrams in tension for the tested materials that the stress at the necking point is higher than the slope of the true stress true strain diagram at this point.

This fact is proved theoretically by the relation:

$$\sigma_{\text{necking}} = \left(\frac{d\sigma}{d\epsilon} \right)_{\text{necking}} + \left(\frac{dP}{dA} \right)_{\text{necking}}$$

where σ = true stress $\frac{d\sigma}{d\epsilon}$ = slope of the true stress true strain diagram. $\frac{dP}{dA}$ = rate of change of the load with respect to the cross section area which is a positive quantity at necking and can be obtained from load vs area diagram as shown in Figures 21 and 22. The above mentioned theoretical and experimental result has therefore to replace the one given in the literature that the true stress at necking equals the slope of the true stress true strain diagram i.e.

$$\sigma_{\text{necking}} = \left(\frac{d\sigma}{d\epsilon} \right)_{\text{necking}}$$

(4) It is also shown from the experimental data of the true stress true strain diagram in tension for all the tested materials that the strain at necking has a different value from the strain hardening exponent. The theoretical relation governing the value of the strain at necking is established as follows:

$$\epsilon_{\text{necking}} = 1 - \frac{m - \left(\frac{dP}{dA} \right)_{\text{necking}}}{\left(\frac{d\sigma}{d\epsilon} \right)_{\text{necking}}}$$

where ϵ = true strain

m = intercept of the straight line portion of the extrapolated true stress true strain diagram with the true stress axis.

The experimental data verifies the above theoretical derivation with varying percentage of difference for each material.

The value of the true strain at necking as derived before has to replace the value given in the literature that the strain at necking equal the strain hardening exponent, i.e.

$$\epsilon_{\text{necking}} = c$$

(5) A new method for treating hyper-elastic pure bending is derived, from which the value of the moment of resistance for any cross section will be:

$$M_t = \frac{D^2}{(\epsilon_{3t} + \epsilon_{3c})^2} \cdot \left\{ \int B \epsilon \left[(a\epsilon)_0^{\epsilon_{1t}} + \left(1 - \frac{\epsilon_{1t} + \epsilon_{2t}}{4}\right) (b\epsilon^c)_{\epsilon_{1t}}^{\epsilon_{2t}} + \left(1 - \frac{\epsilon_{2t} + \epsilon_{3t}}{4}\right) (k\epsilon + m)_{\epsilon_{2t}}^{\epsilon_{3t}} \right] d\epsilon + \right. \\ \left. + \int B \epsilon \left[(a\epsilon)_0^{\epsilon_{1c}} + \left(1 + \frac{\epsilon_{1c} + \epsilon_{2c}}{4}\right) (b\epsilon^c)_{\epsilon_{1c}}^{\epsilon_{2c}} + \left(1 + \frac{\epsilon_{2c} + \epsilon_{3c}}{4}\right) (k\epsilon + m)_{\epsilon_{2c}}^{\epsilon_{3c}} \right] d\epsilon \right\}$$

where the values a , b , c , k , m , ϵ_1 , ϵ_2 and ϵ_3 are as previously mentioned in (1), and the subscript t is for tension and c for compression. D and B = Depth and width of the cross section respectively. M_t = moment of resistance of the cross section. This relation can be used to find the value of the moment of resistance for any given extreme fiber tensile stress σ_{3t} , since ϵ_{3t} can be obtained from the true stress true strain diagram and ϵ_{3c} from the following equation used to define the position of the neutral axis:

$$\int B \rho \left[(a \epsilon)_o^{\epsilon_{1t}} + \left(1 - \frac{\epsilon_{1t} + \epsilon_{2t}}{4}\right) (b \epsilon^c)_{\epsilon_{1t}}^{\epsilon_{2t}} + \left(1 - \frac{\epsilon_{2t} + \epsilon_{3t}}{4}\right) (K \epsilon + m)_{\epsilon_{2t}}^{\epsilon_{3t}} \right] d\epsilon$$

$$= \int B \rho \left[(a \epsilon)_o^{\epsilon_{1c}} + \left(1 + \frac{\epsilon_{1c} + \epsilon_{2c}}{4}\right) (b \epsilon^c)_{\epsilon_{1c}}^{\epsilon_{2c}} + \left(1 + \frac{\epsilon_{2c} + \epsilon_{3c}}{4}\right) (K \epsilon + m)_{\epsilon_{2c}}^{\epsilon_{3c}} \right] d\epsilon .$$

Also the values a , b , c , k , m , ϵ_1 , ϵ_2 and D are known numerically and the value of B for any cross section can be replaced in terms of D and ρ . Then the right hand side of the equation of the moment of resistance can be easily computed giving the required result.

It may be noted that the factors $\left(1 - \frac{\epsilon_1 + \epsilon_2}{4}\right)$ and $\left(1 + \frac{\epsilon_1 + \epsilon_2}{4}\right)$ etc., are introduced in the equations of the moment of resistance and the shift of the neutral axis to take account of the effect of the lateral deformation of the cross section.

This method is based on:

- a. The true stress true strain relation as proposed in (1).
- b. Separate relation between the stress and the strain in tension and in compression.
- c. Effect of lateral deformation is considered.
- d. The shift of neutral axis of the cross section is taken into account.

It is worthy to note that all these basic statements are applied to the problem of hyper-elastic bending for the first time.

(6) This method is applied to square, square on edge, circular and trapezoidal cross sections in pure bending as shown in Chapter II.

(7) As a sample of using the new theory of hyper-elastic pure bending a theoretical computation is made for a square cross section of mild steel, stainless steel, aluminum and magnesium. The result of the

computation is shown in Figures 35, 39, 43, and 47 giving relations between σ_t and M_t and in Figures 37, 41, 45 and 49 giving relations between shift of neutral axis and σ_t . Following the same method of computation and using the corresponding equations, similar relations between σ_t , shift of neutral axis and M_t can be established for the square on edge, circular, and trapezoidal cross sections.

(8) Experimental tests (see Fig. 51) were carried out to verify the theoretical application of the new theory of hyper-elastic bending for the square cross section of mild steel, stainless steel, aluminum, and magnesium. The tests showed:

- a. Close agreement between the theoretical and experimental results as shown in Figures 35, 36, 39, 40, 43, 44, 47, and 48.
- b. The plane cross section remains plane after hyper-elastic bending up to the maximum deformation reached 4% as in Figures 55, 56, 57, and 58.
- c. Poisson's ratio varied gradually from its elastic region value up to 0.5 as shown in Figures 59, 60, 61, and 62.

(9) The designed clip gage shown in Figure 117 proved its ability as a means of measuring strains in the hyper-elastic region.

(10) The electrical 17-4 post yield gage worked successfully in detecting the hyper-elastic strains.

(11) The hyper-elastic pure bending treatment previously mentioned is valuable in case of hyper-elastic design and forming of metals. Economy and better understanding of the behavior of the materials can be obtained by using the new theory than those given in the literature. As an example, the relation between σ_t and M_t --using the new theory, the rectangular distribution theory (page 58) and the trapezoidal distribution

theory (page 64)--is given in Figure 80.

(12) As a sample of application of the new theory for forming of materials, a method of obtaining the moment needed and the die radius required to bend a beam of any cross section to a desired radius is given. Its application for square cross sections of mild steel, stainless steel, aluminum and magnesium were carried out resulting in the curves shown in Figures 73 and 74 giving the Moment vs the desired radius, and the die radius vs the desired radius. Following the same steps similar curves can be obtained for square on edge, circular, and trapezoidal cross sections. These curves are valuable in direct use in the machine shop for forming beams of mild steel, stainless steel, aluminum and magnesium. Similar results can be achieved for other materials.

(13) The photoelastic test for a square cross sectional beam of Fosterite verifies the theory that the bending stress is a uniaxial state of stress.

(14) The comparison between yield strength in tension, compression and the beginning of yielding in bending for mild steel, stainless steel, aluminum, and magnesium shows that they can be considered practically equal to each other. This result disproves the observations found by several investigators that the beginning of yielding in bending is about 40% greater than the tensile yield strength.

In Summary, it is concluded that the true stress true strain relationship has been successfully applied to the problem of hyper-elastic pure bending.

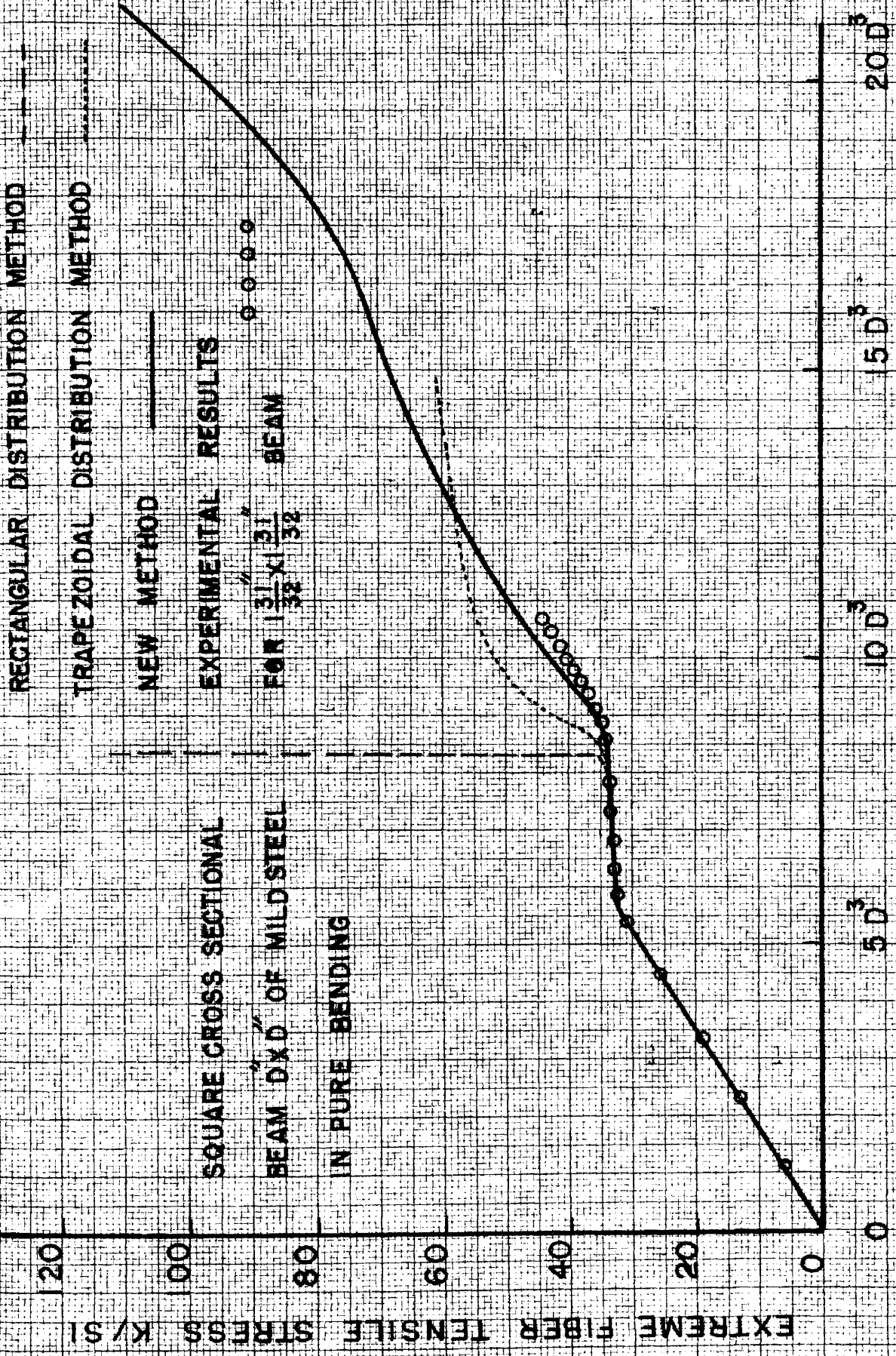


FIG 80 - COMPARISON BETWEEN NEW & PREVIOUS METHODS

BIBLIOGRAPHY

1. Howarth, R. M. "Some Elementary Considerations of the Stress Strain Curve" Aircraft Engineering Vol. XIX, p. 372, December, 1947.
2. Shepherd, W. M. "Plastic Stress Strain Relations" Proceedings of the Institution of Mechanical Engineers Vol. 139 No. 39, p. 95-114, (1948)
3. Glayzal, A. "General Stress-Strain Laws of Elasticity and Plasticity" Journal of Applied Mechanics vol 13, p. A-291, December, 1947.
4. Roop, W. P. "Stress Strain in Plastic Flow" Welding Journal vol. 25, p. 799-823, September, 1946
5. Sturm, R. G. and Templin "Some Stress Strain Studies of Metals" Journal of the Aeronautical Science, vol. 7, p. 189, March, 1940
6. Osgood, W. R. "Stress Strain Formulas" Journal of the Aeronautical Science, vol. 13, p. 45, January, 1946
7. MacGregor "Modification of Stress Strain Diagram" Journal of the Franklin Institute vol. no. 2 p. 111, August, 1944, and no. 3 p. 159, September, 1944
8. Hollomon, J. H. and Jaffe, L. D. "Ferrous Metallurgical Design" John Wiley and Sons Book Co., New York, 1947
9. Nadai, A. "Plasticity" McGraw-Hill Book Co., New York, 1931
10. Donnell, L. H. "Plastic Flow as Unstable Process" Journal of Applied Mechanics vol. 9, p. A-91, June, 1942
11. Prager, W. "Theory of Plasticity" Brown University, 1942
12. Hollomon, J. H. and Lubahn "Plastic Flow of Metals" Physical Review vol. 70, p. 775, November, 1946
13. Timoshenko, S. "Theory of Elastic Stability" McGraw-Hill Book Co., New York, 1936
14. Gill, S. S. "The Bending Strength of Materials with a Non Linear Stress Strain Curve" Aircraft Engineering vol. XIX No. 221, p. 212, July, 1947
15. Arennikoff, A. "Theory of Inelastic Bending with Respect to Limit Design" Proceeding of American Society of Civil Engineers vol. 47, p. 256, March, 1947

16. Wang, T. S. "Elastic and Plastic Bending" Journal of the Aeronautical Science, vol. 14, p. 422, July, 1947
17. Yachter, N. "Note on Bending Beyond the Proportional Limit" Journal of the Aeronautical Science, vol. 12, p. 21, January, 1945
18. Osgood, S. S. "Plastic Bending" Journal of the Aeronautical Science, vol. 12, p. 253, October, 1945, and vol. 11, p. 213, July, 1944
19. Beilschmidt, J. L. "Strength of Light Alloy Engineering" Aircraft Engineering vol. XVI, p. 76-81, March, 1944
20. Bernhult, E. "Yield Point and Stress Distribution in Bars and Tubes Due to Plastic Bending" Engineer's Digest (American edition) vol I, No. 10, p. 555-558, September, 1944
21. Rappleyer, F. A. and Eastman, E. J. "Flexural Strength in the Plastic Range of Rectangular Magnesium Extrusions" Journal of the Aeronautical Science, vol. 11, p. 373, October, 1944
22. Marin, J. and Cotterman "Experiments on Plastic Bending for Aluminum Alloy 175 T" Proceedings American Society Testing Materials vol. 43, pp. 581-599, 1943
23. Volterra, R. "Results of Experiments on Metallic Beams Beyond the Elastic Limit" Journal of the Institution of Civil Engineers March, 1943
24. Beilschmidt, J. L. "The Stresses Developed in Sections Subjected to Bending Moment" Journal of the Royal Aeronautical Society, Vol. XLVI no. 379, pp. 161-182, July, 1942
25. Osgood, W. R. "The Crinkling Strength and the Bending Strength of Round Aircraft Tubing" National Advisory Committee for Aeronautics, Technical report No. 632, 1938
26. Williams, H. "Pure Bending in Plastic Range" Journal of the Aeronautical Science, vol. 14, p. 457, August, 1947
27. Rinagl, F. "Yield Limits and Characteristic of Deflection Lines" Preliminary Publication of 2nd Congress of International Association for Bridges and Structural Engineering, Berlin-Munich, 1936
28. Morkovin, D. and Sidebottom, O. "The Effect of Non Uniform Stress Distribution on the Yield Strength of Steel." Bulletin No. 26, vol. 45, University of Illinois, December, 1947
29. Kuntze, W. "Ermittlung des Einflusses Ungleichformiger Spannungen und Guerschnitte auf die Streckgrenze" Der Stahlbau Berlin vol. 7 1933

30. Luxion, W. and Johnston, B. G. "Plastic Behavior of Wide Flange Beams" The Welding Journal, vol. 27, p. 538, November, 1948
31. Cozzone, F. P. "Bending Strength in Plastic Range" Journal of the Aeronautical Science, vol. 10, p. 137, May, 1943
32. Sturm, R. G. and Fletcher, F. J. "Determining Spring Back" Product Engineering, vol. 12, p. 526, October and p. 596, November, 1941
33. Nakanishi, F. "On the Yield Point of Mild Steel" Imperial University Aeronautical Research Institute, report vol. 6, Tokyo, 1931
34. A. Thum and F. Wunderlich "Restricted Deformation and the Yield Limit" Forschung auf den Gebiete des Ingenieur Wesens, p. 261, 1932
35. Van Iterson "Plasticity in Engineering" Hafner Publishing Co., Inc., New York, 1947
36. Siebel and Vieregge "Dependence of Start of Yield on Distribution of Stresses and on Material" Archivfur Eisenhüttenwesen, Issue 12, p. 679, 1933-34
37. N. Zhudin "On the Yield Point in Flexure" Zhurnal Tekhnicheskoi Fiziki, v. 9, Part 1, p. 968
38. Peterson, E. "Effect of Non Uniform Stress Distribution on the Yield Point" Proceeding A. S. C. E., vol. 72, p. 445, April, 1946
39. Ata, A. K. "Effect of Stress Distribution on Yield Point" Report submitted to Faculty of Engineering, Fouad 1st University, Giza, Egypt, December, 1947
40. Quinney, H. "Further Tests on the Effect of Time in Testing" The Engineer, London, June, 1936
41. Timoshenko, S. "Theory of Elasticity" McGraw-Hill Book Co., New York, 1934
42. Stitz, E. O. and Ata, A. K. "Preliminary Tests with "E" and "17-4" Special Type Strain Gages" Technical Memorandum P-11 Purdue University, June, 1950
43. Frocht, "Photoelasticity" Vol I, 1941 and Vol II, 1947, John Wiley and Sons Book Co., New York

APPENDIX

1. Tensile Ordinary Stress Strain Diagrams

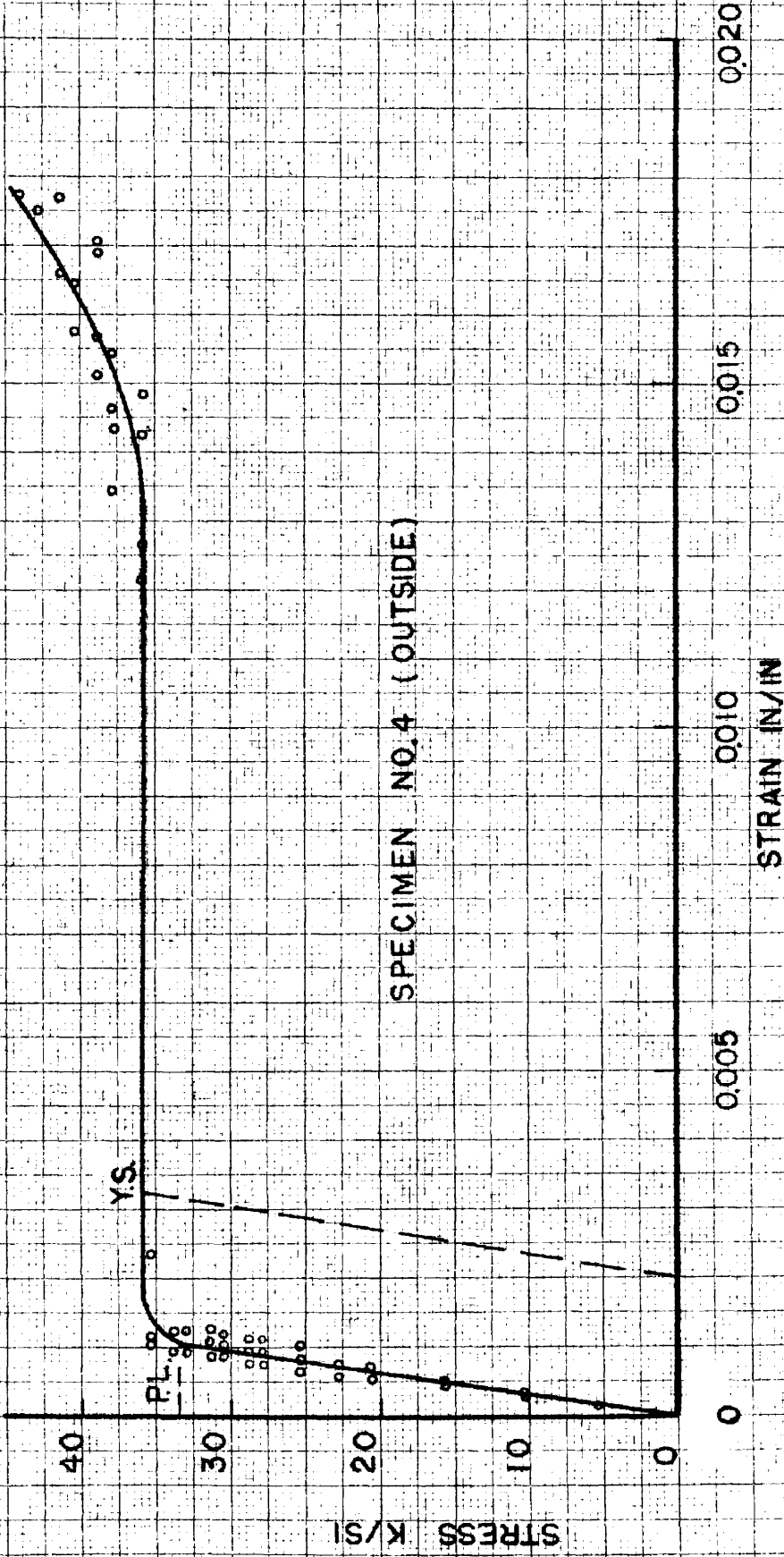
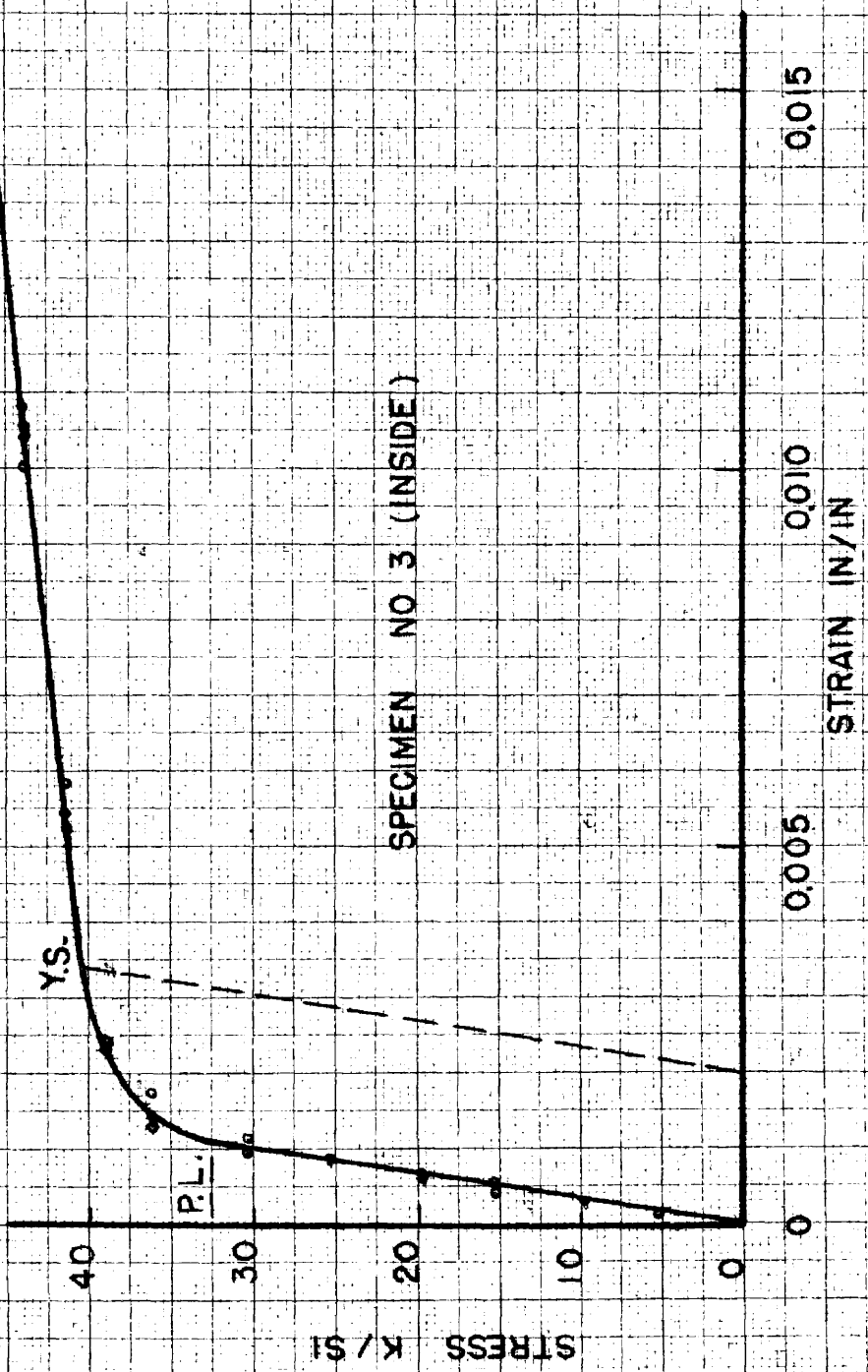
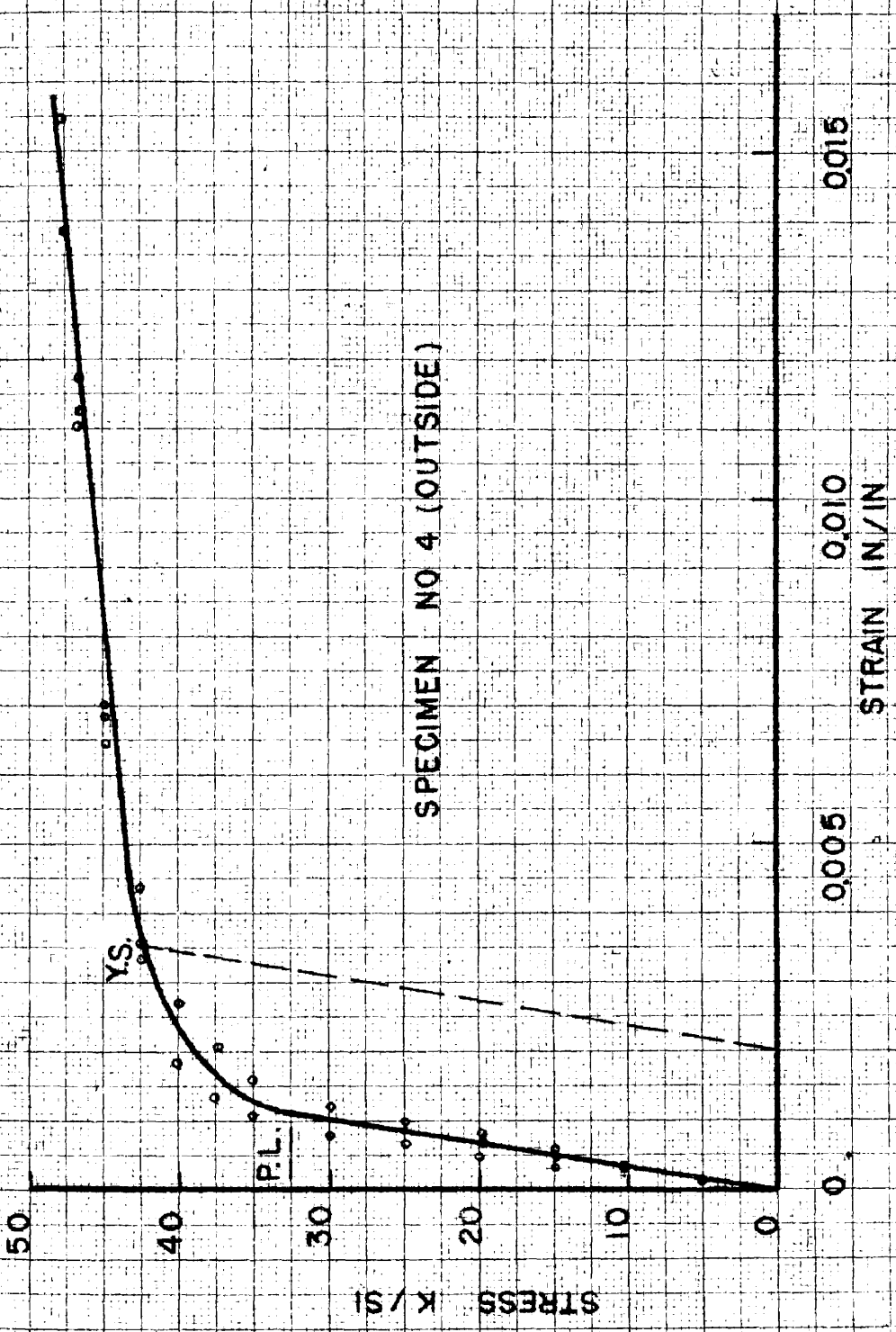


FIG. 81 ORDINARY STRESS STRAIN DIAGRAM FOR MILD STEEL IN TENSION



SPECIMEN NO 3 (INSIDE)

FIG. 82-ORDINARY STRESS STRAIN DIAGRAM FOR STAINLESS STEEL IN TENSION



SPECIMEN NO 4 (OUTSIDE)

FIG.83 ORDINARY STRESS STRAIN DIAGRAM FOR STAINLESS STEEL IN TENSION

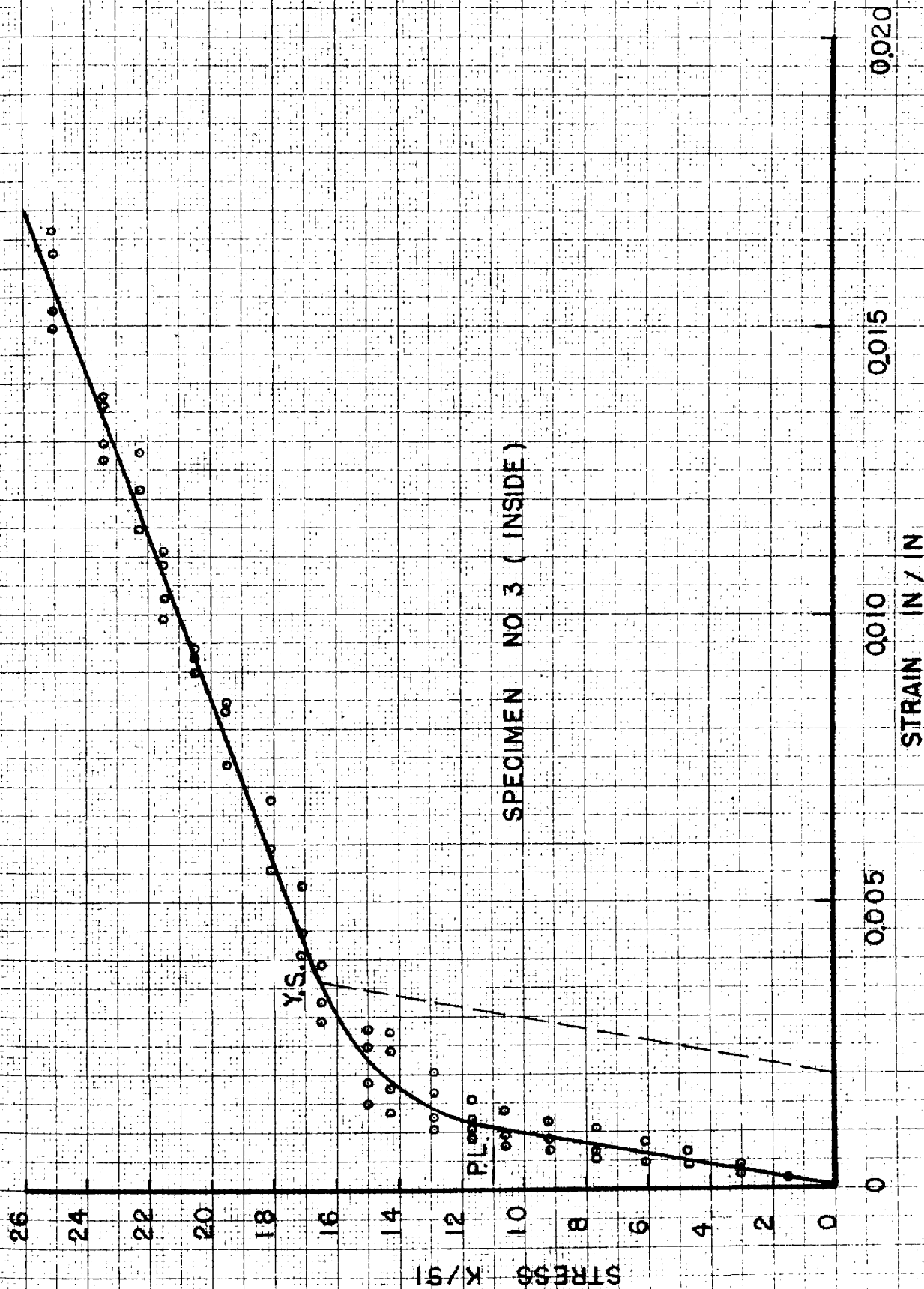


FIG. 84-ORDINARY STRESS STRAIN DIAGRAM FOR ALUMINUM IN TENSION

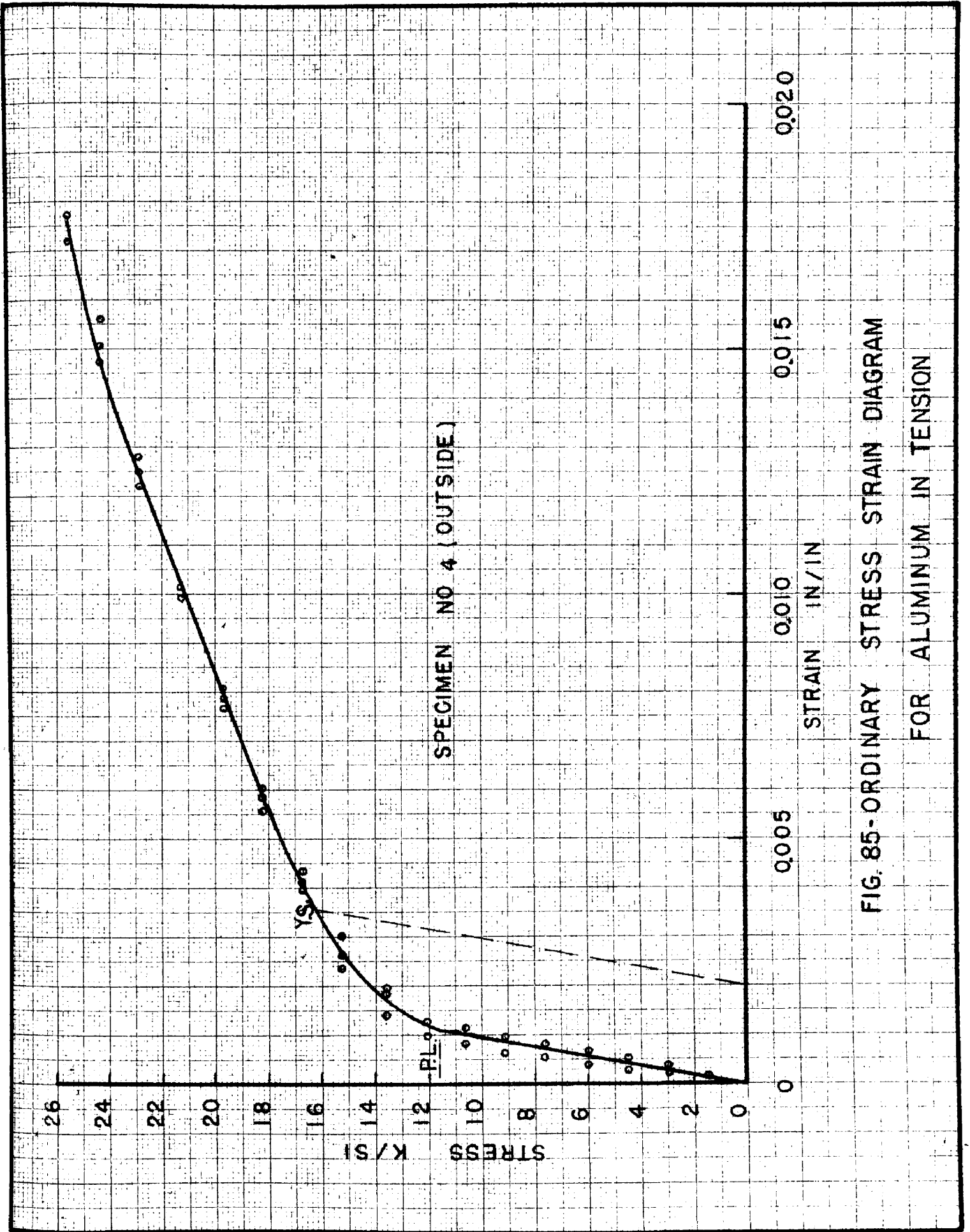


FIG. 85-ORDINARY STRESS STRAIN DIAGRAM FOR ALUMINUM IN TENSION

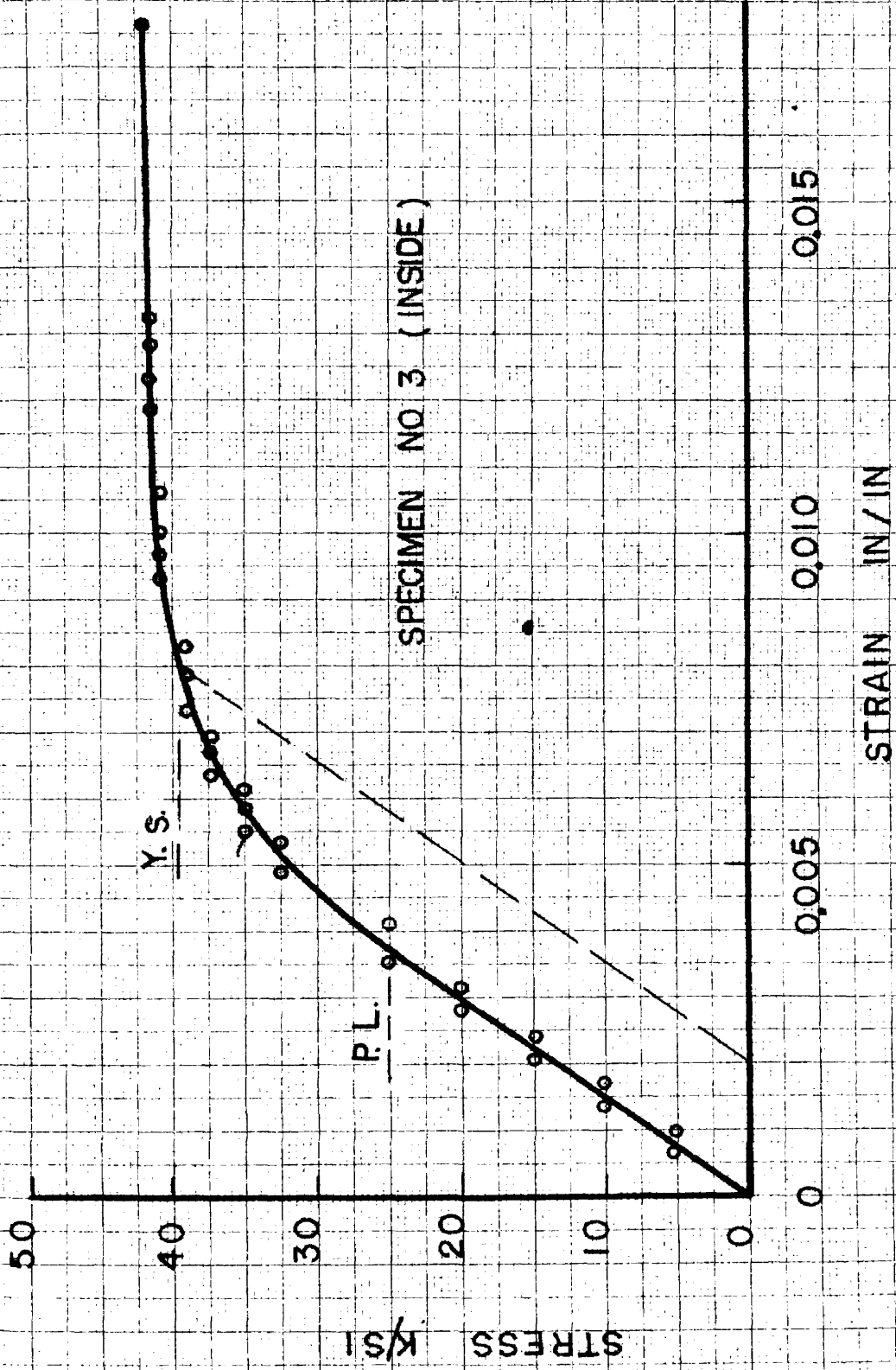


FIG.86 - ORDINARY STRESS STRAIN DIAGRAM FOR MAGNESIUM IN TENSION

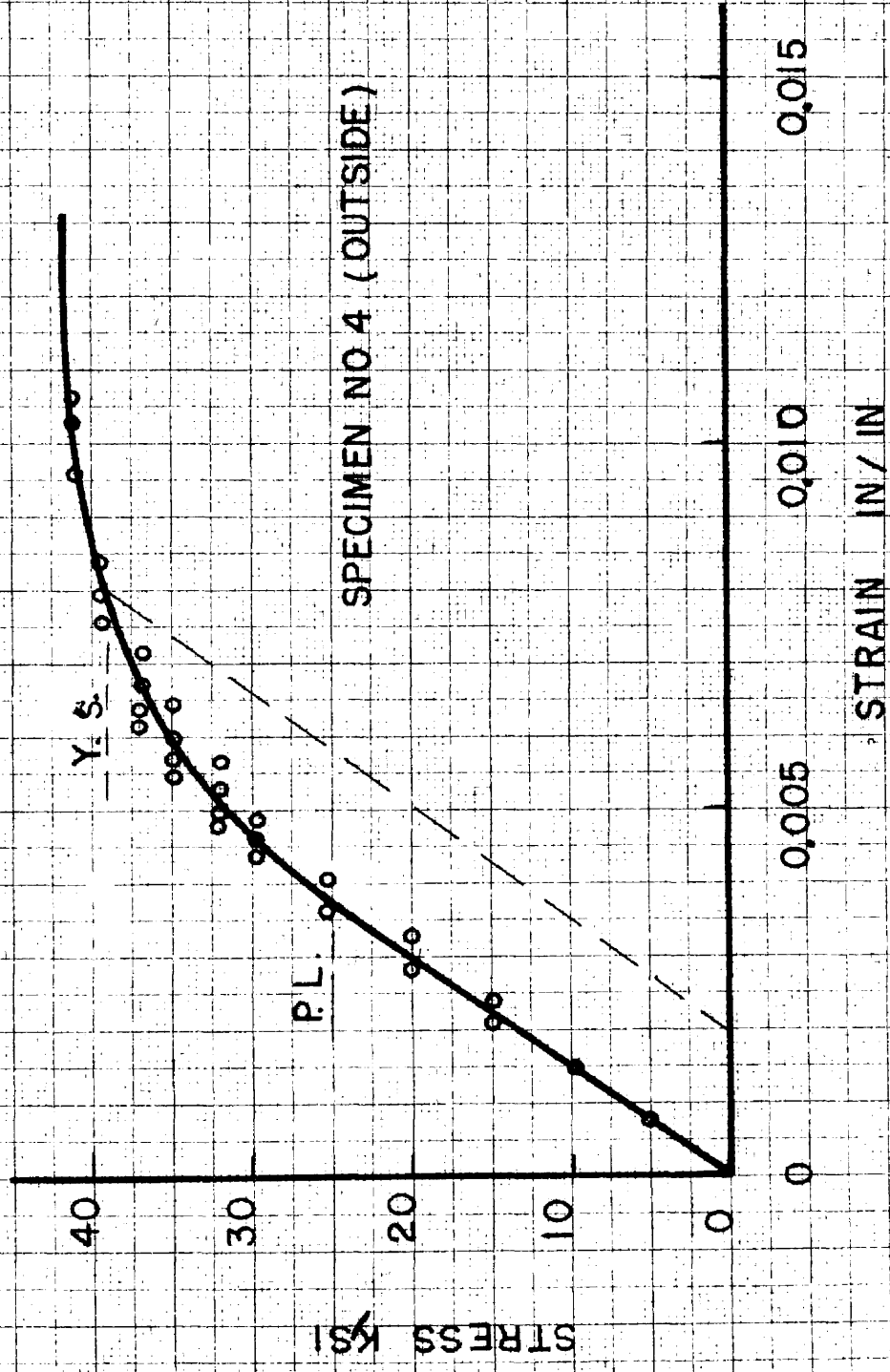
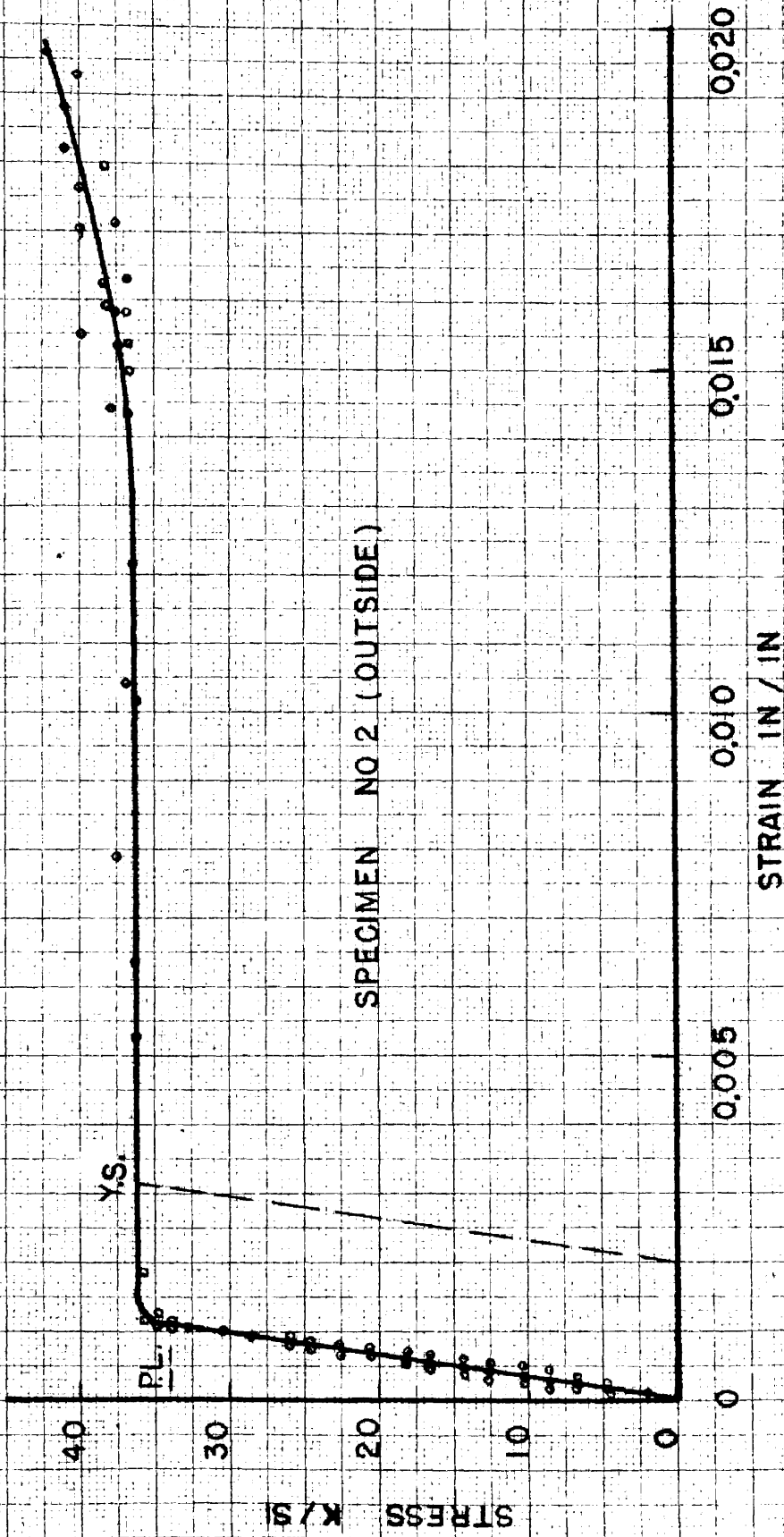


FIG87 - ORDINARY STRESS STRAIN DIAGRAM FOR MAGNESIUM IN TENSION

2. Compressive Ordinary Stress Strain Diagrams



SPECIMEN NO 2 (OUTSIDE)

FIG. 88 - ORDINARY STRESS STRAIN DIAGRAM FOR MILD STEEL IN COMPRESSION

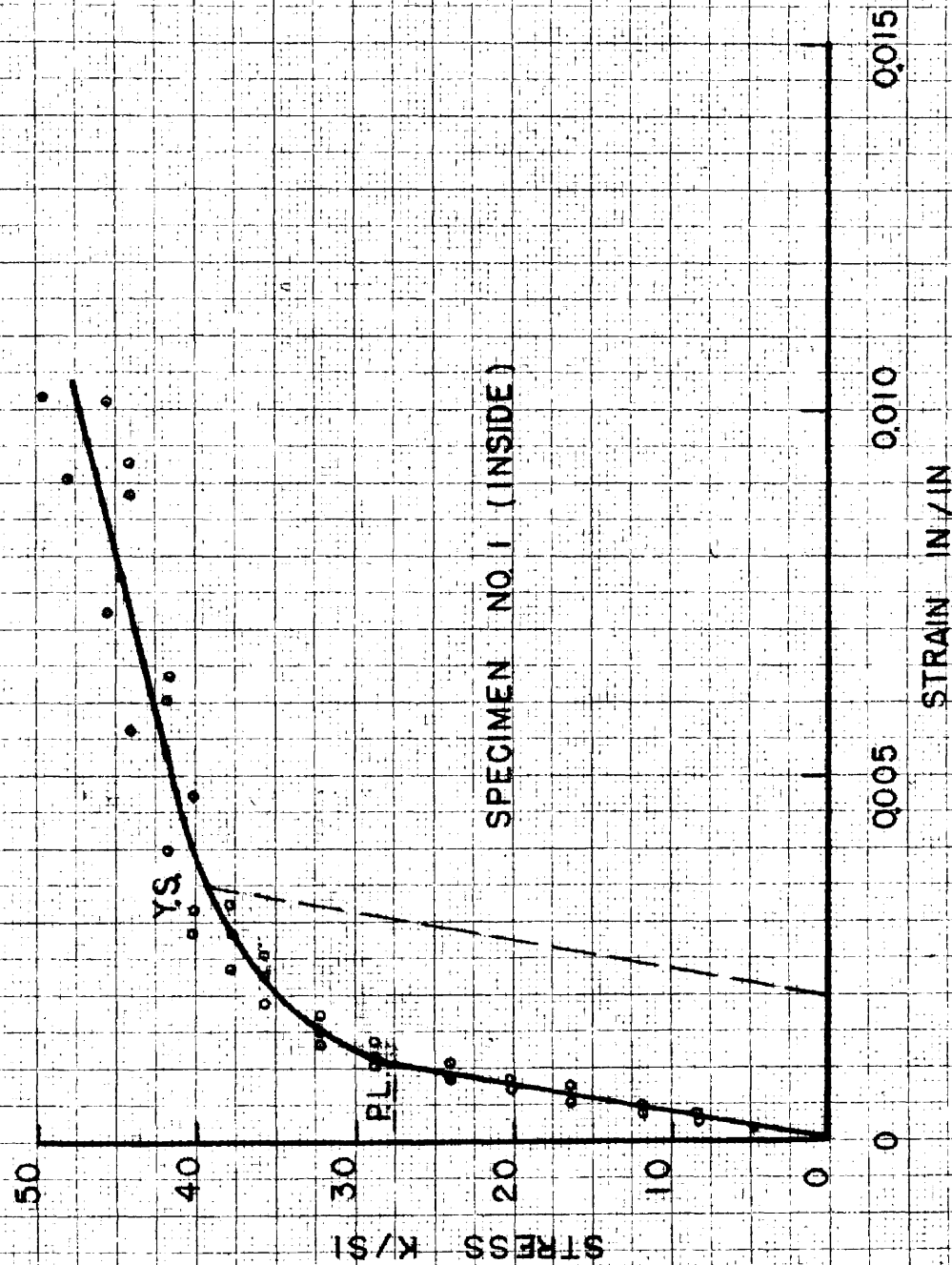
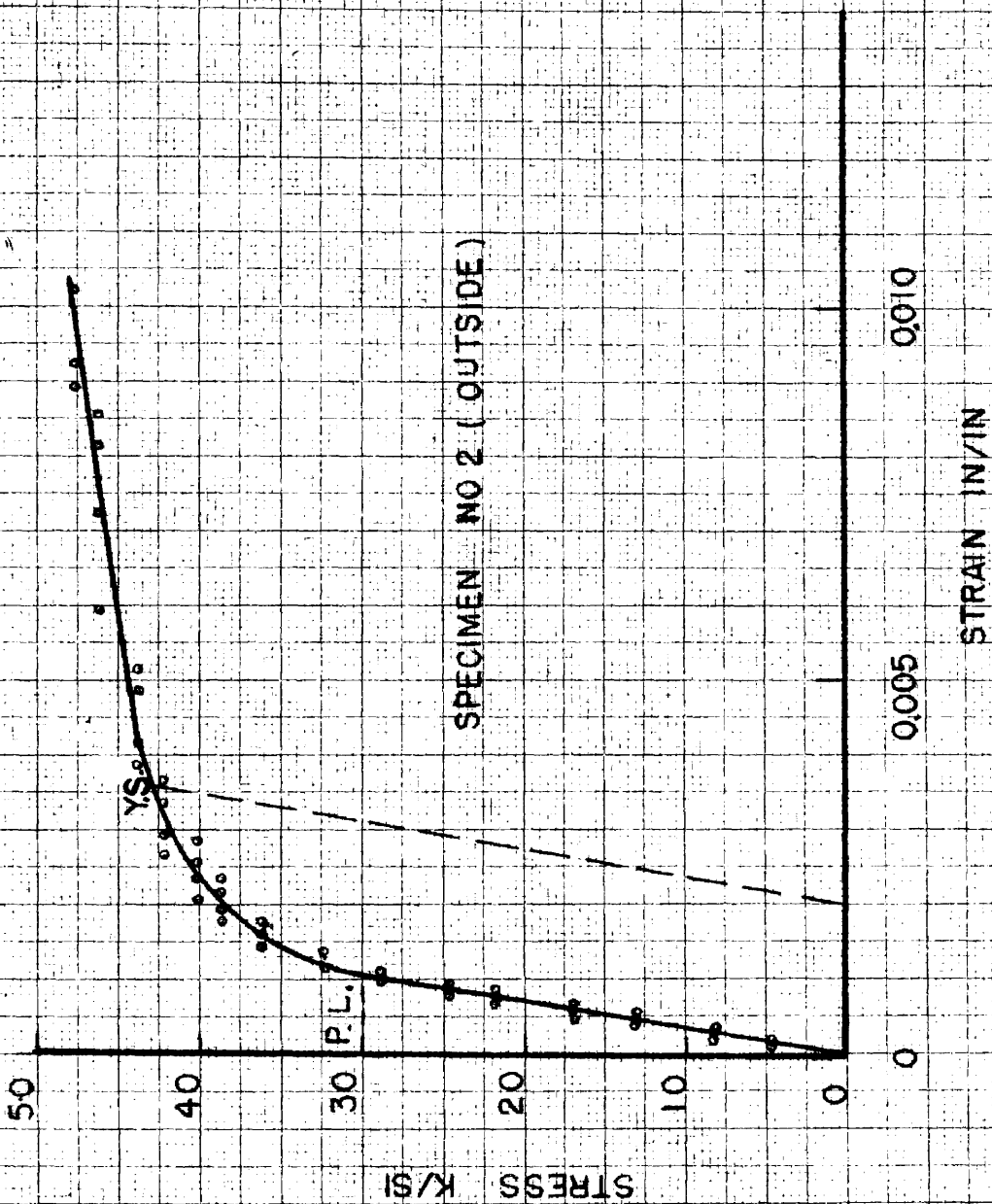


FIG. 89 - ORDINARY STRESS STRAIN DIAGRAM FOR STAINLESS STEEL IN COMPRESSION



SPECIMEN NO 2 (OUTSIDE)

FIG. 90-ORDINARY STRESS STRAIN DIAGRAM FOR STAINLESS STEEL IN COMPRESSION

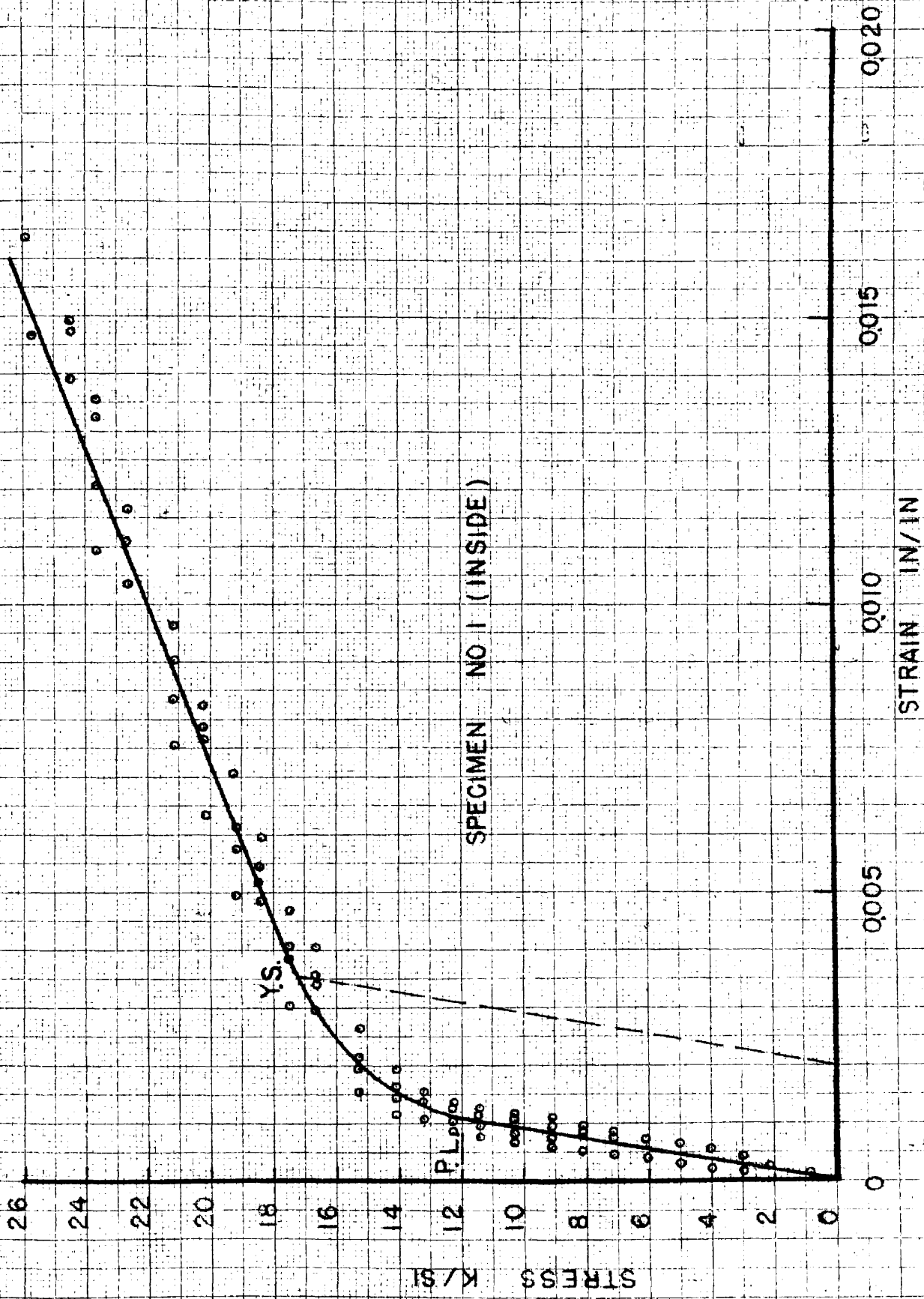
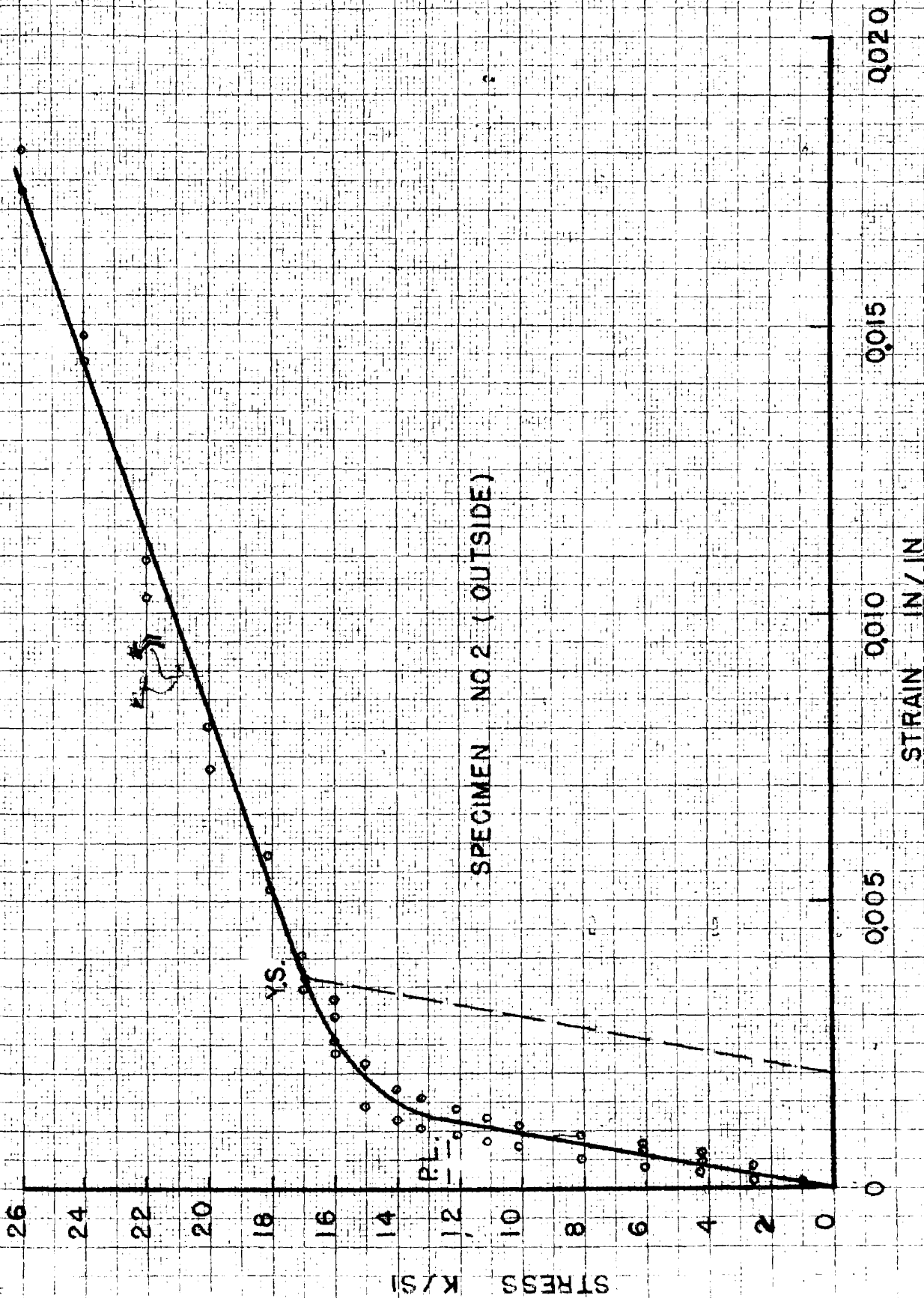


FIG. 91 - ORDINARY STRESS STRAIN DIAGRAM FOR ALUMINUM IN COMPRESSION



SPECIMEN NO 2 (OUTSIDE)

FIG. 92 - ORDINARY STRESS STRAIN DIAGRAM FOR ALUMINUM IN COMPRESSION

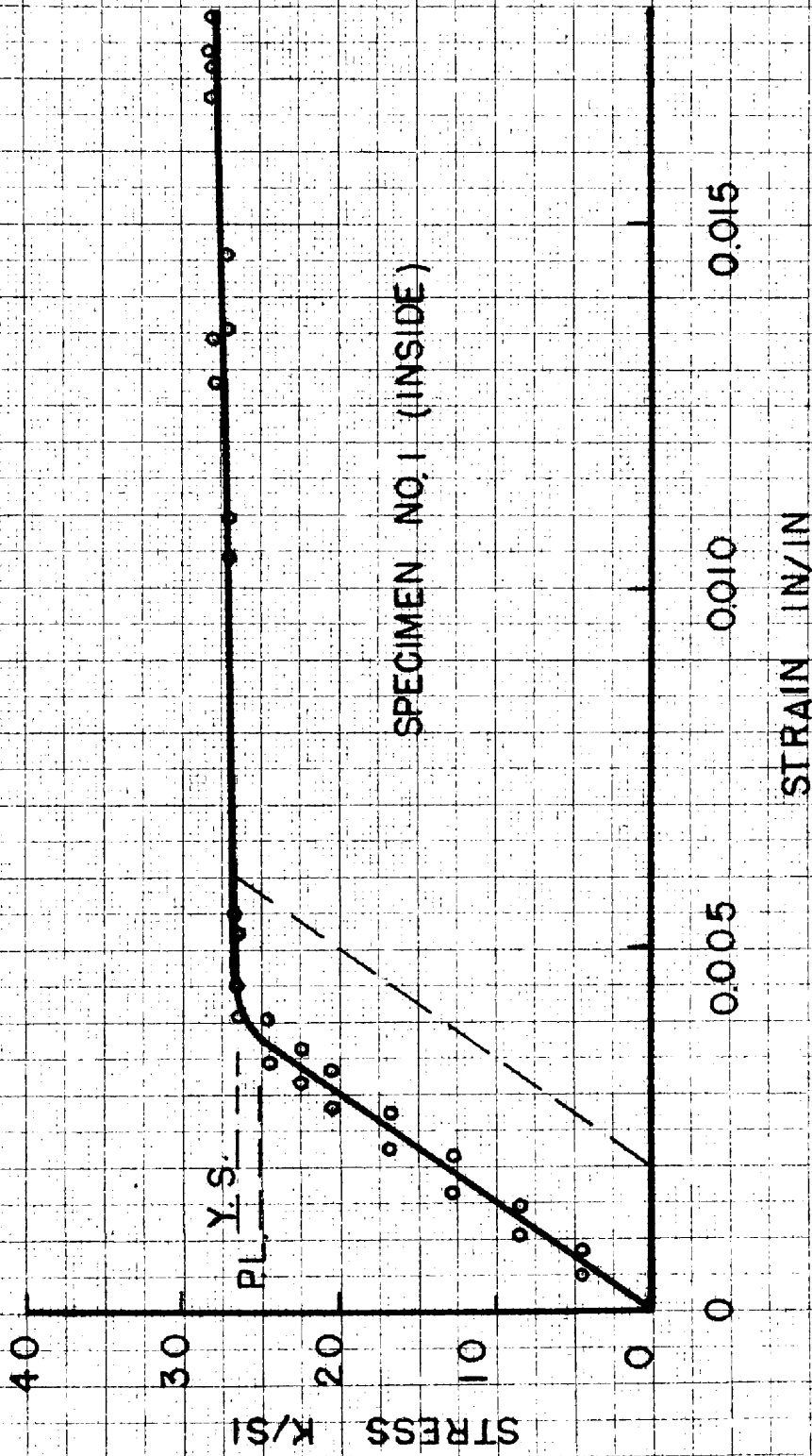


FIG 93 - ORDINARY STRESS STRAIN DIAGRAM FOR MAGNESIUM IN COMPRESSION

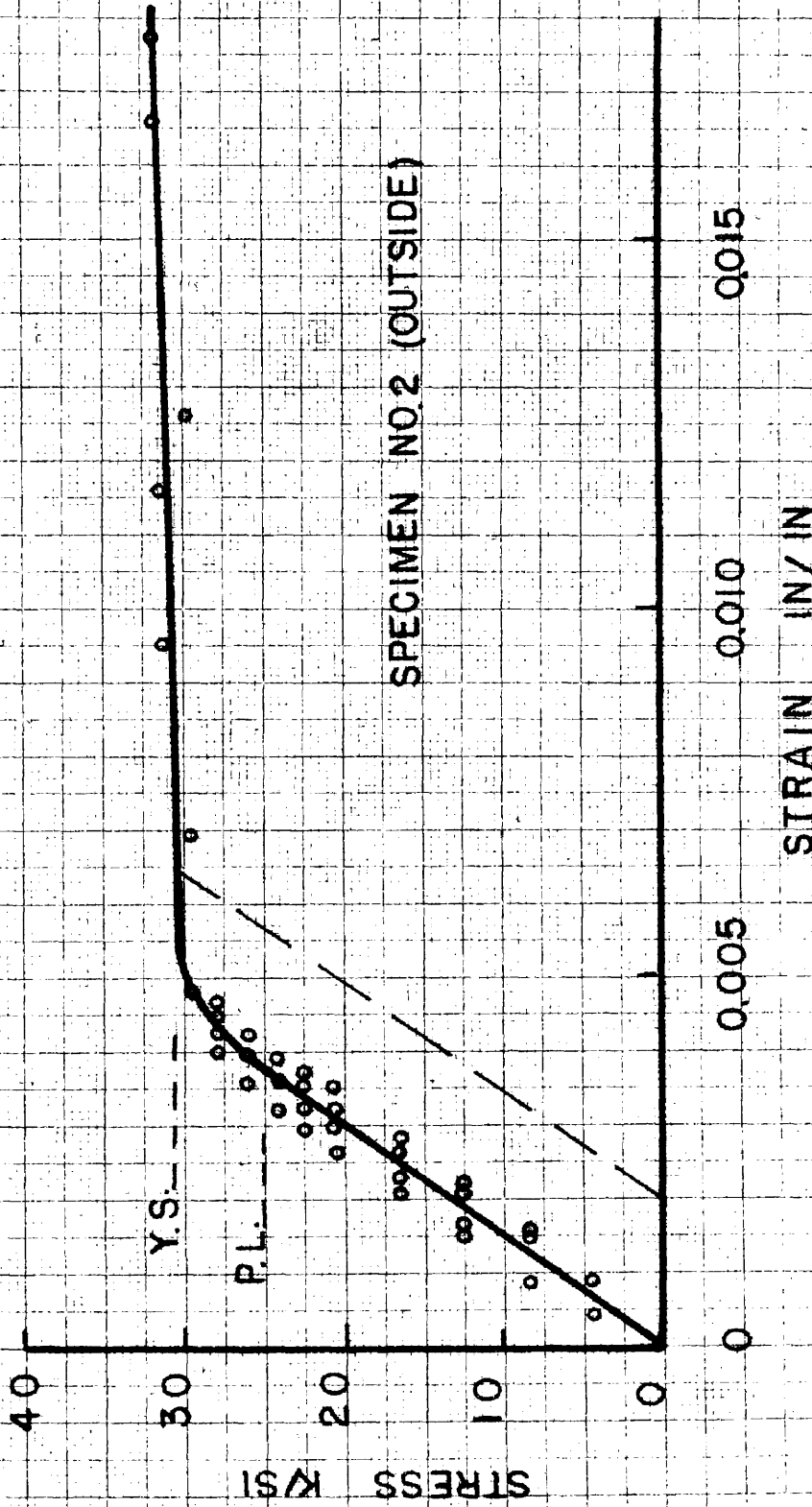
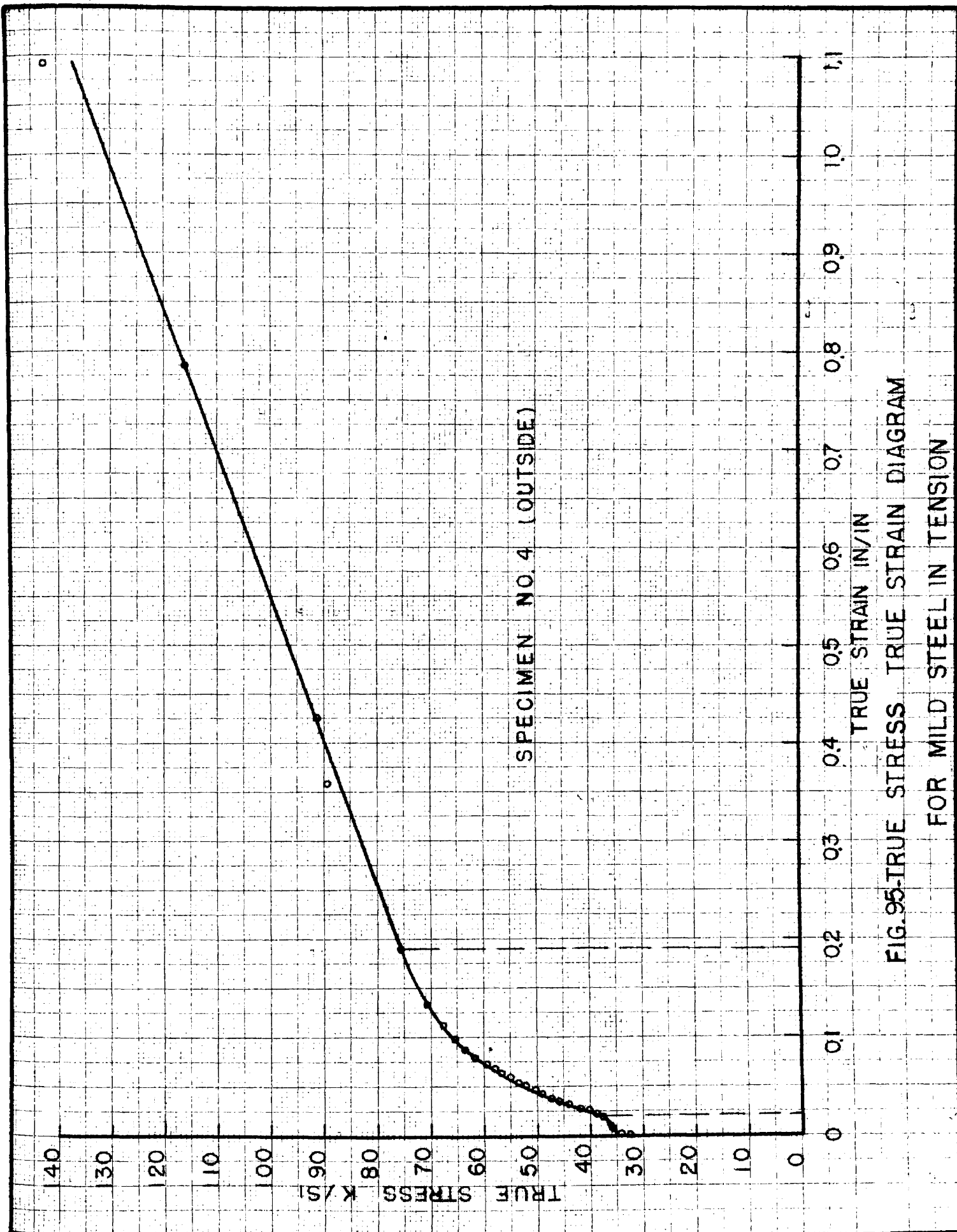


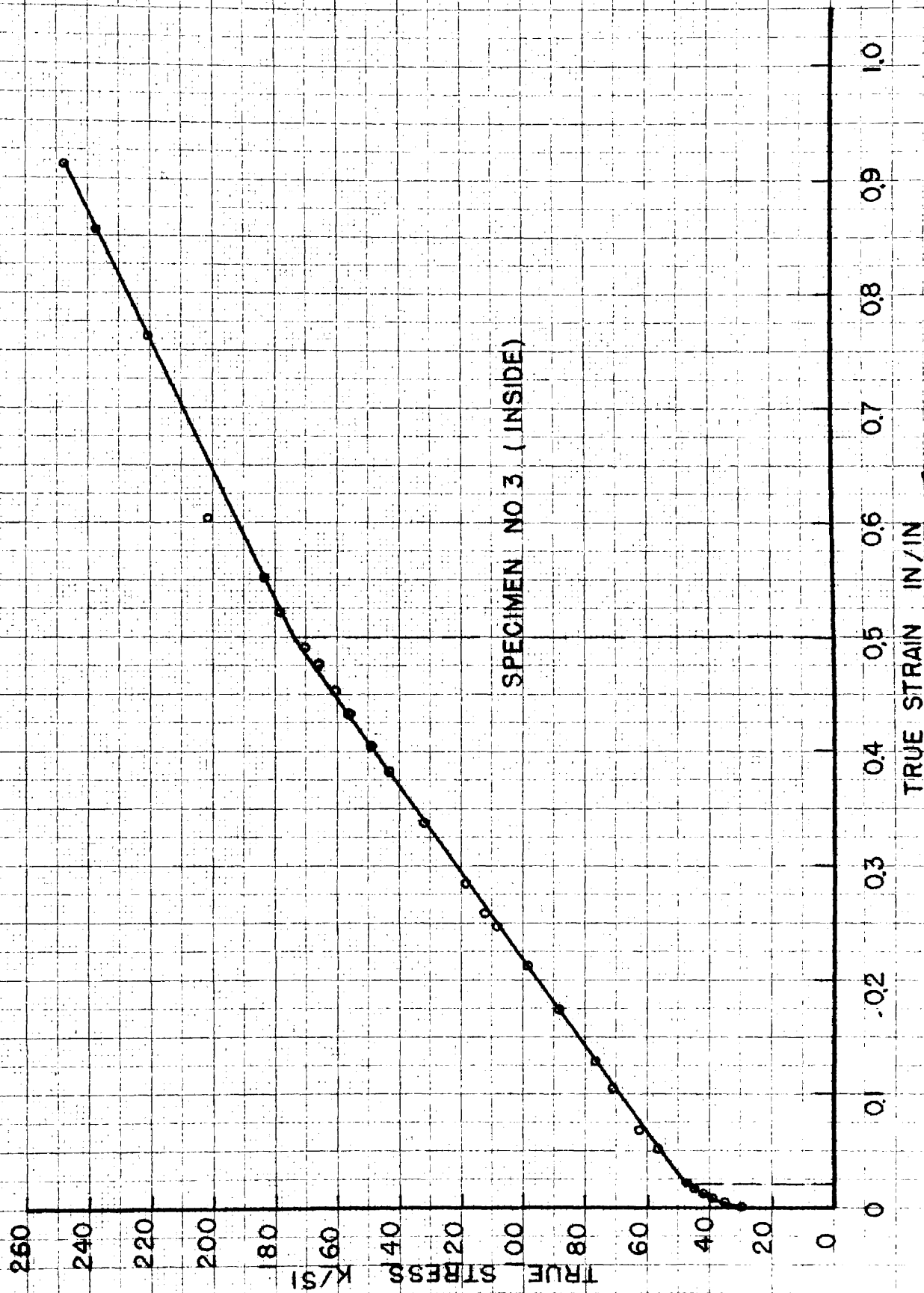
FIG.94 - ORDINARY STRESS STRAIN DIAGRAM FOR MAGNESIUM IN COMPRESSION

3. Tensile True Stress True Strain Diagrams



SPECIMEN NO. 4 (OUTSIDE)

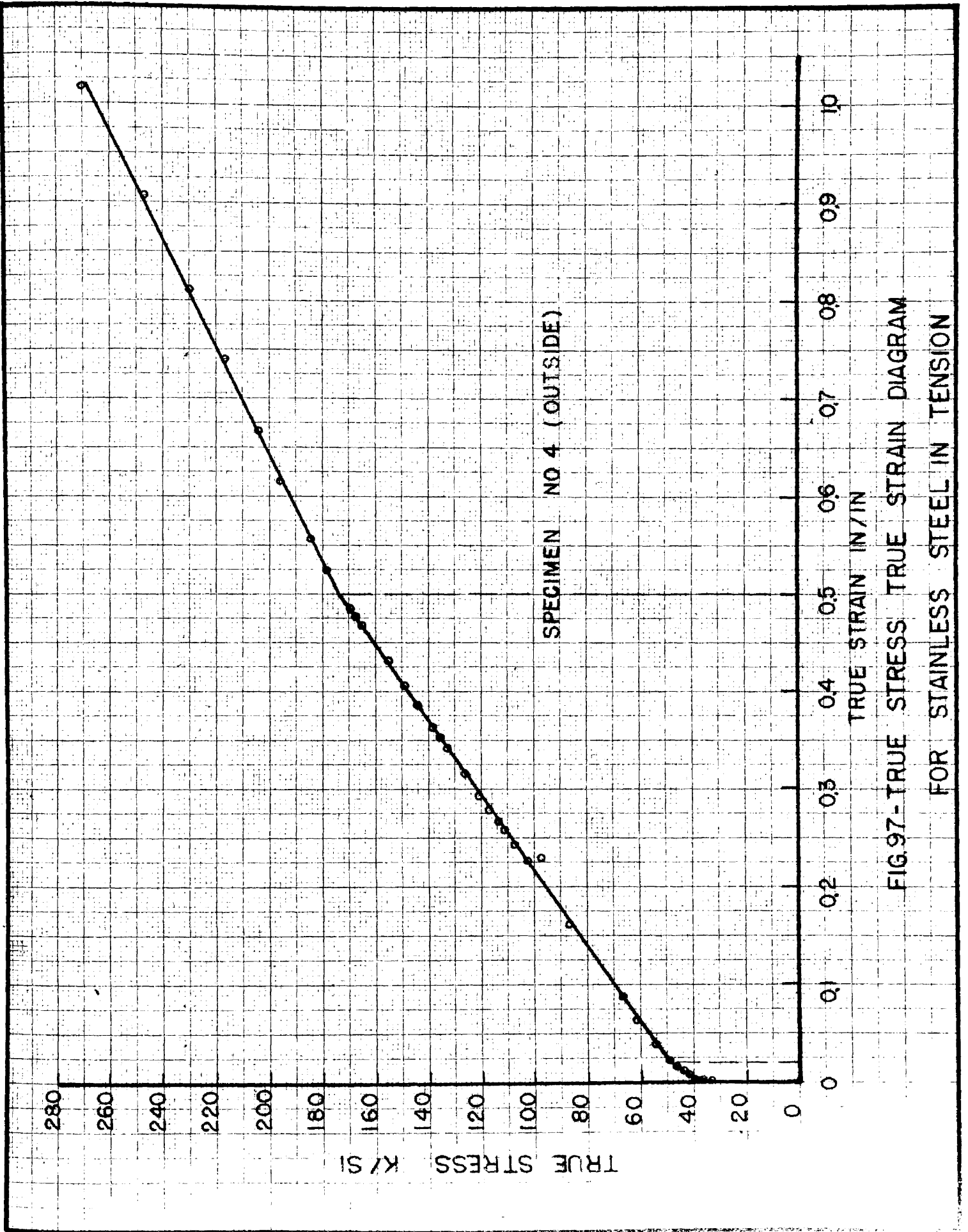
FIG. 95-TRUE STRESS TRUE STRAIN DIAGRAM FOR MILD STEEL IN TENSION



SPECIMEN NO 3 (INSIDE)

FIG.96-TRUE STRESS TRUE STRAIN DIAGRAM

FOR STAINLESS STEEL IN TENSION



SPECIMEN NO 4 (OUTSIDE)

FIG.97-TRUE STRESS TRUE STRAIN DIAGRAM FOR STAINLESS STEEL IN TENSION

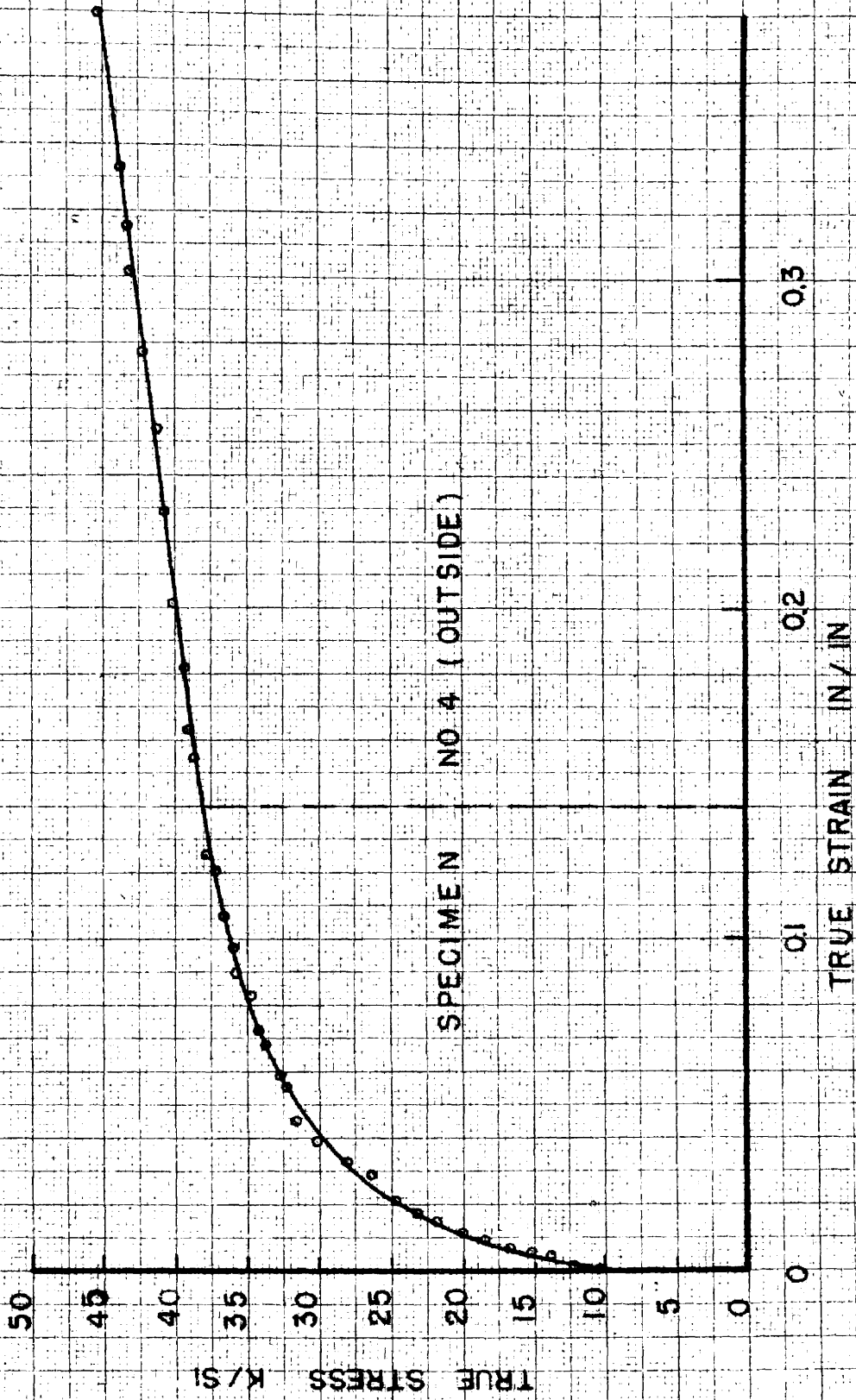


FIG.98-TRUE STRESS TRUE STRAIN DIAGRAM
FOR ALUMINUM IN TENSION

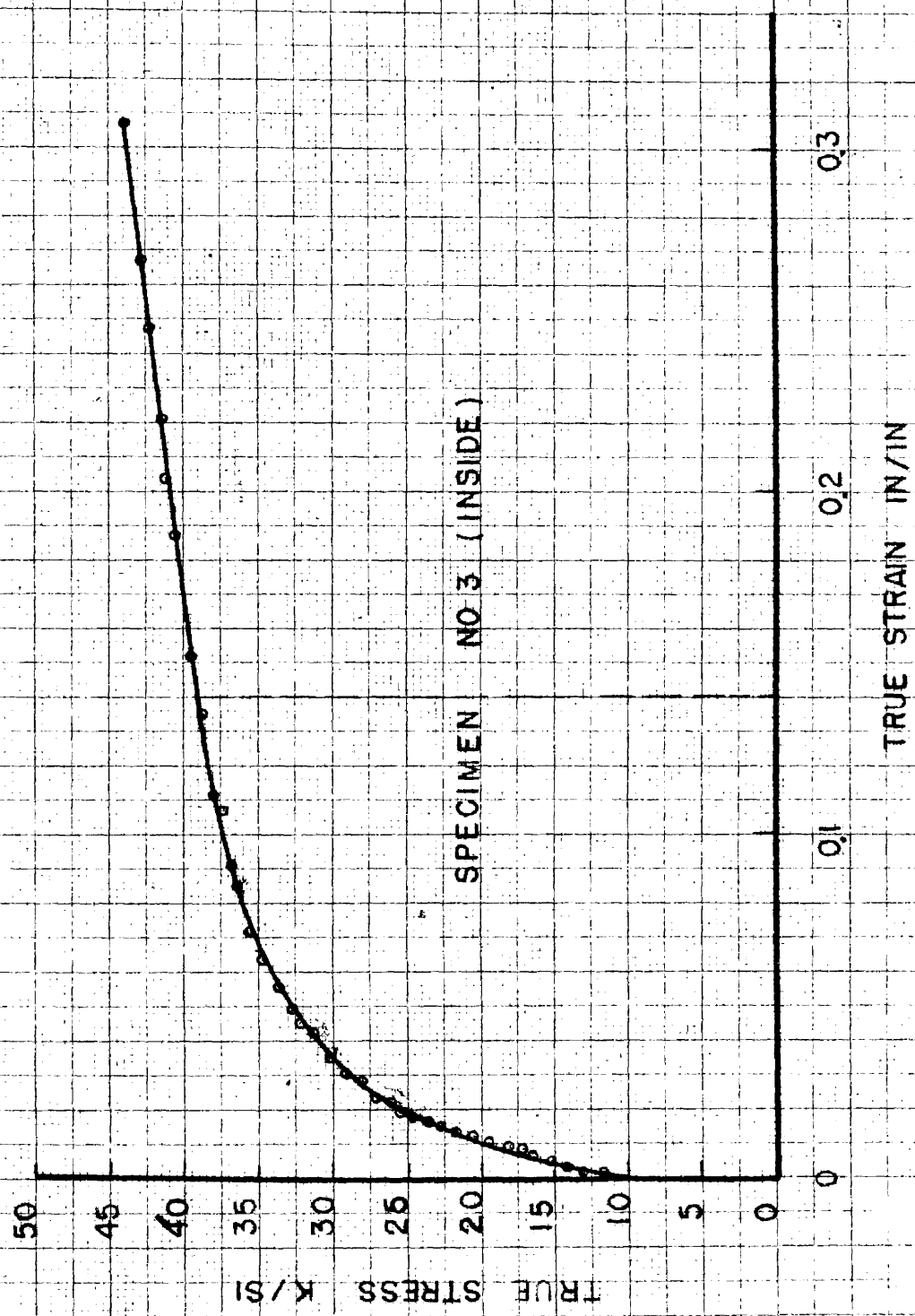
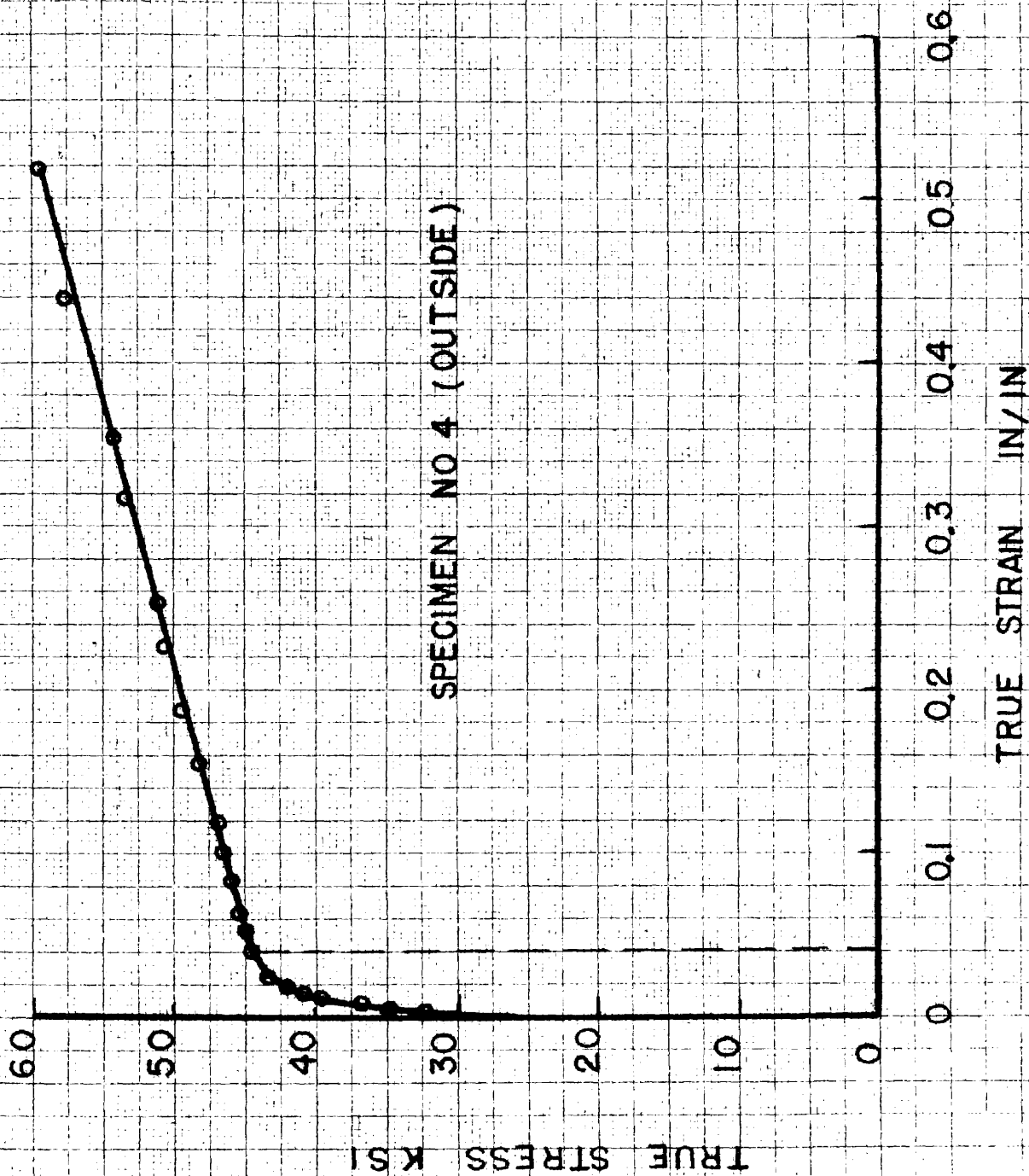
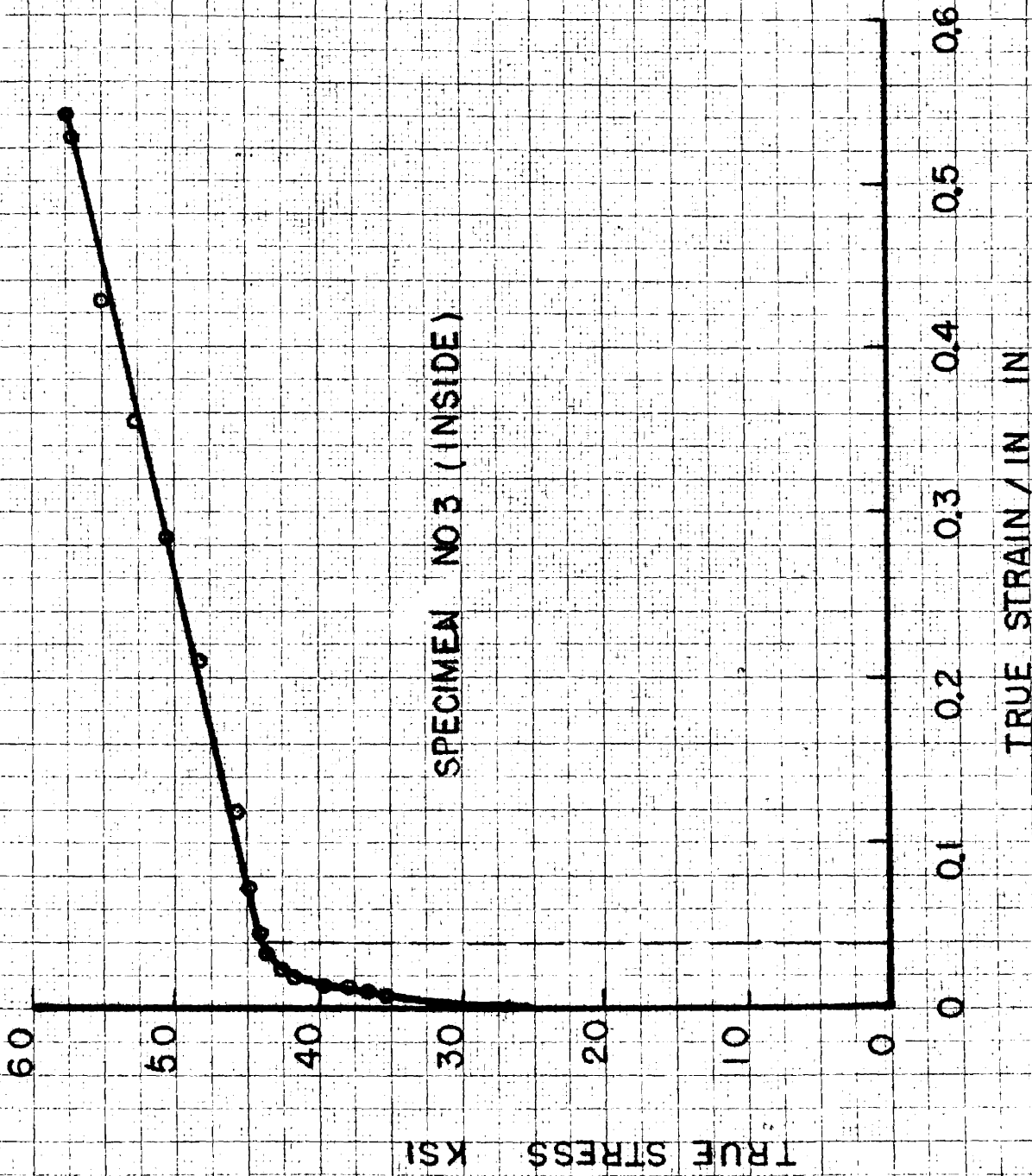


FIG. 99 - TRUE STRESS TRUE STRAIN DIAGRAM FOR ALUMINUM IN TENSION



SPECIMEN NO 4 (OUTSIDE)

FIG.100- TRUE STRESS TRUE STRAIN DIAGRAM
FOR MAGNESIUM IN TENSION



SPECIMEN NO 3 (INSIDE)

FIG.101 - TRUE STRESS TRUE STRAIN DIAGRAM FOR MAGNESIUM IN TENSION

4. Compressive True Stress True Strain Diagrams

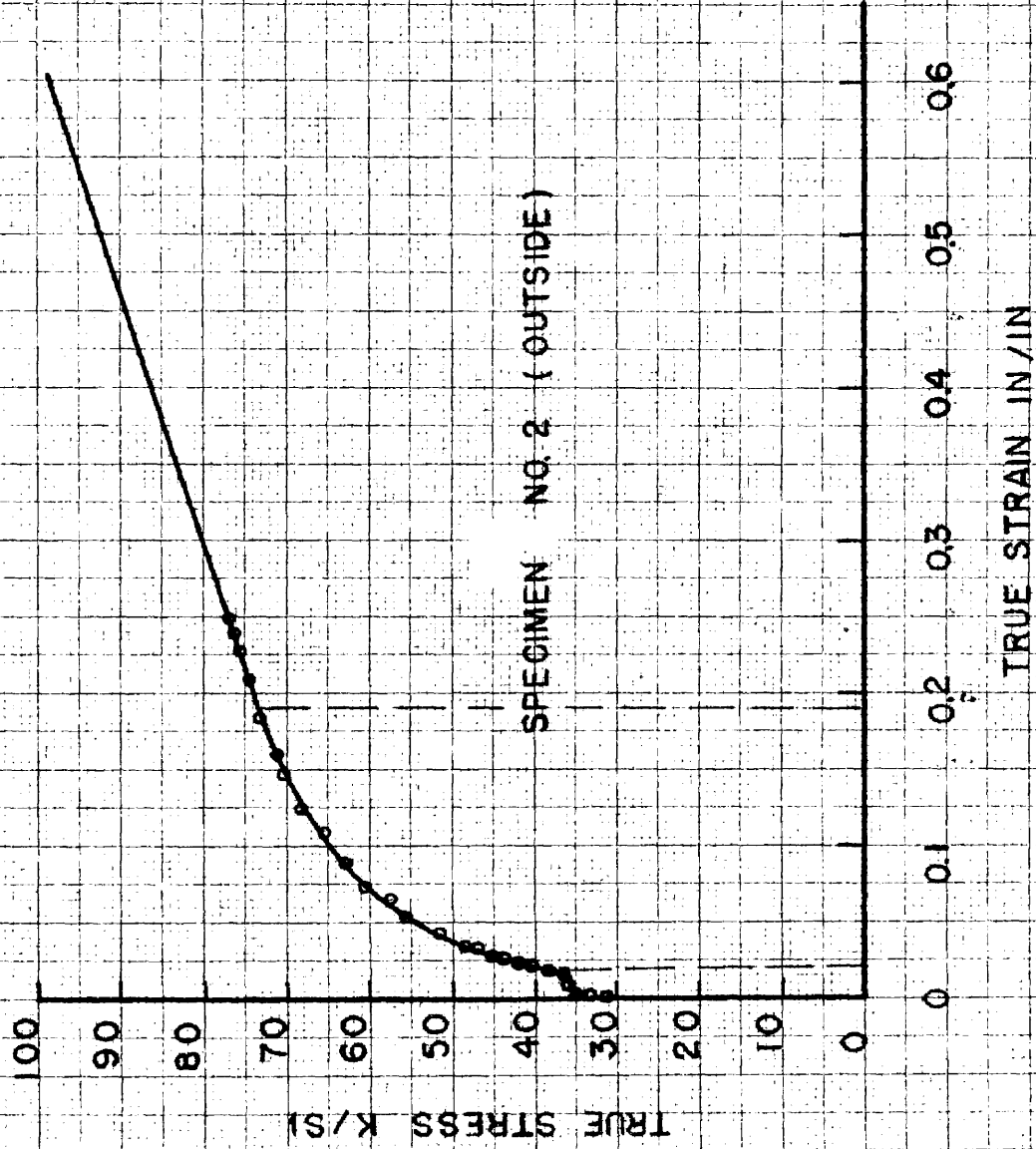
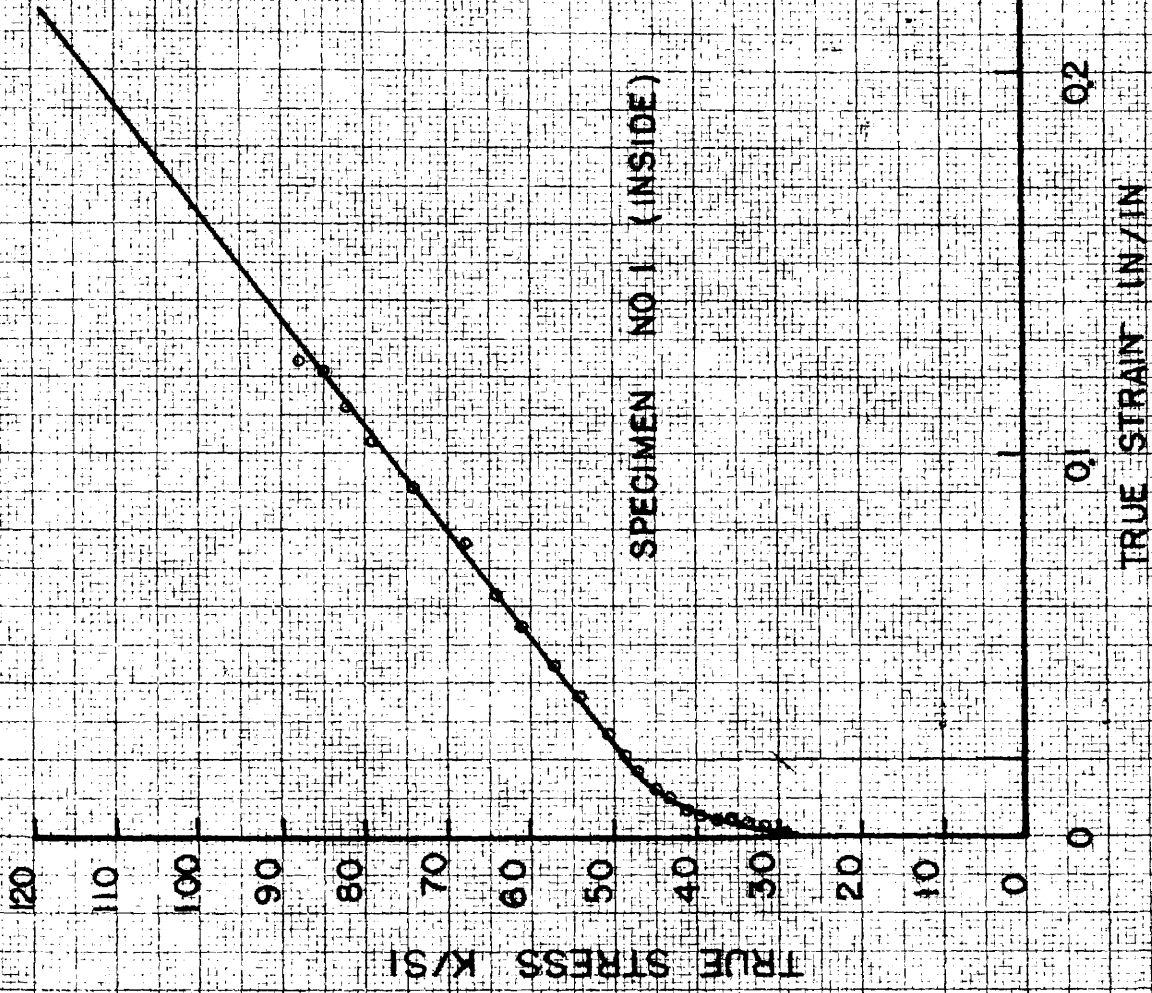


FIG. 102-TRUE STRESS TRUE STRAIN DIAGRAM FOR MILD STEEL IN COMPRESSION



SPECIMEN NO. 1 (INSIDE)

FIG. 103-TRUE STRESS TRUE STRAIN DIAGRAM FOR STAINLESS STEEL IN COMPRESSION

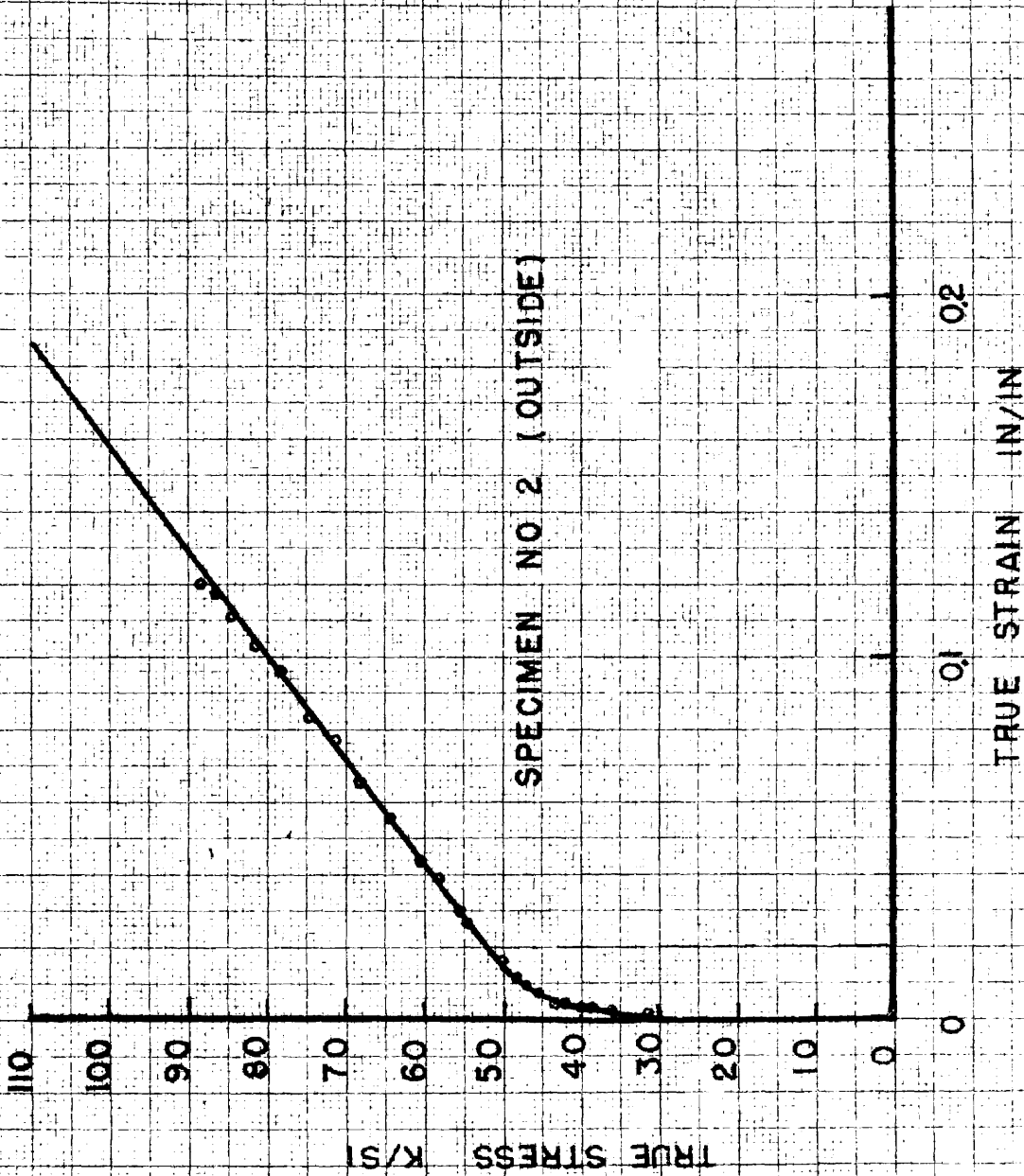


FIG.104-TRUE STRESS TRUE STRAIN DIAGRAM FOR STAINLESS STEEL IN COMPRESSION

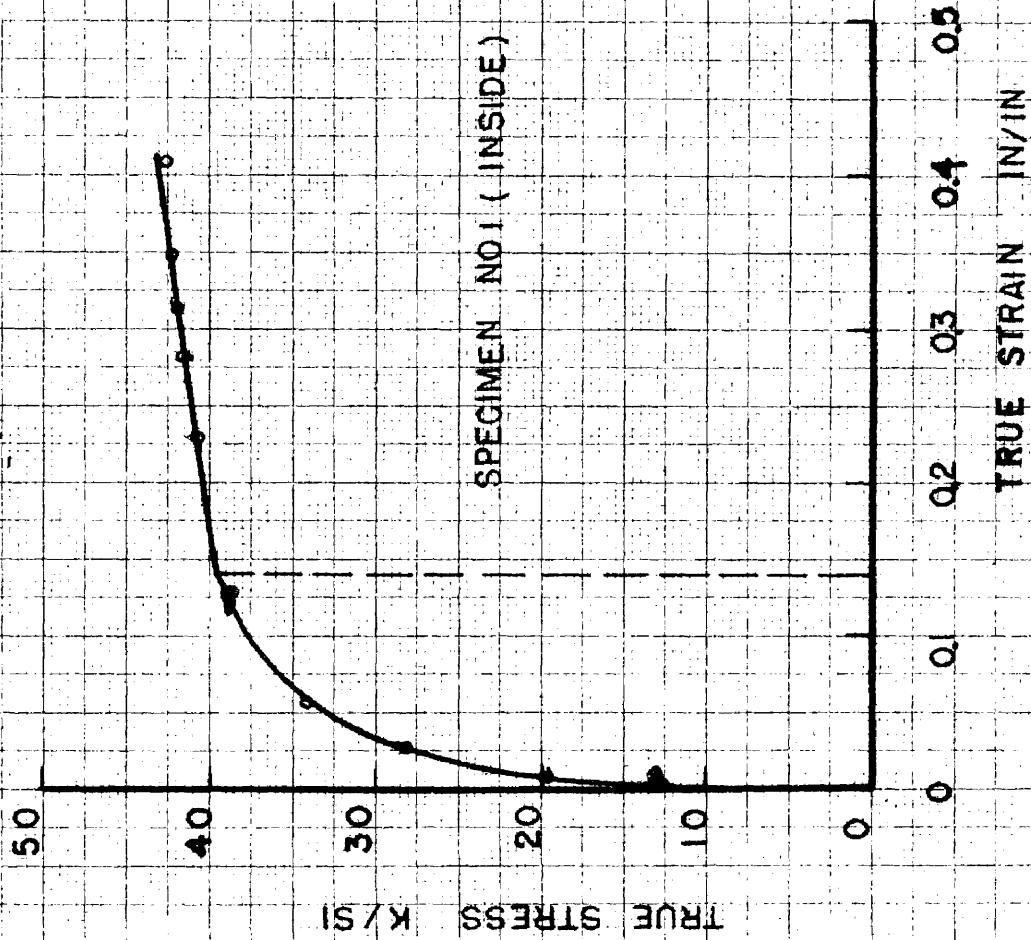


FIG.105-TRUE STRESS TRUE STRAIN DIAGRAM FOR ALUMINUM IN COMPRESSION

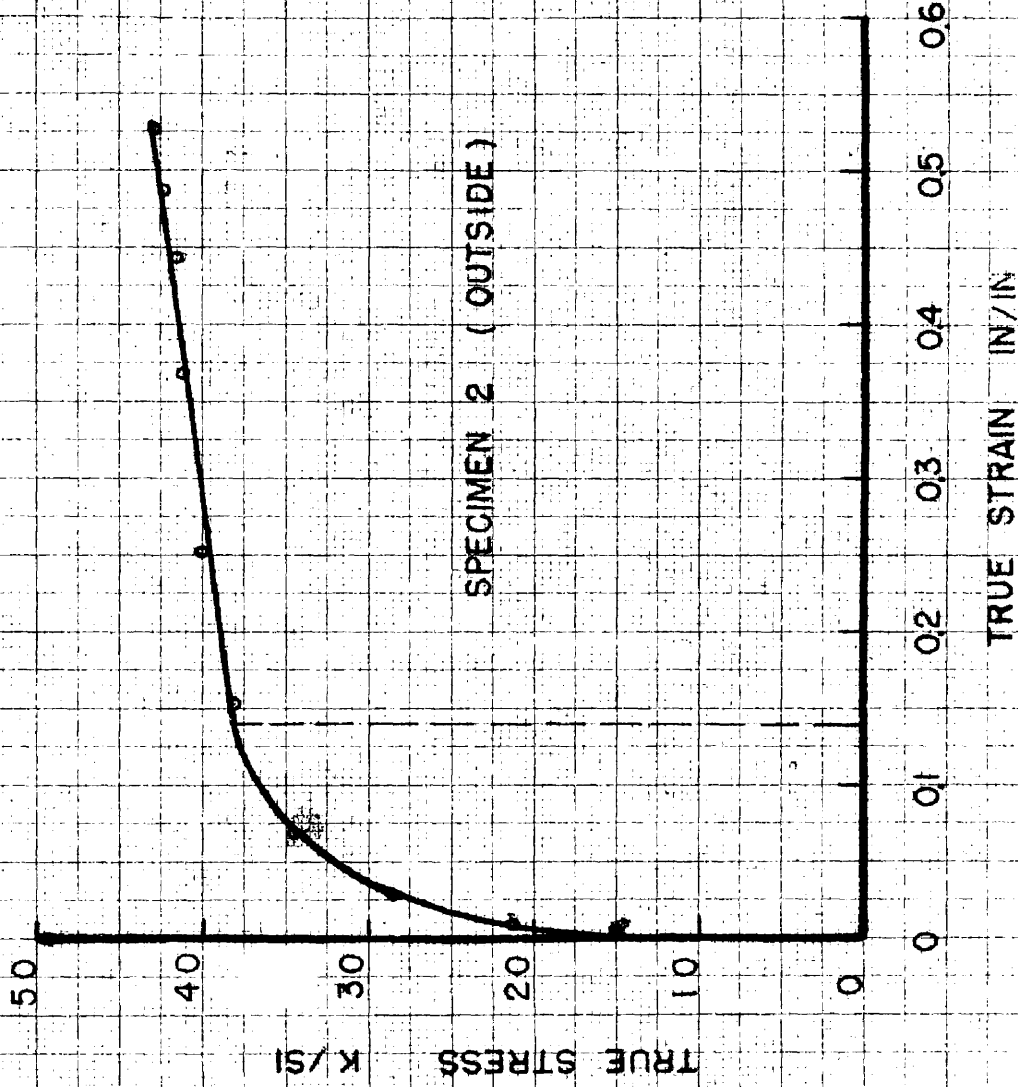


FIG 106 TRUE STRESS TRUE STRAIN DIAGRAM
FOR ALUMINUM IN COMPRESSION

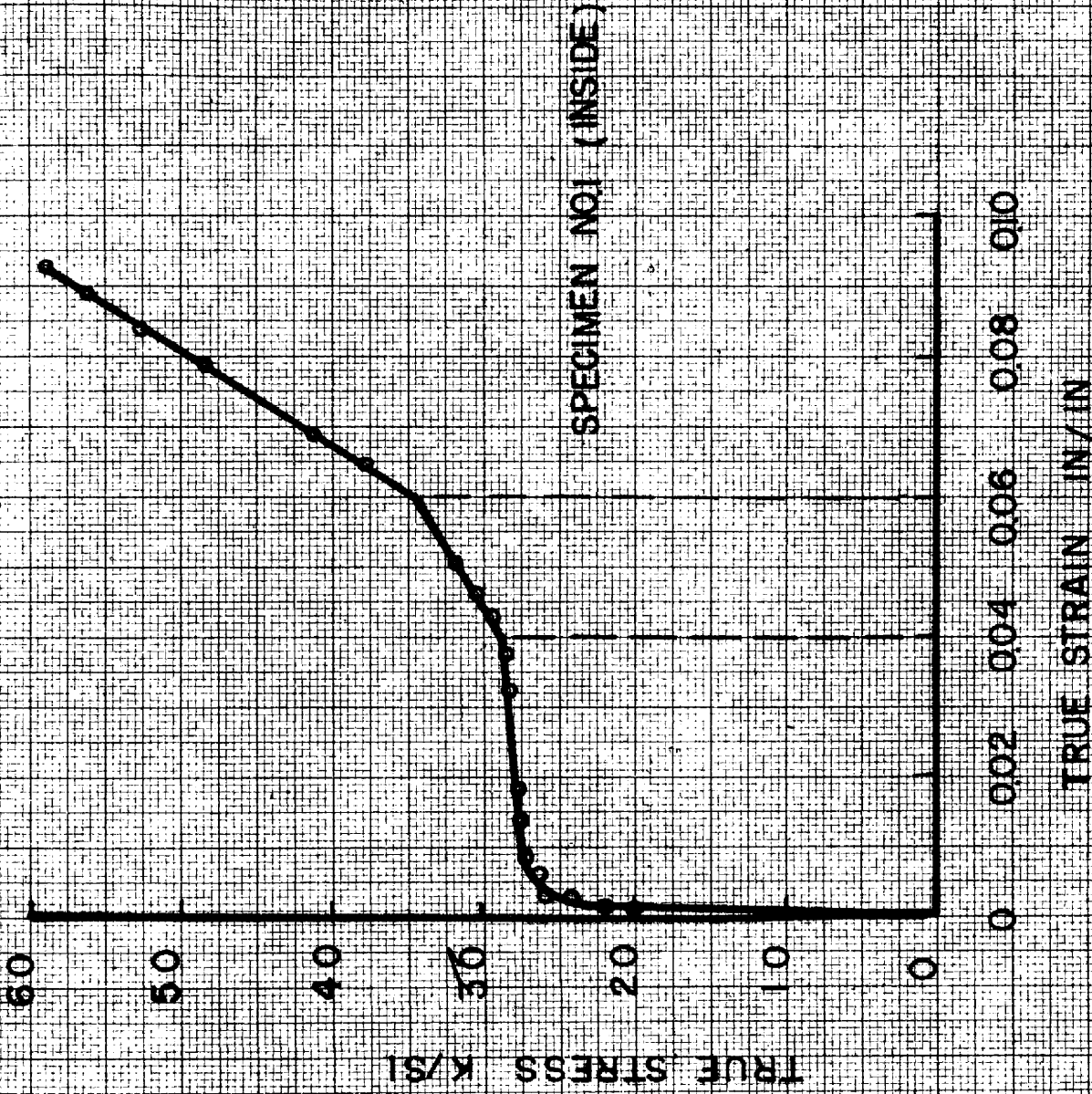


FIG.107 - TRUE STRESS TRUE STRAIN DIAGRAM FOR MAGNESIUM IN COMPRESSION

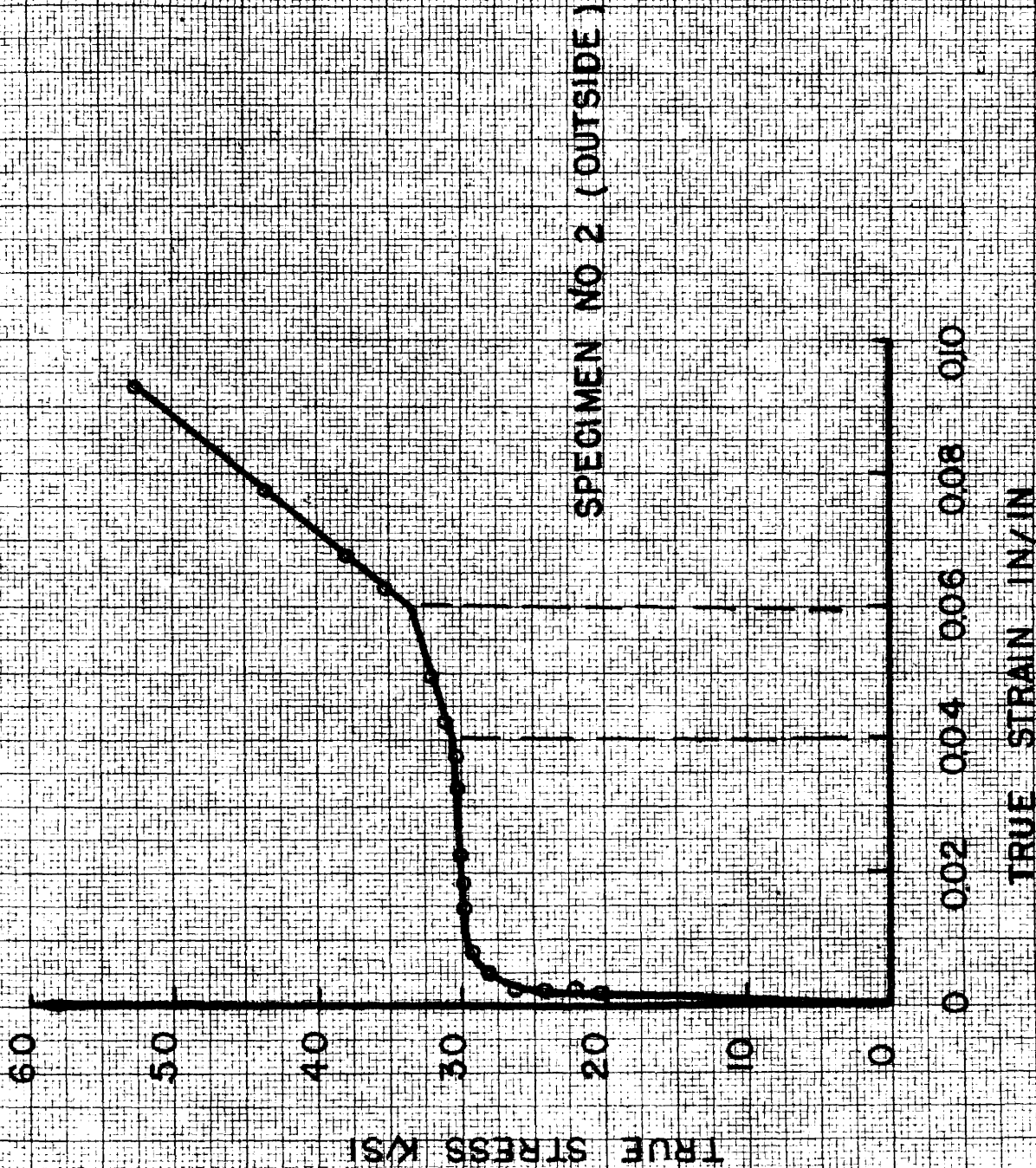


FIG. 108- TRUE STRESS TRUE STRAIN DIAGRAM FOR MAGNESIUM IN COMPRESSION

5. Tensile Logarithmic True Stress True Strain Diagrams

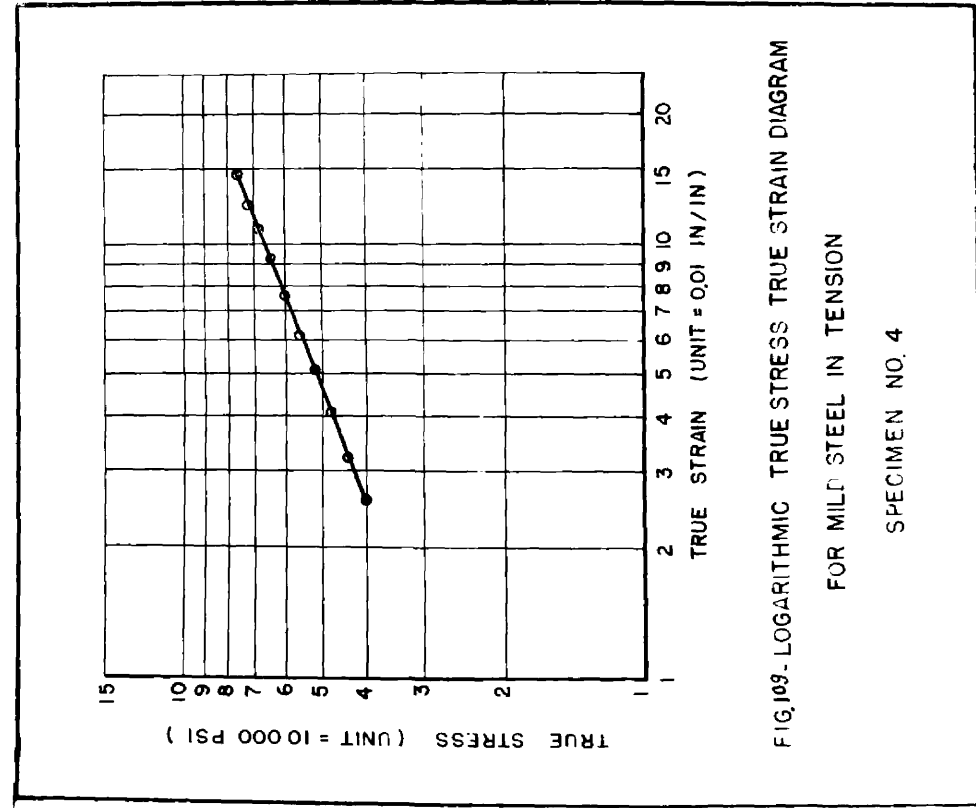


FIG.109. LOGARITHMIC TRUE STRESS TRUE STRAIN DIAGRAM

FOR MILD STEEL IN TENSION

SPECIMEN NO. 4

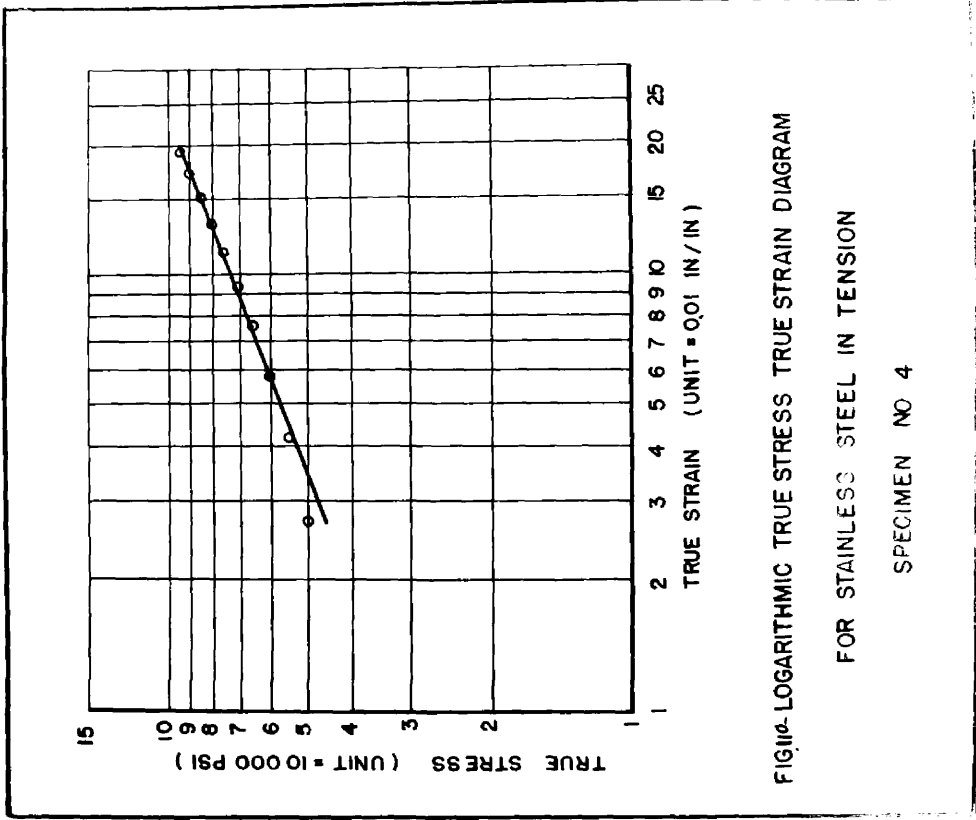


FIG.108. LOGARITHMIC TRUE STRESS TRUE STRAIN DIAGRAM

FOR STAINLESS STEEL IN TENSION

SPECIMEN NO. 4

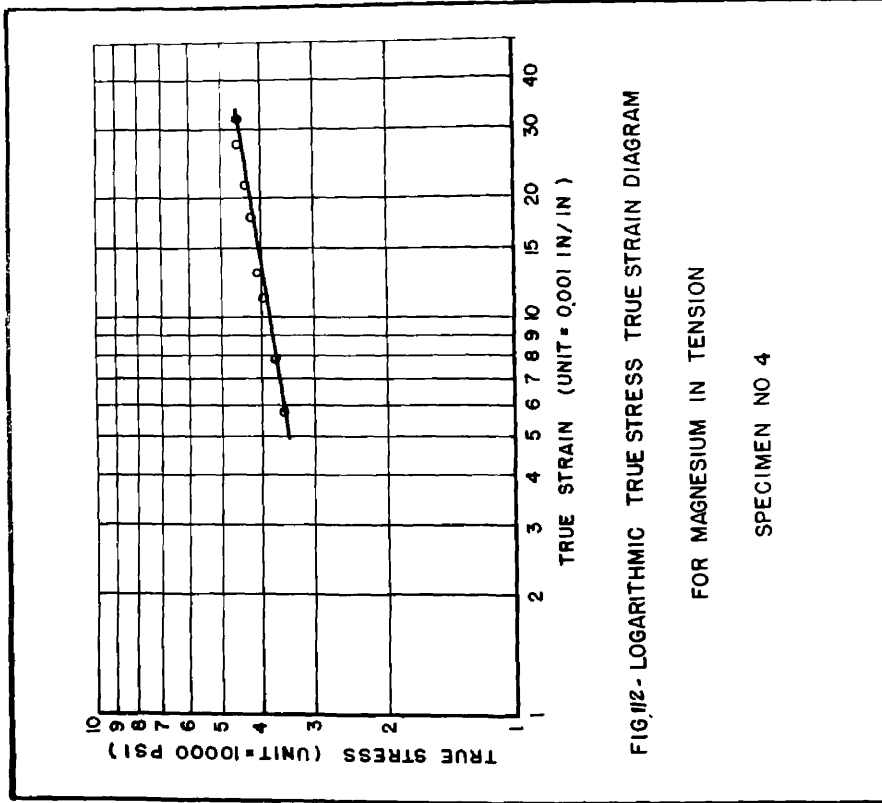


FIG. II/2 - LOGARITHMIC TRUE STRESS TRUE STRAIN DIAGRAM

FOR MAGNESIUM IN TENSION

SPECIMEN NO 4

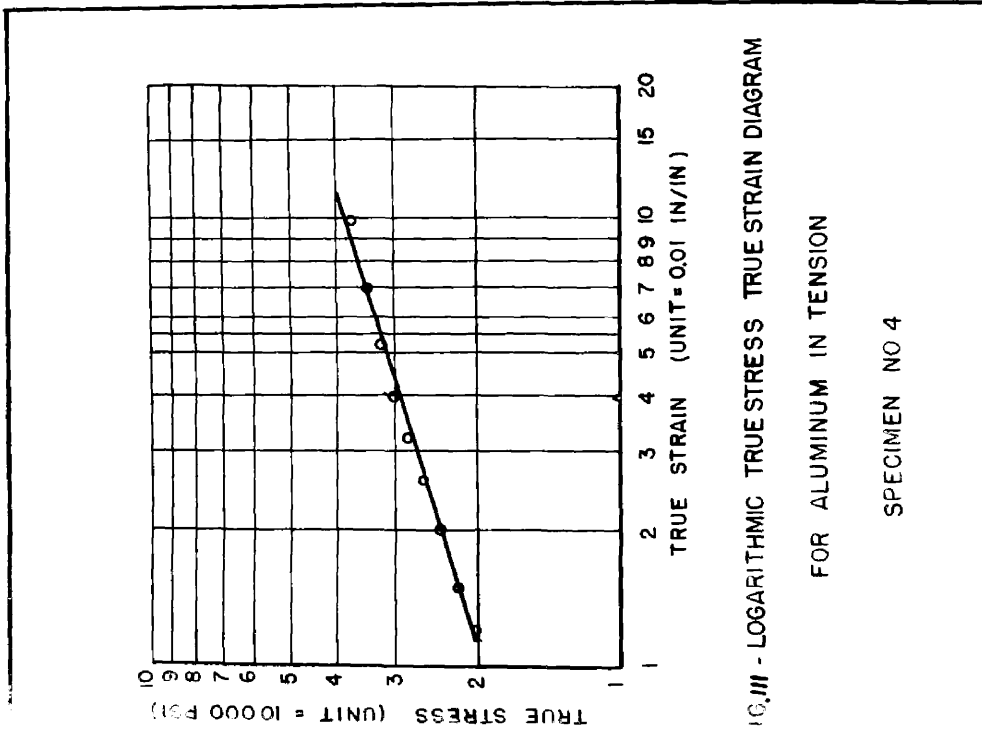
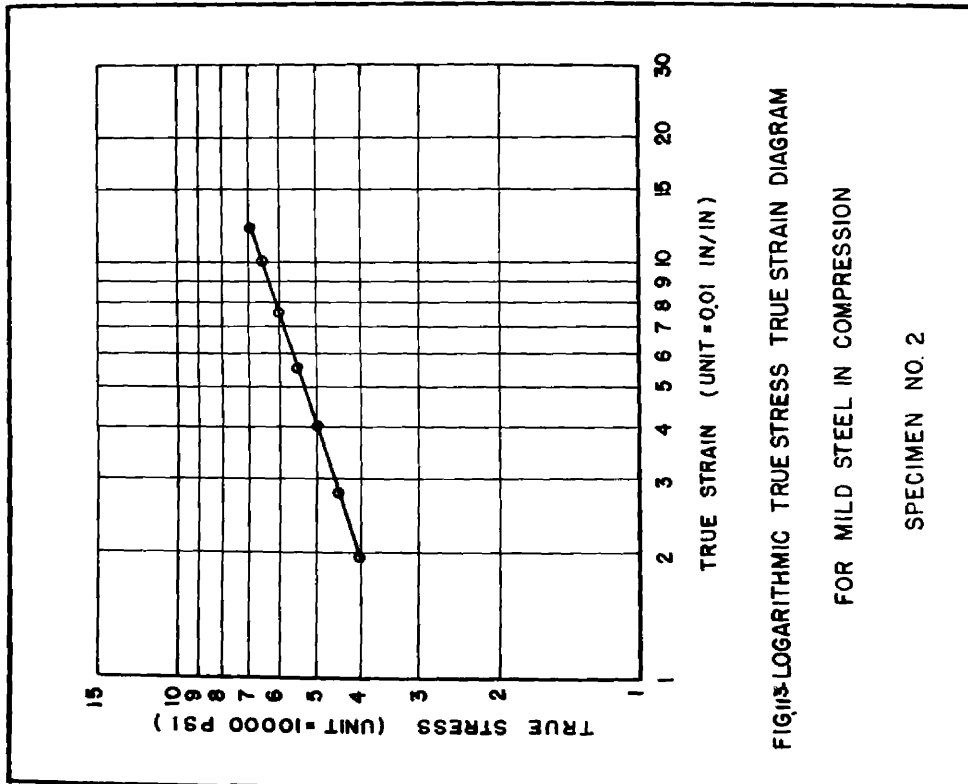
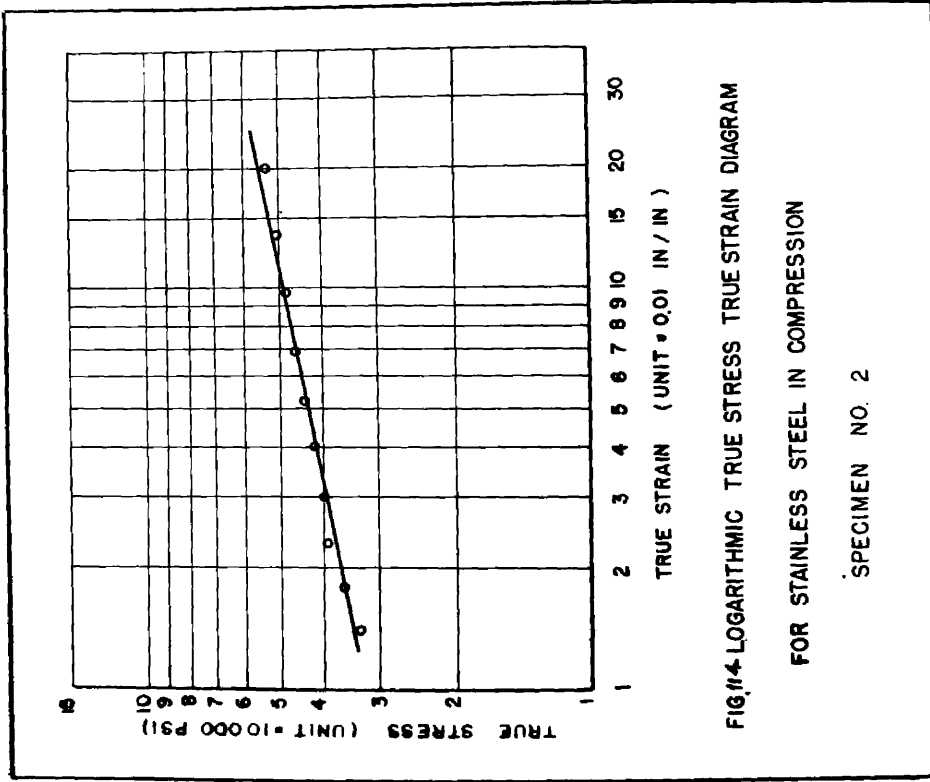


FIG. III - LOGARITHMIC TRUE STRESS TRUE STRAIN DIAGRAM

FOR ALUMINUM IN TENSION

SPECIMEN NO 4

6. Compressive Logarithmic True Stress True Strain Diagrams



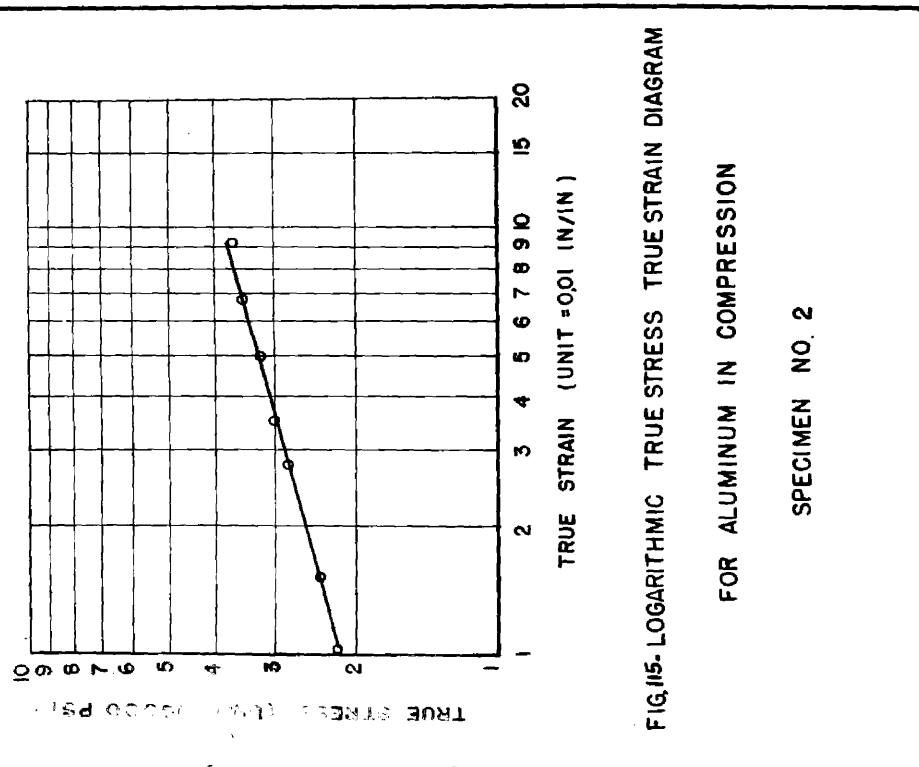


FIG.15- LOGARITHMIC TRUE STRESS TRUE STRAIN DIAGRAM

FOR ALUMINUM IN COMPRESSION

SPECIMEN NO. 2

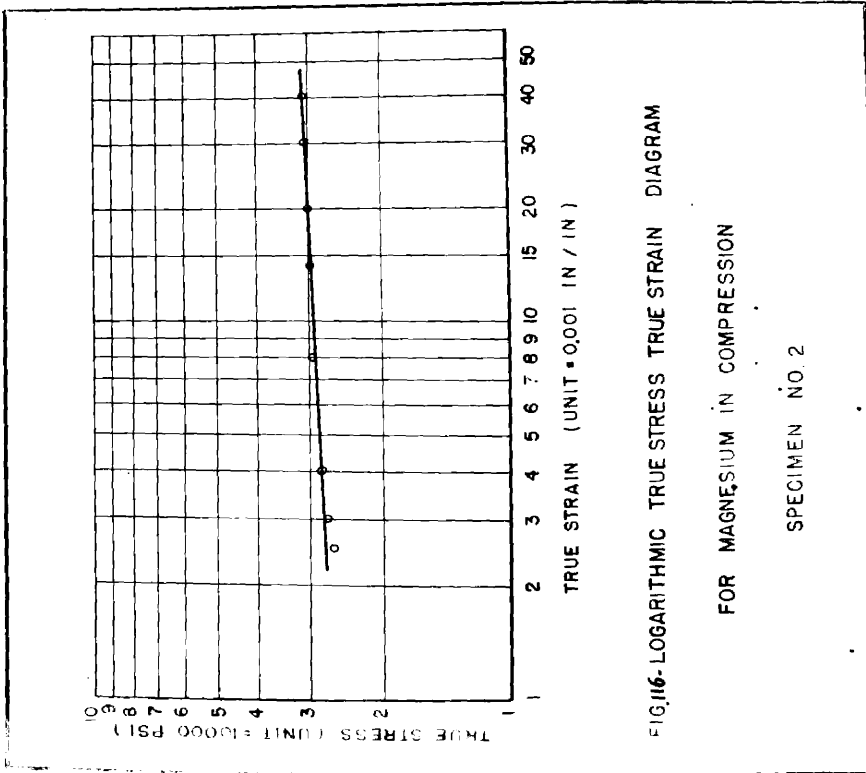


FIG.16- LOGARITHMIC TRUE STRESS TRUE STRAIN DIAGRAM

FOR MAGNESIUM IN COMPRESSION

SPECIMEN NO. 2

7. Clip Gage

Clip Gage

This gage was designed to meet the requirements of the bending tests discussed previously for measuring high strains, since the SR-4 gages have an average maximum range of strain of about 0.020 to 0.030 in/in. It consists of a phosphor bronze strip to which SR-4 gages were cemented as shown in Fig. 117. This strip was mounted on the tested beams by resting freely thru two side holes on two balls attached rigidly to supports which were fixed to the tested beams. The fixation was made either by brazing the supports to the beam or attaching them by a screw thru a tiny hole drilled and tapped in the beam. The movement of the two supports will press or release the phosphor bronze strip thru the pressure of the two end balls on the strip thru the side holes. This pressure or release of the phosphor bronze strip will affect the cemented SR-4 gages. This effect is linear up to 14% strain as shown by comparing the clip gage reading with that of a micrometer by pressing the micrometer thru the two side holes of the clip gage as shown in Figures 118 and 120.

Therefore large strains at the supports are reduced to small measurable strains by the SR-4 gage cemented on the clip gage. The factor of reduction or the multiplication factor of the clip gage was determined by calibrating the clip gage with SR-4 gage mounted on the tested specimen (Fig. 121) till the failure of the SR-4 gage. The multiplication factor obtained was used to translate the clip gage reading to the actual strain.

It was observed that the multiplication factor varied according to the depth of the tested beam and the position of the clip gage on tensile or compressive side. As a sample, the multiplication factor for pure compression where the micrometer was used, is 73.8, while for the mild steel beams 1" x 1" and 1 31/32" x 1 31/32" cross sections in pure bending, the multiplication factors are 35 and 50 respectively. Also the factor all over the bending tests carried was around 50 since the depths of tested beams were 1 31/32", 2 1/4" and 2".

It is worthy to note that the strain measured by the clip gage was for the horizontal distance between the fixed clip supports all over the bending test and not the strain of the curved surface of the bended beam which is the actual strain. In our case the difference between the two cases up to 5% deformation, which is over the range reached, is less than 1% which is practically negligible.

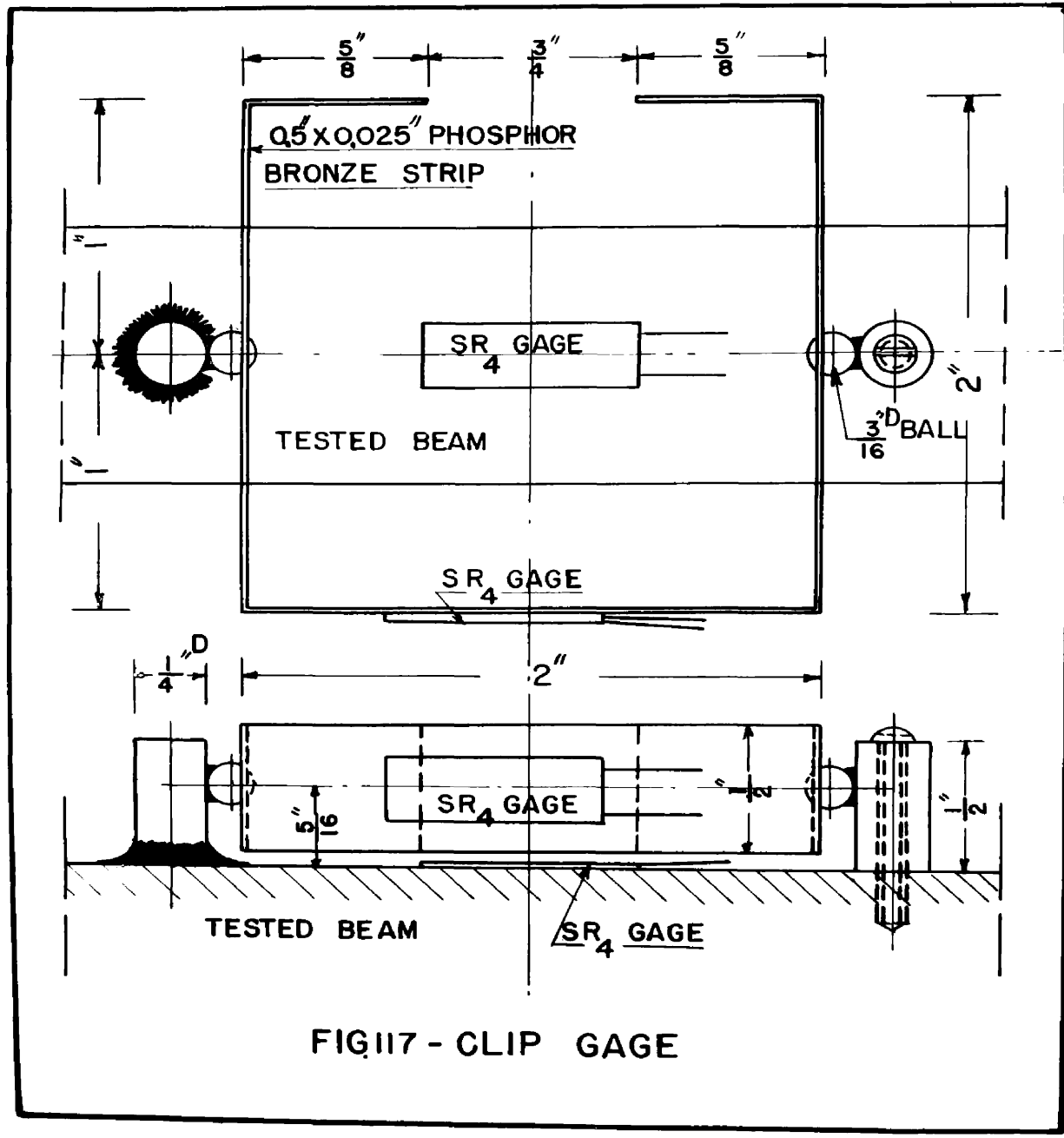


FIG117 - CLIP GAGE

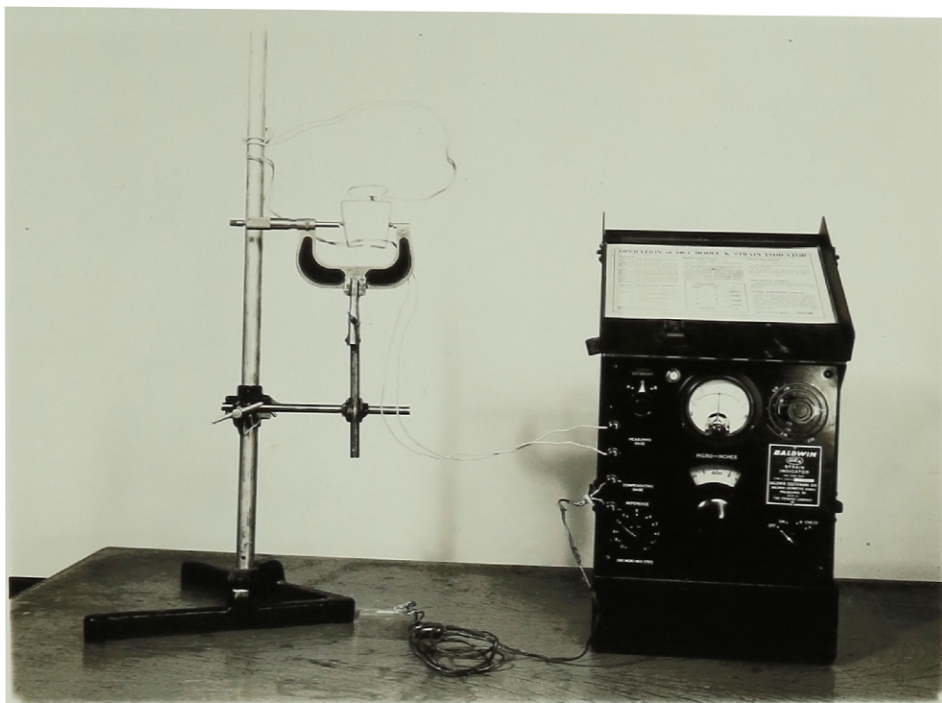
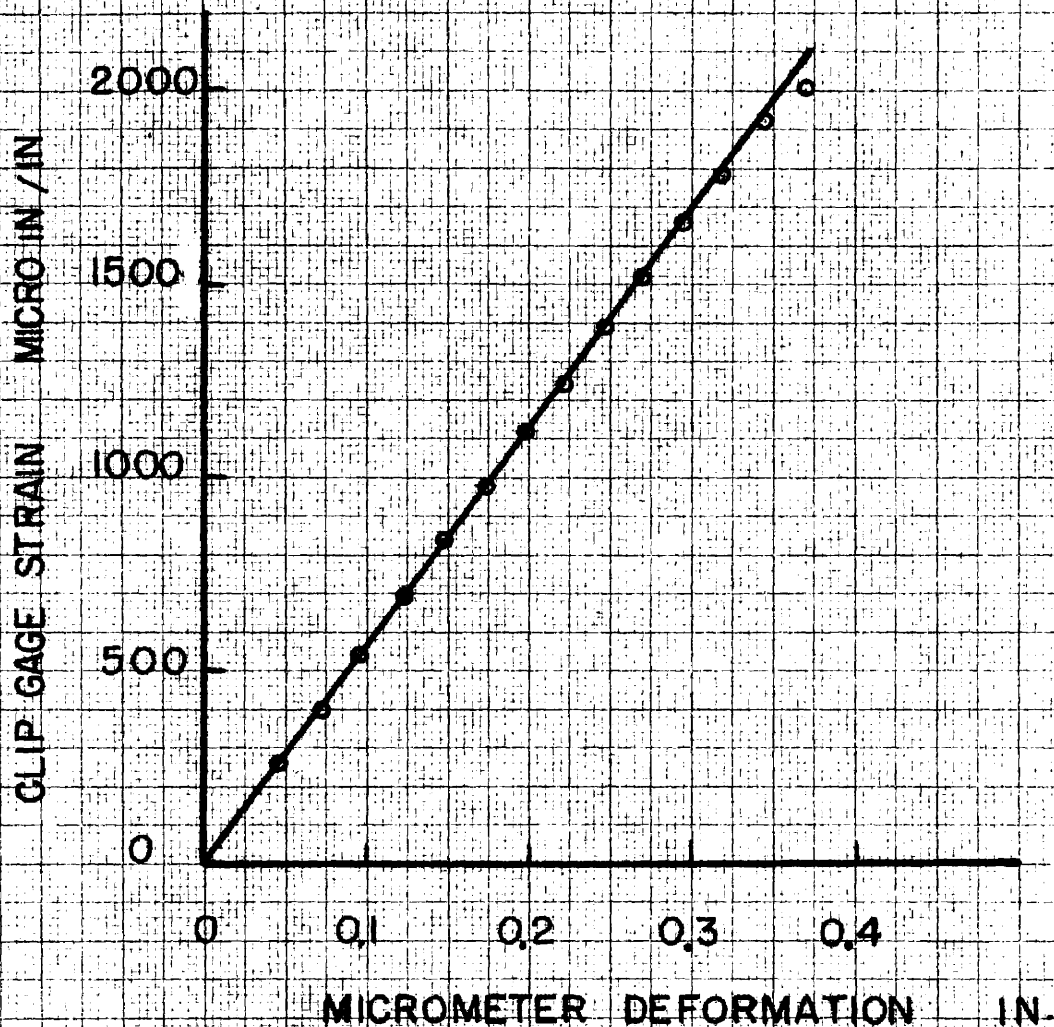


FIG.118 - CALIBRATION OF CLIP GAGE BY MICROMETER



FIG.119 - CALIBRATION OF CLIP GAGE BY SR-4 GAGE



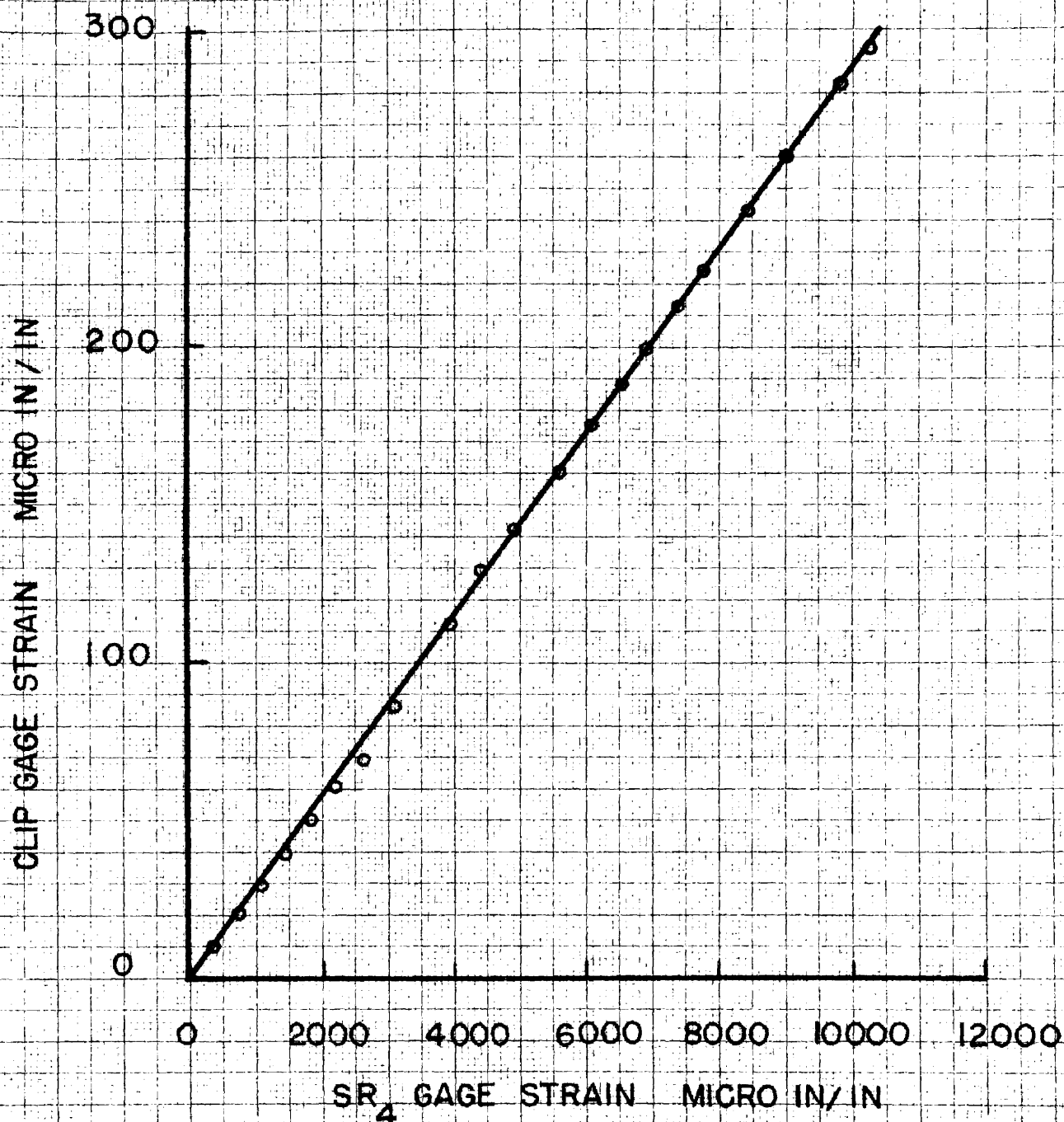
GAGE LENGTH = 2.370 INS.

MAXIMUM STRAIN REACHED = $\frac{.35}{2.370} = 0.1475$ IN/IN

= 14.75 % DEFORMATION

MULTIPLICATION FACTOR OF CLIP GAGE = SLOPE OF
MICROMETER & CLIP GAGE STRAINS = 73.8

FIG 20- MICROMETER DEFORMATIONS VS CLIP GAGE
STRAINS FOR AXIAL COMPRESSION



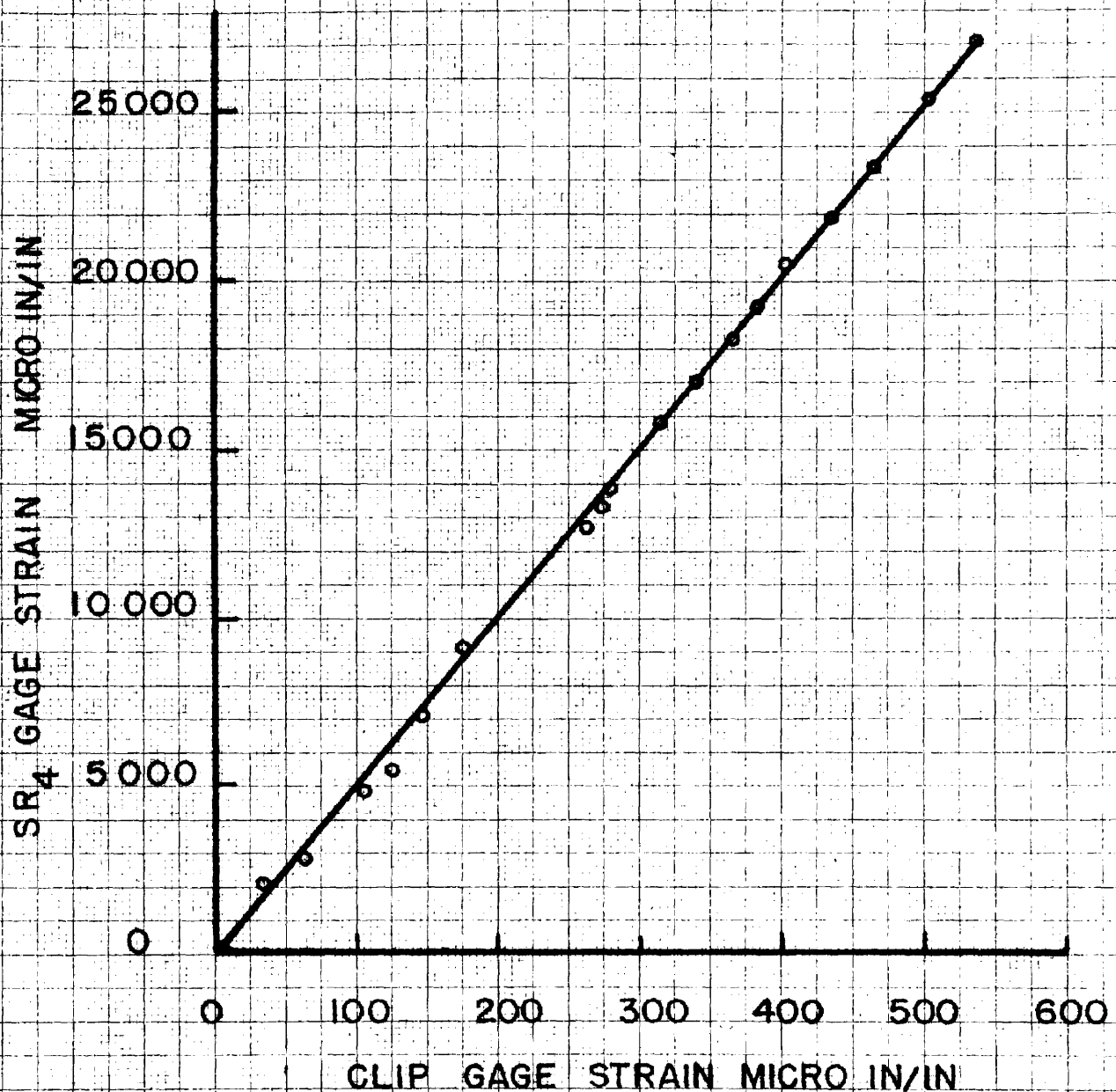
MAXIMUM STRAIN REACHED = 0.0103

= 1.03 % DEFORMATION

MULTIPLICATION FACTOR OF CLIP GAGE = 35

FIG 21 - SR STRAINS VS CLIP GAGE STRAINS FOR SQUARE
CROSS SECTION "I" MILD STEEL BEAM IN PURE BENDING

COMPRESSION SIDE OF THE BEAM



MAXIMUM STRAIN REACHED = 0.027 IN/IN

= 2.70% DEFORMATION

MULTIPLICATION FACTOR OF CLIP GAGE = 50

FIG.122- SR_4 STRAINS VS CLIP GAGE STRAINS FOR SQUARE
 CROSS SECTION $1\frac{31}{32} \times 1\frac{31}{32}$ MILD STEEL BEAM IN PURE BENDING

VITA

Abd el-Kerim Mohamed Ata was born on November 4, 1918, at Rashid, Egypt. He graduated in 1935 from Abbasiah Secondary School, Alexandria, Egypt. Then he entered Fouad 1st University, Giza, Egypt, in October, 1935, in the Civil Engineering section of the faculty of engineering. After attending five years in civil engineering education, he took his B. Sc. degree with honor June, 1940. He then joined the government municipality department as structural engineer from 1940 to 1942. In December, 1942, he was elected to be a staff member of the structural department of faculty of engineering, Fouad 1st University, where he taught full time from 1942 to 1948. During this period he worked for his M. Sc. degree and obtained it in July, 1945. Then he was promoted to the post of lecturer "B" on the staff of the university March, 1946. In February, 1948, he was awarded a fellowship from his university at Egypt to complete his graduate work in the United States. He entered the University of California, Berkeley, California, in March, 1948, where he attended the spring and the summer sessions. During this time, he was promoted to the post of lecturer "A" on the staff of Fouad 1st University, Egypt, July, 1948. He then enrolled at Purdue University, West Lafayette, Indiana, in the School of Civil Engineering and Engineering Mechanics working towards the Ph. D. degree.